Flight Simulator Benchmarking

A Simulator Comparison Study into the Effects of Motion Filter Order on Pilot Control Behavior

M. A. Pieters

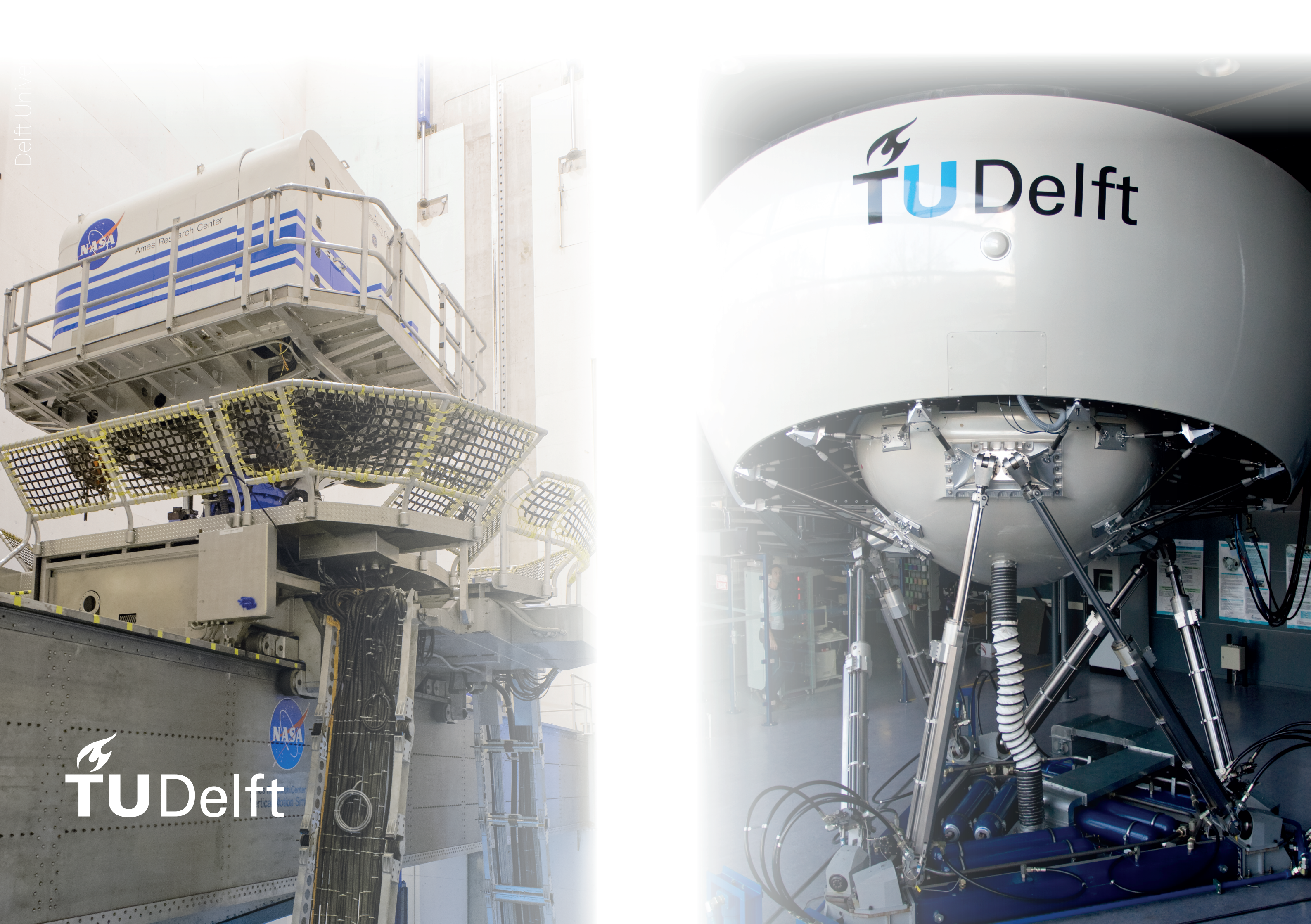

TU Delft

Flight Simulator Benchmarking

A Simulator Comparison Study into the Effects of Motion Filter Order on Pilot Control Behavior

by

M. A. Pieters

to obtain the degree of Master of Science
at the Delft University of Technology.

Student number:	4282248	
Project duration:	January 2018 - December 2018	
Thesis committee:	prof. dr. ir. M. Mulder,	TU Delft
	dr. ir. D. M. Pool,	TU Delft
	dr. ir. P. M. T. Zaal,	NASA Ames Research Center
	ir. O. Stroosma,	TU Delft
	dr. ir. J. F. C. de Winter	TU Delft

An electronic version of this thesis is available at `http://repository.tudelft.nl/`.

TUDelft

Delft University of Technology

DELFT UNIVERSITY OF TECHNOLOGY
DEPARTMENT OF
CONTROL AND SIMULATION

The undersigned hereby certify that they have read and recommend to the Faculty of Aerospace Engineering for acceptance a thesis entitled **"Flight Simulator Benchmarking: a Simulator Comparison Study into the Effects of Motion Filter Order on Pilot Control Behavior"** by **Marc Antoine Pieters** in partial fulfillment of the requirements for the degree of **Master of Science**.

Dated: 4 December 2018

Readers:

prof. dr. ir. M. Mulder

dr. ir. D. M. Pool

dr. ir. P. M. T. Zaal

ir. O. Stroosma

dr. ir. J. F. C. de Winter

Preface

This report presents my Master of Science thesis at the faculty of Aerospace Engineering of Delft University of Technology, in the Control and Simulation department. The thesis project consisted of two phases: a preliminary phase and an experiment phase. The preliminary phase focused on performing a literature review, developing theory and defining a research plan for an actual experiment, which was subsequently performed in the experiment phase. This report contains the results of both phases.

I started this thesis project in January 2018 in Delft and relocated to Mountain View, California, in February. After concluding part of the work in the United States in June 2018, I moved back to Delft, the Netherlands. In the United States, I was part of the NASA Ames Research Center division on Human-Systems Integration. More specifically, I worked in the Human-Centered Control and Simulation Laboratory (the logo of which can be found below), which also hosted me during my internship in 2017. Doing my internship at NASA Ames Research Center gave me the chance to experience several different projects. I worked in close relation with the team of the Vertical Motion Simulator and many other departments around the center. Eventually this internship lead to the thesis project. The thesis project was aptly named Motion Algorithm Development (MAD) at NASA. The logo that was made for this project can be found below.

I would like to express my gratitude to my supervisor in Delft, dr. ir. Daan Pool for setting up the contact which would eventually lead to me working at NASA. Furthermore, I would like to thank dr. ir. Peter Zaal, my supervisor at NASA Ames. All the help and guidance both of you offered throughout this project proved extremely valuable. Furthermore, I would like to thank the simulator engineers of both the Vertical Motion Simulator and SIMONA Research Simulator in Delft, Stephan Norris and ir. Olaf Stroosma, respectively. Your input in the project was extremely helpful to me.

Finally, I would like to thank all my friends and family, both in the Netherlands and abroad. Your support made this work possible.

M. A. Pieters
Delft, December 2018

Contents

List of Figures

List of Tables

Nomenclature

Abbreviations

ANOVA	analysis of variance
CG	center of gravity
DES	Dynamic Environment Simulator
ERP	eye reference point
FC	Fourier coefficient
GFORCE	Generic Fighter Operations Research Cockpit Environment
GRACE	Generic Research Aircraft Cockpit Environment
ICR	instantaneous center of rotation
IDMS	Image Delay Measurement System
IRB	Institutional Review Board
KW	Kruskall-Wallis test
LAMARS	Large Amplitude Multi-Mode Aerospace Research Simulator
MF	motion filter
MLE	maximum likelihood estimation
NASA	National Aeronautics and Space Administration
NLR	National Aerospace Laboratory
OMCT	Objective Motion Cueing Test
PFD	primary flight display
PS	pilot station
REF	reference motion conditions
RMS	root mean square
SIMONA	Simulation, Motion and Navigation Institute
SRH	Schreirer-Ray-Hare extension
SRS	SIMONA Research Simulator
SS	sum-of-squares
T-CAB	transport aircraft cabine
UTIAS	University of Toronto Institute for Aerospace Studies
VAF	variance accounted for
VDMS	Visual Delay Measurement System
VFR	visual flight rules
VMS	Vertical Motion Simulator

Symbols

δ_c	Control deflection	$[deg]$
δ_e	Elevator deflection	$[deg]$
μ	Average	$[-]$
ω_b	Third order motion filter break frequency	$[rad/s]$
$\omega_{c,d}$	Open-loop disturbance crossover frequency	$[rad/s]$
$\omega_{c,t}$	Open-loop target crossover frequency	$[rad/s]$
ω_{mf}	Motion filter break frequency	$[rad/s]$
ω_{nm}	Pilot model neuromuscular frequency	$[rad/s]$
ω_{phug}	Phugoid frequency	$[rad/s]$
ω_{sp}	Short period frequency	$[rad/s]$
ϕ	Roll angle	$[deg]$
Φ_S	Motion filter break frequency at 1 rad/s	$[deg]$
ψ	Yaw angle	$[deg]$
ρ	Correlation coefficient	$[-]$
σ	Standard deviation	$[-]$

σ_u^2	Variance of control signal	$[deg^2]$
τ_m	Pilot model motion time delay	$[s]$
τ_v	Pilot model visual time delay	$[s]$
θ	Pitch angle	$[deg]$
$\varphi_{m,d}$	Open-loop disturbance phase margin	$[deg]$
$\varphi_{m,t}$	Open-loop target phase margin	$[deg]$
ζ_{nm}	Pilot model neuromuscular damping constant	$[-]$
a	Linear acceleration	$[m/s^2]$
e	Visual error signal	$[deg]$
F^{ab}	Aircraft body frame of reference	$[-]$
F^{pa}	Aircraft pilot station frame of reference	$[-]$
F^{ps}	Simulator pilot station frame of reference	$[-]$
F^{sb}	Simulator body frame of reference	$[-]$
F^{si}	Simulator inertial frame of reference	$[-]$
$f_{t,d}$	target / disturbance forcing function	$[deg]$
H_c	Controlled dynamics	$[-]$
H_θ	Aircraft pitch response function	$[-]$
H_{mf}	Motion filter	$[-]$
H_{motion}	Simulator motion hardware dynamics	$[-]$
$H_{p_{mot}}$	Pilot motion response	$[-]$
$H_{p_{vis}}$	Pilot visual response	$[-]$
H_{SRS}	SRS motion dynamics	$[-]$
H_{stick}	Side stick dynamics	$[-]$
H_{VMS}	VMS motion dynamics	$[-]$
K_m	Pilot model motion gain	$[-]$
K_S	Motion filter gain at 1 rad/s	$[-]$
K_s	Stick gain	$[-]$
K_v	Pilot model visual gain	$[-]$
K_{mf}	Motion filter gain	$[-]$
l	Linear distance	$[m]$
n	Remnant signal	$[deg]$
O_{mf}	Motion filter order	$[-]$
s	Laplace variable	$[-]$
t	Time	$[s]$
T_L	Pilot model lead time constant	$[s]$
T_m	Measurement time	$[s]$
u	Control input signal	$[deg]$

1
Introduction

Recently, there has been a lot of interest for studies comparing pilot behavior and performance between flight simulators with the purpose of developing human-centered simulator benchmark tests. In 2017, a Royal Aeronautical Society conference in London was held specifically to discuss the topic [1]. This thesis presents an experiment which compared the Vertical Motion Simulator at NASA Ames Research Center and SIMONA Research Simulator, which is located at Delft University of Technology, with the purpose of taking steps in developing a human-centered simulator benchmark test. The goal of such a benchmark test would be to put the human in a central role in simulator benchmarking, instead of regarding simulator subsystems separately.

Another topic of interest in current research is the order of magnitude of the motion filters that are present in flight simulators. Whereas the individual parameters of the motion filter (gain, break frequency, etc.) have received attention in many previous experiments (for example work by Pool et al. [2, 3]), the effects of the order O_{mf} of the filters on pilot performance and control behavior have not received attention, even though filters of different orders are used in different simulators, or even within a simulator.

Hence, this project features two main goals: Firstly, gaining insight into the effects of motion filter orders on pilot manual control behavior, which ties directly to Delft University of Technology simulator fidelity research [2]. This is done by performing an experiment with a variation of the order of the motion filters O_{mf}. Secondly, taking a step into developing a human-centered simulator performance benchmark. This is done by performing the experiment on both the Vertical Motion Simulator and the SIMONA Research Simulator and comparing the results.

In order to present the content of this report as clearly as possible, it is structured as follows. The first part of the report presents a scientific paper describing the final experiment. A version of this paper was also published on the 2019 AIAA SciTech conference in San Diego, CA, USA. Several appendices are present to support the final experiment. Appendix A goes more into detail on the results, presenting an analysis excluding several participants and a description of the procedure of verification of the results and the statistical analysis. Furthermore, in Appendix B, a closer look is taken at the matching of the motion systems of both simulators. Appendix C discusses differences between the sidesticks of the VMS and SRS. Finally, Appendix D presents several documents that were necessary in the experiment, such as the experiment briefing, the runtables and the participant consent forms.

The second part of the report contains the preliminary thesis. It is structured as follows. Firstly, two chapters of literature are present, to treat the two goals respectively: Chapter 2 presents a literature survey on motion filter order O_{mf} and Chapter 3 presents a literature survey on simulator benchmarking. Both these chapters start with some general theory, which is followed by an overview of previous works into the topic. From this basis research questions are posed. Then, Chapter 4 presents the methodology and results of two preliminary experiment iterations. The results are discussed and several recommendations for a future experiment are made. Finally, Chapter 6 concludes the preliminary phase of the report.

I

Scientific Paper

To be graded as part of AE5310 - Thesis Control and Operations

A Simulator Comparison Study into the Effects of Motion Filter Order on Pilot Control Behavior

Marc A. Pieters
Delft University of Technology
Delft, the Netherlands
Supervisors: Daan M. Pool, Peter M. T. Zaal, Olaf Stroosma, Max Mulder

This paper describes an experiment investigating the effects of motion filter order on human manual control tracking behavior and performance. The experiment was performed on two simulators: the Vertical Motion Simulator at NASA Ames Research Center and the SIMONA Research Simulator at Delft University of Technology. Eighteen pilots in the Vertical Motion Simulator and twenty pilots in the SIMONA Research Simulator performed the experiment with a full factorial variation of three motion filter orders and two motion filter frequencies, in addition to a reference no-motion and full-motion condition. Motion shaping filters derived from Objective Motion Cueing Test measurements on the Vertical Motion Simulator were included in the SIMONA Research Simulator motion logic to match the motion cues between both simulators. Furthermore, the side sticks were set to matching characteristics and the visual cues were matched in terms of time delay, graphics size and screen characteristics. With increased motion filter order, pilots showed worse performance and a lowered contribution of motion feedback in their control strategy. Increasing the motion filter break frequency had similar effects, which were stronger than the effects of increasing the motion filter order, for the eight experimental conditions that were considered in this experiment. For the same motion condition the simulators showed offsets in the results. However, the trends between the motion conditions were similar, leading to the conclusion that for simulator comparisons relative trends are easier to replicate between simulators than absolute results within one condition.

Nomenclature

Symbols

e	error signal, deg
$f_{t,d}$	target / disturbance forcing function, deg
H_c	controlled dynamics
H_{mf}	motion filter
H_{motion}	motion hardware dynamics
$H_{shaping}$	motion shaping filter
H_{stick}	stick dynamics
H_{SRS}	SRS motion dynamics
$H_{p_{mot}}$	pilot motion response
$H_{p_{vis}}$	pilot visual response
H_{VMS}	VMS motion dynamics
K_m	motion gain, $-$
K_S	gain of motion filter at 1 rad/s, $-$
K_v	visual gain, $-$
n	pilot remnant, deg
O_{mf}	motion filter order, -
s	Laplace operator, $-$
t	time, s
T_L	pilot lead time constant, s
T_m	measurement time, s
u	pilot control input, deg
δ_c	control deflection, deg
ζ_{nm}	neuromuscular damping, $-$
θ	pitch angle, deg
μ	average, $-$
ρ	correlation coefficient, $-$
σ	standard deviation, $-$
σ_u^2	variance of control signal, deg^2
τ_m	motion time delay, s
τ_v	visual time delay, s
φ_m	open-loop phase margin, deg
Φ_S	phase of motion filter at 1 rad/s, deg
ω_c	open-loop crossover frequency, rad/s
ω_n	stick natural frequency, rad/s
ω_{mf}	motion filter frequency, rad/s
ω_{nm}	neuromuscular frequency, rad/s
ω_{phug}	phugoid frequency, rad/s
ω_{sp}	short period frequency, rad/s

Abbreviations

ANOVA	analysis of variance
CG	center of gravity
ERP	eye reference point
ICR	instantaneous center of rotation
IDMS	Image Delay Measurement System
KW	Kruskall-Wallis test
MLE	maximum likelihood estimation
OMCT	Objective Motion Cueing Test
PFD	primary flight display
REF	reference motion conditions
RMS	root mean square
SRH	Scheirer-Ray-Hare extension
SRS	SIMONA Research Simulator
T-CAB	transport aircraft cab
VAF	variance accounted for
VDMS	Visual Delay Measurement System
VMS	Vertical Motion Simulator

I. Introduction

This paper presents the results of an experiment that was performed on two simulators investigating changes in pilot control behavior and performance for different motion filter orders.

The aviation market is growing and over the next 20 years it is estimated that over 600,000 new pilots are required.[1,2] With such a predicted increase, industry is eager to train pilot control skills efficiently. Traditionally, in order to train pilots efficiently, flight simulators are designed to present pilots with high fidelity simulation cues,[3] such as motion cues. However, even though the benefit of using motion-enabled flight simulators in the training of pilot control skills is subject of much debate,[4–7] current pilot training requirements still focus heavily on the availability of motion in flight simulators. The focus on motion is even growing, which is illustrated by the new requirement for airline pilots to receive stall training in full-motion flight simulators starting in 2019.[8–10] Hence, with the increasing need for skilled pilots in the growing aviation industry, the role of motion in flight simulators will become more important.

Flight simulators are bound by their available motion space in presenting pilots with motion cues. A large variety of motion washout filters has been applied in the past, in order to make pilots perceive the onset of a maneuver without exceeding the physical limits of the motion system.[11] Classical washout filters are commonly used since they ensure different pilots are presented with the same motion cues, independent of their control behavior.[12] The settings of classical washout filters have been shown to influence pilot control behavior in numerous studies.[13–21] Hence, the effects of the motion filter settings on pilot control behavior and performance need to be known, in order to determine how pilots could benefit from motion in flight simulators.

Whereas the parameters of the classical washout filters (gains, break frequencies, rate limits, etc.) have been the subject of numerous studies,[7,13,14,22–24] the order of the washout filters O_{mf} has not received the same attention. For example, Pool et al.[13,14] consolidated the results of ten studies into the effects of motion fidelity on pilot control behavior using quantitative cybernetic pilot models. They found consistent results indicating that a decreasing motion filter gain K_{mf} and an increasing motion filter break frequency ω_{mf}, result in degraded pilot performance, lower visual gains and increased use of visual information for lead generation. Furthermore, the parameters have been the subject of studies in which procedures for tuning the washout filters were investigated.[7,22–24]

Furthermore, despite the need for verification of human performance results, experiments on full-motion flight simulators are rarely replicated due to high costs involved and challenges in comparing simulator subsystems. In a series of previous flight simulation experiment replications where a yaw-capture task with varying sway and yaw cueing was considered, generally similar results were found.[25–31] However, differences between the simulators were present even though considerable effort was spent on matching all experiment setups. Another replication by Jex et al.[32,33] considered a tracking task, which proved valuable in comparing the control behavior of pilots between simulators, and identifying the source of the possible differences. Hence, repeating a manual control tracking experiment on two simulators while matching simulation cues, would allow for verification of current findings of filter order effects and might aid in drawing conclusions for future simulator comparisons.

This paper has two main goals. The first goal is to gain insight into the effects of motion filter order O_{mf} and motion filter break frequency ω_{mf} on pilot manual control behavior and performance. This was achieved by performing an experiment with a variation of the order of the motion filters. A pitch task based on Ref. 34 was performed, which allowed to use cybernetic pilot models to assess changes in control behavior and performance in a quantitative manner. In total, 38 pilots participated in the experiment. The second goal of this paper is to determine factors for generalizability of experimental findings into human control behavior and performance on multiple simulators, in order to aid future experiment replications. This was done by performing the experiment on both the Vertical Motion Simulator

(VMS) and the SIMONA Research Simulator (SRS) and comparing the results. Because of the dual goal of the paper, two sets of hypotheses are present: the first three hypotheses discuss the motion filter effects and two hypotheses are added to cover the simulator comparison aspect.

Section II presents the methodology of the experiment. Then, Section III elaborates on the efforts to match the cues the pilots perceived in both simulators. Section IV presents the experimental results. In Section V, the results are discussed. Finally, Section VI concludes the paper.

II. Method

II.A. Control Task

The manual pitch control task that participants performed in both the VMS and SRS can be represented by the closed-loop diagram in Figure 1. The task was based on a previous experiment by Zaal and Zavala.[34] Comparing the results of Ref. 34 to the current experimental results allowed to verify correct implementation of the task on both simulators. Furthermore, using an existing task allowed to minimize development time on the two flight simulators. Participants were asked to minimize the pitch error e, which was presented on a compensatory display, by making inputs with a side stick. The display represented a simplified version of a primary flight display (PFD). Using the side stick pilots generated control inputs u. The inputs acted on the pitch dynamics transfer function $H_\theta(s)$, which resulted in the pitch angle θ. This pitch angle θ was used to calculate the visual pitch error signal e. Furthermore, in the motion feedback path, it was filtered through a motion filter $H_{mf}(s)$. The motion filter $H_{mf}(s)$ was varied between experimental conditions (see Section II.E). The pilot perceived the motion cues resulting from the motion system $H_{motion}(s)$. In the VMS the motion system just consisted of the VMS motion system dynamics $H_{motion_{VMS}}(s)$. In the SRS a motion shaping filter $H_{shaping}(s)$ was present in front of the SRS motion system dynamics: $H_{motion}(s) = H_{shaping}(s) \cdot H_{motion_{SRS}}(s)$, in order to match the motion system response of the SRS to the VMS (see Section III.A). Finally, two forcing functions were present which allowed to identify a multi-channel quasi-linear human pilot model which consisted of a visual response function $H_{p_{vis}}(s)$, a motion response function $H_{p_{mot}}(s)$ and a remnant signal n.[35] The remainder of this section goes more into depth on the individual elements of Figure 1.

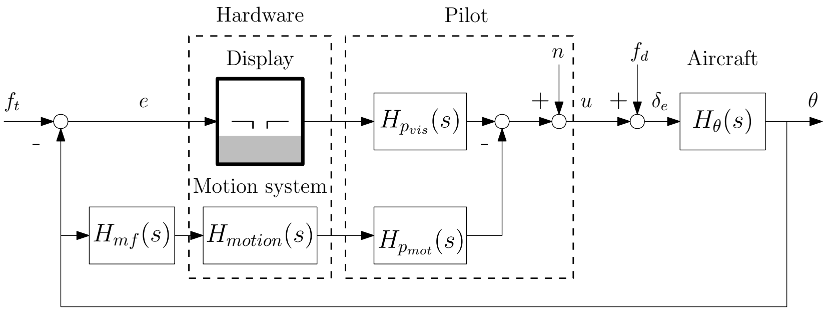

Figure 1: The considered pitch control task and human pilot model

II.A.1. Controlled Dynamics

The controlled dynamics $H_\theta(s)$ were defined by Eq. (1). They represent a mid-size twin-engine commercial transport aircraft with a weight of 185,000 lbs, trimmed close to its stall point at 41,000 ft and with an indicated airspeed of 150 kts. The controlled dynamics feature a stable short period eigenmode ($\omega_{sp} = 0.6892$ rad/s) and an unstable phugoid eigenmode ($\omega_{phug} = 0.0638$ rad/s), with eigenvalues at $\lambda_{1,2} = -0.2230 \pm 0.6522i$ and $\lambda_{3,4} = 0.0069 \pm 0.0634i$ in the complex plane, respectively. These controlled dynamics were used earlier in Ref. 34.

$$H_\theta(s) = \frac{\theta(s)}{\delta_e(s)} = \frac{28.4474 \cdot \left(346.5s^2 + 32.03s + 1\right)}{(245.6s^2 - 3.409s + 1) \cdot (2.105s^2 + 0.9387s + 1)} \tag{1}$$

Vertical motion of the center of gravity (CG) of the aircraft results in CG heave. Instantaneous center of rotation (ICR) pitch-heave results from the location of the pilot station in front of the center of rotation. The pilot of a real aircraft feels a combination of both heave components. To accommodate the motion space of both simulators, no CG heave was present and only ICR pitch-heave was included in the task. A previous study showed that this did not significantly affect pilot control behavior.[36] The ICR pitch-heave response to pitch variations was defined by Eq. (2).

$$H_{a_{z_{\theta,ICR}}}(s) = \frac{a_{z_{\theta,ICR}}(s)}{\theta(s)} = -11.49s^2 \tag{2}$$

Eq. (2) shows that the pilot station was located 11.49 m in front of the instantaneous center of rotation. Analogous to ICR pitch heave, the z-position of the pilot station above or below the x-axis of the aircraft body-fixed reference frame results in ICR pitch surge. In the considered aircraft, the pilot station was placed on the x-axis, such that no pitch surge was present. Furthermore, no CG surge was modelled.

II.A.2. Human Pilot Model

In order to investigate the control behavior of the pilot, linear transfer functions were identified for both the visual and the motion channel, as depicted in Figure 1. McRuer and Jex[37] state that pilots adapt themselves to the controlled dynamics to ensure that the open-loop response approximates a single integrator in the region of the crossover frequency. For the controlled dynamics of Eq. (1), pilots thus need to generate lead in the region of the crossover frequency. Hence, the pilot visual and motion responses are defined by Eq. (3) and (4), respectively.

$$H_{p_{vis}}(s) = K_v\,(1 + T_L s)\, e^{-\tau_v s} \frac{\omega_{nm}^2}{s^2 + 2\zeta_{nm}\omega_{nm}s + \omega_{nm}^2} \tag{3}$$

$$H_{p_{mot}}(s) = sK_m e^{-\tau_m s} \frac{\omega_{nm}^2}{s^2 + 2\zeta_{nm}\omega_{nm}s + \omega_{nm}^2} \tag{4}$$

These two equations formed the pilot model, which has a total of seven parameters that quantify pilots' selected control behavior. The pilot lead equalization is captured with the equalization parameters: the visual gain K_v, the motion gain K_m, and the lead time constant T_L. The human limitations of the pilots are captured with the visual time delay τ_v and the motion time delay τ_m. Furthermore, pilots are limited by their neuromuscular actuation, which is captured with the neuromuscular parameters: the damping constant ζ_{nm} and frequency ω_{nm}. Previous research has shown that a second-order mass-spring-damping model is able to adequately describe the combined stick and neuromuscular dynamics of the pilots.[15,36,38]

II.A.3. Forcing Functions

Two forcing functions were used in the pitch tracking task, a target and a disturbance signal, which resulted in a combined target-following and disturbance-rejection task. Using two independent forcing function signals allowed to estimate the two separate describing functions that are part of the pilot model as introduced in Section II.A.2: the pilot visual response $H_{p_{vis}}$ and the pilot motion response $H_{p_{mot}}$.[14] Both forcing functions were defined as sum-of-sines signals:

$$f_{t,d}(t) = \sum_{k=1}^{N_{t,d}} A_{t,d}(k) \sin\left[\omega_{t,d}(k)t + \phi_{t,d}(k)\right] \tag{5}$$

In Eq. (5) $A_{t,d}(k)$, $\omega_{t,d}(k)$ and $\phi_{t,d}(k)$ represent the amplitude, frequency and phase of the k^{th} sine in the target and disturbance forcing functions f_t and f_d, respectively. The number of sine waves in these functions is represented by $N_{t,d}$. The considered forcing function parameter values for the f_t and f_d signals, both with $N_{t,d} = 10$ sinusoids, can be found in Table 1.

Table 1: Properties of the forcing functions, as found in Ref. 34

Target, f_t				Disturbance, f_d			
n_t [-]	ω_t [rad/s]	A_t [deg]	ϕ_t [rad]	n_d [-]	ω_d [rad/s]	A_d [deg]	ϕ_d [rad]
3	0.2301	0.5818	-1.4796	2	0.1534	0.0105	0.1355
6	0.4602	0.5306	-0.0745	5	0.3835	0.0098	-0.1664
13	0.9971	0.3711	0.7006	11	0.8437	0.0091	2.9016
27	2.0709	0.1674	-1.9563	23	1.7641	0.0283	5.6383
41	3.1447	0.0901	-2.8131	37	2.8379	0.0403	2.8648
53	4.0650	0.0605	2.1026	51	3.9117	0.0477	4.8718
73	5.5990	0.0375	-2.6178	71	5.4456	0.0569	1.0245
103	7.9000	0.0238	2.2550	101	7.7466	0.0725	5.0337
139	10.6612	0.0174	-0.6739	137	10.5078	0.0967	4.1487
194	14.8796	0.0135	0.1942	191	14.6495	0.1458	0.4274

The frequencies for the sinusoids ($\omega_{t,d}$) were all integer multiples ($n_{t,d}$) of the measurement time base frequency, $\omega_m = 2\pi/T_m = 2\pi/81.92$ s $= 0.0767$ rad/s, to avoid spectral leakage. The integer multiples were selected to ensure that the typical frequency range of human control was covered with regular intervals on a logarithmic scale.[34] Both the target forcing function f_t and the disturbance forcing function f_d had a time-domain variance of 0.4 deg^2, which has been applied successfully in previous experiments.[34]

The runs lasted 94.92 seconds. The first 3 seconds contained no forcing functions, followed by 5 seconds of ramp-in, to allow pilots to stabilize the controlled element. Then, a measurement window of 81.92 seconds was used for the analysis. The last 5 seconds were a fade-out of the forcing functions, in order to return the simulators to their initial positions gradually.

II.B. Dependent Measures

The goal of the experiment was to investigate how the order of the motion washout filter O_{mf} and the motion filter frequency ω_{mf} influenced the control behavior of the pilots and if results were comparable between two flight simulators. Hence, human control behavior and performance parameters were the variables of interest.

The root mean square (RMS) of the error signal e (i.e. RMS_e) and control signal u (i.e. RMS_u) were determined. RMS_e is a measure of performance, where a lower RMS_e signifies a lower overall error score and hence a better performance. RMS_u is a measure of control activity; a higher RMS_u indicates a higher control activity.

Furthermore, the pilot model defined in Eqs. (3) and (4) featured seven dependent variables: K_v, K_m, T_L, τ_v, τ_m, ζ_{nm} and ω_{nm}. These parameters were estimated using a time-domain parameter estimation technique, based on maximum likelihood estimation (MLE).[36] In this technique, a genetic algorithm provides an initial estimate for the parameters, which is subsequently refined by a gradient based Gauss-Newton estimation. The variance accounted for (VAF) is a measure of how much of the control signal u could be explained by the linear pilot model transfer functions. Using the linear pilot model transfer functions, the variance of the control signals of both the visual and motion channel, $\sigma^2_{u_v}$ and $\sigma^2_{u_m}$, respectively, were computed. The fraction of these variances showed how much of the total control signal u could be explained by the two channels of the quasi-linear pilot model.

Finally, the crossover frequencies and phase margins of the open-loop dynamics describe the pilot performance in attenuating the target and disturbance signals.[34] Looking at Figure 1, an open-loop response can be constructed, for both the target and disturbance inputs, which can be seen in Eq. (6) and (7), respectively.

$$H_{ol,t}(s) = \frac{\theta(s)}{E(s)} = \frac{H_{p_{vis}}(s)H_\theta(s)}{1 + H_{mf}(s)H_{motion}(s)H_{p_{mot}}(s)H_\theta(s)} \tag{6}$$

$$H_{ol,d}(s) = -\frac{U(s)}{\delta_c(s)} = H_\theta(s)\left[H_{p_{vis}}(s) + H_{mf}(s)H_{motion}(s)H_{p_{mot}}(s)\right] \tag{7}$$

The open-loop crossover frequencies and phase margins for both the target and disturbance signal were determined, using Eqs. (6) and (7): $\omega_{c,t}$, $\omega_{c,d}$, $\varphi_{m,t}$ and $\varphi_{m,d}$.

II.C. Participants

In the VMS 18 pilots participated in the experiment and in the SRS 20 pilots participated. All participants were active general aviation pilots. Table 2 presents information on the pilot population. Four VMS pilots had considerably more flight hours than the rest: 5300, 2800, 1637 and 1200 hours. Similarly, two SRS pilots had flown considerably more hours than the rest: 6800 and 1018 hours. Most pilots in both groups had experience in fixed-base or full-motion flight simulators. Most of the VMS pilots had experience with similar experiments (for example, Ref. 37), whereas the recruited SRS pilots did not.

Data from one VMS pilot and one SRS pilot were removed. For the VMS pilot the data were not sufficient to generate accurate parameter estimates and the SRS pilot was not able to complete the experiment. Consequently, the analysis of the results was performed with another two random SRS pilots omitted, such that for both simulators the data of 17 pilots were present, as one of the statistical tests assumed an equal number of participants in both groups, as explained in Section IV.A.

Table 2: Overview of pilot population characteristics

	Age		Flight hours		Simulator hours		Flight and simulator hours past 3 months	
	μ	σ	μ	σ	μ	σ	μ	σ
VMS	28.9	4.97	751	1341	45.7	91.0	17.3	40.3
SRS	31.5	5.52	636	1445	27.9	60.2	37.3	58.4

II.D. Procedures

At the start of the experiment, each pilot was given a briefing, detailing the purpose of the experiment and the procedures, including suggestions and examples on how to best follow the target and compensate for the disturbance. No specifics about the (number of) motion conditions were given, apart from that a no-motion condition was present. Pilots were informed of the current best score and encouraged to improve it. After each run the head down display showed the RMS_e of that run to give the pilots feedback on their performance.

The experiment consisted of three simulator sessions, all performed on the same day, with breaks in between sessions. The pilots performed 24, 20 and 12 runs in the first, second and third session, respectively. During and between each session pilots were informed that they could take additional or longer breaks if they so desired (for example, due to fatigue). The first 16 runs were used as training and the last 40 runs were used to calculate the results. A randomized latin square experiment matrix was followed. Over the full experiment, each pilot performed each experimental condition 7 times.

Brown noise resembling aircraft engines was played over noise-cancelling headphones to mask the sound made by the motion actuators throughout the experiment.

II.E. Independent Variables

Table 3 shows the eight tested experimental conditions. The motion filters in these conditions were applied to the pitch, heave and surge axes of the simulators. Three motion filter orders and two break frequencies were tested. C0 and C7 are reference (REF) motion conditions. C0 is a reference no-motion condition and C7 acts as a reference full-motion condition. The no-motion condition C0 was present to isolate the effects of the motion system of the simulators. For C0 the pilot model only consisted of a visual channel. The full-motion condition C7 was implemented as a second order filter with a break frequency of $\omega_{mf} = 0.2$ rad/s, in order to prevent the simulator from drifting. It was present to generate the motion shaping filters $H_{shaping}(s)$ (see Section III) and as a reference motion value for the prediction equations. In all conditions, the damping constant was set to $\zeta_{mf} = 1/\sqrt{2} = 0.707$. Figure 2 shows the motion fidelity of the motion conditions on the fidelity criteria proposed by Sinacori[39] and Schroeder.[25] With increasing filter order O_{mf}, the conditions move further away from the high fidelity region. This effect is present for increasing motion filter frequency ω_{mf} as well, with even bigger changes visible.

Table 3: Experimental conditions

Condition	Filter order O_{mf} [-]	ω_{mf} [rad/s]	Motion Filter	K_S [-]
C0	No motion	-	$H_{mf}(s) = 0$	0.000
C1	1	0.5	$H_{mf}(s) = \frac{s}{s+0.5}$	0.894
C2	1	2.0	$H_{mf}(s) = \frac{s}{s+2.0}$	0.447
C3	2	0.5	$H_{mf}(s) = \frac{s^2}{s^2+2\cdot\zeta_{mf}\cdot 0.5\cdot s+0.5^2}$	0.970
C4	2	2.0	$H_{mf}(s) = \frac{s^2}{s^2+2\cdot\zeta_{mf}\cdot 2.0\cdot s+2.0^2}$	0.243
C5	3	0.5	$H_{mf}(s) = \frac{s}{s+0.5} \cdot \frac{s^2}{s^2+2\cdot\zeta_{mf}\cdot 0.5\cdot s+0.5^2}$	0.868
C6	3	2.0	$H_{mf}(s) = \frac{s}{s+2.0} \cdot \frac{s^2}{s^2+2\cdot\zeta_{mf}\cdot 2.0\cdot s+2.0^2}$	0.109
C7	Full motion	0.2	$H_{mf}(s) = \frac{s^2}{s^2+2\cdot\zeta_{mf}\cdot 0.2\cdot s+0.2^2}$	0.999

II.F. Hypotheses

Pool et al. formulated a series of equations in Ref. 13 that predict the effects of different motion filter settings on the dependent variables mentioned before. Using these equations, the effects of changing O_{mf} and ω_{mf} could be predicted. By analyzing data from numerous studies where motion conditions were varied and the effects on pilot tracking and control behavior were investigated, it was found that K_S, the magnitude of the motion filter at a frequency of 1 rad/s, was the most suitable predictor variable.[13] K_S is part of the motion fidelity criteria as proposed by Sinacori[39] and adapted by Schroeder.[25] It was calculated using Eq. (8).

$$K_S = \left| H_{mf}(j\omega) \right|_{\omega=1\ rad/s} \tag{8}$$

The prediction equations relate the pilot model parameters to the motion fidelity of a certain motion condition, using K_S. Using the value of a reference full-motion condition with $K_S = 1$, the K_S of the desired condition allows to

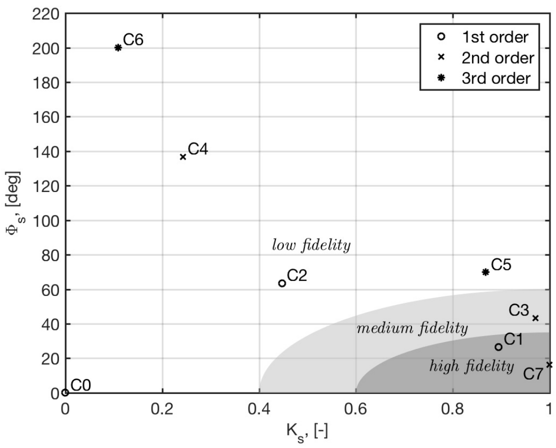

Figure 2: Experiment conditions shown on motion fidelity plot, as proposed by Ref. 39 and Ref. 25

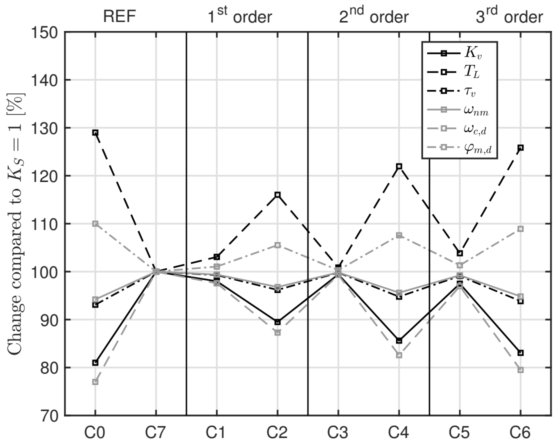

Figure 3: Predicted relative change of pilot model parameters, in comparison to full-motion C7

compute the corresponding predicted pilot model parameter. The prediction equations are given by Eq. (9) to (14).

$$\hat{K}_v(K_S) = K_v(1)\,[0.19\,(K_S - 1) + 1] \tag{9}$$

$$\hat{T}_L\,(K_S) = T_L(1)\,[-0.29\,(K_S - 1) + 1] \tag{10}$$

$$\hat{\tau}_v\,(K_S) = \tau_v(1)\,[0.069\,(K_S - 1) + 1] \tag{11}$$

$$\hat{\omega}_{nm}\,(K_S) = \omega_{nm}(1)\,[0.058\,(K_S - 1) + 1] \tag{12}$$

$$\hat{\omega}_{c,d}(K_S) = \omega_{c,d}(1)\,[0.23\,(K_S - 1) + 1] \tag{13}$$

$$\hat{\varphi}_{m,d}(K_S) = \varphi_{m,d}(1)\,[-0.10\,(K_S - 1) + 1] \tag{14}$$

For example, for $\hat{T}_L$, the prediction of the lead time constant T_L, the value of the lead time constant in a condition with $K_S = 1$ is indicated by $T_L(1)$ and K_S is the value of the motion condition of the desired prediction. The numerical factor that follows (-0.29 in the case of $\hat{T}_L$) indicates the percentage change that occurs when K_S equals 0: the lead time constant is predicted to be 29% higher for $K_S = 0$ than for $K_S = 1$.[13] Pool et al.[13] found sufficiently strong linear regressions between K_S and the following pilot model parameters: K_v, T_L, τ_v, ω_{nm}, $\omega_{c,d}$ and $\varphi_{m,d}$. For K_m, τ_m, ζ_{nm}, $\omega_{c,t}$ and $\varphi_{m,t}$ no such linear relationships were found.

Figure 3 shows the predicted relative change for each experimental motion condition compared to C7, with $K_S = 1$ in percent. Because C7 was implemented as a second order filter with $\omega_{mf} = 0.2$ rad/s, its K_S was equal to 0.999, see Table 3. For increasing motion filter order O_{mf}, increases in T_L and $\varphi_{m,d}$ can be seen. Furthermore, K_v and $\omega_{c,d}$ show a decrease for increasing filter order. τ_v and ω_{nm} show slight decreases for increasing O_{mf} as well. The effects are similar, but more pronounced for increasing motion filter break frequency ω_{mf}. For the increasing filter order O_{mf}, mainly the $\omega_{mf} = 2.0$ rad/s conditions show the changes.

Based on the offline prediction equations, three hypotheses were formulated for the change in dependent measures due to the change in filter order O_{mf} and filter frequency ω_{mf}, respectively:

H1: **Effect of motion filter order** O_{mf} - With increasing motion filter order more of the low frequency content of the aircraft output is filtered out by the motion filter. Furthermore, a higher filter order leads to more induced phase lead on the simulator motion. In Figure 3 it can be seen that for an increase in motion filter order the prediction equations predicted a decrease in visual gain K_v, an increase in visual lead time constant T_L and a slight decrease in visual time delay τ_v and neuromuscular frequency ω_{nm}. Mainly for the higher motion filter break frequency $\omega_{mf} = 2.0$ rad/s the effects for increasing the motion filter order are visible. Thus, it was expected that pilots would control with a smaller gains, while using more of the visual channel to generate lead. Furthermore, the prediction equations predicted a decrease in disturbance crossover frequency and a corresponding increase in disturbance phase margin. This suggested that the pilot model motion channel $H_{p_{mot}}$ would contribute less to the open-loop responses. Hence, it was hypothesized that pilots would use less motion and their performance would decrease for increasing motion filter order.

H2: **Effect of motion filter frequency** ω_{mf} - Similar to H1, with increasing motion filter break frequency ω_{mf}, more of the low-frequency content of the aircraft output is filtered out by the motion filter. Figure 2 relates this to a lowered motion fidelity. Looking at Figure 3 it can be seen that most of the effects are similar to the ones stated in hypothesis H1, albeit stronger. It was expected that with an increase in motion filter break frequency ω_{mf}, pilots would display an increase in T_L and $\varphi_{m,d}$ and a decrease K_v and $\omega_{c,d}$ and a slight decrease in τ_v and ω_{nm}. Thus, it was hypothesized that pilots would also use less motion and their performance would decrease for increasing motion filter frequency ω_{mf}.

H3: **Motion filter order versus motion filter frequency** - When comparing the different motion filter break frequencies to the motion filter orders in Figure 2 and 3, the change in frequency ω_{mf} showed larger changes in K_S. Subsequently, the prediction equations predicted larger changes on the pilot model parameters for changing ω_{mf} than for changing O_{mf}. Therefore, the effects of O_{mf} were hypothesized to be less severe than the effects of ω_{mf}, for the considered experimental conditions.

Hypotheses H1, H2 and H3 treat the effects of the independent variables O_{mf} and ω_{mf}. They will be supplemented with another two hypotheses in Section III that focus on the use of two different simulators.

III. Simulator Equalization

The experiment was first performed on the VMS at NASA Ames Research Center, using the transport aircraft cab (T-CAB), see Figure 4. The SRS at Delft University of Technology was used to replicate the experiment, see Figure 5. Their respective cockpits are visible in Figures 6 and 7. Figures 8 and 9 present the dimensions of the cockpit and location of the control device, the head-down display and the eye reference point (ERP) of both simulators.

Figure 4: The VMS (Ref. 40)

Figure 5: The SRS (Ref. 41)

Figure 6: VMS cockpit (Ref. 42)

Figure 7: SRS cockpit (Ref. 15)

Figure 10 shows a high-level schematic overview of a pilot executing a task in a flight simulator.[43] The pilot receives cues from the task and several simulator systems involved in the simulation: the motion system, the visual system, the control device feedback, proprioceptive feedback and feedback from secondary cues. The following sections discuss the equalization of these systems and their cues across both simulators, according to the division in Figure 10.

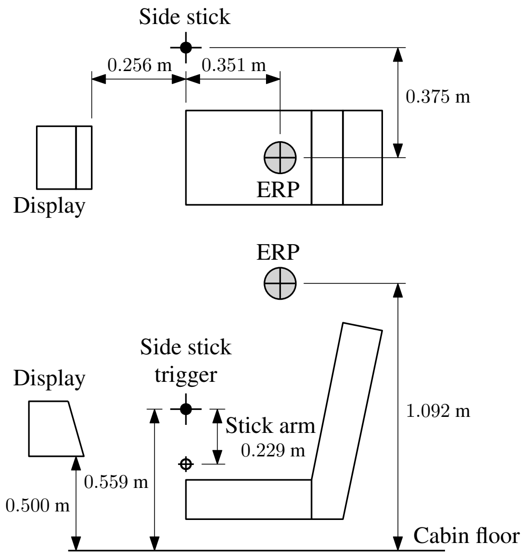

Figure 8: VMS cockpit dimensions, not to scale

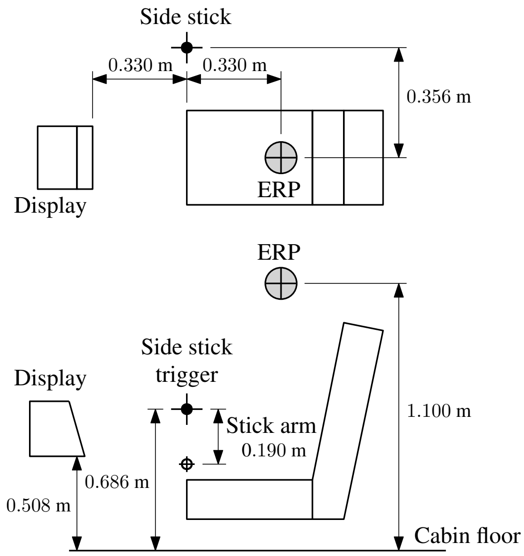

Figure 9: SRS cockpit dimensions, not to scale

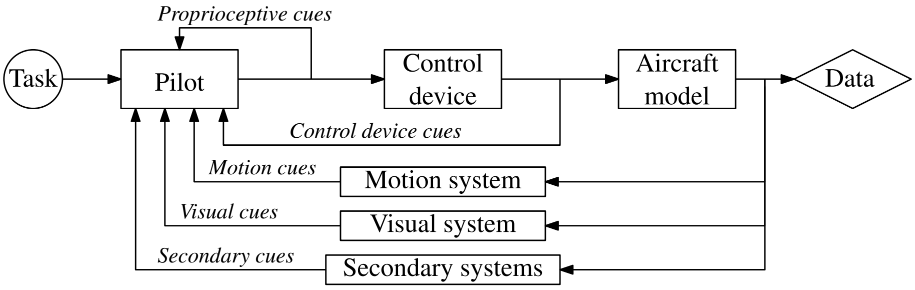

Figure 10: Schematic representation of a pilot executing a task in a flight simulator, as adapted from Ref. 43

III.A. Motion System

The VMS was built to provide the motion fidelity needed to simulate vertical take-off and landing vehicles and hence features a heave range of motion of ± 9.14 m. The cabin can also move ± 6.10 m laterally and ± 1.22 m longitudinally.[40] The vertical and lateral motion is provided by electric motors, while for the longitudinal and rotational motions hydraulic actuators are used. The 6 degrees-of-freedom are uncoupled. On the other hand, the SRS has a hydraulic hexapod motion system with linear actuators that have an operational stroke length of 1.15 m.[12]

Shaping filters were estimated to equalize the motion response between simulators for the pitch and heave axes. The shaping filters had the following form[29] and were placed between the aircraft output and the motion filters on the SRS, see Figure 1:

$$H_{shaping}(s) = H_{SRS}^{-1}(s) \cdot H_{VMS}(s) \tag{15}$$

where $H_{SRS}(s)$ and $H_{VMS}(s)$ represent the unaltered motion frequency responses of the SRS and VMS, respectively. Objective Motion Cueing Test (OMCT)[44] measurements were performed for the full-motion experimental condition C7 on both simulators prior to the experiment to determine the unaltered motion response at twelve discrete OMCT measurement frequencies. Then, transfer functions of the form presented in Eq. (16) were fitted through the twelve OMCT response measurement points using a quadratic cost function,[29] to determine the simulator motion dynamics.

$$H_{SRS,VMS}(s) = \frac{A \cdot s^2}{B \cdot s^2 + C \cdot s + D} \cdot e^{-E \cdot s} \tag{16}$$

The resulting simulator motion dynamics for the relevant degrees of freedom of the VMS and SRS were as follows:

$$H_{VMS_z}(s) = \frac{0.911 \cdot s^2}{0.883 \cdot s^2 + 0.280 \cdot s + 0.036} \cdot e^{-0.098 \cdot s} \tag{17}$$

$$H_{VMS_q}(s) = \frac{0.893 \cdot s^2}{0.916 \cdot s^2 + 0.254 \cdot s + 0.035} \cdot e^{-0.045 \cdot s} \tag{18}$$

$$H_{SRS_z}(s) = \frac{0.908 \cdot s^2}{0.900 \cdot s^2 + 0.256 \cdot s + 0.036} \cdot e^{-0.045 \cdot s} \tag{19}$$

$$H_{SRS_q}(s) = \frac{0.908 \cdot s^2}{0.891 \cdot s^2 + 0.259 \cdot s + 0.035} \cdot e^{-0.026 \cdot s} \tag{20}$$

Because of limitations due to the chosen experimental motion conditions (Section II.E), the standard OMCT test signal amplitudes as specified in Ref. 44 did not fit in the available motion space: some of the lower frequencies exceeded limits in the SRS and some of the higher frequencies exceeded limits in the VMS. This was due to the motion filter gain being $K_{mf} = 1.0$ in all conditions. Hence, using simulations of the motion systems of both simulators, the amplitudes were adapted according to Table 4. Two sets of OMCT tests were performed. Firstly, the full-motion simulator settings (experimental condition C7) were used to construct the shaping filters of Eqs. (17) to (20). Secondly, with the shaping filters present, the motion filter settings of experimental condition C5 were used as verification, as this experimental condition was the furthest away from the full-motion condition C7, in terms of motion filter order: it had a third order filter. Condition C5 had a break frequency of $\omega_{mf} = 0.5$ rad/s, which allowed to construct the motion frequency responses with a sufficiently high test signal-to-noise ratio. Due to its break frequency of $\omega_{mf} = 2.0$ rad/s, C6 could not be used for the verification OMCT data, as too much of the low frequency signals were found to be filtered away with the adapted amplitude settings.

Table 4: OMCT signal amplitudes

	Standard OMCT amplitudes		C7 OMCT amplitudes		C5 OMCT amplitudes	
Frequency	Linear [m/s^2]	Rotational [deg/s^2]	Linear [m/s^2]	Rotational [deg/s^2]	Linear [m/s^2]	Rotational [deg/s^2]
1	1.000	0.060	0.010	0.060	0.500	1.000
2	1.000	0.150	0.010	0.150	0.500	1.000
3	1.000	0.251	0.020	0.251	0.250	0.251
4	1.000	0.398	0.050	0.398	0.250	0.398
5	1.000	0.631	0.050	0.631	0.250	0.631
6	1.000	1.000	0.100	1.000	0.500	1.000
7	1.000	1.585	0.500	1.585	1.000	1.585
8	1.000	2.512	1.000	2.512	1.000	2.512
9	1.000	3.981	1.000	3.500	1.000	3.500
10	1.000	6.310	1.000	6.000	1.000	6.000
11	1.000	10.000	1.000	7.000	1.000	7.000
12	1.000	10.000	1.000	7.000	1.000	7.000

Figure 11 shows the unaltered motion responses of both simulators and the SRS response with the shaping filter included for C7. Figure 12 shows the same for experimental condition C5. In both figures it can be seen that the shaping filter succeeds in matching the SRS to the original unaltered VMS motion response for the heave degree-of-freedom. The pitch degree-of-freedom showed similar results, which are omitted here for the purpose of brevity.

III.B. Control Device

The VMS featured a electro-hydraulic McFadden control side stick,[45] whereas the SRS has an electrical Moog side stick. Both simulators featured an armrest. The armrest in the VMS was covered with a canvas fabric, which allowed the pilots' arm to slide relatively freely over the armrest. The armrest in the SRS was covered with artificial leather, which prevented free movement of the arm to a certain degree. Table 5 presents the parameters of the side stick used in the experiment. In both simulators the side stick settings were set to these values, which were subsequently verified using a force-displacement plot on both simulators and a frequency sweep on the SRS. Figure 13 shows the force-displacement plot. The force-displacement allowed to verify that the gradient, the breakout and the range of motion of the side sticks was the same. Figure 14 shows a frequency sweep that was performed on the SRS. The natural

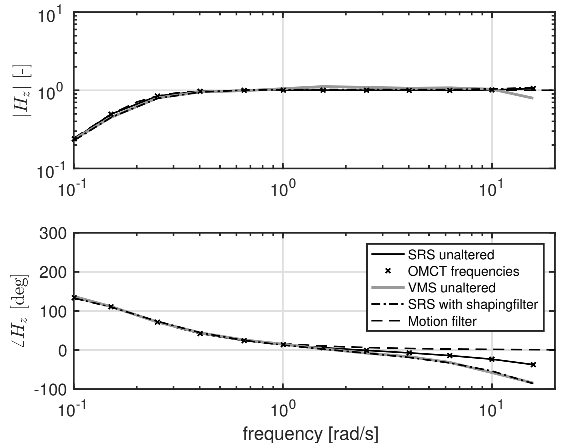

Figure 11: Motion response of the VMS compared to the SRS with and without shaping filter for the full-motion condition C7, that was used to construct the shaping filters

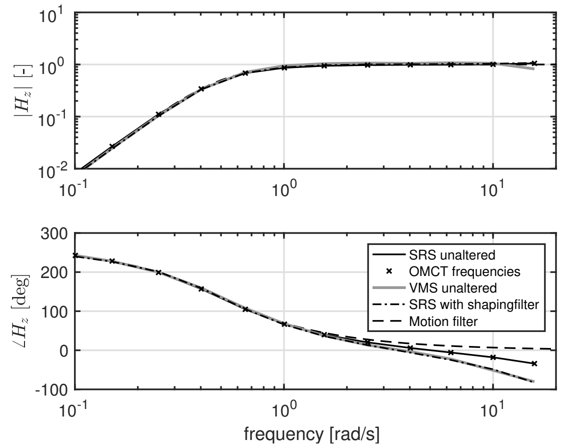

Figure 12: Motion response of the SRS with the shaping filters included and the unaltered response of the VMS for a third order motion filter (experimental condition C5)

frequency of the SRS stick was found by fitting a mass-spring-damper transfer function to the stick dynamics H_{stick} that were determined from the frequency sweep data. The stick dynamics H_{stick} were determined as follows:

$$H_{stick}(s) = \frac{U(s)}{F(s)} \tag{21}$$

where $U(s)$ and $F(s)$ are the Fourier-transformed control signal (i.e. stick position) and stick stick force, respectively. The natural frequency of the VMS side stick was found to be $\omega_n = 11.04$ rad/s by manually adjusting a mechanical damping factor in the side stick hardware and subsequently letting the stick oscillate in its natural frequency after a small perturbation. Figure 14 shows that the mass-spring-damper transfer function that was fitted on the SRS frequency sweep data crosses the -90 degrees phase line at $\omega_n = 11.08$ rad/s. One difference between the two side sticks that could not be adjusted was the length of the stick arm, which was 0.229 m in the VMS and 0.190 m in the SRS, as measured from the turning point to the trigger, as can be seen in Figure 8 and 9. Furthermore, the design of the grip of both sticks was different. The position of the side sticks with respect to the seat differed 0.02 m. No adjustments were made to correct for this offset.

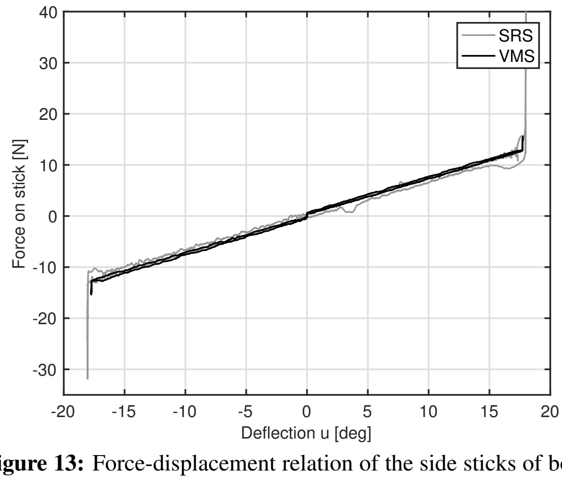

Figure 13: Force-displacement relation of the side sticks of both simulators

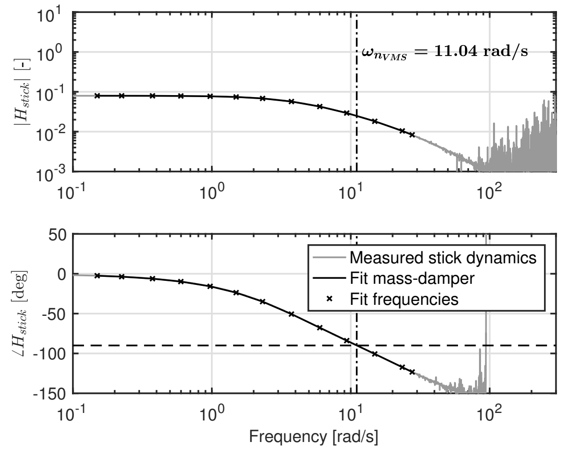

Figure 14: SRS frequency sweep compared to $\omega_{n_{VMS}}$

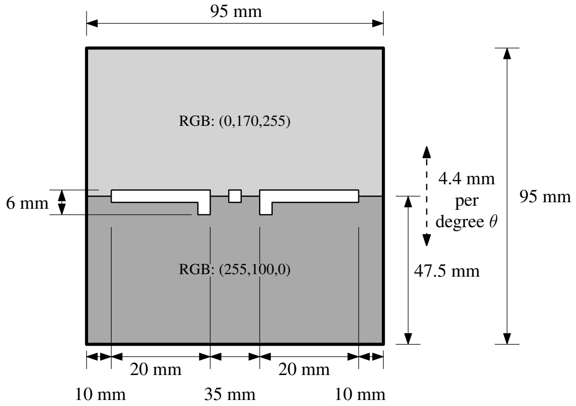

Figure 15: The dimensions of the primary flight display

Table 5: Overview of side stick settings

Parameter	Unit	Set value
Max deflections	deg	$\pm$ 18.0
Force gradient	N/deg	0.6987
Breakout force	N	0.0
Stick damping	Ns/deg	0.1747
Stick inertia	Ns^2/deg	0.0057
Stick natural frequency	rad/s	11.04

III.C. Visual System

In order to eliminate the effects of different out-of-the-window visual systems and in order to simplify the replication of the experiment, only head-down displays were used. The display graphics on the head-down displays were generated from the same C/OpenGL code. The size of the visuals on the screen was measured and adjusted such that the artificial horizon shown on the SRS replicated the one shown in the VMS, in terms of its dimensions and movement during the experiment runs. Figure 15 shows the dimensions of the PFD on the screen.

In a previous simulator comparison, the dynamics of the displays were modelled as pure time delays.[29] The time delay in the visual system of the VMS was measured using the Image Dynamic Measurement System (IDMS)[46] and was found to be 36.3ms. The IDMS is based on detecting a change from black to white on the screen. It uses an instrument with a video input that measures the time it takes between the command being generated and the change to happen on the display. The total time delay of SRS was measured using the Visual Delay Measurement System (VDMS).[47] The VDMS test is based on a sinusoidal input signal on the pitch angle. The image on the head-down display was compared to a reference image, that was provided to a human observer through shutter glasses which sampled at twice the sinusoid frequency. The shutter glasses have a known, constant and small time delay. The observers adjusted the shutter glasses' time delay until the head-down display image and the image through the shutter glasses coincided. This was repeated for three frequencies (2, 4 and 8Hz). Two different observers performed the procedure, resulting in an estimated visual delay of approximately $33-39$ms. Because this fell within the same range of the VMS visual time delay, no adjustments were needed to match both simulators.

Furthermore, the dimensions of the cockpit, the ERP in relation to the head-down display and the position of the chair in relation to the side stick were compared. The only relevant difference was a vertical offset in the position from the ERP to the screen: the SRS ERP was 5 cm higher to the bottom of the screen, compared to the VMS, as can be seen in Figure 8 and 9. No correction for this offset was made.

III.D. Hypotheses

The experiment was repeated on two simulators, with considerable effort to match the cues the pilots perceived from the different simulator systems: the motion response of the simulators was equalized, the side sticks were verified to have equivalent characteristics and the visual system was matched. Furthermore, the task was the same. On top of the three motion filter hypotheses from Section II.F, two hypotheses on the effects of the different simulators were proposed:

H4: **No differences in absolute value of dependent measures** - Because the pilot population was similar in characteristics (type, experience, age) and size, it was hypothesized that both experiments would deliver the same results between simulators, in terms of the dependent variables considered for each experimental condition separately.

H5: **No differences in relative trends between conditions** - Similarly to hypothesis H4, it was hypothesized that the pilot control behavior data collected in both simulators would show the same relative effects between the different tested motion conditions.

IV. Results

Because the experiment featured two sets of hypotheses, two separate statistical analyses were performed. Section IV.A explains the purpose of these two statistical analyses. The following sections present the results of the tracking performance and control activity, the pilot model parameters and the open-loop parameters, respectively.

IV.A. Statistical Analysis

The first statistical test focused on the effects across the two simulators, while the second statistical test focused on the effects of motion filter order O_{mf} and motion filter frequency ω_{mf}.

IV.A.1. Statistical Analysis for Differences Across Simulators

Firstly, a two-way mixed ANOVA was performed to detect statistically significant interactions between the used simulator and motion condition, as well as the main effects of motion condition and simulator for each dependent measure. In this statistical test, a significant interaction implied that the differences between motion conditions were not the same in both simulators and hence different relative trends were present in the data. The main effect of simulator considered each condition individually to see if there was a bias between the results.

The ANOVA assumptions were tested as follows. Firstly, for the ANOVA assumption regarding outliers, the studentized residuals were used to check if data were within $\pm$ 3 standard deviations. Secondly, the Shapiro-Wilk test was used to assess the normality of the data ($p > 0.05$). Thirdly, to assess the assumption of homogeneity of variance Levene's test of equality of error variances ($p > 0.05$) was used. Fourthly, the assumption of similarity of covariance was tested with Box's test of equality of covariance matrices ($p < 0.001$). Fifthly, Mauchly's test of sphericity was used to test the assumption of sphericity ($p > 0.05$).

The ANOVA is considered robust against violations of the assumption of normality[48] and the assumption of homogeneity of variance.[49] However in some of the dependent measures the violations were considered too severe to ignore and a non-parametric equivalent to a two-way mixed ANOVA was used. The Shreirer-Ray-Hare extension of the Kruskall-Wallis (SRH-KW) test[50,51] was used in case the assumption of normality was violated in at least four out of sixteen cases or the assumption of homogeneity of variances was violated in three out of eight cases or more. This non-parametric test assumed an equal number of participants in both simulator groups. If a significant difference between simulators was present, post-hoc Mann-Whitney U tests were performed to detect the conditions from which this difference originated. The purpose was to assess whether a single condition, or set of conditions, repeatedly gave rise to these simulator differences. No post-hoc tests to further investigate significant differences across motion conditions were performed, as this was the focus of the second statistical analysis. Table 6 presents the results of the statistical analysis for the differences across the simulators, including the test that was used.

IV.A.2. Statistical Analysis for Effects of Motion Filter Order O_{mf} and Motion Filter Frequency ω_{mf}

Following the statistical tests for the differences across simulators, a two-way repeated measures ANOVA was performed twice on the experiment data of C1 to C6: once for the VMS data and once for the SRS data. This division was made because the first statistical analysis indicated offsets in the results across the simulators, see Table 6.

In case the assumption of normality was violated in three out of six conditions or more for either the VMS or the SRS data, the SRH-KW test was used for both simulators. The interaction term $O_{mf} \times \omega_{mf}$ indicated whether the value of either O_{mf} or ω_{mf} influenced the effect of the other. Table 7 presents the results of the second statistical analysis.

In the following section, the dependent variables are presented on either boxplots or 95% confidence interval plots, depending on statistical test that was performed. In all plots, both the means and medians are indicated, as circles and horizontal dashes, respectively. The means of medians of condition C7 were used as baseline for the prediction equations. Where no mention is made of the ANOVA assumptions in the following section, all assumptions were met.

IV.B. Performance and Control Activity

Figure 16 shows pilot tracking performance in terms of RMS_e. Both simulators showed similar differences in tracking performance over the different motion conditions, which is supported by an insignificant interaction term, as can be seen in Table 6. Best tracking performance was seen in the full-motion C7. As expected, a significant increase was observed in RMS_e with increasing motion filter order O_{mf} of around 8% and 5% on average per motion filter order for the VMS and SRS, respectively. Furthermore, with increasing ω_{mf}, RMS_e increased significantly by 8% and 6% on average for the VMS and SRS, respectively, as can be seen in Table 7. Both in the VMS and SRS data, the $\omega_{mf} = 2.0$ rad/s conditions showed a four times larger decrease in performance with increasing motion filter order than the $\omega_{mf} = 0.5$ rad/s conditions, as also indicated by the significant interaction between motion filter order and ω_{mf}, see Table 7. There were significant differences between the simulators, as can be seen in Table 6. Post-hoc Mann Whitney U tests indicated that only in condition C4 and C7 the difference between simulators was statistically significant.

Figure 17 shows the pilot control activity in terms of RMS_u. The data showed violations of the assumption of normality in seven conditions, as well as six violations of the assumption equality of variances. In both the VMS and SRS the same relative difference between motion conditions could be seen: the interaction of simulator and motion condition was not significant, as can be seen in Table 6. In the no-motion condition C0 the median of the data was lowest, for both simulators. In the full-motion condition C7, the median was highest, indicating that pilots controlled more actively in this condition. However, according to the non-parametric statistical test, the main effect of motion condition was not significant, see Table 6. This was supported by the second statistical analysis: no significant effect of filter order O_{mf} or filter frequency ω_{mf} on the control activity was detected for the VMS or the SRS, see Table 7 There were significant differences between the two simulators. The VMS data showed a significantly larger range of RMS_u, as indicated by the taller boxplots in Figure 17: the data of the VMS contained four pilots that controlled with larger control inputs. Post-hoc Mann-Whitney U tests indicated that for all conditions a significant difference in RMS_u between the two simulators was present, which supported this finding.

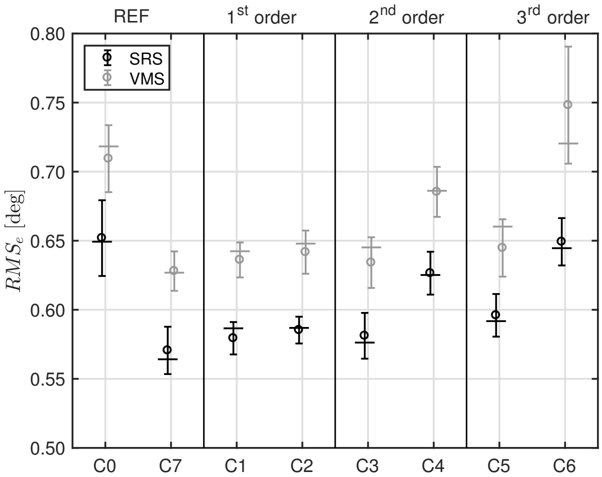

Figure 16: Pilot tracking performance

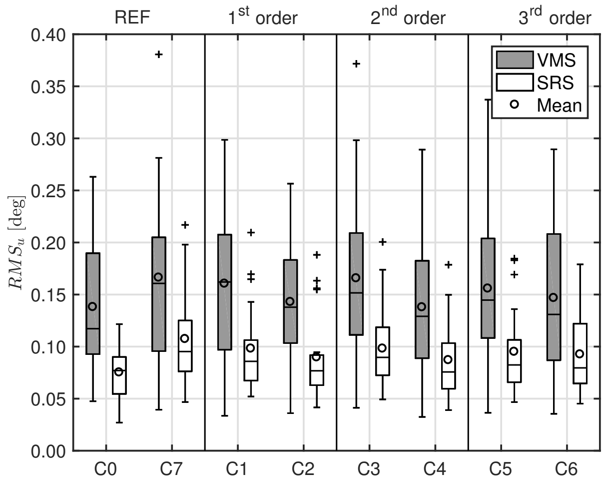

Figure 17: Pilot control activity

IV.C. Pilot Model Parameters

For each estimated pilot model, the VAF was calculated to assess the quality of the estimation. A VAF of 100% signifies that the corresponding pilot model was able to perfectly explain all the variance in the pilot control signal u. Figure 18 shows the VAF. It can be seen that values range from 70% to 92%. In previous experiments similar VAF values were found.[34,52]

Figure 19 shows the variance of the output signal of the motion pilot model $\sigma^2_{u_m}$ over the variance of the output signal of the visual pilot model $\sigma^2_{u_v}$ as a measure of how much motion was used by the pilots. A higher variance fraction signifies more motion used. A variance fraction of 100% indicates that the variance of the motion and visual signals are equal. The values ranged from 100.4% in C7 to 0% in motion condition C6. For the no-motion condition C0 no data was available, because the motion channel of the pilot model was not estimated for C0 (see Section II.E). Both the VMS and SRS data violated the ANOVA assumption of normality for three motion conditions. Both simulators showed similar trends in the data, as illustrated by an insignificant interaction between simulator and motion condition, see Table 6. A significant decrease in motion channel usage with increasing filter frequency ω_{mf} was found, see Table 7. For the VMS the average decrease was 65% and for the SRS the average decrease was 70%, for the change from $\omega_{mf} = 0.5$ rad/s to $\omega_{mf} = 2.0$ rad/s, over the three filter orders. Furthermore, the data showed a decrease in $\sigma^2_{u_m}/\sigma^2_{u_v}$ with increasing motion filter order O_{mf} for the $\omega_{mf} = 2.0$ rad/s conditions, which averaged at 31% for the VMS and 41% for the SRS per filter order. For the $\omega_{mf} = 0.5$ rad/s conditions no change was seen with increasing

O_{mf}. Although this was visible in the data, no significant main effect of motion filter order O_{mf} was found in either simulator, see Table 7. Furthermore, the interaction between ω_{mf} and filter order O_{mf} was insignificant, see Table 7. There were significant differences between the VMS and SRS within single conditions, as indicated by the significant main effect of simulator, see Table 6. Post-hoc Mann-Whitney U tests indicated that for conditions C4 and C6 the data was significantly different. In Figure 19 these two conditions are the only ones where the median of the SRS data falls below the first quartile of the VMS data.

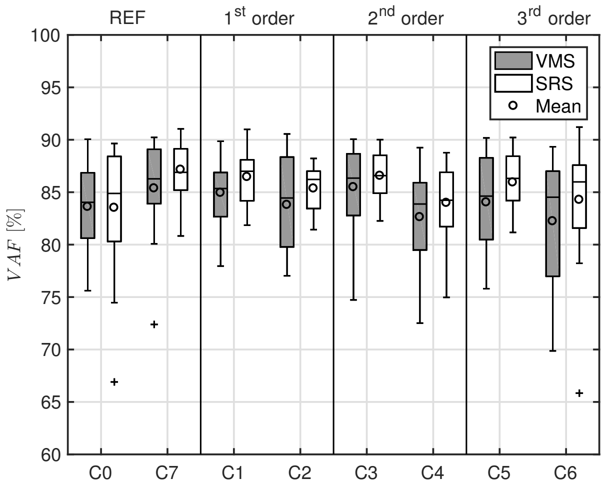

Figure 18: Pilot model variance accounted for

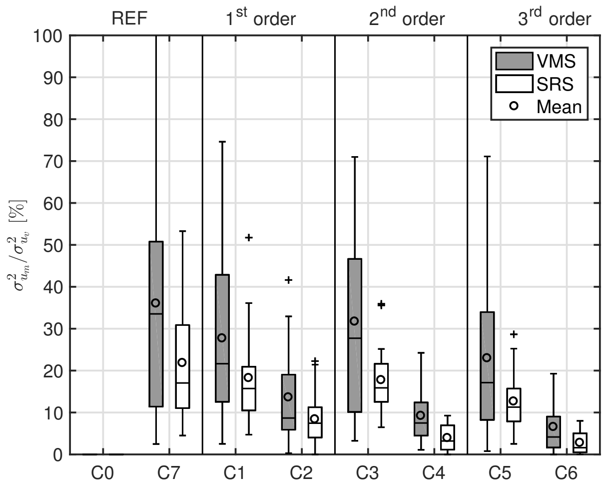

Figure 19: Variance of visual over motion control signal

Figure 20 shows the pilot model visual gain K_v. A higher K_v indicates that pilots responded with larger inputs to visual cues. The data severely violated the assumption of normality, as well as the assumption of equality of error variances, in 12 and 5 cases in total, respectively. No significant interaction between simulator and motion filter condition was found: both simulators showed similar relative differences between conditions, see Table 6. No significant main effect of motion filter order O_{mf} was found, see Table 7. The interaction between O_{mf} and ω_{mf} was not found to be significant for both simulators either. However, for both simulators a significant decrease in median K_v with increasing ω_{mf} was found, of 19% and 13% average, for the VMS and SRS, respectively, over the three filter orders. There were significant differences between the VMS and SRS, as indicated by a significant main effect of simulator, see Table 6. Two VMS pilots had notably higher visual gains. Both these pilots also belonged to the group of four VMS pilots with notably higher RMS_u and in C1 and C4 their effect was significant, as assessed with post-hoc Mann Whitney U tests. In the no-motion condition C0, the two simulators showed similar medians ($K_{v_{VMS}} = 0.0437$ and $K_{v_{SRS}} = 0.0431$), indicating that with no motion present, pilots controlled with similar gains in both the VMS and SRS. In both simulators, the prediction equations from Ref. 13 supported the results, with correlation coefficients of $\rho = 0.83$ and $\rho = 0.91$ for the VMS and SRS, respectively. The equations predicted the trends in the SRS results of K_v well. The largest difference between the experimental results and predicted K_v was 8.9%. The VMS data showed higher medians than predicted for most conditions, apart from C0 and C6 where the median K_v of the experiment data was found below the predicted value $\hat{K}_v$.

Figure 21 shows the pilot model motion gain K_m. A higher K_m indicates that pilots responded with larger inputs to motion cues. The assumption of equality of error variances was violated in all but two conditions. Like the visual pilot model gain K_v, the motion gain K_m displayed similar relative trends over the motion conditions for both simulators: the interaction between simulator and motion condition was insignificant, see Table 6. However, the main effect of simulator was significant. Post-hoc Mann-Whitney U tests indicated a difference in distribution for C4. The VMS data of K_m did not reveal any significant change with increasing filter order O_{mf}, see Table 7. However, the SRS data did show an average 20% significant decrease in K_m with increasing filter order O_{mf} in the $\omega_{mf} = 2.0$ rad/s conditions. A significant interaction between O_{mf} and ω_{mf} was observed in the SRS data, where K_m in the $\omega_{mf} = 2.0$ rad/s conditions decreased almost 3 times more over the three filter orders than in the $\omega_{mf} = 0.5$ rad/s conditions, in contrast to the VMS data where no significant interaction was found. Both the VMS and SRS data showed a significant decrease in K_m with increasing ω_{mf}, meaning that pilots responded less to motion information in the $\omega_{mf} = 2.0$ rad/s conditions.

Figure 22 shows the pilot model visual lead time constant T_L. A higher lead time constant indicates that pilots use more visual cues to generate lead to control the aircraft. The only violation of the ANOVA assumptions was due to outliers: the data showed four outliers in one VMS pilot and one outlier in an SRS pilot. An ANOVA was performed with and without the outliers, which produced the same results. Therefore, the outliers were left in the dataset. The data of both simulators showed similar trends, with little differences between the simulators: no significant interaction between simulator and motion condition was observed, see Table 6. A significant increase in visual lead time T_L with increasing O_{mf} was found in both simulators, see Table 7. Like RMS_e and K_m, this effect was mostly visible in the $\omega_{mf} = 2.0$ rad/s conditions, which increased by 23% and 12% on average for the three filter orders, for the VMS and SRS, respectively. Furthermore, both simulators also showed a significant increase in T_L with increasing ω_{mf}, of 35% and 20% on average. The VMS data did not show a significant interaction between O_{mf} and ω_{mf}, whereas the SRS data did, see Table 7. No significant differences between the two flight simulators were found, as indicated by an insignificant main effect of simulator, see Table 6. The prediction equations supported the results, correctly indicating the trends of increasing T_L for increasing ω_{mf} and O_{mf} for both the VMS and SRS, with correlation coefficients of $\rho = 0.86$ and $\rho = 0.95$, respectively. In both C0 and C6 the prediction equations estimated $\hat{T}_L$ to be lower than the experimental results, mirroring what was seen for the prediction equations of $\hat{K}_v$. In the no-motion condition C0 the means of the data of both simulators were found at the inverse of the short period frequency of the controlled dynamics: $1/\omega_{sp} = 1/0.6892$ rad/s $= 1.4509$ s, with little difference between them.

The three equalization parameters together showed that mainly for the higher filter frequency $\omega_{mf} = 2.0$ rad/s (conditions C2, C4 and C6) the pilots controlled with smaller gains and used more visual information to generate lead for larger filter orders O_{mf}, even though the statistical analysis did not support this completely, see Table 6 and Table 7. The following four parameters are the limitation parameters. The limitation parameters showed that pilots' frequency response was more damped and more of the frequency response was attenuated by the neuromuscular system for higher O_{mf}, once again mainly in the $\omega_{mf} = 2.0$ rad/s conditions.

Figure 23 shows the pilot model visual time delay τ_v. The ANOVA showed no significant interaction between simulator and motion condition, see Table 6. A significant difference between simulators for conditions C3, C5, C6 and C7 was present, as indicated by post-hoc Mann-Whitney U tests. However, the data of both simulators did not show significant main effects of motion condition, see Table 6. This was supported by the second statistical analysis. The data did not reveal any significant effect of O_{mf} or ω_{mf} for neither of the two simulators, see Table 7. Furthermore, no significant interaction between O_{mf} and ω_{mf} was found. However, the prediction equations did estimate there would be effects visible, see Figure 23. The predictions correlated to the VMS and SRS data with $\rho = -0.03$ and $\rho = -0.79$, respectively. Hence, the predictions of $\hat{\tau}_v$ were not supported by the results of the current experiment.

Figure 24 shows the pilot model motion time delay τ_m. Like the visual time delay τ_v, the motion time delay τ_m remained relatively constant over the different motion conditions. Compared to previous studies,[34] the values found in C4 and C6 were disproportionately high, which indicated that in these conditions τ_m could not be estimated accurately. In Ref. 53, a similar situation was encountered. The motion time delay showed little to no difference over the other conditions or between simulators. The SRS data violated the assumption of normality in all conditions and the VMS violated this assumption in 2 conditions. The non-parametric statistical test confirmed the findings: no significant effects were found, see Table 6. The second statistical test was not performed.

Figure 25 shows the neuromuscular damping constant ζ_{nm}. A smaller ζ_{nm} indicates that the pilot model frequency response is less damped. In both simulators similar trends were present, see Table 6. A significant increase in ζ_{nm} for increasing filter order O_{mf} was found, see Table 7. This average increase of 11% and 5% in the VMS and SRS, respectively, was visible only in the $\omega_{mf} = 2.0$ rad/s conditions. The $\omega_{mf} = 0.5$ rad/s conditions did not show an increase. Hence, for both simulators there was a significant interaction between O_{mf} and ω_{mf}, see Table 7. Furthermore, both simulators showed a significant increase in ζ_{nm} with increasing ω_{mf}, see Table 7: in the VMS ζ_{nm} increased by 17% and in the SRS by 15% on average. The difference of 0.12 in ζ_{nm} in the no-motion C0 indicated that the motion was not the source of the differences across simulators, but the other systems of which the pilots received cues, such as the side stick or the visuals. Finally, the main effect of simulator was significant, indicating that differences between the simulators were present, see Table 6. Post-hoc Mann-Whitney U tests subsequently indicated that for all conditions, except C5 and C6, there were differences between the simulators.

Figure 26 shows the neuromuscular frequency ω_{nm}. A smaller ω_{nm} indicates that the pilot model neuromuscular system attenuated a smaller bandwidth of the frequency response. The data of the VMS and SRS showed the same trends: no significant interaction was found between simulator and motion condition and there were also no significant differences between the two simulators, see Table 6. The data did not show any significant effect of ω_{mf} or O_{mf} in the SRS data, see Table 7. However, the VMS data did show a significant increase in ω_{nm} with increasing ω_{mf}. No significant interactions between O_{mf} and ω_{mf} were found. The prediction equations predicted opposite trends than the data showed: they correlated to the VMS and SRS data with $\rho = -0.79$ and $\rho = -0.71$, respectively. Hence, the prediction equation of $\hat{\omega}_{nm}$ was not supported by the results of the current experiment.

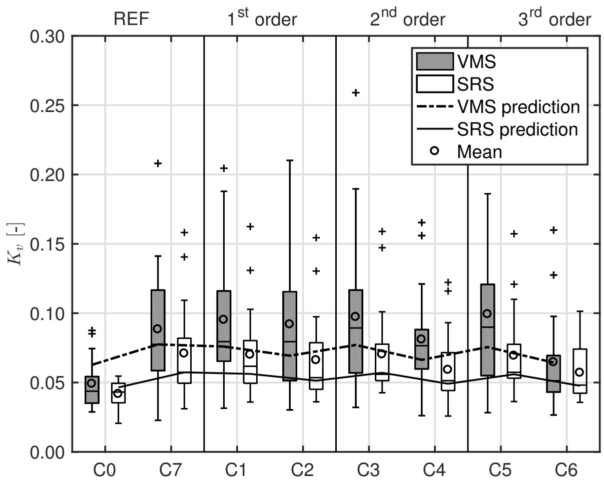

Figure 20: Pilot model visual gain K_v

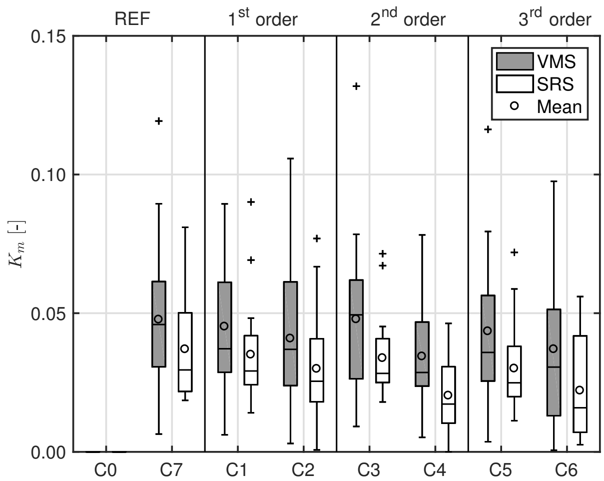

Figure 21: Pilot model motion gain K_m

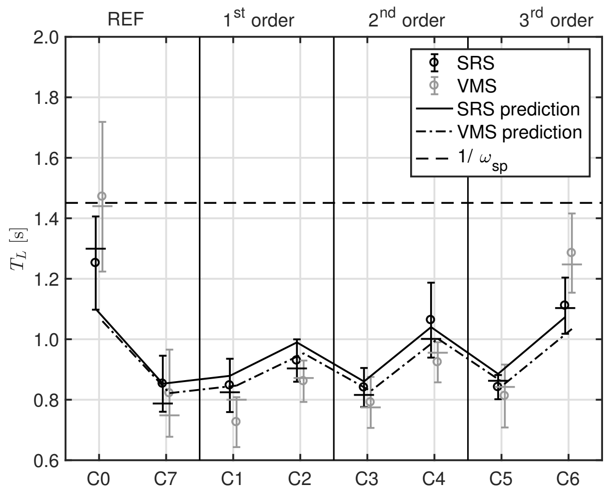

Figure 22: Pilot model lead time constant T_L

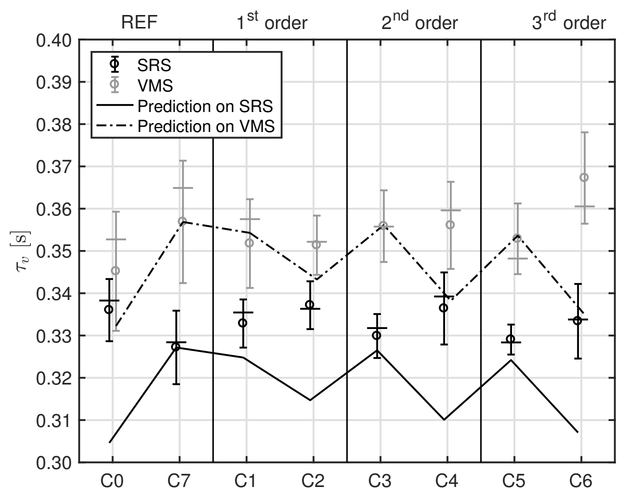

Figure 23: Pilot model visual time delay τ_v

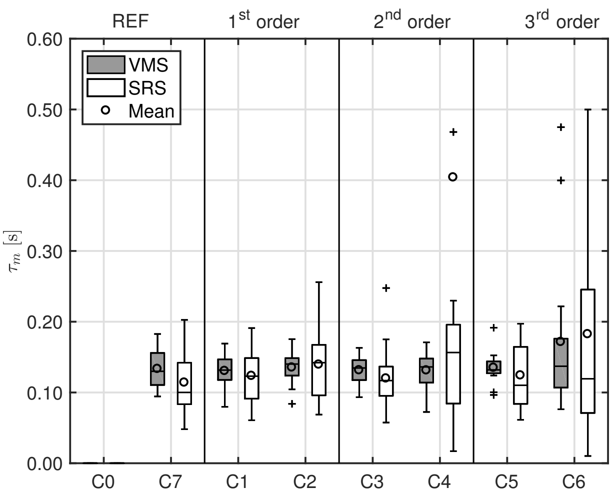

Figure 24: Pilot model motion time delay τ_m

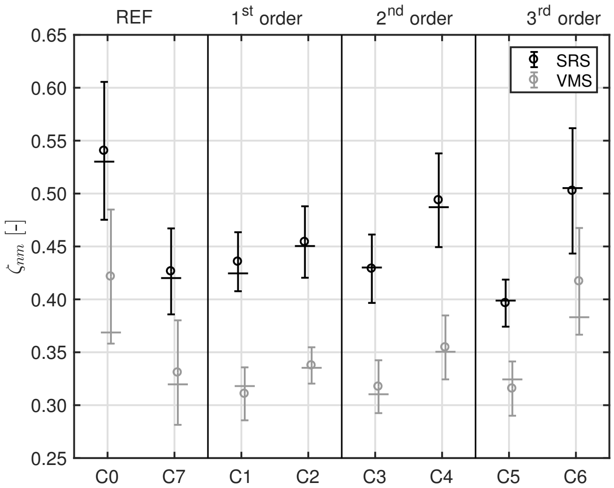

Figure 25: Pilot model neuromuscular damping ζ_{nm}

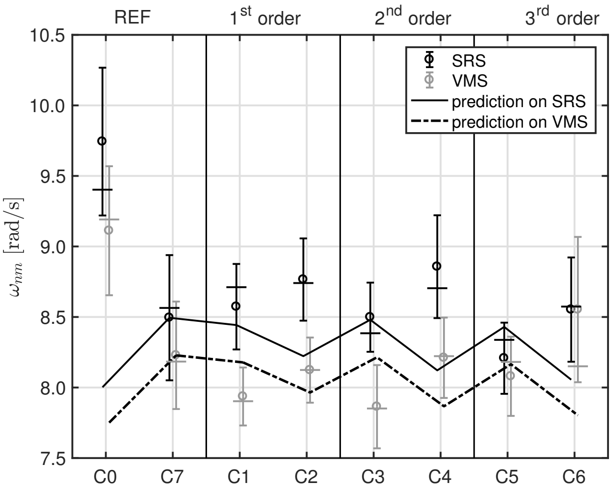

Figure 26: Pilot model neuromuscular frequency ω_{nm}

IV.D. Open-loop Dynamics

The closed-loop tracking task that was performed in this experiment was a combined target-following and disturbance-rejection task. Performance depended on attenuating errors caused by both the target and disturbance forcing functions.[54] Overall, as can be seen in Figures 27 to 30, the values of the open-loop parameters found in this experiment were similar to previous research, Ref. 34 for example.

Figure 27 shows the open-loop target crossover frequency $\omega_{c,t}$. The SRS data violated the assumptions of normality in three conditions. The same trends were observed in both simulators: no significant interaction was found between the effects of simulator and motion condition, see Table 6. Also no significant difference between simulators was present, see Table 6. In both simulators, no significant change in $\omega_{c,t}$ with increasing O_{mf} was found, see Table 7. Furthermore, no significant interaction between O_{mf} and ω_{mf} was found. However, both simulators showed an average significant increase of 19% in $\omega_{c,t}$ from the $\omega_{mf} = 0.5$ rad/s conditions to the $\omega_{mf} = 2.0$ rad/s conditions.

Figure 28 shows the open-loop disturbance crossover frequency $\omega_{c,d}$. The data of $\omega_{c,d}$ violated the assumption of normality in 5 cases in total. The SRH-KW test indicated a significant interaction between simulator and motion condition on $\omega_{c,d}$, as can be seen in Table 6. The data of the two simulators showed the same trends, except for the difference between C5 and C6, see Figure 28. The medians of $\omega_{c,d}$ of the SRS data decreased 7.0% more from C5 to C6 (third order conditions), as compared to the VMS data. With these two conditions excluded, the SRH-KW test did not return a significant interaction effect. Because the second largest difference in trends was a 5.8% larger increase in $\omega_{c,d}$ from C0 to C7 in the VMS data, the significant interaction between simulator and motion condition was not considered relevant for the results. No significant main effect of O_{mf} was found, see Table 7. Both simulators did show a significant average decrease of 15.6% and 11.5%, for the VMS and SRS, respectively, with the increase from $\omega_{mf} = 0.5$ rad/s to $\omega_{mf} = 2.0$ rad/s. Furthermore, the main effect of simulator was significant, indicating that there were differences between the simulators, see Table 6. A post-hoc Mann-Whitney U test indicated that this difference originated from C0, similar to what was seen in the data of ζ_{nm} and ω_{nm}. The prediction equations from Ref. 13 supported the experimental results, showing similar trends for both simulators, with strong correlations of $\rho = 0.94$ for both simulators.

Figure 29 shows the open-loop target crossover phase margin $\varphi_{m,t}$. Both simulators showed similar trends in the data: no significant interaction between simulator and motion condition on $\varphi_{m,t}$ was found, see Table 6. In both simulators the data showed a significant decrease with increasing O_{mf}: over the three filter orders $\varphi_{m,t}$ decreased on average 6.1% and 6.9% for the VMS and SRS, respectively. Furthermore, with increasing ω_{mf}, the $\varphi_{m,t}$ decreased significantly as well in both simulators: on average 26% in the VMS and 23% in the SRS for the change from $\omega_{mf} = 0.5$ rad/s to $\omega_{mf} = 2.0$ rad/s. The interaction between O_{mf} and ω_{mf} was only significant in the SRS, however, see Table 7. The main effect of simulator was significant, see Table 6, and post-hoc tests pointed to C4 being the source of the simulator differences.

Figure 30 shows the open-loop disturbance crossover phase margin $\varphi_{m,d}$. No significant interaction between simulator and motion filter was found, see Table 6, which indicated that the similar trends were present in the data. The disturbance crossover phase margin $\varphi_{m,d}$ showed a significant decrease for increasing O_{mf}, see Table 7. This effect was mainly visible in the $\omega_{mf} = 2.0$ rad/s conditions, with a decrease of around 10% per motion filter order for both simulators. In the $\omega_{mf} = 0.5$ rad/s conditions $\varphi_{m,d}$ remained constant. Hence, for both simulators the interaction between O_{mf} and ω_{mf} was significant, see Table 7. Both simulators also showed a significant decrease in $\varphi_{m,d}$ for increasing ω_{mf}, of around 15% and 10%, for the VMS and SRS respectively. This result was opposed by the prediction equations, which predicted a slight increase in $\varphi_{m,d}$ for increasing ω_{mf}. The correlation coefficients confirmed this finding: for the VMS $\rho = -0.77$ and for the SRS $\rho = -0.84$. The prediction equations did not support the results of this experiment. Finally, a significant difference between simulators was found, see Table 6. Post-hoc Mann-Whitney U tests indicated that these differences could be found in C1, C3 and C5.

The combination of open-loop parameters indicated a decrease in motion channel use for both increasing ω_{mf} and increasing O_{mf} in the open-loop response. Most notably, the decreasing $\omega_{c,d}$ and decreasing $\varphi_{m,t}$ reflected this, as well as the increasing $\omega_{c,t}$.

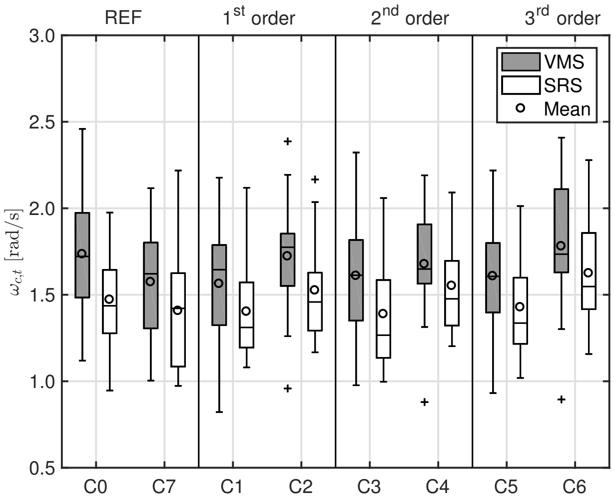

Figure 27: Open-loop target crossover frequency $\omega_{c,t}$

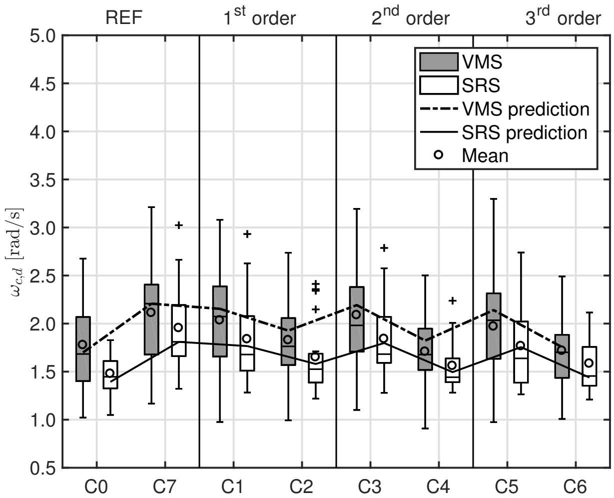

Figure 28: Open-loop disturbance crossover frequency $\omega_{c,d}$

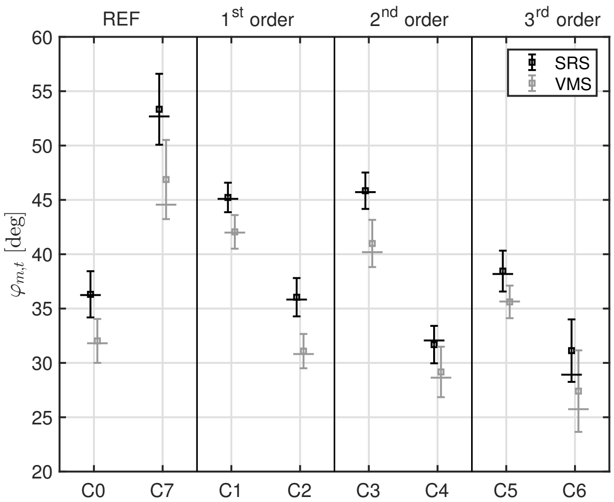

Figure 29: Open-loop target phase margin $\varphi_{m,t}$

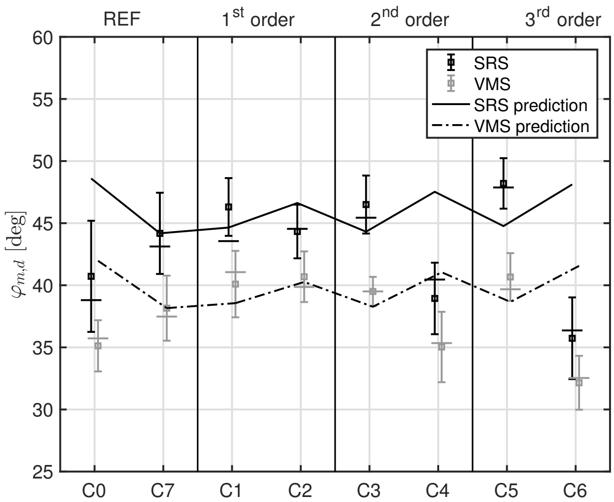

Figure 30: Open-loop disturbance phase margin $\varphi_{m,d}$

Table 6: Summary of statistical analysis for simulator differences

		Simulator			Motion condition			Simulator × Motion condition		
	Test	*df*	*F*	*p*	*df*	*F*	*p*	*df*	*F*	*p*
RMS_e	ANOVA	1.0, 32.0	0.184	0.031	3.2, 102.6^{gg}	26.657	<0.001	3.2, 102.6^{gg}	0.957	0.420
RMS_u	SRH-KW	1.0, 256.0	55.006	<0.001	7.0, 256.0	4.602	0.121	7.0, 256.0	0.719	0.081
$\sigma^2_{u_m}/\sigma^2_{u_v}$	SRH-KW	1.0, 256.0	12.339	<0.001	7.0, 256.0	92.062	<0.001	7.0, 256.0	1.417	0.062
K_v	SRH-KW	1.0, 256.0	19.371	<0.001	7.0, 256.0	41.357	<0.001	7.0, 256.0	1.915	0.052
K_m	SRH-KW	1.0, 237.0	21.187	<0.001	6.0, 237.0	18.051	0.002	6.0, 237.0	1.278	0.054
T_L	ANOVA	1.0, 32.0	0.006	0.938	2.7, 91.4^{gg}	26.624	<0.001	2.7, 91.4^{gg}	2.632	0.061
τ_v	ANOVA	1.0, 32.0	6.76	0.014	4.5,143.6^{gg}	0.975	0.429	4.5, 143.6^{gg}	1.491	0.202
τ_m	SRH-KW	1.0, 237.0	1.537	0.149	6.0, 237.0	6.600	0.100	6.0, 237.0	3.998	0.135
ζ_{nm}	ANOVA	1.0, 32.0	6.34	0.017	3.5, 118.8^{gg}	8.591	<0.001	3.5, 118.8^{gg}	0.507	0.706
ω_{nm}	ANOVA	1.0, 32.0	0.773	0.386	4.1,131.5^{gg}	9.591	<0.001	4.1,131.5^{gg}	1.017	0.347
$\omega_{c,t}$	ANOVA	1.0, 32.0	4.143	0.051	3.9, 124.8^{gg}	21.239	<0.001	3.9, 124.8^{gg}	1.114	0.352
$\omega_{c,d}$	SRH-KW	1.0, 256.0	21.992	<0.001	7.0, 256.0	28.428	<0.001	7.0, 256.0	0.767	0.009
$\varphi_{m,t}$	ANOVA	1.0, 32.0	1139.7	0.034	3.4, 108.9^{gg}	77.521	<0.001	3.4, 108.9^{gg}	0.794	0.514
$\varphi_{m,d}$	ANOVA	1.0, 32.0	1809.8	0.02	4.3, 138.3^{gg}	14.04	<0.001	4.3, 138.3^{gg}	0.702	0.602

gg = Greenhouse-Geisser correction
= significant ($p < 0.050$)
= not significant ($p \geq 0.050$)

Table 7: Summary of statistical analysis for motion filter effects

		O_{mf}			ω_{mf}			$O_{mf} \times \omega_{mf}$		
VMS										
	Test	*df*	*F*	*p*	*df*	*F*	*p*	*df*	*F*	*p*
RMS_e	ANOVA	1.5, 23.8^{gg}	21.866	<0.001	1.0, 16.0	18.302	<0.001	1.5, 23.8^{gg}	7.045	0.007
RMS_u	SRH-KW	2.0, 96.0	0.066	0.484	1.0, 96.0	1.317	0.180	2.0, 96.0	0.243	0.443
$\sigma^2_{u_m}/\sigma^2_{u_v}$	SRH-KW	2.0, 96.0	3.691	0.079	1.0, 96.0	23.903	<0.001	2.0, 96.0	0.529	0.384
K_v	SRH-KW	2.0, 96.0	2.416	0.149	1.0, 96.0	3.651	0.034	2.0, 96.0	1.984	0.185
K_m	ANOVA	2.0, 32.0	0.781	0.467	1.0, 16.0	11.862	0.003	2.0, 32.0	1.505	0.237
T_L	ANOVA	2.0, 32.0	34.842	<0.001	1.0, 16.0	34.186	<0.001	2.0, 32.0	6.740	0.444
τ_v	ANOVA	2.0, 32.0	1.778	0.185	1.0, 16.0	1.438	0.248	2.0, 32.0	1.670	0.204
τ_m	SRH-KW	2.0, 96.0	0.327	0.425	1.0, 96.0	0.400	0.516	2.0, 96.0	0.207	0.451
ζ_{nm}	ANOVA	1.4, 21.7^{gg}	5.915	0.015	1.0, 16.0	14.814	0.001	1.4,21.7^{gg}	3.998	0.047
ω_{nm}	ANOVA	2.0, 32.0	2.233	0.124	1.0, 16.0	7.136	0.017	2.0, 32.0	0.379	0.688
$\omega_{c,t}$	SRH-KW	2.0, 96.0	0.263	0.438	1.0, 96.0	4.544	0.019	2.0, 96.0	0.279	0.435
$\omega_{c,d}$	SRH-KW	2.0, 96.0	0.750	0.344	1.0, 96.0	8.1097	0.002	2.0, 96.0	0.743	0.345
$\varphi_{m,t}$	ANOVA	2.0, 32.0	15.62	<0.001	1.0, 16.0	55.507	<0.001	2.0, 32.0	2.181	0.129
$\varphi_{m,d}$	ANOVA	2.0, 32.0	9.737	<0.001	1.0, 16.0	12.923	0.002	2.0, 32.0	8.324	0.001
SRS										
		O_{mf}			ω_{mf}			$O_{mf} \times \omega_{mf}$		
	Test	*df*	*F*	*p*	*df*	*F*	*p*	*df*	*F*	*p*
RMS_e	ANOVA	2.0, 32.0	22.592	<0.001	1.0, 16.0	17.972	<0.001	2.0, 32.0	7.346	0.002
RMS_u	SRH-KW	2.0, 96.0	$6.05 \cdot 10^{-04}$	0.500	1.0, 96.0	1.069	0.2261	2.0, 96.0	0.578	0.375
$\sigma^2_{u_m}/\sigma^2_{u_v}$	SRH-KW	2.0, 96.0	6.095	0.024	1.0, 96.0	46.283	<0.001	2.0, 96.0	2.297	0.159
K_v	SRH-KW	2.0, 96.0	0.902	0.319	1.0, 96.0	4.952	0.015	2.0, 96.0	0.703	0.352
K_m	ANOVA	2.0, 32.0	7.44	0.002	1.0, 16.0	27.328	<0.001	2.0, 32.0	6.305	0.005
T_L	ANOVA	2.0, 32.0	4.164	0.045	1.0, 16.0	13.208	0.002	2.0, 32.0	4.328	0.027
τ_v	ANOVA	2.0, 32.0	0.717	0.496	1.0, 16.0	2.249	0.153	2.0, 32.0	0.052	0.949
τ_m	SRH-KW	2.0, 96.0	0.043	0.489	1.0, 96.0	2.442	0.075	2.0, 96.0	0.012	0.497
ζ_{nm}	ANOVA	2.0, 32.0	0.392	0.618	1.0, 16.0	15.193	<0.001	2.0, 32.0	2.924	0.070
ω_{nm}	ANOVA	2.0, 32.0	2.281	0.119	1.0, 16.0	3.266	0.09	2.0, 32.0	0.254	0.777
$\omega_{c,t}$	SRH-KW	2.0, 96.0	0.975	0.307	1.0, 96.0	9.334	0.001	2.0, 96.0	0.253	0.441
$\omega_{c,d}$	SRH-KW	2.0, 96.0	0.329	0.424	1.0, 96.0	6.726	0.005	2.0, 96.0	0.532	0.383
$\varphi_{m,t}$	ANOVA	2.0, 32.0	23.524	<0.001	1.0, 16.0	91.859	<0.001	2.0, 32.0	5.366	0.010
$\varphi_{m,d}$	ANOVA	2.0, 32.0	5.145	0.025	1.0, 16.0	23.458	<0.001	2.0, 32.0	8.519	0.001

gg = Greenhouse-Geisser correction
= significant ($p < 0.050$)
= not significant ($p \geq 0.050$)

V. Discussion

This paper presents the results of a human-in-the-loop tracking experiment that was performed to evaluate the effects of varying motion filter order O_{mf} and motion filter break frequency ω_{mf} on pilot tracking performance and behavior. Whereas the effects of parameters of the motion filter on pilot control behavior and performance have been previously researched,[13,14] the filter order O_{mf} has not been subject of the same attention. By making use of a multimodal pilot model that was fitted on time traces that were recorded in a combined target-following and disturbance-rejection task with eight different motion conditions, changes in pilot control behavior were investigated. The motion filter order O_{mf} and motion filter break frequency ω_{mf} were varied between motion conditions. To compare the results and investigate the effects of a different flight simulator, the experiment was performed in two full-motion research flight simulators, the VMS and the SRS, respectively.

V.A. Discussion of Hypotheses

It was hypothesized that with increasing filter order O_{mf}, pilots would display lower performance and less use of motion feedback in their control strategy (Hypothesis H1). Looking at RMS_e, an increase with increasing O_{mf} indicated that performance decreased. Furthermore, with increasing O_{mf}, a significant increase in T_L suggested that pilots relied more on visual cues to generate lead to control the aircraft. Both these effects were predominantly present in the higher motion filter break frequency setting $\omega_{mf} = 2.0$ rad/s. The data from the SRS experiment showed a 20% significant decrease in K_m with increasing O_{mf}, which indicated that pilots responded less to the motion signal. This effect was also visible in the data of the VMS, even with relative differences between conditions of the same magnitude. However, a larger spread between participants in the VMS data was observed and the decrease of K_m with increasing motion filter order was not found to be significant. Finally, even though in both simulators the crossover frequencies $\omega_{c,t}$ and $\omega_{c,d}$ showed an increase and decrease with increasing O_{mf}, respectively, these effects were not found to be significant. The corresponding phase margins, however, did show significant decreases of 10% per filter order, indicating the pilots controlled less stably for increasing motion filter order. Even though the fraction of control signal variances $\sigma^2_{u_m}/\sigma^2_{u_v}$ did not return any significant differences, the data did show a slight decrease for increasing motion filter order. Overall, hypothesis H1 could be accepted: pilots showed lower performance and less use of motion feedback for increasing motion filter order. This result is in line with the fidelity criteria proposed by Ref. 39 and 25 and previous experiments where motion conditions of differing fidelity were tested, Ref. 15 for example. The experimental conditions with $\omega_{mf} = 2.0$ rad/s showed larger decreases in motion fidelity using the criteria by Sinacori[39] and Schroeder[25] for increasing O_{mf}, which explained the significant interactions between O_{mf} and ω_{mf}. The motion filters themselves caused 90 degrees of phase lead for every increasing order. In the conditions with $\omega_{mf} = 2.0$ rad/s this phase distortion was present on a larger bandwidth, as compared to $\omega_{mf} = 0.5$ rad/s. Hence, it could have impacted the pilots more. This phase lead translated into the open-loop phase margins, as visible in Eq. (6) and (7). This is supported by the significant interaction between O_{mf} and ω_{mf} that was found for $\varphi_{m,t}$ and $\varphi_{m,d}$, see Table 7.

It was hypothesized that with increasing motion filter frequency ω_{mf}, pilots would show similar effects as to an increasing motion filter order O_{mf}: lower performance and less use of motion feedback in their control strategy (Hypothesis H2). Furthermore, it was expected that the effects of ω_{mf} would be stronger than the effects of motion filter order O_{mf} (Hypothesis H3). Except for RMS_u, τ_v and τ_m, all dependent measures showed a significant effect of increasing ω_{mf}. Furthermore, whereas both simulators showed an increase in ω_{nm} for increasing ω_{mf}, this was only significant in the VMS. In the data of both simulators, pilots showed a higher RMS_e with increasing ω_{mf}. Furthermore, the fraction of $\sigma^2_{u_m}/\sigma^2_{u_v}$ indicated that with increasing ω_{mf}, less use was made of motion feedback. The motion gain K_m supported this, with a similar significant decrease. The visual equalization parameters K_v and T_L showed a significant decrease and an increase for increasing ω_{mf}, respectively. This indicated that pilots used more visual cues to generate lead, while controlling with smaller gains. All four open-loop parameters showed significant effects of ω_{mf}. The increase in $\omega_{c,t}$ with increasing ω_{mf} indicated an improved target-following performance and the corresponding decrease in $\varphi_{m,t}$ signified lower stability. The decrease in $\omega_{c,d}$ with increasing ω_{mf} indicated a degraded disturbance-rejection performance and the corresponding decrease in $\varphi_{m,d}$ signified lower stability. These four parameters together indicated a decreasing dependence on the motion channel of the pilot model in the open-loop responses, with increasing ω_{mf}. Hypothesis H2 could be accepted: pilots showed a decrease in use of the motion channel and a decrease in performance with increasing ω_{mf}. This finding is consistent with previous experiments.[14,15]

Furthermore, hypothesis H3 could be accepted as well: the effects of ω_{mf} were more prevalent than O_{mf} for the chosen experimental conditions. However, it is important to realize that only two ω_{mf}'s were present in the experiment and the relative change between the two frequencies might have been more severe than the change with each order of the motion filter. The change in ω_{mf} resulted in larger differences in the dependent variables than the changes in

O_{mf}, even in the $\omega_{mf} = 2.0$ rad/s conditions where the fidelity criteria of Sinacori[39] and Schroeder[25] predicted large effects for both ω_{mf} and O_{mf}. The results indicated that a first order motion filter resulted in the best performance. However, when ω_{mf} was sufficiently low, the filter order did not influence pilot behavior. A low ω_{mf} did result in better pilot performance. Hence, to compensate for lower a ω_{mf}, a larger filter order (i.e. second or third order) could be used to prevent the simulator from drifting without causing a decrease in pilot performance.

Even though meticulous attention was paid to match the VMS and SRS, most dependent measures did show clear offsets between both simulators: Hypothesis H4 was rejected. These differences between simulators were partially caused by four VMS pilots who used substantially larger control inputs during the task, which had a direct effect on RMS_u, K_v, K_m and the open-loop parameters, and hence also on $\sigma^2_{u_m}/\sigma^2_{u_v}$. Furthermore, the differences could also be caused by the difference in side stick arm. The side stick of the VMS had a 4.9 cm longer arm, which might have prompted the pilots to control with higher a RMS_u. Furthermore, the armrest in the VMS was covered with a canvas fabric, which allowed the pilots' arm to slide freely over the armrest. The armrest in the SRS, however, was covered in artificial leather, which prevented free movement of the arm to a certain degree. The difference in ζ_{nm} in C0 supported both these theories. Finally, many of the VMS pilots had experience in tracking tasks, whereas the SRS pilots usually performed such a task for the first time. Even though training runs ensured pilots showed constant performance (as assessed with RMS_e), this difference could have also caused the VMS pilots to control with a higher RMS_u.

With a few minor exceptions, all relative trends between the different tested motion conditions were highly consistent across simulators and therefore hypothesis H5 could be accepted. The only case where a significant interaction between motion condition and simulator was found, was for the disturbance crossover frequency $\omega_{c,d}$. Although this interaction was significant, it was not found to be relevant for the results, as the interaction was due to a single pair of conditions and the difference in trend was only 1% larger than other differences between conditions which did not cause a significant interaction.

V.B. Discussion of Statistical Analysis

Even though the ANOVA is considered by some to be essentially non-parametric,[48] in several cases the violations of its assumptions were quite severe. Hence, for some of the dependent variables a different statistical test was used: the Scheirer-Ray-Hare extension of the Kruskall-Wallis test.[50,51] This test is deemed to be a viable non-parametric alternative to an ANOVA, but it is found to lack statistical power in case interaction effects other than the main effects that are being tested are present.[55] Lower statistical power translates to a higher Type-II (false negative) error probability, which could have influenced some of the conclusions, as some of the variables where this test was applied (K_v, for example) did show consistent variation across conditions, but none were found significant.

V.C. Discussion of Prediction Equations

The prediction equation equations from Ref. 13 were compared to the experimental data. The predictions of K_v, T_L and $\omega_{c,d}$ were supported very well by the results, with correlation coefficients above $\rho > 0.8$. In C0 and C6, the prediction equations indicated higher $\hat{T}_L$'s than measured in the experiment. $1/\omega_{sp}$ appeared to be a more accurate predictor for T_L in conditions where little use was made of motion feedback. The equations for τ_v, ω_{nm} and $\varphi_{m,d}$ did not predict the results of this experiment, with correlation coefficients ranging from $\rho = -0.84$ to $\rho = -0.71$, which indicated that the equations predicted opposite trends. For τ_v a correlation of $\rho = 0$ was found. The experimental data of τ_v did not show significant results and the predictions indicated variations, which caused this low correlation. For $\varphi_{m,d}$, the opposite trend might have been present in the experimental results due to the phase lead introduced by the motion filter orders. In general, the equations for K_v, T_L and $\omega_{c,d}$ were found to be accurate predictors. For τ_v and $\varphi_{m,d}$, no conclusion on the prediction equations could be drawn, due to the absence of effects in the current experimental data and the experimental conditions themselves, respectively.

V.D. Human-Centered Simulator Benchmark

The experiment in this paper was performed in two flight simulators. More experiment replications in a broader environment consisting of more flight simulators, are necessary to strengthen the conclusions drawn. Consequently, a human-centered benchmark test is required, that has the purpose of identifying the effects of each simulator on the pilots that perform the experiment. The experiment in this paper indicated that relative trends between conditions are well reproducible across simulators, even in the presence of clear between-simulator biases in the results. A human-centered simulator comparison benchmark therefore might focus on at least two (motion) conditions, in order to investigate the relative effects between these conditions, instead of using one condition to find absolute differences. This may help overcome the pilot factors[29] of which experiment replications are subject.

VI. Conclusion

This paper describes the results of a tracking experiment performed to investigate the effects of different motion filter break frequencies ω_{mf} and motion filter orders O_{mf} on human control performance and behavior. Three motion filter orders and two motion filter break frequencies were tested in a factorial variation, in addition to two reference motion conditions: a full-motion and a no-motion condition. The experiment was performed on the VMS at NASA Ames Research Center and repeated on the SRS at Delft University of Technology in order to verify replication of the results. The motion system of the SRS was matched to the VMS using shaping filters. Head-down displays were used with the same graphics and the side stick was set to the same settings.

The effects of increasing the motion filter order O_{mf} on pilot behavior are equivalent to those of increasing the motion filter break frequency ω_{mf}, albeit less strong for the eight motion conditions considered in this experiment: pilots showed a similar decrease of performance and decrease in contribution of motion feedback on their control strategy. The results of this experiment indicate that pilots perform best with a low ω_{mf}. To prevent flight simulators from drifting, a low ω_{mf} could be compensated by a higher order filter (second or third order), without severely affecting pilot behavior.

The relative trends over the eight motion conditions were replicated well across the two simulators. However, even with meticulous attention paid to equalizing the simulator systems and the pilot population, the exact results between simulators for the same motion conditions were not replicated: biases were present within motion conditions between the two simulators. A future replication of experiments on multiple simulators, or even a human-centered benchmark test, might thus benefit from a focus on relative effects between a number of experimental motion conditions, instead of one setting in which the effects of the simulator are quantified.

References

[1] Boeing, *Commercial Market Outlook: 2018 - 2037*, Boeing Commercial Airplane Group, Seattle WA, USA, 2018, Retrieved from: https://www.boeing.com/commercial/market/commercial-market-outlook/.

[2] Airbus, *Global Market Forecast: 2018 - 2037*, Airbus S.A.S., Toulouse, France, 2018, Retrieved from: https://www.airbus.com/aircraft/market/global-market-forecast.html.

[3] Caird, J. K., "Persistent issues in the application of virtual environment systems to training," *Proceedings of the Third Annual Symposium on Human Interaction with Complex Systems*, Aug. 1996, pp. 124–132.

[4] Burki-Cohen, J. and Go, T., "The Effect of Simulator Motion Cues on Initial Training of Airline Pilots," *AIAA Modeling and Simulation Technologies Conference and Exhibit*, aug 2005.

[5] Burki-Cohen, J., Sparko, A., and Bellman, M., "Flight Simulator Motion Literature Pertinent to Airline-Pilot Recurrent Training and Evaluation," *AIAA Modeling and Simulation Technologies Conference*, aug 2011.

[6] Zaal, P. M. T. and Mobertz, X., "Effects of Motion Cues on the Training of Multi-Axis Manual Control Skills," *AIAA Modeling and Simulation Technologies Conference*, jun 2017.

[7] Zaal, P. M. T., Schroeder, J. A., and Chung, W. W., "Transfer of Training on the Vertical Motion Simulator," *Journal of Aircraft*, Vol. 52, No. 6, nov 2015, pp. 1971–1984.

[8] Federal Aviation Administration, "Stall Prevention and Recovery Training," Advisory Circular 120-109A, Nov. 2015.

[9] Zaal, P. M. T., Popovici, A., and Zavala, M. A., "Effects of False Tilt Cues on the Training of Manual Roll Control Skills," *AIAA Modeling and Simulation Technologies Conference*, jan 2015.

[10] Popovici, A., Zaal, P. M. T., and Pieters, M. A., "Time-Varying Manual Control Identification in a Stall Recovery Task under Different Simulator Motion Conditions," *AIAA Modeling and Simulation Technologies Conference*, jun 2018.

[11] Reid, L. D. and Nahon, M., "Flight Simulation Motion-Base Drive Algorithms: Part 1 - Developing and Testing the Equations," Tech. rep., UTIAS, 1985.

[12] Gouverneur, B., Mulder, J. A., van Paassen, M. M., Stroosma, O., and Field, E., "Optimisation of the SIMONA Research Simulator's Motion Filter Settings for Handling Qualities Experiments," *AIAA Modeling and Simulation Technologies Conference and Exhibit*, aug 2003.

[13] Pool, D. M., Damveld, H., van Paassen, M. M., and Mulder, M., "Tuning Models of Pilot Tracking Behavior for a Specific Simulator Motion Cueing Setting," *AIAA Modeling and Simulation Technologies Conference*, aug 2011.

[14] Pool, D. M., van Paassen, M. M., and Mulder, M., "Effects of Motion Filter Gain and Break Frequency Variations on Pilot Roll Tracking Behavior," *AIAA Modeling and Simulation Technologies Conference*, aug 2013.

[15] Pool, D. M., Zaal, P. M. T., Damveld, H., van Paassen, M. M., and Mulder, M., "Evaluating Simulator Motion Fidelity using In-Flight and Simulator Measurements of Roll Tracking Behavior," *AIAA Modeling and Simulation Technologies Conference*, aug 2012.

[16] Pool, D. M., Zaal, P. M. T., van Paassen, M. M., and Mulder, M., "Effects of Heave Washout Settings in Aircraft Pitch Disturbance Rejection," *Journal of Guidance, Control, and Dynamics*, Vol. 33, No. 1, 2010, pp. 29–41.

[17] Wieringen, A. T. V., Pool, D. M., van Paassen, M. M., and Mulder, M., "Effects of Heave Washout Filtering on Motion Fidelity and Pilot Control Behavior for a Large Commercial Airliner," *AIAA Modeling and Simulation Technologies Conference*, Aug. 2011.

[18] Steurs, M., Mulder, M., and van Paassen, M. M., "A Cybernetic Approach to Assess Flight Simulator Fidelity," *AIAA Modelling and Simulation Technologies Conference and Exhibit*, 2004.

[19] Bergeron, H. P., "Investigation of Motion Requirements in Compensatory Control Tasks," *IEEE Transactionson Man-Machine Systems*, Vol. MMS-11, No. 2, June 1970, pp. 123–125.

[20] van Gool, M. F. C., "Influence of Motion Washout Filters on Pilot Tracking Performance," *Piloted Aircraft Environment Simulation Techniques*, , No. AGARD-CP-249, 1978, pp. 19–1 – 19–5.

[21] Bray, R. S., "Visual and Motion Cueing in Helicopter Simulation," *TM-86818, NASA Ames Research Center*, 1985.

[22] Grant, P. R. and Reid, L. D., "Motion Washout Filter Tuning: Rules and Requirements," *Journal of Aircraft*, Vol. 34, No. 2, mar 1997, pp. 145–151.

[23] Hosman, R. J. A. W. and Advani, S. K., "Are Criteria for Motion Cueing and Time delays possible? Part 2," *AIAA Modeling and Simulation Technologies Conference*, aug 2013.

[24] Zaal, P. and Mobertz, X., "Effects of Motion Cues on the Training of Multi-Axis Manual Control Skills," *AIAA Modeling and Simulation Technologies Conference*, jun 2017.

[25] Schroeder, J. A., "Helicopter Flight Simulation Motion Platform Requirements," Tech. rep., NASA Ames Research Center, 1999.

[26] Grant, P. R., Yam, B., Hosman, R. J. A. W., and Schroeder, J. A., "The Effect of Simulator Motion on Pilot's Control Behavior for Helicoptor Yaw Tasks," *AIAA Modeling and Simulation Technologies Conference and Exhibit*, aug 2005.

[27] Ellerbroek, J., Stroosma, O., Wentink, M., Groen, E., and Smaili, H., "Effect of Sway and Yaw Motion on Perception and Control: A Multi-Simulator, Follow-Up Study," *AIAA Modeling and Simulation Technologies Conference and Exhibit*, aug 2006.

[28] Ellerbroek, J., Stroosma, O., Mulder, M., and van Paassen, M., "Identification of the Roles of Yaw and Sway Motion in Helicopter Yaw Control Tasks," *AIAA Modeling and Simulation Technologies Conference and Exhibit*, aug 2007.

[29] Ellerbroek, J., Stroosma, O., Mulder, M., and van Paassen, M. M., "Role Identification of Yaw and Sway Motion in Helicopter Yaw Control Tasks," *Journal of Aircraft*, Vol. 45, No. 4, jul 2008, pp. 1275–1289.

[30] Hodge, S., Perfect, P., Padfield, G., and White, M., "Optimising the yaw motion cues available from a short stroke hexapod motion platform," *The Aeronautical Journal*, Vol. 119, No. 1211, jan 2015, pp. 1–21.

[31] Hosman, R. J. A. W., Grant, P. R., and Schroeder, J. A., "Pre and Post Pilot Model Analysis Compared to Experimental Simulator Results." *AIAA Modeling and Simulation Technologies Conference and Exhibit*, aug 2005.

[32] Jex, H. R., Magdaleno, R. E., and Junker, A. M., "Roll tracking effects of G-vector tilt and various types of motion washout," *The 14th Annual Conference on Manual Control*, Nov. 1978, pp. 463–502.

[33] Jex, H. R., Jewell, W. F., Magdaleno, R. E., and Junker, A. M., "Effects of Various Lateral-Beam Washouts on Pilot Tracking and Opionio in the Lamar Simulator," Tech. rep., AFFDLTR-79-3134, 1979.

[34] Zaal, P. M. T. and Zavala, M. A., "Effects of Different Heave Motion Components on Pilot Pitch Control Behavior," *AIAA Modeling and Simulation Technologies Conference*, jun 2016.

[35] van Paassen, M. M. and Mulder, M., "Identification of Human Operator Control Behaviour in Multiple-Loop Tracking Tasks," *IFAC Proceedings Volumes*, Vol. 31, No. 26, sep 1998, pp. 455–460.

[36] Zaal, P. M. T., Pool, D. M., de Bruin, J., Mulder, M., and van Paassen, M. M., "Use of Pitch and Heave Motion Cues in a Pitch Control Task," *Journal of Guidance, Control, and Dynamics*, Vol. 32, No. 2, mar 2009, pp. 366–377.

[37] McRuer, D. and Jex, H., "A Review of Quasi-Linear Pilot Models," *IEEE Transactions on Human Factors in Electronics*, Vol. HFE-8, No. 3, sep 1967, pp. 231–249.

[38] Damveld, H. J., Abbink, D. A., Mulder, M., Mulder, M., van Paassen, M. M., van der Helm, F. C. T., and Hosman, R. J. A. W., "Measuring the Contribution of the Neuromuscular System During a Pitch Control Task," *AIAA Modeling and Simulation Technologies Conference*, aug 2009.

[39] Sinacori, J. B., "The Determination of Some Requirements for a Helicopter Research Simulation Facility," Tech. rep., NASA-CR-152066, Systems Technology Inc., 1977.

[40] Aponso, B. L., Beard, S. D., and Schroeder, J. A., "The NASA Ames Vertical Motion Simulator A Facility Engineered for Realism," *Royal Aeronautical Society Spring 2009 Flight Simulation Conference, London, UK*, June 2009.

[41] Pool, D. M., Mulder, M., van Paassen, M. M., and van der Vaart, J. C., "Effects of Peripheral Visual and Physical Motion Cues in Roll-Axis Tracking Tasks," *Journal of Guidance, Control, and Dynamics*, Vol. 31, No. 6, nov 2008, pp. 1608–1622.

[42] Zaal, P. M. T., Schroeder, J. A., and Chung, W. W., "Transfer of Training on the Vertical Motion Simulator," *Journal of Aircraft*, Vol. 52, No. 6, nov 2015, pp. 1971–1984.

[43] Schroeder, J. A. and Grant, P. R., "Pilot Behavioral Observations in Motion Flight Simulation," *AIAA Modeling and Simulation Technologies Conference*, aug 2010.

[44] ICAO, "Document 9625, Volume 1, Attachement F: Frequency-Domain Motion Cueing System Performance Test," Tech. rep., ICAO, 2009, ISBN 978-92-9231-341-8, obtained online.

[45] Danek, G. L., "Vertical Motion Simulator Familiarization Guide," Tech. rep., NASA-TM-103923, 1993.

[46] Lehmer, R. and Chung, W., "Image Dynamic Measurement System (IDMS-2) for flight simulation fidelity verification," *AIAA Modeling and Simulation Technologies Conference and Exhibit*, aug 1999.

[47] Stroosma, O., van Paassen, M. M., Mulder, M., and Postema, F., "Measuring Time Delays in Simulator Displays," *AIAA Modeling and Simulation Technologies Conference and Exhibit*, aug 2007.

[48] Sawilowsky, S. S., "Nonparametric Tests of Interaction in Experimental Design," *Review of Educational Research*, Vol. 60, No. 1, mar 1990, pp. 91–126.

[49] Field, A., *Discovering Statistics Using SPSS (Introducing Statistical Methods series)*, Sage Publications Ltd, 2005.

[50] Scheirer, C. J., Ray, W. S., and Hare, N., "The Analysis of Ranked Data Derived from Completely Randomized Factorial Designs," *Biometrics*, Vol. 32, No. 2, jun 1976, pp. 429.

[51] Sokal, R. R. and Rohlf, F. J., *Biometry: The Principles and Practices of Statistics in Biological Research*, W. H. Freeman, 1994.

[52] Zaal, P. M. T., Pool, D. M., Chu, Q. P., Mulder, M., van Paassen, M. M., and Mulder, J. A., "Modeling Human Multimodal Perception and Control Using Genetic Maximum Likelihood Estimation," *Journal of Guidance, Control, and Dynamics*, Vol. 32, No. 4, jul 2009, pp. 1089–1099.

[53] Valente Pais, A. R., Pool, D. M., De Vroome, A. M., van Paassen, M. M., and Mulder, M., "Pitch Motion Perception Thresholds During Passive and Active Tasks," *Journal of Guidance, Control, and Dynamics*, Vol. 35, No. 3, may 2012, pp. 904–918.

[54] Nieuwenhuizen, F. M., Mulder, M., van Paassen, M. M., and Bülthoff, H. H., "Influences of Simulator Motion System Characteristics on Pilot Control Behavior," *Journal of Guidance, Control, and Dynamics*, Vol. 36, No. 3, may 2013, pp. 667–676.

[55] Toothaker, L. E. and Horng Shing Chang, "On "The Analysis of Ranked Data Derived from Completely Randomized Factorial Designs"," *Journal of Educational Statistics*, Vol. 5, No. 2, 1980, pp. 169.

II

Preliminary Thesis

To be graded as AE4020 - Literature Study

2

Motion Filter Order

Because flight simulators are restricted by their motion space, the simulated aircraft motion needs to be attenuated. Typically, a combination of gain attenuation and high-pass filtering is used. In order to start investigating the effects of changing motion filter order, first a metric to compare motion filters is required. For this reason, Section 2.1 provides a brief review of some commonly used simulator motion fidelity criteria. Then, Section 2.2 presents the motion filters and its parameters. A wide variety of washout filters can be found in operational flight simulators, each with their own motion fidelity. Section 2.3 illustrates this by reviewing a large body of literature on motion filter research. Although there have been numerous investigations into the effects of the motion filter parameters, the motion filter order has received less attention. Finally, Section 2.4 identifies a research gap from the previous sections and states a research question for an experiment into the effects of motion filter order.

2.1. Simulator Motion Fidelity Criteria

Several studies considered defining fidelity criteria for simulator motion filters, in order to achieve certain levels of fidelity. In 1977 Sinacori [4] used a helicopter model to relate motion filter characteristics to the motion fidelity experienced by a pilot. Four test points were used to postulate the criteria in Figure 2.1, indicated with the dashed lines. These fidelity regions assume that the gain and phase distortion of the motion filter at a frequency of 1 rad/s allow to characterize the motion that is experienced by a human pilot. The frequency of 1 rad/s was chosen since it is at this frequency that the frequency response of the semicircular canals has the highest gain [5]. This delivers the parameters K_S and Φ_s, as can be seen in Equation 2.1 and 2.2.

$$K_S = \left|H_{mf}(j\omega)\right| \quad \text{with} \quad \omega = 1 \quad \text{rad/s} \tag{2.1}$$

$$\Phi_S = \angle H_{mf}(j\omega) \quad \text{with} \quad \omega = 1 \quad \text{rad/s} \tag{2.2}$$

Schroeder [5] then revisited these criteria with a series of experiments on the VMS, retaining the principle of evaluating the motion filter at a frequency of 1 rad/s, but refining the boundaries of the fidelity regions. The results can be seen in Figure 2.1. For both Sinacori's and Schroeder's experiments, the motion fidelity regions were determined using subjective motion ratings from pilots. In recent research by Zaal et al. [6], the Objective Motion Cuing Test (OMCT) has been applied to define motion fidelity criteria. This test differs from the previous described ones, as it regards a frequency range, rather than an evaluation at a single frequency. Furthermore, the motion criteria are being determined objectively, based on pilot performance. The OMCT is further discussed in Section 3.1.1.

2.2. Simulator Washout Filters

Flight simulators are bound by their limited motion space in providing motion cues to pilots. The goal of the high-pass washout filters is to make the pilot perceive the onset of a maneuver, without actually exceeding the bounds of the motion platform. High-pass filters, which pass the higher frequencies and attenuate lower ones, succeed in doing so. Often, also a tilt coordination low-pass filter is present in the motion algorithm. This filter converts surge and sway specific forces to pitch and roll angles to simulate low-frequency specific forces [7]. An example of this is the force a pilot feels when decelerating after touchdown.

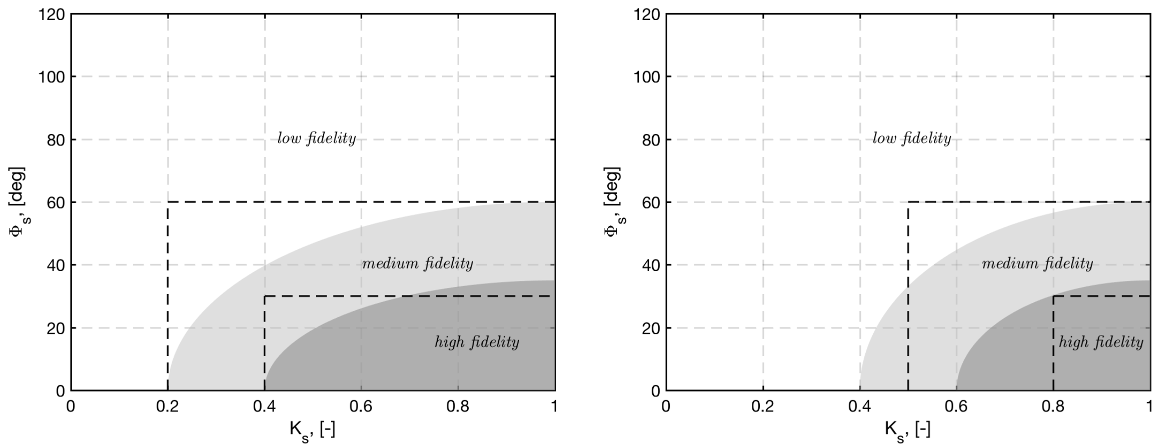

(a) Rotational

(b) Translational

Figure 2.1: Sinacori fidelity criteria [4] indicated by dashed lines, with adaptations by Schroeder visible as shaded areas [5]

Different types of simulator washout filters have been applied in the past, for instance adaptive filters and classical washout filters [8], which are the subject of this research. The classical washout filter has a linear structure, which ensures different subjects are presented with the same motion cues, independent of their control behavior, as explained by Gouveneur et al. [9]. This is vital in evaluating simulator motion fidelity, as it allows to compare results for a population of participants. Motion filters of several orders exist, as indicated in Equation 2.3 to 2.6.

$$\text{zeroth order:} \quad H_{mf}(s) = K \tag{2.3}$$

$$\text{first order:} \quad H_{mf}(s) = K\frac{s}{s+\omega_{mf}} \tag{2.4}$$

$$\text{second order:} \quad H_{mf}(s) = K\frac{s^2}{s^2+2\zeta_{mf}\omega_{mf}s+\omega_{mf}^2} \tag{2.5}$$

$$\text{third order:} \quad H_{mf}(s) = K\frac{s^2}{s^2+2\zeta_{mf}\omega_{mf}s+\omega_n^2}\frac{s}{s+\omega_b} \tag{2.6}$$

Motion filter order influences the fidelity of the simulator motion cues. As Pool et al. explain in [2]: *"For constant parameter settings, motion fidelity decreases with increasing filter order, as increasingly more low-frequency motion is attenuated and phase distortion increases rapidly for higher filter orders."*. Figure 2.2 illustrates this for the motion filters in Equations 2.3 to 2.6, with $K = 1$, $\omega_{mf} = 1$ rad/s, $\zeta_{mf} = 0.7$ and $\omega_b = 0.3$ rad/s. Figure 2.3 shows the frequency response of these motion filters.

2.3. Previous Research

There has been a lot of research into the effects of varying motion washout filter parameters. Pool et. al. [2], for instance, consolidate a large set of experiments and derive equations from the found data, such that the effects of the motion filter parameters can be predicted. Ten experiments are included, which are separated in rotational and translational degrees of freedom, to correspond to the fidelity plots of Sinacori [4] and Schroeder [5]. There is no distinction between the different axes in this research. Four studies were present in the translational degrees of freedom and six in the rotational degrees. The studies spans all three regions of the fidelity criteria. Only one of the ten studies compares motion filters of different orders.

In 1978 Jex et al. [10] investigated pilot manual control behavior in a combined target following and disturbance rejection task. Their experiment included motion washout filters ranging from zeroth order to second order. It was found that the second order washout was least desirable, and that the first order washout filter produced most realistic results. Realistic here was defined as resulting in similar pilot model parameters, compared to a real-world flying task [10]. This corresponds with the notion presented in Section 2.2 that higher orders result in lower fidelity motion cues. However, in this study difficulties in analyzing the second

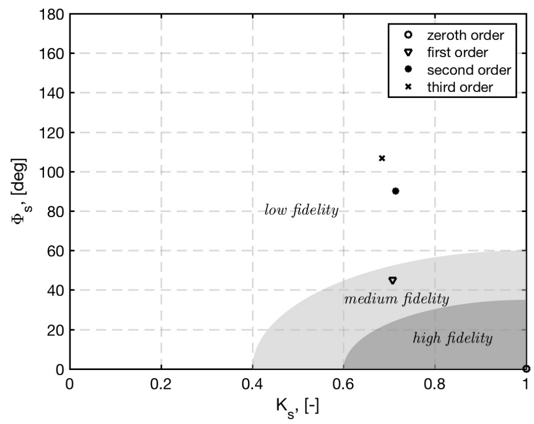

Figure 2.2: Motion filters with constant parameters plotted on fidelity criteria plot

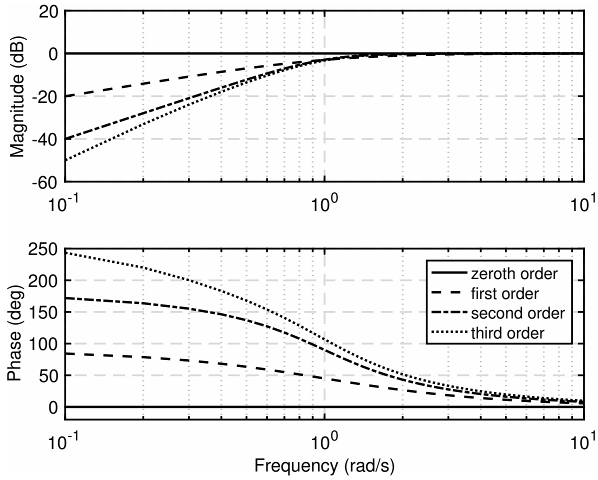

Figure 2.3: Frequency response of several different orders of motion filters

order filter arose, because of the design of the simulator, which might have influenced the results. So no direct comparison between the effects of orders on pilot manual control behavior was made.

In 2013 Pool et al. [3] analyzed the motion filter break frequency and gain influence and gathered data from another large set references to show how the research compared to previous work. Figure 2.4 shows the motion filter fidelity criteria for all these experiments. The studies considered are only roll tasks, and only four of the studies are also used in the overview of [2]. The figure succeeds in illustrating that the body of research into motion filter influence is large, and all three fidelity regions are spanned. The settings of each of the conditions, and the corresponding reference, can be found in [3] and are omitted here for brevity.

Figure 2.5 shows a similar overview for a set of experiments with only heave motion cue variation. Figure 2.6 shows an overview for experiments using different pitch motion filters. Only the experiments used in these two overviews already succeed in spanning all three fidelity regions. Nevertheless, neither Figure 2.5 nor Figure 2.6 contain any experiments where the focus lied explicitly on identifying the effects of the different motion filter orders.

Figure 2.5 contains more references with higher order motion filters than Figure 2.6. While these figures are by no means exhaustive lists of all the research performed, this difference can be explained. For the translational degrees of freedom, such as heave, the high-pass filters should be able to return the simulator back to its neutral position in response to a step on specific force, as explained by Stroosma et al. [7]. A third order filter, as shown in Equation 2.6, can be proven to do this with the final value theorem. In Equation 2.7, $\frac{1}{s}$ represents the Laplace transform of a step input and the double integrator $\frac{1}{s^2}$ is present to transform from acceleration to position.

$$\lim_{t\to\infty} x(t) = \lim_{s\to 0} sX(s) = \lim_{s\to 0} s\left(H_{mf}(s)\frac{1}{s}\right)\frac{1}{s^2} = \lim_{s\to 0} s\left(\frac{Ks^2}{s^2+2\zeta_{mf}\omega_{mf}s+\omega_{mf}^2}\frac{s}{s+\omega_b}\frac{1}{s}\right)\frac{1}{s^2} = 0 \tag{2.7}$$

Steps in specific force occur in operations of flight simulators, for instance on the take-off. However, steps in rotational acceleration are exceptional, and therefore filters in the rotational degrees of freedom usually have a lower order [7].

The publications discussed in this section [2–5, 7, 10], show that there is a large body of literature on the effects of the parameters of the motion washout filter, but it seems that little attention has been paid to comparing washout filters of different orders, with the explicit goal of comparing the order effects. The next section proposes a research question for a possible experiment to investigate these effects.

2.4. Research Question

In the previous sections, some common measures of simulator motion fidelity and motion washout filters were presented. Furthermore, a review of a body of literature revealed that there has been a lot of research into varying motion washout filter parameters and looking into the effects on human control behavior and

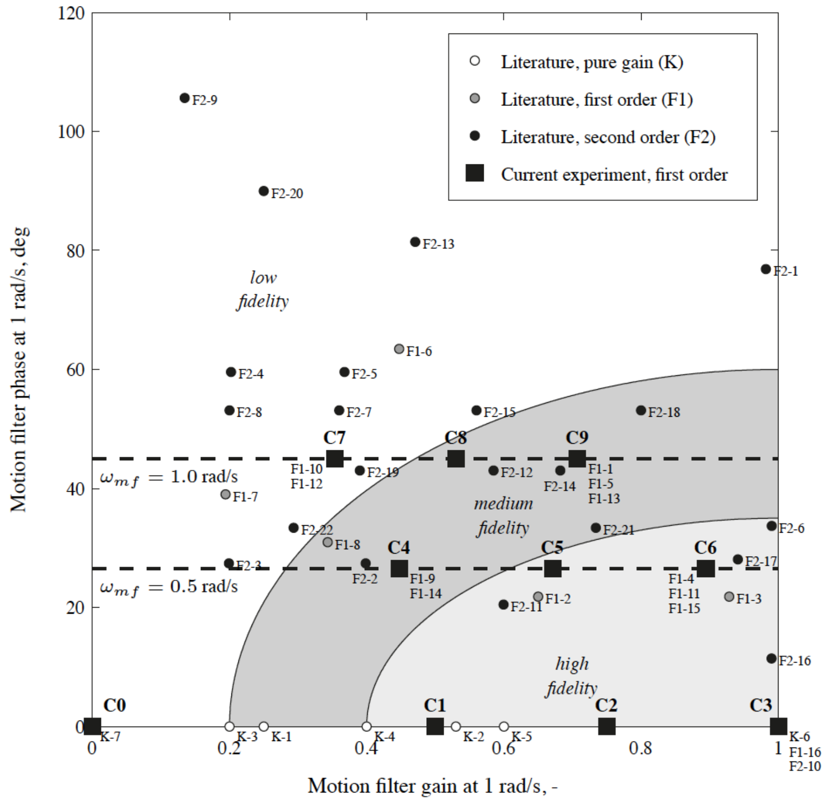

Figure 2.4: Compiled roll motion filter settings used in the research by Pool et al. [3] shown on simulator motion fidelity criteria plots proposed by Sinacori [4] and Schroeder [5]

performance, for all axis of flight simulators. However, the order of classical washout filters has not yet received this attention, even though many different orders can be found in currently operational simulators, sometimes even within one simulator. Hence, the following research question arises: *"How does changing the motion washout filter order influence human manual control behavior?"*

The research question could be investigated in a tracking experiment, which allows to estimate a human pilot model, with its parameters. The motion filter order could be varied and the subsequent differences in pilot control behavior could be used to analyze the effects of motion filter order.

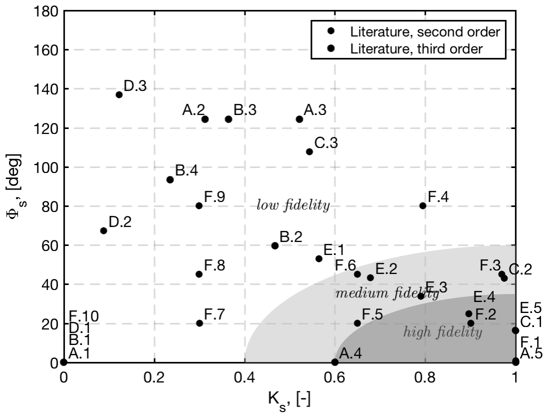

Second Order		Third Order	
Symbol	Ref.	Symbol	Ref.
C1 - C3	[11]	A1 - A5	[12]
D1 - D3	[13]	B1 - B4	[14]
E1 - E5	[15]		
F1 - F10	[5]		

Figure 2.5: Heave motion cueing settings of six experiments compared to translational simulator motion fidelity criteria proposed by Sinacori [4] with modified fidelity regions as suggested by Schroeder [5]

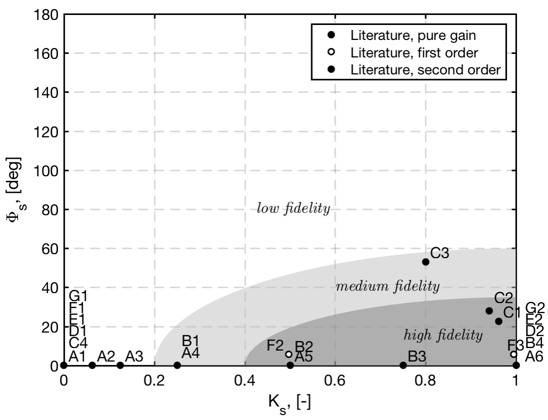

Zeroth Order		First Order		Second Order	
Symbol	Ref.	Symbol	Ref.	Symbol	Ref.
A1 - A6	[16]	F1 - F3	[13]	C1 - C4	[17]
B1 - B4	[18]				
D1 - D2	[12]				
E1 - E2	[14]				
G1 - G2	[19]				

Figure 2.6: Pitch motion cueing settings of six experiments compared to rotational simulator motion fidelity criteria proposed by Sinacori [4] with modified fidelity regions as suggested by Schroeder [5]

3
Simulator Benchmarking

Benchmarking, the concept of comparing results to known reference plays a major role in any science: comparisons can only be made once there is something to compare to. However, in the domain of human flight simulation, a simulator benchmark is absent. Borrowing from other domains of science, relevant information on how to create a benchmark, with its tests and necessary requirements was be found. For example, in the domain of computer sciences, many benchmarks exist, and many new ones are being created constantly, for a wide variety of purposes. Huppler lists the following five characteristics for a good benchmark test [20]:

- Relevant: The results of the test must directly relate to the factor of interest.
- Repeatable: The test can be run numerous times and produce similar results.
- Fair: The test is objective and allows all participants to perform equally.
- Verifiable: The test must represent the actual system and the results inspire confidence that it does.
- Economical: The test requires resources such that it does not impact other functioning of the equipment and it can be performed with minimal resource investment.

Also more close to home, in aerospace engineering, relevant information on how to create a benchmark can be found. For instance, Oberkampf and Smith [21] propose six attributes that need to be documented clearly for a study to be repeated well:

- The experimental facility (e.g. the flight simulator and all its subsystems)
- The instrumentation and signal processing
- The boundary and initial conditions (e.g. the task)
- The material properties (e.g. the pilots)
- The test conditions
- The system responses (e.g. the results)

These characteristics and requirements for documentation, form a basis from which to commence the search for a human-centered flight simulator benchmark test. This chapter explores the literature for past attempt to incorporate these characteristics in a benchmark for flight simulators. To do so, however, first a look into the concept of flight simulation itself is taken. Flight simulators are complex machines, replicating a complex environment. Therefore, the problem has to be subdivided. Firstly, Section 3.1 introduces a schematic overview of a pilot executing a task in a simulator. Then, in Section 3.2, some previous flight simulator experiment repetitions are presented, in which different simulators were used, since this is relevant for benchmarking. From this basis a research question is distilled in Section 3.3.

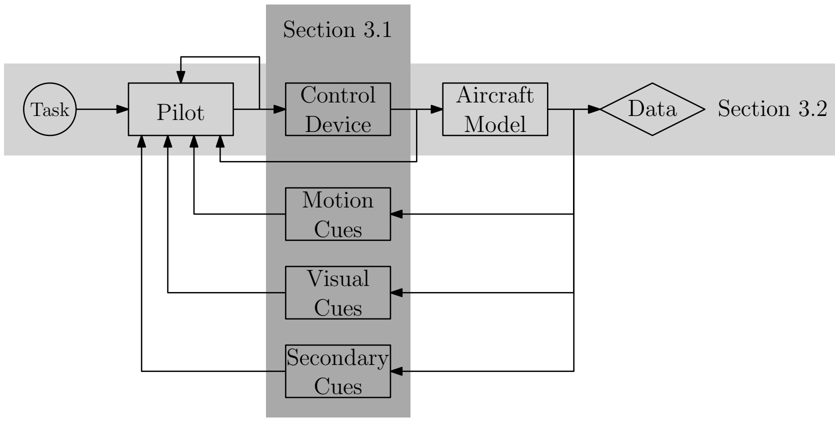

Figure 3.1: Schematic block diagram of a pilot executing a task in a flight simulator, as adapted from [22]

3.1. Flight Simulation Loop

A schematic representation of a pilot executing a task in a flight simulator can be seen in Figure 3.1. The pilot perceives cues from several different systems, such as the motion cues and the visual cues. Secondary cues include sound and smell cues, for example. In trying to identify simulator elements to document and define, the overview of Figure 3.1 will be used. Some possible methods to test each of these elements are discussed. Firstly, Section 3.1.1 focuses on the motion system. Secondly, Section 3.1.2 discusses the visual system. Thirdly, Section 3.1.3 presents ways of characterizing the control device. Finally, Section 3.1.4 examines the secondary cues a pilot might perceive. With an idea of how these four blocks in Figure 3.1 can be characterized and compared, in the next part of this chapter, Section 3.2, literature on previous experiments is reviewed, in order to get a better understanding of how to select the task, the pilots and the aircraft model.

3.1.1. Motion System Testing

Firstly, for the motion system, the Objective Motion Cuing Test (OMCT) is a standardized test to characterize a simulator motion system. It is part of the ICAO 9625 simulator qualification guidelines [23] and is meant to objectively evaluate the physical motion of a flight simulator, as opposed to subjective evaluation by test pilots.

Because the motion system of current-day flight simulators is able to provide high quality cueing, the role of the motion cueing algorithm is more important in the pilot's motion perception, as explained by Stroosma et al. in [7]. Hence, previous tests, such as AGARD-AR-144 [24], which only focus on the motion system hardware, are not fully applicable anymore to completely characterize the motion system of a particular simulator. The OMCT does include the motion cueing algorithm response.

The OMCT works by inserting sinusoid functions into separate axis of the motion algorithm, and measuring the responses of the platform. Estimates of the response in the form of linear transfer functions can be made. To capture all degrees of freedom and combinations thereof, ten different tests are executed, six of which report direct transfer relations (such as pitch response due to aircraft pitch input) and four of which show cross-coupling effects (such as roll rate due to aircraft sway input). The results are the frequency responses which relate the real aircraft rotation rates and accelerations at the pilot station to those in the simulator, as explained by Zaal et al. in [6].

The OMCT has been applied in several previous studies in simulators of various uses, in order to develop motion cuing guidelines and criteria [6, 7]. It is useful for simulator comparisons, because it allows to fully characterize the motion response of a simulator in all its degrees of freedom. It allows to quantify the differences in motion systems. Figure 3.2 shows how the sinusoid signal generator is used as input signal instead of the aircraft model to compare the simulated to the actual pilot station [23].

Figures 3.3 and 3.4 show some fictional OMCT results for two examples, to illustrate the usefulness of the results. In Figure 3.3, it can be observed that example test 2 (surge due to pitch) has a high phase range, while its gain range is relatively low. The example in Figure 3.4 has a relatively high gain over all frequencies and a relatively low phase range. In the ICAO 9526 manual [23], it is stated that the 6 direct transformation test should display high gains and low phases, while the four cross-coupling tests should also show low gains. Figure 3.4 shows the results of a direct transformation and Figure 3.3 of a cross-coupling test.

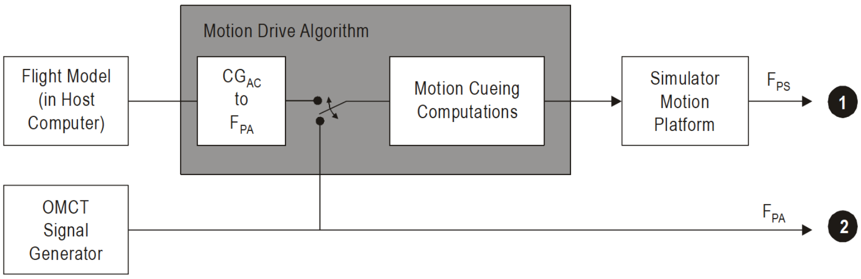

Figure 3.2: The OMCT working principle: a signal generator allows to compare the motion states of the actual aircraft to those in the simulator, both at the pilot station [23]

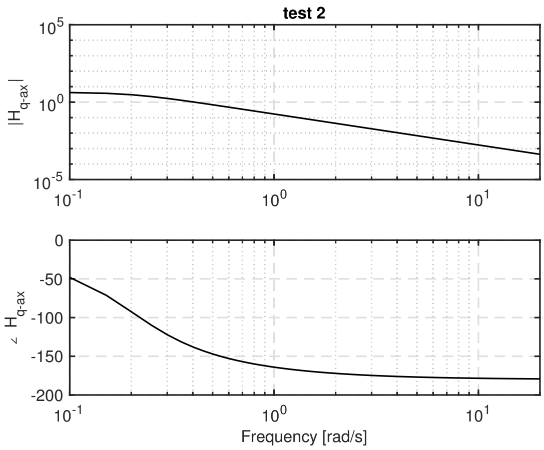

Figure 3.3: OMCT example results for surge due to heave

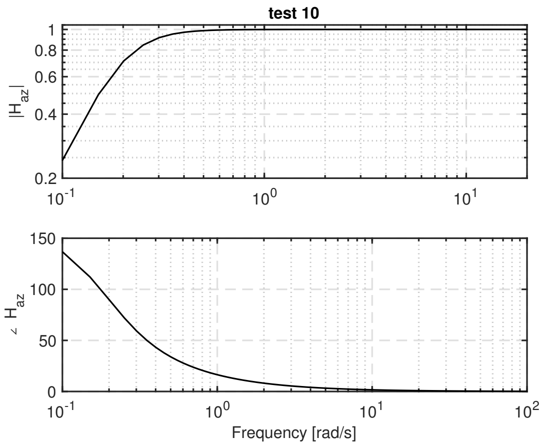

Figure 3.4: OMCT example results for heave due to heave

Zaal et al. [6] used the OMCT for all conditions of an experiment where the influence of motion on transfer of training was investigated. Sixty-one general aviation pilots divided over four motion conditions performed four challenging flight tasks and subsequently transferred to a full motion condition on the VMS. The OMCT was used in this experiment to quantify the fidelity of each condition. The difference between conditions was used to predict trends in pilot ratings and performance. Hence, the OMCT could be useful to provide information on differences within one simulator. However, for similar conditions on a different simulator the OMCT also provides a useful and tangible way to compare motion systems.

3.1.2. Visual System Testing

The next important system to understand is the visual system of the flight simulator, since it is the source of numerous factors which might influence pilots, for example time delays. Numerous investigations have shown that visual time delays can have severe detrimental effects on human manual control behavior. For instance, Sheridan [25] reviews a large body of literature in the context of spacecraft teleoperations. He concludes that *"By 1980 there was abundant experimental evidence that time delay was a serious problem for teleoperation, at least one which could not be ignored."* [25], page 2. Another example supporting this notion can be found in the work of Miall and Jackson [26]. In their experiment, two groups of participants were asked to perform a tracking task: one group controlled undelayed dynamics and while the other was subjected to a 300ms visual time delay. As stated in [26], page 1: *"Introduction of the visual feedback delay significantly disrupted tracking performance, with an increase in errors and a reduction in frequency of corrective movements."* Visual time delays are thus a significant factor in influencing human manual control behavior.

Aggravating the situation in case of a simulator comparison, is the fact that many different techniques exist to provide pilots with visual cues in flight simulators. These techniques are dependent on the simulators intended purpose. For instance, a training simulator intended to teach VFR flying will have a larger benefit of high-fidelity out-of-the-window visuals than a research simulator intended to investigate display design. Allerton [27] provides a large volume of information on simulator visual systems, and the different techniques that can be used. For instance, different simulators have different field of views, which leads to different use of the peripheral vision. This has been investigated before, for instance by Pool et al. [28], who concluded that the use of visual peripheral cues has an increasing effect on tracking performance. The out-of-the-window view of a simulator is thus an influencing factor in a simulator comparison study.

One method of eliminate these large differences between simulators, is to limit the visual cues pilots receive to a more controllable influx of information. For instance, only head-down displays with simple visuals could be used, as they are easier to control and compare. For a full simulator comparison study, however, also the differences in visual system have to be accounted for. While focusing on the head-down displays lowers this benchmark usability, it gives more control over differences, as there simply are less. However, even these displays might have different time delays in different simulators and hence this should still be examined.

A possible method is proposed by Stroosma et al. [29], the Visual Delay Measurement System. This test can be used for out-of-the-window visuals as well as other displays. It is based on minimizing the observed phase difference between a driver signal and a displayed signal, by using shutter glasses (with a known or negligible time delay) which open at twice the frequency of the driver signal. The time delay is found at the moment where a single stable image is observed by a participant, because the shutter glasses open at the moment where the driver signal and displayed signal plus the time delay overlap, as can bee seen in Figure 3.5.

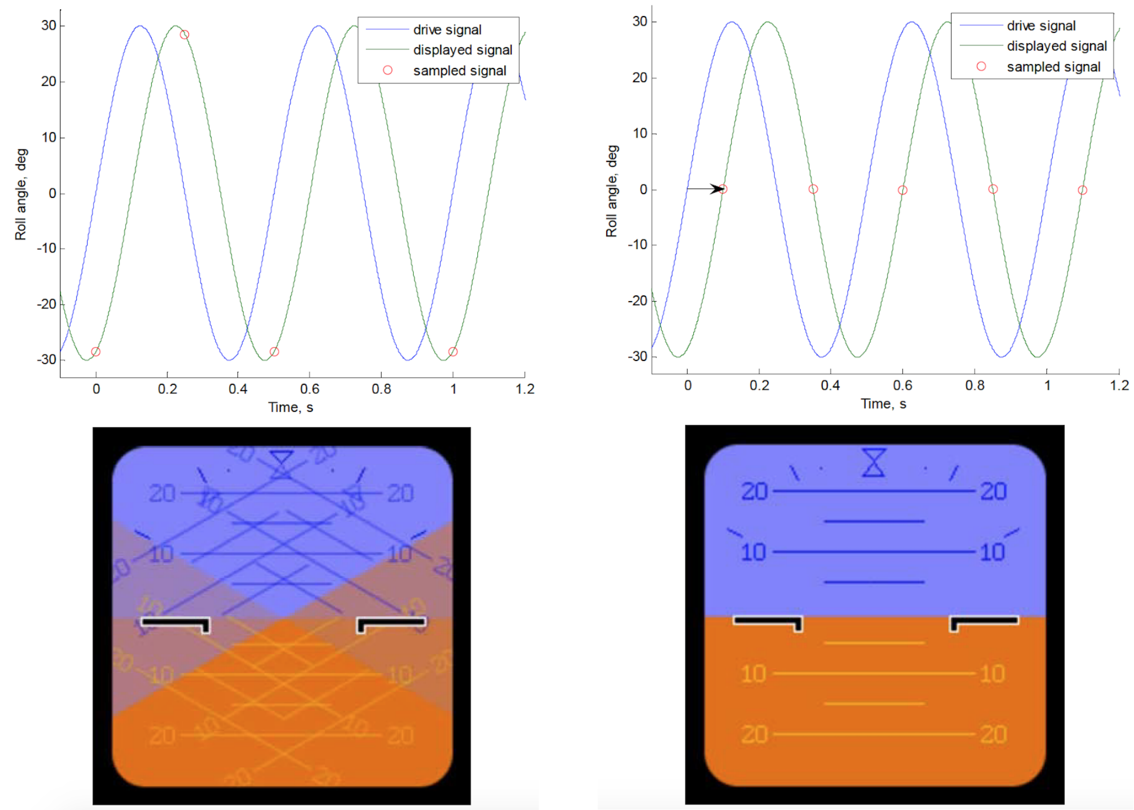

(a) No time offset, phase difference exists

(b) Correct time offset, stable image

Figure 3.5: Visual Delay Measurement System operating principle, as found in [29]

3.1.3. Control Device Testing

The control actuator is the device that the operator uses to control the system. The interaction between it and the operator therefore can be of high influence in the control strategy. Two metrics to characterize the actuator are the force / displacement relation and the actuator's frequency response.

The force / displacement relation of an actuator shows how much force is needed for a certain displacement. Some of the actuator characteristics that can be found from this figure are the break-out force, the force gradient(s) and the travel. This information can be used to characterize the pilots feel of the stick, for example. Another method to characterize the response of a control actuator is a frequency sweep. In this manner the frequency response can be found.

3.1.4. Secondary Cues Testing

Some secondary cues which a pilot flying a simulator might perceive are sound cues are smell cues, for instance. In order to eliminate the effect of the actuator movements, typically a loud (engine) noise signal is played to the pilot through headphones. This audio signal is relatively easy to standardize between simulators, if chosen well. Furthermore, the seat and cockpit have to be made to feel equal. In this manner the "seat-of-the-pants" feeling for the participants between the simulators is made equal.

Apart from these cues, many more can influence the operator in simulator, such as smell, temperature and atmospheric conditions inside the simulator [30]. Some are under control and some are not. Therefore, most of all, it is vital to fully document the simulation environment.

3.2. Previous Experiments

Although there is a pressing need to validate experimental results in human centered flight simulation research, not many studies have been replicated with this purpose. Three series of experiment replications were identified, however. Firstly, Jex et al. performed a study in 1987 investigating pilot manual control for roll tracking, which was replicated on another simulator a year later, as discussed in Section 3.2.1. Secondly, an experiment by Schroeder focusing on a helicopter yaw task was replicated in three different simulators, which is discussed in Section 3.2.2. Thirdly, a de-crab maneuver experiment was performed on two different simulators, as discussed in Section 3.2.3. Furthermore, an experiment where a certain motion platform was simulated on another one is presented in Section 3.2.4. Finally, the implications on a benchmarking test found with this literature are discussed in Section 3.2.5.

3.2.1. Roll Tracking Task

Firstly, Jex et al. [10] performed an experiment on the Dynamic Environment Simulator, which can be seen in Figure 3.6. The effects of several types of motion washout filters on pilot roll tracking behavior were investigated. The simulator is a centrifuge, as is described in [31], however for the experiment in question only the roll degree of freedom was used. In the experiment four well-trained non-pilot participants had to follow a target roll angle, while also suppressing a disturbance, both sitting upright and in a supine position. The latter allowed to remove the effect of the gravity vector generating false tilt cues. Then, a year later, another simulator, the Large Amplitude Multi-Mode Aerospace Research Simulator, described in [32], was used to replicate this experiment [33]. The results were similar, implying that a second simulator could be used in performing a task with similar outcomes. Most notably, the use of a cybernetic approach allowed to ascertain that the subjects made use of the same control strategy. The non-pilot subjects in the first study used the same strategy as the pilots in the second study. The main practical conclusion of these two experiments was that the DES could substitute for for LAMARS, as DES was more easily available. Hence, with the purpose of benchmarking, in this two-simulator comparison, a standard was proven to exist which allowed to compare results between the simulators.

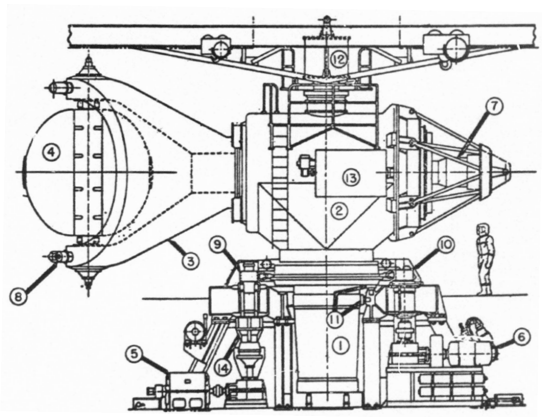

Figure 3.6: DES [31]

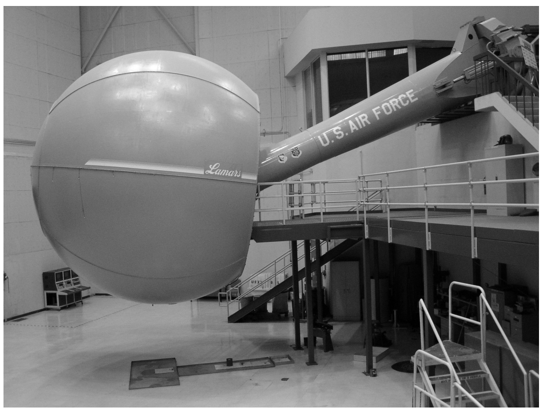

Figure 3.7: LAMARS [34]

The controlled dynamics of the LAMARS experiment were adapted to include some of the DES dynamics [33], page 5: the first experiment revealed *"a simulator-drive mode having a frequency of 10 rad/s and damping-ratio of 0.37 was unavoidably present."* This means that the dynamics of the DES simulator were included in the controlled element as shown in Equation 3.1.

$$Y_c(s) = \frac{\phi}{\text{control force } c} = \frac{15000}{s \cdot \underbrace{\left(1+\frac{s}{1.7}\right)}_{\text{Roll subsidence}} \cdot \underbrace{\left(1+\frac{s}{5.0}\right)}_{\text{Servo lag}} \cdot \underbrace{\left(1+\frac{2\cdot(0.37)\cdot s}{10.0}+\frac{s^2}{10.0^2}\right)}_{\text{DES mode}}} \frac{[\text{deg}]}{[\text{lb}]} \tag{3.1}$$

From a benchmarking point of view, there is also information absent, such as the visual field of view and the manipulator characteristics. However, the results could be compared since it was found that pilots behaved similarly. Hence, it seems of importance to characterize the behavior of pilots. Looking back at the criteria proposed before, the cybernetic approach used in this series of two experiments allows for a "verifiable" set of results. The task is "fair" and allowed participants to perform equally and is "repeatable" with the same results.

3.2.2. Series of Helicopter Experiments

The second example deals with a series of experiments following from a helicopter yaw capture task. The incentive for the series of yaw capture experiments was a study by Meiry [35], where a yaw disturbance rejection task was performed. Three participants controlled a first order system in three experimental conditions: only visual feedback, only vestibular feedback and combined visual and vestibular feedback. It was found that pilot time delay decreased with yaw motion present, compared to visual feedback only. However, Schroeder performed two experiments on the NASA VMS (Figure 3.8) which yielded results that contradicted these findings [36, 37]: In a disturbance rejection task and a yaw capture task no beneficial effects of yaw feedback were found. Following these two experiments, Schroeder performed another set of experiments on the VMS, in order to investigate these conflicting findings [5]. Three helicopter yaw tasks were considered: a 180-degree turn, another yaw capture task and a disturbance rejection task. Pilots had to control all helicopter axes. Four conditions were performed: no motion, translational motion only, yaw (rotational) motion only and translation and yaw combined. Two objective measures were used: the number of target overshoots in the yaw capture task and the RMS of the pedal rate. Furthermore, the 6 pilots supplied some subjective data: the pilots rated the level of compensation and motion fidelity. The results from the three tasks were similar: no benefit from yaw motion was found in any of the tasks.

Hosman used his Descriptive Pilot Model to analyze the experimental results of Schroeder's study [38]. The offline analysis results largely support Schroeder's conclusions, indicating how theoretic models could be used to compare results of experiments. The found differences might have been due to unknown factors in the simulator setup, which were not present in the model. Hosman's analysis was executed in parallel with another follow-up experiment in this series: the UTIAS (Figure 3.9) flight simulator study executed by Grant [39]. The analysis was readjusted with the results of this validation study. Hosman concludes that using offline analysis is a valuable tool to predict the effects of motion feedback.

In order to minimize the simulator differences, and to explore the possibilities of the tasks becoming benchmark tasks, several measures were taken to reproduce the VMS characteristics on the flight simulator of UTIAS. For instance, shaping filters were inserted between the aircraft model and the motion logic, in order to approximate the frequency response of the VMS. These shaping filters were determined via a trial-and-error procedure, with the goal of emulating the VMS response on UTIAS [39]. The low-order approximation of the VMS motion response was obtained from an earlier work by Schroeder [36], and can be seen in Equation 3.2. The shaping filter can be seen in Equation 3.3 and the resulting response can be seen in Figure 3.10.

$$\frac{\dot{\psi}_s}{\dot{\psi}_c} = \frac{11^2}{s^2 + s(0.6)(11)s + 11^2} \tag{3.2}$$

$$H_{shaping}(s) = \frac{10^2}{s^2 + 2(0.6)(10)s + 10^2} \frac{0.08s+1}{0.001s+1} \tag{3.3}$$

The three helicopter tasks were replicated and executed by three test pilots. The results were similar to what Schroeder originally found, with a difference being that a significant effect of yaw on performance was found. It was speculated that the differences might be due to one of three factors. Firstly, the number of pilots

Figure 3.8: VMS [40]

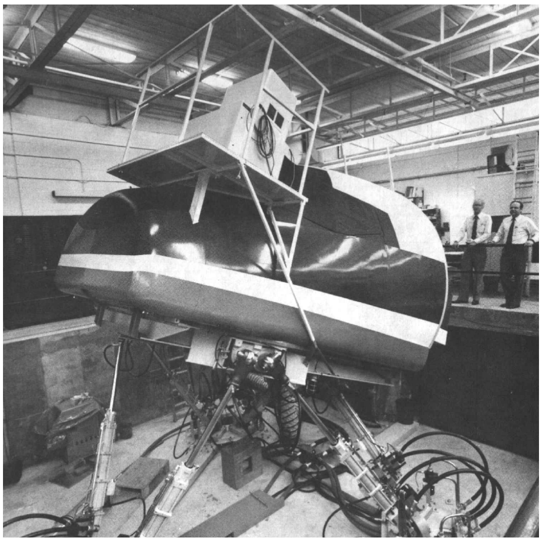

Figure 3.9: UTIAS flight simulator [41]

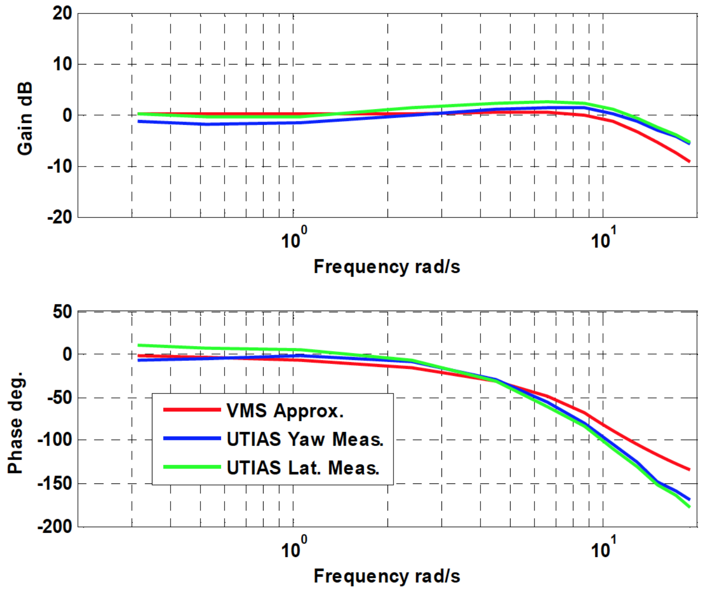

Figure 3.10: UTIAS and VMS motion responses, as found in [39]

in this study was lower (three versus six in the original). Secondly, the fact that pilots are usually recruited in groups and different groups might control differently could have played a role. Thirdly, the different simulators might have contributed to the differences. For example, the nature of the motion system (electric driving in the VMS and hydraulic in UTIAS). Therefore Grant concludes in [39], page 15: *"The study demonstrates the difficulty in repeating experiments at different facilities. It is a large effort and there are often simulator differences that cannot be eliminated."* From a benchmarking point of view it already becomes apparent that factors such as the pilot type or the briefing become highly relevant.

Ellerbroek et al. took on this challenge and attempted another replication of Schroeder's experiment on the SIMONA Research Simulator [42, 43], located at Delft University of Technology (Figure 3.12). The yaw capture task and the target tracking task with turbulence were repeated, but only in the yaw tracking task the characteristics of the VMS were replicated. The same low order approximation as in the UTIAS experiment (Eq. 3.2) was used to represent the VMS motion response and here as well shaping filters were applied to match the VMS dynamics, both in rotational as in translational degrees of freedom, which consisted of two parts, as indicated by Equation 3.4.

$$H_{shaping}(s) = H_{SRS}^{-1}(s) \cdot H_{app}(s) \tag{3.4}$$

The $H_{SRS}(s)$ term represents the inverse of the SRS motion system dynamics, which Ellerbroek et al. approximated using a second-order low-pass filter and a time delay [43]:

$$H_{SRS}(s) = \frac{n_a s^2 + n_b s + 1}{d_a s^2 + d_b s + 1} \cdot e^{-\tau_d s} \tag{3.5}$$

$$H_{app}(s) = \frac{n_a s^2 + n_b s + 1}{d_a s^2 + d_b s + 1} \tag{3.6}$$

However, only the low-pass filter is used and the time delay was accounted for in $H_{app}(s)$. Using frequency sweeps and minimizing the difference between $H_{SRS}(s)$ and the measured frequency response $\tilde{H}_{SRS}(s)$ using a quadratic cost function, the SRS dynamics were approximated. Then, $H_{app}(s)$ was determined by minimizing the quadratic cost function in Equation 3.7, where $\theta = [n_a, n_b, d_a, d_b]$.

$$J(\theta) = \sum_{s=\omega_0}^{\omega_1} \left| H_{SRS}^{-1}(s) \cdot H_{app}(s,\theta) \cdot \tilde{H}_{SRS}(s) - H_{VMS}(s) \right|^2 \tag{3.7}$$

$H_{VMS}(s)$ represents the low-order VMS approximation in Equation 3.2.

The results of this experiment replication largely support the prior experiments. The paper is concluded with the following statement [43], page 14: *"Although motion systems can be matched relatively well with shaping filters, differences that are not captured with a linear model, such as actuator noise and parasitic accelerations, can be significant and can influence experimental results."* Furthermore, it is noted that extra attention should be paid to the selection of the human participants. Even though the facilities were documented well, the differences between individual human subjects, and even subject types, will remain highly variable in simulator comparisons.

Other than adapting the motion logic with shaping filters such that the simulators approximated the VMS motion response, the previous experiments looked at other differences between the facilities as well. For instance, the visual system was compared. The results can be seen in Figure 3.11. In the SRS, an additional time delay was added to match the VMS visual system. The controlled dynamics were chosen to be equal in the three replications: all representing a low order model for an unaugmented AH-64 helicopter in hover, as can be seen in Equation 3.8.

$$\frac{\psi^{ab}}{\delta_p} = \frac{19.45}{s(s+0.27)} \tag{3.8}$$

Using these relatively simple controlled dynamics, a realistic experiment task could still be constructed. Hence, from an economical perspective, the use of this kind of controlled vehicle is favourable, as it is easy to implement on different simulator devices.

As stressed before, also the pilot population was compared. However, due to the scarcity of test pilots, as used in Schroeder's original, Grant and Ellerbroek were not able to fully match the subjects used. The control device was compared as well to the VMS pedals: through a trial-and-error process the characteristics were matched. However, still large differences remained, especially between the VMS and the SRS, for instance in the force gradient.

The final paper that will be considered in this series of experiment repetitions, is the work of Hodge [44] at the University of Liverpool, using the HELIFLIGHT-R simulator (Figure 3.13). Although this experiment also had the goal of continuing the series of yaw capture tasks, it did so using different controlled vehicle dynamics and a short stroke hexapod motion system. In this initial study only one pilot was used. Because of these fundamental differences, the study mainly adds value to the results of the motion filter research question originally set out by Schroeder [5]: here as well the results were supported, albeit with a larger effect from platform translational motion than found before. However, from the perspective of benchmarking this study features some difficulties, as large differences in experimental setup remain. As suggested in [44], a follow-up study should feature more participants and perhaps another controlled vehicle, such that the effects of pilot position could become more clear and the results can be tied to previous work.

So since this series includes four experiments, it seems promising to look for conclusions on the problem of simulator benchmarking. And because the helicopter yaw capture task was repeated, some promising results to develop it further into a human-centered test for simulator benchmarking were present. Firstly, the

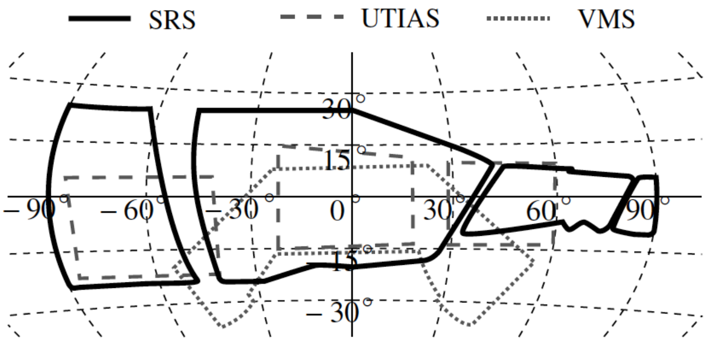

Figure 3.11: Hammer–Aitoff projection of the outside visual field of view of the VMS, UTIAS and SRS simulators [43]

Figure 3.12: SRS

Figure 3.13: HELIFLIGHT-R flight simulator [44]

task was relatively easy to implement in different simulators, due to the simple controlled dynamic. Furthermore, the vehicle dynamics and the task in general remain difficult enough to ensure the effects of motion were used by the participants. Several things in this experiment series should be taken into account for further studies attempting to set up simulator benchmarks. For example, a large visual database, with an airport and supporting structures, was used in the first experiment and hence required in all follow-ups. The fact that different simulators feature different visual characteristics complicated this even more. Moreover, only a helicopter task with the yaw pedals as inputs was present. This had a limited applicability for further operations in real life. Continuing on the task itself, it seemed that the pilot population was relevant for the results: the selected dependent variables were not insensitive for the different control strategies that might have been used. Also the briefing could have had an impact on how the participants opted to control. So perhaps it could be concluded that even though meticulous attention was spent on replicating the simulator characteristics, this series of experiments lacked a quantitative method to observe pilot control behavior more objectively. This is in contrast with the two experiments by Jex et al. [10, 33] seen before: here a cybernetic approach proved to be of great value to compare pilot behavior in different simulators.

3.2.3. De-crab Experiment

The final replication study that is discussed is a de-crab experiment, performed in 2005 by Groen [45, 46] on NLR's GEFORCE fighter simulator. Eleven pilots were asked to provide subjective ratings on a series of de-crab maneuvers. The pilots did not fly the task themselves. This experiment was repeated on the NLR GRACE simulator in 2017 [47] where 14 pilots were asked to perform the de-crab themselves. The results of the second experiment support the first: motion positively influences perceived motion fidelity. Because the pilots performed a control task in the second study, it could be concluded that motion also had a positive effect on performance. The absence of an active control task in the first experiment limits the applicability to drawing conclusions on simulator benchmarking to fit the criteria posed in the introduction of this chapter however.

3.2.4. Motion System Replication

Nieuwenhuizen et al. [48] performed an experiment in 2013 where a low-cost motion system (a Stewart platform simulator located at the Max Planck Institute in Germany) was simulated on a high-performance full-motion flight simulator (SRS). This study is interesting since it looked at the effects of approximating a certain simulator setup on another simulator with different characteristics. The study started with determining the frequency response of the low-cost Stewart platform. The motion response of this platform can be described with Equation 3.9 and includes a platform break frequency and a time delay [48]. The break frequency was set to $f_b = 1$ Hz by the manufacturer and the time delay was found to be $\tau = 35$ ms.

$$H_{MPI}(s) = \frac{1}{(1+\frac{1}{2\pi f_b})^2} \cdot e^{-\tau s} \tag{3.9}$$

This frequency response was approximated on the SRS. Apart from the pure frequency response of the low-cost platform, also its noise characteristics were determined separately and simulated on the SRS. The experiment had three independent variables: platform break frequency, time delay and noise presence. Each of these variables had two levels: SRS or Max Planck Stewart platform. This delivered 8 experimental conditions. No significant difference in performance due to the noise characteristics or the inherent simulator time delay was found in this experiment. The difference in motion response time delay between the simulators was $10ms$. The time delays of the pilot models were at least a factor 10 larger, which might explain the absence of a significant effect. Furthermore, Niewenhuizen et al. [48], page 9, conclude: *"platform noise characteristics could play an important role in detecting simulator motion in other types of experiments, such as measurements on motion thresholds of pilots."*.

3.2.5. Implications

Initially a simulator benchmark test has to be applicable for a large number of simulators and a large variety of subject types. However, in the initial proposal and design of such a task, in order to truly isolate the effects of the different simulators, it is important to verify that the participants operate in a similar manner. Some measure to do so are the selection of the type of participants and controlling environmental factors that might influence them. However, to fully make sure this is the case, analytic measures are required to quantify pilot control behavior and strategy. Participants have to be required to adopt the same strategy regardless of their type (test pilot, student, commercial pilot, etc.). The research of Jex et al. [10, 33] illustrates the importance of using such a method. A manual control tracking task which allows for pilot model estimation seems to be a promising direction to look for a task. Looking more closely at the simulator subsystems, the 5 criteria posed by Huppler [20] pose some requirements on the systems that are used, and the way in which they are used. The motion system, the visual system and the control device should be subject of investigation.

Firstly, in order to compare simulators and develop a benchmark for when different motion systems exist, the motion system needs to be equal in response and cues presented to the pilots. Several test exist to quantify simulator motion, of which the OMCT is a recent but proven option. Secondly, since for many simulators the visual system is designed in a different manner, or with a different goal in mind, this could give rise to unintended influences in simulator comparisons. Because the visual system is the host of vast differences, a proposed initial benchmarking study might focus on head-down displays. These are easier to control and compare, especially if simple (yet realistic) display graphics are used. A full simulator benchmark should include all visual systems, however. Thirdly, the pilots interact with the control device to perform the task. This device is their main interface to interact with the system and hence deviations between simulators can give rise to unintended differences. The characteristics of the control device thus need to be known and made equal.

Even with all these factors described, all repeated experiment series considered in this section revealed the difficulties of performing comparative studies using flight simulator. Above all, therefore, it is vital that in the development of the benchmark test all steps and considerations are well documented. The next section proposes a research question following from the conclusion presented here.

3.3. Research Question

In the previous sections general requirements for scientific benchmarks were discussed, followed by a schematic overview of a pilot in a flight simulation task. The overview allowed to identify crucial elements of the system as a whole which need to be analyzed and compared, in order to perform a comparison at simulator level. Then, a review of experiments found in literature was presented. This review allowed to distill characteristics to develop a simulator comparison task. For example, in order to verify that participants operate in a similar manner, especially in multiple simulators, a method to characterize pilot control behavior is necessary. Multiple experiments illustrate that a cybernetic approach, using a tracking task for example, could be of value [5, 10, 33, 39, 43, 44, 46, 48]. Hence, the following research question arose: *"To what extent can a tracking task be used as a benchmark test for simulator motion fidelity comparisons?"*

In order to answer this research question, an experiment using a tracking task is proposed. This experiment is developed such that it can be executed on two simulators. By performing an experiment on the VMS and replicating it on the SRS it can be investigated how well the task holds up as a benchmarking task to compare flight simulators. In order to develop this experiment further a preliminary experiment was performed. Chapter 4 presents the experiment design and discusses the results. From these results a final experiment is proposed, in Chapter 5.

4

Preliminary Experiment

In order to look into the research questions for the two topics, that were posed in Sections 2.4 and 3.3 respectively, a preliminary experiment was proposed. Firstly, Section 4.1 discusses the setup of this experiment, and the work on which it is based. Secondly, the conditions that were flown, a theoretical model and subsequent hypotheses are presented, in Sections 4.2, 4.3 and 4.4, respectively. Then, this chapter presents two iterations of this preliminary experiment that were performed, in Section 4.5 and 4.6, respectively. Finally, the results and recommendations for future work are discussed.

Conducting a preliminary experiment is important for several reasons: firstly, it allows to collect and analyze data, as it would be done in the final experiment, aiding in identifying mistakes in the process and reasoning. Secondly, it provides a preview for the results of the final experiment: an opportunity for a sanity check. Conducting a preliminary experiment thus serves to improve the process and quality of a final experiment with a larger sample of participants.

4.1. Experiment Setup

The literature study indicated the importance of a quantitative method to compare pilot control strategies in a flight simulator comparison. In 2016, Zaal and Zavala [15] performed an experiment on the VMS where the effect of heave cues on pilot manual control behavior was investigated. The results indicated that motion cuing with more pitch heave compared to center of gravity heave, results in pilot manual control behavior more similar to full aircraft motion. In order to minimize the development time and effort of an experiment on two separate simulators, this work was chosen as a basis for the preliminary experiment. The model-based cybernetic method allowed to estimate multi-modal visual-vestibular pilot control models and hence provides a way to characterize pilot control behavior.

The task that participants performed in [15] is presented in Figure 4.1. Participants were asked to minimize the pitch error e, which was presented on a compensatory display, by making inputs with a side stick control device. The display represented a simplified version of a primary flight display. Using the side stick pilots generated control inputs u. A stick gain K_s was present, which was set to $K_s = 0.8$ in the original experiment. The inputs acted on the pitch dynamics transfer function $H_\theta(s)$, which subsequently outputted the pitch angle θ. In addition to the visual error, which is the difference between the target signal f_t and the system output θ, the participants also perceived motion cues. In the original experiment the motion cues were a mix of pitch, pitch heave and heave cues. The difference is explained by Figure 4.2: the pilot sat a distance $l_{x_{PS}} - l_{x_{ICR}}$ in front of the aircraft instantaneous center of rotation, which gave rise to the pitch-heave cues. The center of gravity of the aircraft was subject to heave accelerations $a_{z_{CG}}$ and finally the pilot also perceived the actual pitch angle accelerations $\ddot{\theta}$ of the aircraft.

In [15] the motion filter $H_{mf}(s)$ and heave components were varied. For the preliminary experiment of this thesis, however, only the motion filter was varied. The pilot perceived the motion cues resulting from this filter. Together with the visual cues, and a remnant signal n, a human operator model can be constructed. Finally, two forcing functions were present which allowed to identify this human operator model. The remainder of this section goes more into depth on all individual elements of Figure 4.1.

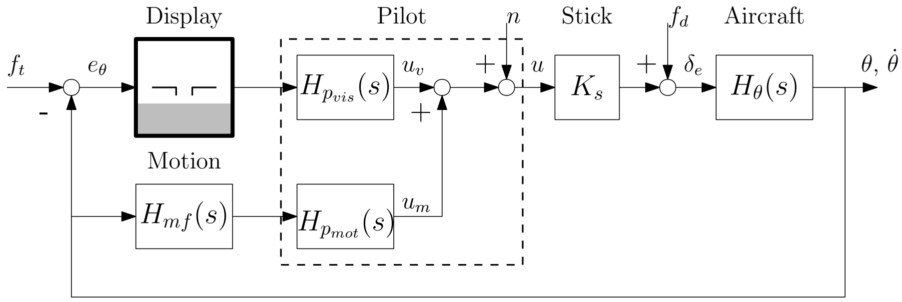

Figure 4.1: Pitch control task

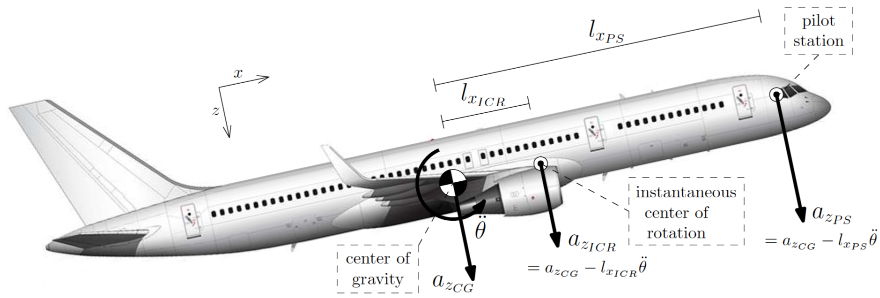

Figure 4.2: Aircraft pitch, pitch-heave and heave motion during a pitch control task, as found in [15]

Controlled Dynamics The controlled dynamics are defined in Equation 4.1. They represented a mid-size twin-engine commercial transport aircraft with a weight of 185,000 lbs, trimmed close to its stall point at 41,000 ft and with an airspeed of 150 kts [15]. Around the frequencies in which a human operator typically controls, these controlled dynamics resembled a double integrator. This resulted in a fairly difficult acceleration based task.

$$H_\theta = \frac{\theta}{\delta_e} = \frac{28.4474 \cdot \left(346.5s^2 + 32.03s + 1\right)}{\left(245.6s^2 - 3.409s + 1\right) \cdot \left(2.105s^2 + 0.9387s + 1\right)} \tag{4.1}$$

In the original experiment, the experimental conditions varied the CG heave, the CG pitch-heave, the ICR heave and the ICR pitch-heave, each with their own response functions [15]. Removing all of these heave degree of freedom responses would have resulted in an unrealistic task. For the purpose of simplicity, while retaining realism, it was decided to only include ICR pitch-heave in the proposed preliminary experiment. The ICR pitch-heave response to pitch variations is defined in Equation 4.2.

$$H_{a_{z_{\theta,ICR}}} = \frac{a_{z_{\theta,ICR}}}{\theta} = -37.685s^2 \text{ [ft]} = -11.49s^2 \text{ [m]} \tag{4.2}$$

Equation 4.2 shows that the pilot station was located 37.685 ft in front of the instantaneous center of rotation. The negative is present to account for the direction of the reference frame: the z-axis pointed downwards.

Human Operator Model In order to investigate the control behavior of the human operator, linear transfer functions were estimated for both the visual and the motion channel, as depicted in Figure 4.1. McRuer [30] states that a human operator adjust his or her control behavior to the controlled dynamics such that the open loop response approximates a single integrator near the crossover frequency. For the controlled dynamics of Equation 4.1, the human operator thus needed to generate lead in the region of the crossover frequency. Hence, the pilot visual and motion responses are defined by Equation 4.3 and 4.4, respectively.

$$H_{p_{vis}}(s) = K_v\,(1 + T_L s)\,e^{-\tau_v s}\,\frac{\omega_{nm}^2}{s^2 + 2\zeta_{nm}\omega_{nm}s + \omega_{nm}^2} \tag{4.3}$$

$$H_{p_{mot}}(s) = sK_m e^{-\tau_m s}\,\frac{\omega_{nm}^2}{s^2 + 2\zeta_{nm}\omega_{nm}s + \omega_{nm}^2} \tag{4.4}$$

These two equations, together with the remnant signal n, formed the human operator model. The equalization parameters were the visual gain K_v, the motion gain K_m and the lead time constant T_L. The limitation parameters were the visual time delay τ_v, the motion time delay τ_m and the neuromuscular parameters, the damping constant ζ_{nm} and frequency ω_{nm}.

As stated in [15], page 6: *"In the frequency domain, pilot performance in attenuating the target and disturbance signals is determined by the crossover frequencies and phase margins of the target and disturbance open-loop dynamics."* Looking at Figure 4.1, two open loop responses could be constructed, the target and disturbance, which can be seen in Equation 4.5 and 4.6, respectively.

$$H_{ol,t}(s) = \frac{\theta(s)}{E(s)} = \frac{H_{p_{vis}}(s) K_s H_\theta(s)}{1 + H_{mf}(s) H_{p_{mot}}(s) K_s H_\theta(s)} \tag{4.5}$$

$$H_{ol,d}(s) = -\frac{U(s)}{\delta_e(s)} = K_s H_\theta(s) \left[H_{p_{vis}}(s) + H_{mf}(s) H_{p_{mot}}(s) \right] \tag{4.6}$$

Forcing Functions Two forcing functions were present in the experiment, a target and a disturbance signal. Both were defined as sum-of-sines signals, according to Equation 4.7.

$$f_{t,d}(t) = \sum_{k=1}^{N_{t,d}} A_{t,d}(k) \sin\left[\omega_{t,d}(k) t + \phi_{t,d}(k)\right] \tag{4.7}$$

In Equation 4.7 $A_{t,d}(k)$, $\omega_{t,d}(k)$ and $\phi_{t,d}(k)$ represent the amplitude, frequency and phase of the k^{th} sine in the target and disturbance forcing functions f_t and f_d, respectively. The number of sine waves in these functions is represented by $N_{t,d}$. The forcing functions used in [15] and in the proposed preliminary experiment can be found in Table 4.1.

Table 4.1: Properties of the forcing functions, as found in [15]

target, f_t				disturbance, f_d			
n_t, –	ω_t, rad/s	A_t, deg	ϕ_t, rad	n_d, –	ω_d, rad/s	A_d, deg	ϕ_d, rad
3	0.2301	0.5818	-1.4796	2	0.1534	0.0105	0.1355
6	0.4602	0.5306	-0.0745	5	0.3835	0.0098	-0.1664
13	0.9971	0.3711	0.7006	11	0.8437	0.0091	2.9016
27	2.0709	0.1674	-1.9563	23	1.7641	0.0283	5.6383
41	3.1447	0.0901	-2.8131	37	2.8379	0.0403	2.8648
53	4.0650	0.0605	2.1026	51	3.9117	0.0477	4.8718
73	5.5990	0.0375	-2.6178	71	5.4456	0.0569	1.0245
103	7.9000	0.0238	2.2550	101	7.7466	0.0725	5.0337
139	10.6612	0.0174	-0.6739	137	10.5078	0.0967	4.1487
194	14.8796	0.0135	0.1942	191	14.6495	0.1458	0.4274

The frequencies used in these sinusoids were all integer multiples $n_{t,d}$ of the measurement time base frequency, $\omega_m = 2\pi/T_m = 2\pi/81.92$ s $= 0.0767$ rad/s. The runs lasted 90 seconds, but only the last 81.92 seconds of data were used. The integer multiples were selected to ensure that the range of human control was covered.

To determine the amplitudes and the phases, the following procedure was performed in [15]: Both the variance of the target and of the disturbance function were scaled to 0.4 deg^2. This relative strength delivered a challenging but not too difficult task. In order to achieve this, a second order low-pass filter was used to reduce the amplitudes at the higher frequencies. The phase distributions were selected from a large set of random phases. The phase sets were checked to be sufficiently normally distributed and to have average crest factors.

Participant, Procedure and Apparatus For the proposed preliminary experiment only one participant performed all experimental conditions. Having only one participant inhibited the ability to infer (statistically sound) conclusions. However, for the purposes of this preliminary experiment it is sufficient. The participant had knowledge of the conditions and experimental goal. The SIMONA Research Simulator located at Delft University of Technology was used for the preliminary experiment.

Dependent Measures The goal of the preliminary experiment was to investigate in what manner the order of the motion washout filter influences the control behavior of the human operator. Hence, human control behavior and performance parameters were the variables of interest. From the control loop shown in Figure 4.1, the Root Mean Square of the error signal e and control signal u could be determined. The RMS_e was a measure of performance; a lower RMS_e signified a lower error score and hence a better performance. The RMS_u was a measure of control activity; a higher RMS_u indicated a higher control activity. Furthermore, the pilot model defined in Equations 4.3 and 4.4 featured seven dependent variables: K_v, K_m, T_L, τ_v, τ_m, ζ_{nm} and ω_{nm}. These parameters were estimated using a time-domain parameter estimation technique, based on maximum likelihood estimation [19]. In this technique, a genetic algorithm provided an initial estimate for the parameters, which was subsequently refined by a gradient based Gauss-Newton estimation. The Variance Accounted For (VAF) is a measure of how much of the control signal u can be explained by the linear pilot model transfer functions. Finally, the open loop crossover frequencies and phase margins for both the target and disturbance signal were determined, using Equations 4.5 and 4.6.

4.2. Preliminary Experiment Conditions

Figures 4.3 and 4.4 show the influence of both motion filter gain K_{mf} and motion filter break frequency ω_{mf} on the motion fidelity criteria K_S and Φ_S. Figure 4.3 shows that K_S is linearly dependent on the motion filter gain K_{mf}. Furthermore, Figure 4.4 shows that Φ_S is not dependent on K_{mf} at all. However, both figures show an influence of ω_{mf}. Looking at the derivative of Φ_S over ω_{mf}, Figure 4.5, it can be seen that the range of 0.0 rad/s to 1.0 rad/s is highest; most change is observed here. Thus, for the preliminary experiment break frequencies of 0.0 rad/s, 0.5 rad/s and 1.0 rad/s are chosen. The gains are chosen equal to these values. Table 4.2 shows the overview of conditions for the (first) preliminary experiment. Because one of the purposes is to identify the effects of the individual parameters in the filter (ie. K_{mf} and ω_{mf}), the number of conditions is high. These conditions spanned the three motion fidelity regions, as can be seen in Figure 4.6.

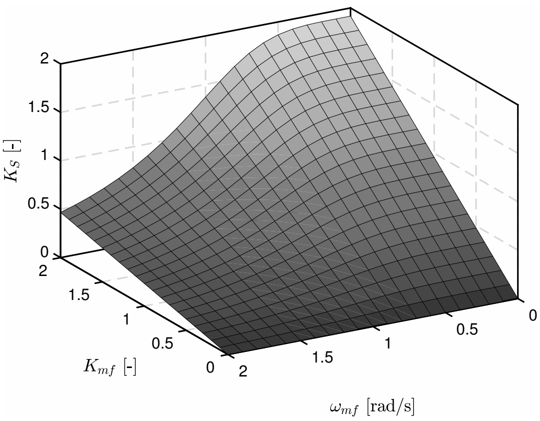

Figure 4.3: The effects of K_{mf} and ω_{mf} on K_S

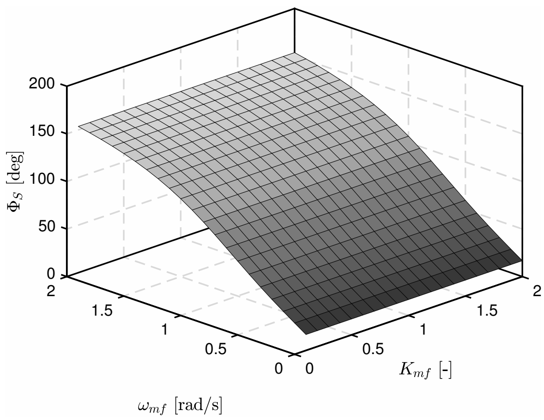

Figure 4.4: The effects of K_{mf} and ω_{mf} on Φ_S

For the purpose of simplicity, the first preliminary experiment only used pitch motion in most conditions. In the final experiment, to add realism to the task, ICR pitch-heave is present. However, if only pitch would have been varied, while keeping the ICR pitch-heave motion filter constant, the participants would have increasingly relied on pitch-heave for lower fidelity pitch conditions and less on pitch angle. Therefore, to eliminate this confounding factor, also four conditions where pitch-heave was varied were present. These conditions aim to identify the effects of adding ICR pitch-heave and have the same motion filter as the pitch angle. For all filters, the damping constant was set to $\zeta_{nm} = 0.7$ and the third order frequency to $\omega_b = 0.3$ rad/s.

4.3. Prediction of Effects on Pilot Model Parameters

With the experiment conditions known, the effects on the pilot model parameters of the different motion conditions were predicted using Equations 4.8 to 4.13, as presented in [2]. This served two purposes. Firstly, it aided in hypothesizing the effects of the different conditions on the pilot control behavior. Secondly, it proved to be an opportunity to verify the prediction equations in this context, such that they can be used

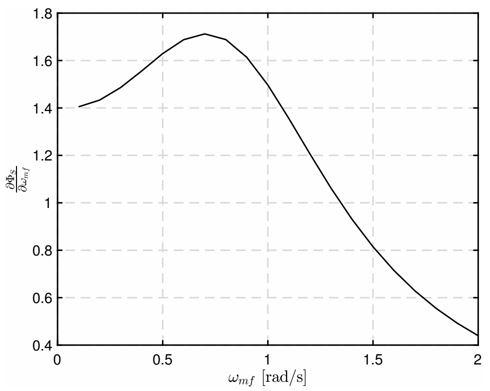

Figure 4.5: Derivative of motion filter phase at 1 rad/s $\frac{\partial \Phi_S}{\partial \omega_{mf}}$

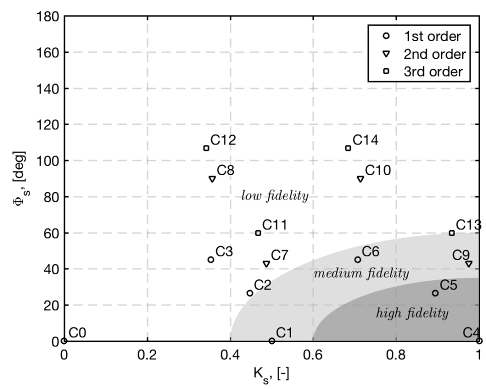

Figure 4.6: The motion filter conditions of the preliminary experiment shown on a motion fidelity plot, as proposed by [4] and [5]

Table 4.2: Conditions for preliminary experiment in SRS

Condition	Order	K_{mf} [-]	ω_{mf} [rad/s]	Heave	K_S [-]
0	No motion	0.0	0.0	-	0.0000
1	1	0.5	0.0	-	0.5000
2	1	0.5	0.5	-	0.4472
3	1	0.5	1.0	-	0.3536
4	Full motion	1.0	0.0	-	1.0000
5	1	1.0	0.5	-	0.8944
6	1	1.0	1.0	-	0.7071
7	2	0.5	0.5	-	0.4874
8	2	0.5	1.0	-	0.3571
9	2	1.0	0.5	-	0.9747
10	2	1.0	1.0	-	0.7143
11	3	0.5	0.5	-	0.4668
12	3	0.5	1.0	-	0.3421
13	3	1.0	0.5	-	0.9336
14	3	1.0	1.0	-	0.6842
15	Full motion	1.0	0.0	yes	1.0000
16	1	0.5	1.0	yes	0.3536
17	2	0.5	1.0	yes	0.3571
18	3	0.5	1.0	yes	0.3421

in the final experiment as well. Pool et al. were not able to find a relation dependent on K_S for K_m, τ_m, ζ_{nm}, $\omega_{c,t}$ and $\varphi_{m,t}$. All of the prediction equations below are dependent on K_S. For all conditions of the preliminary experiment K_S can be seen in Table 4.2 Furthermore, each equation features a $K_S = 1$ parameter, which determines the baseline full-motion level of the parameter. The value can be obtained from literature, which is done in [3] for example.

$$K_v(K_S) = K_v(1)\,[0.19\,(K_S - 1) + 1] \tag{4.8}$$

$$T_L(K_S) = T_L(1)\,[-0.29\,(K_S - 1) + 1] \tag{4.9}$$

$$\tau_v(K_S) = \tau_v(1)\,[0.069\,(K_S - 1) + 1] \tag{4.10}$$

$$\omega_{nm}(K_S) = \omega_{nm}(1)\,[0.058\,(K_S - 1) + 1] \tag{4.11}$$

$$\omega_{c,d}(K_S) = \omega_{c,d}(1)\,[0.23\,(K_S - 1) + 1] \tag{4.12}$$

$$\varphi_{m,d}(K_S) = \varphi_{m,d}(1)\,[-0.10\,(K_S - 1) + 1] \tag{4.13}$$

However, even though a previous experiment is present on which the predictions could be based, it was decided to solve for the parameters analytically. Firstly, because this added an extra step of verification, but mostly because the experiment by Zaal and Zavala [15] differed in some ways. For example, in the preliminary SRS experiment, no CG heave is present, as this would require a motion space comparable to the VMS. Equation 4.14 and 4.15 show that the absolute of the target and disturbance open loop is equal to 1 at the crossover frequency. By assuming certain parameters in the pilot model, these equations allow to solve for the others. Equation 4.16 is proposed after observing this relation in the results of previous experiment using pilot models, [3, 49] for example. It is not a strict relation, but it does allow to compute predictions of the parameters. Before attempting this, however, some assumptions as to the used pilot model needed to be made.

$$\left|H_{ol,t}(j\omega)\right|_{\omega=\omega_{c,t}} = \left|\frac{K_s \cdot H_{p_{vis}}(j\omega) \cdot H_\theta(j\omega)}{1 + K_s \cdot H_{p_{mot}}(j\omega) \cdot H_\theta(j\omega)}\right|_{\omega=\omega_{c,t}} = 1 \tag{4.14}$$

$$\left|H_{ol,d}(j\omega)\right|_{\omega=\omega_{c,d}} = \left|\left[H_{p_{vis}}(j\omega) + H_{p_{mot}}(j\omega)\right] \cdot K_s \cdot H_\theta(j\omega)\right|_{\omega=\omega_{c,d}} = 1 \tag{4.15}$$

$$K_v \cdot T_L = K_m \tag{4.16}$$

Firstly, in [15] the stick gain $K_s = 0.8$, but in the preliminary experiment it was set to $K_s = 1.6$, to achieve adequate control authority. The neuromuscular parameters were assumed to be $\zeta_{nm} = 0.35$ and $\omega_{nm} = 8.5$ rad/s. The visual time delay $\tau_v = 0.4$ s and the motion time delay $\tau_m = 0.2$ s. Assuming both crossover frequencies $\omega_{ol,t}$ and $\omega_{ol,d}$ and solving for K_v, K_m and T_L proved difficult, as no real solution exists for this set of equations. By assuming $\omega_{c,t} = 1.3$ rad/s and $K_m = 0.05$, Equation 4.14 and 4.16 could be solved for K_v and T_L. These assumptions originate from [15]. No prediction equations for K_m and $\omega_{ol,t}$ exist: the effects of the different motion conditions on these two parameters are thus not predicted and they can be assumed without hindering the further analysis. Solving Equation 4.14 and 4.16 with these assumed parameters lead to a solution with $K_v = 4.927$ deg and $T_L = 0.6394s$. Both correspond to the results of [15]. Hence, for the first iteration of the preliminary experiment predictions of the motion filter order effects could be made using Equations 4.8 to 4.13. The results of the prediction equation are directly shown compared to the results of the first iteration of the preliminary experiment in Section 4.5.

4.4. Preliminary Experiment Hypotheses

The preliminary experiment has two objectives: Firstly, it functions as a sanity check to see if any of the theoretical results can be observed in practice. Secondly, it is performed to narrow the focus for an actual experiment.

Two hypotheses are proposed for the preliminary experiment to meet these objectives. Firstly, in Figure 4.6, the distribution of conditions for this selection of motion filter gains and break frequencies, can be observed to show more interaction mainly over the Φ_S axis. Figures 4.3 and 4.4 support this and show that Φ_S is dependent on ω_{mf} and not dependent on K_{mf}. The fidelity regions in Figure 4.6 show that higher filter orders move the conditions into lower motion fidelity regions, leading to the second hypothesis.

1. Changing the motion filter break frequency has a larger interaction in influencing human control behavior than changing the motion filter gain.
2. With increasing motion filter order, a human operator will show:
    a. worse performance
    b. more control activity
    c. less contribution of motion feedback on his or her behavior

4.5. First Iteration

For the first preliminary experiment, only condition C0, C4, C15, C17, C18, C3, C8 and C12 were flown (in that order). The reason for this is that without any heave motion present, the participant reported to reel little to no motion at all in most filtered conditions. Some of the results are presented here. It was chosen to only use the prediction results for the heave conditions, as the pilot models were more accurate here.

Figure 4.7 shows the pilot model visual gain K_v. Apart from C15, which is the heave full-motion condition, the heave conditions show notably higher visual gains than the pitch-only conditions. Figure 4.8 shows the pilot model lead time constant T_L. C15 allows the pilot to generate the least lead. The no motion condition C0 requires most lead by the pilot. All heave conditions show lower T_L's. The predictions made with Equation 4.9 match the experimental results well, with only a relatively constant offset due to the initial assumption.

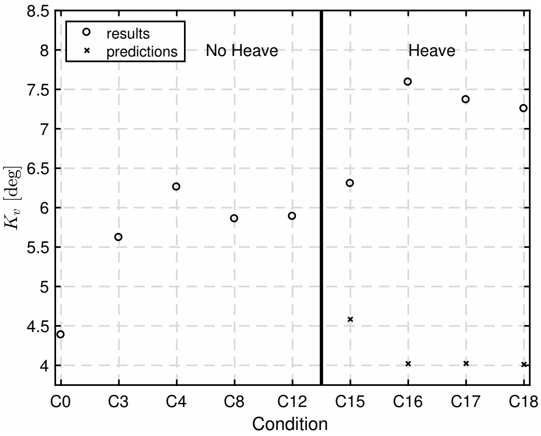

Figure 4.7: Pilot model visual gain K_v of the first preliminary experiment

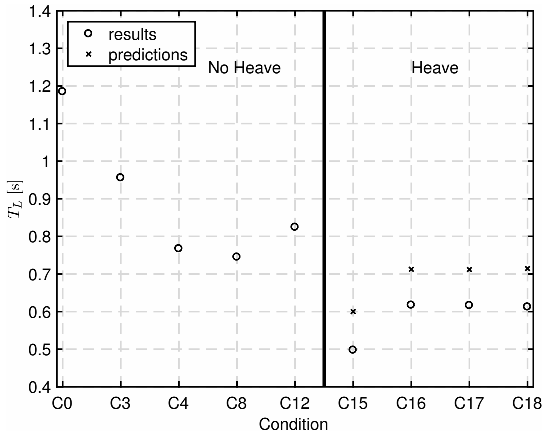

Figure 4.8: Pilot model lead time constant T_L of the first preliminary experiment

Figure 4.9 shows the motion time delay τ_m. In this figure, it can be seen that in the conditions with heave motion the time delay is relatively constant between conditions. The pitch-only full motion condition C4 also lies on this level. All time delays are relatively small. However, in this preliminary experiment only one subject performed the task and this subject has substantial experience on this type of task. To verify these results, the pilot model frequency responses were compared to analytically computed Fourier Coefficients. The frequency responses followed the Fourier Coefficients, as can be seen in Figure 4.11 and 4.12, which shows the pilot model and Fourier Coefficients for C15. Furthermore, the Variance Accounted For of C4, and C15 to C18 is 90%. The motion time delay illustrates that in the conditions without heave being present, the pilot models could not be estimated. The τ_m of condition C3 falls far beyond the axis of this figure. This result was verified by inspecting the frequency response of the models. The participant in the simulator indicated that in condition C3, C8 and C12 hardly any motion was present. Figure 4.10 also indicates this: the conditions with heave motion deliver larger phase margins and the conditions without heave have a phase margin close to the no-motion condition C0.

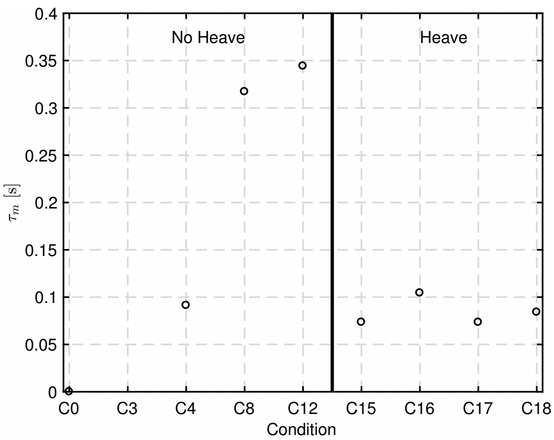

Figure 4.9: Pilot model motion time delay τ_m of the first preliminary experiment

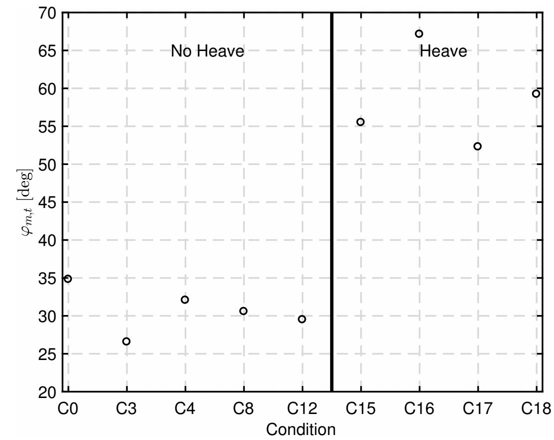

Figure 4.10: Open loop target phase margin $\varphi_{m,t}$ of the first preliminary experiment

The motion in the conditions without heave was not large enough to allow for the identification of pilot models. Because of the limited number of conditions that was flown, it was not possible to reflect on the hypotheses for this preliminary experiment. For the second iteration of the preliminary experiment, condition

C0 to C14 of Table 4.2 were flown with both pitch and ICR heave using the same motion filter.

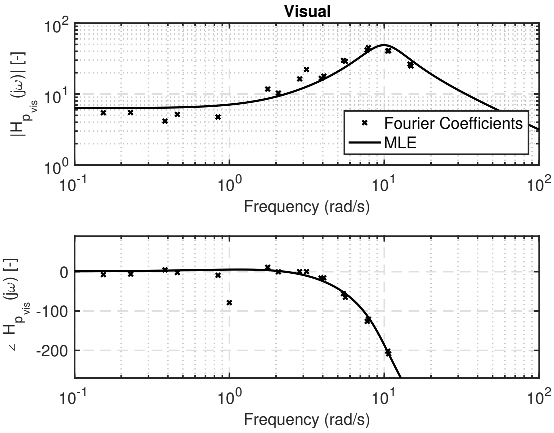

Figure 4.11: First preliminary experiment C15 visual pilot model and Fourier Coefficients

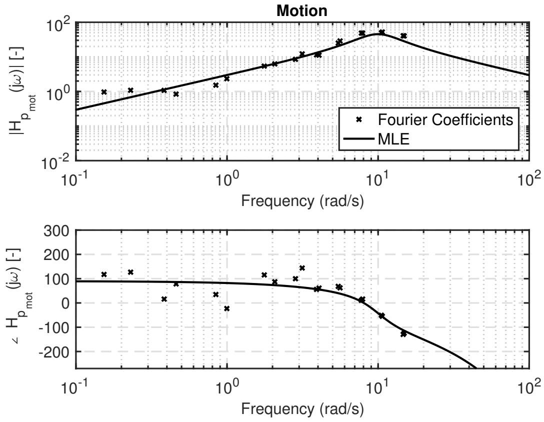

Figure 4.12: First preliminary experiment C15 motion pilot model and Fourier Coefficients

4.6. Second Iteration

Using the conclusions from the first preliminary experiment iteration, a second series of measurements was taken on SRS. The conditions from Table 4.2 and Figure 4.6 were re-used, with the addition of ICR heave motion for every condition. The heave filter is the same as the pitch filter. This made conditions C15, C16, C17 and C18 obsolete and hence these were omitted. The results of C15 from the first iteration were used as $K_S = 1$ values in the prediction equations for the second iteration.

In order to select the signal for the identification, and to investigate the effects that might have been caused by the difference between the simulator body frame F^{sb} and the simulator inertial frame F^{si}, the VAFs of six different identification signals were compared. Figure 4.13 shows the VAF of the pilot models for six different identification signals: three in the simulator body frame of reference F^{sb} (θ, q and $\dot{q}$) and three in a reference frame parallel to the earth F^{si} (z, $\dot{z}$ and a_z). The difference between the two reference frames is the transformation matrix of Equation 4.17, which transforms the earth frame to the body frame [50]. Only the pitch angle rotation is relevant, as the other two euler angles are fixed. In Figure 4.13 it can be seen that the pilot models identified with the pitch rate q show the highest VAF's for most conditions. However, most movement comes from the heave degree of freedom. To investigate the effect that the change of reference frame might have, the pilot models from these six signals were used to simulate the response and calculate the VAF with the corresponding data in the other reference frame. The results for the pitch rate pilot model on $\dot{z}$ data and vice versa are shown in Figure 4.14. This figure shows that the reference frame lowers the VAF of the pilot model fits by several percents. For the pitch rate q model on the $\dot{z}$ data, the effect is smaller than 5% in most conditions. Furthermore, for the $\sin\theta$ and $\cos\theta$ elements in the transformation matrix a small angle approximation was valid. For the remaining data analysis it was thus chosen to use the pitch rate q for the identification.

$$\mathbb{T}_{bE} = \begin{bmatrix} \cos\theta & 0 & -\sin\theta \\ 0 & 1 & 0 \\ \sin\theta & 0 & \cos\theta \end{bmatrix} \tag{4.17}$$

Figure 4.15 shows the pilot performance in terms of the RMS_e. The no-motion condition C0 shows the highest RMS_e. The best performance is in C4, which is the full-motion condition. Both the gain and break frequency show an influence on the performance. Figure 4.16 shows the pilot control activity in terms of the RMS_u. The control activity remained relatively constant throughout the experiment.

In order to isolate the contribution of motion, using the identified pilot models, simulations of the control signal u in both the motion and visual channel were made. In the block diagram in Figure 4.1, RMS_{u_v} and RMS_{u_m} can be found after the pilot models. Figure 4.17 shows the results. Generally, when filter order increases, the motion channel control activity RMS_{u_m} appears to decrease somewhat. This effect is small though. Figure 4.18 shows the fraction of the variance of the motion control signal over the visual control

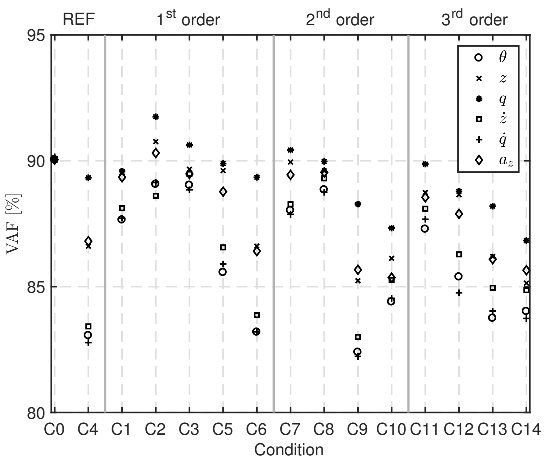

Figure 4.13: VAF of pilot models using different identification signals

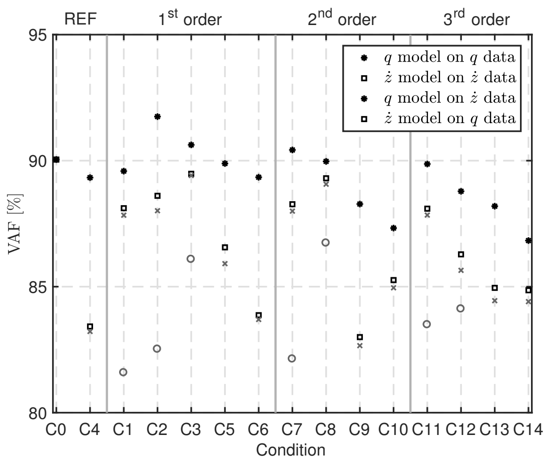

Figure 4.14: VAF of pilot models identified in different reference frames

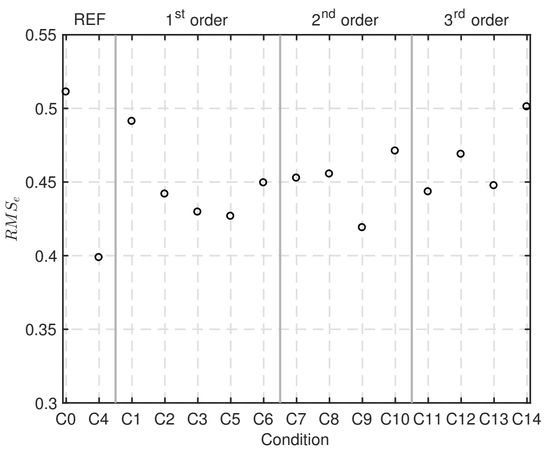

Figure 4.15: RMS_e

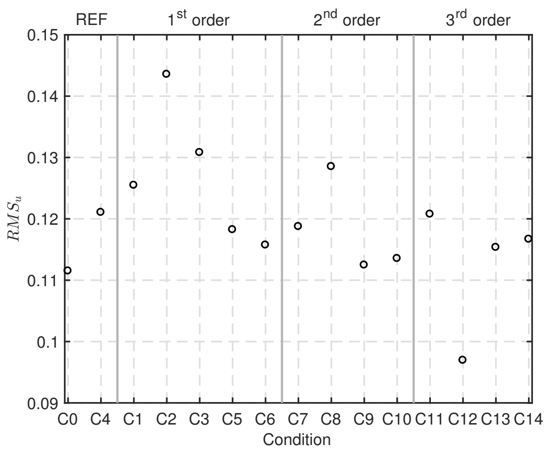

Figure 4.16: RMS_u

signal variance. This metric allows to look at the use of motion versus visual information. In the full motion condition C4 most motion is used, as indicated by the highest percentage. The figure shows a trend of decreasing use of motion with increasing filter order, except when condition C3, C8 and C12 are compared.

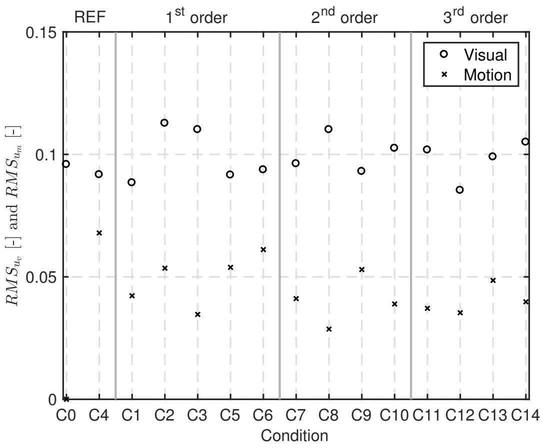

Figure 4.17: RMS_u of visual channel and of motion channel separated

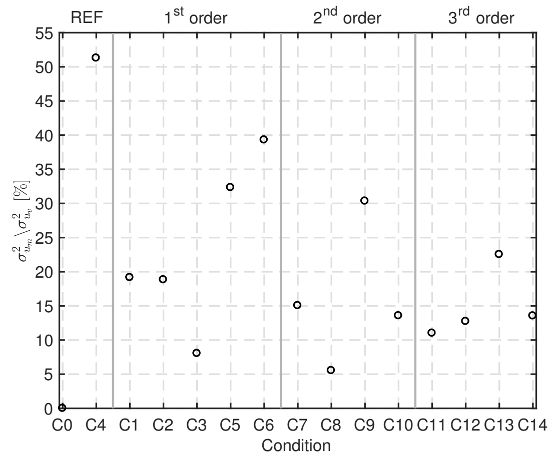

Figure 4.18: Control signal u variance fractions of visual and motion channel

Figure 4.19 shows the pilot model visual gain K_v together with the results of the prediction equations. It can be observed that the experimental results show higher gains than were predicted. Furthermore, for conditions where the break frequency was changed, larger interactions were seen in the experimental results than in the predictions, for example comparing C7 with C8 and C9 with C10. Figure 4.20 shows the pilot model motion gain K_m. Apart from condition C12, increasing the motion filter order shows a decrease in K_m.

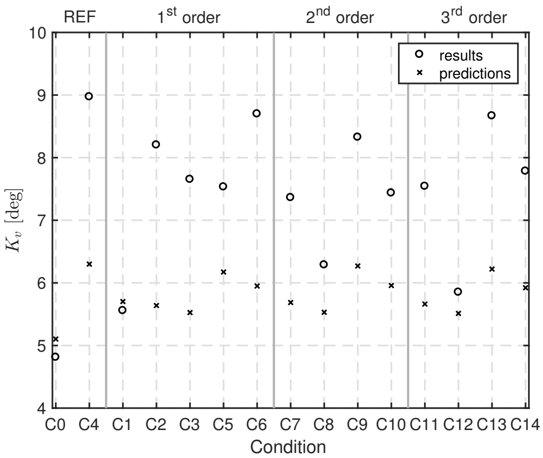

Figure 4.19: Pilot model visual gain K_v

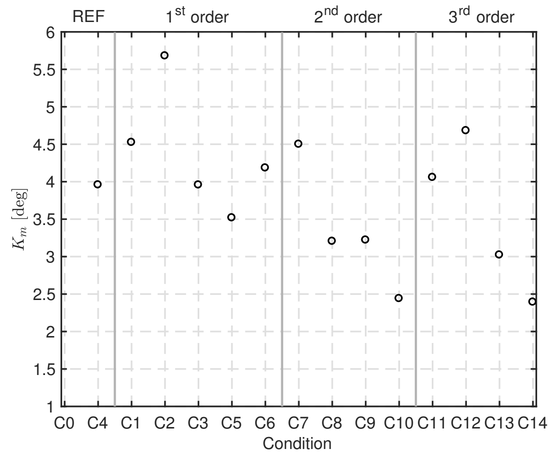

Figure 4.20: Pilot model motion gain K_m

Figure 4.21 shows the pilot model lead time T_L together with its predictions. The pilot has to generate most lead in the no-motion condition C0 and least lead in the full-motion condition C4. Little influence of motion filter order is seen in this figure. The predictions match with the experimental results relatively well in C2, C3, C7, C9, C11 and C13. All these conditions have a motion filter gain of $K_{mf} = 0.5$. However, when changing the motion filter break frequency of these conditions, much larger differences between the predicted values and experimental results are observed, for example in C8 and C12.

Figure 4.22 shows the visual time delay τ_v and Figure 4.23 shows the motion time delay τ_m. Both time delays show relatively constant results over the experimental conditions. Similar to the first preliminary experiment, the motion time delay is relatively small. However, the same participants performed the runs. This participant had very substantial experience in performing such tasks.

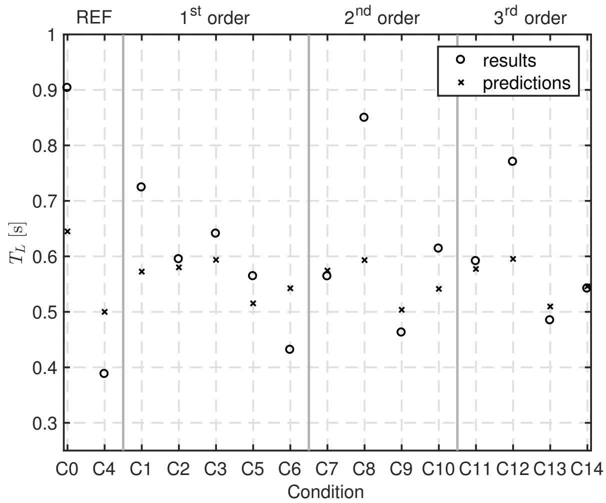

Figure 4.21: Pilot model lead time constant T_L

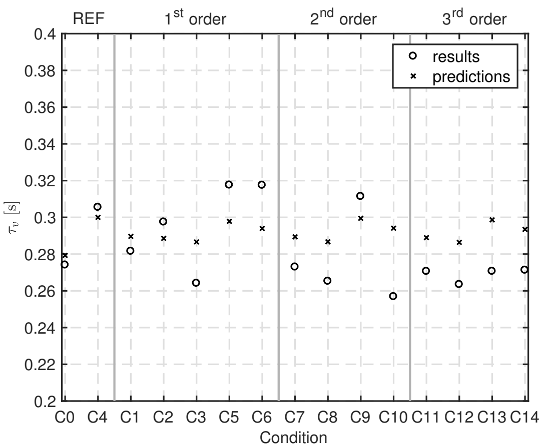

Figure 4.22: Pilot model visual time delay τ_v

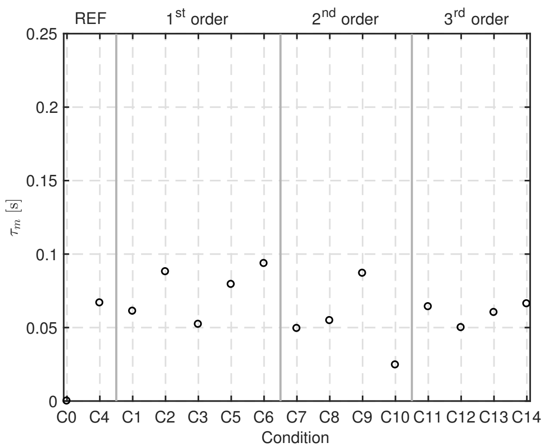

Figure 4.23: Pilot model motion time delay τ_m

Figure 4.24 shows the neuromuscular damping constant: it is relatively constant over the conditions. Figure 4.25 shows the neuromuscular frequency and its predictions. It can be observed that the larger interactions than predicted are present when the break frequency is adapted over the condition for condition C11 compared to C12 and C13 to C14 for example.

Figure 4.26 shows the target open-loop crossover frequency. No effects of motion filter order become clear from this data. Figure 4.27 shows the disturbance open-loop crossover frequency, with its predictions. The predicted effects seem to counteract the experimental results. No immediate effect of motion filter order can be identified. Furthermore, the motion filter gain appears to influence the crossover frequency more than the break frequency.

Figure 4.28 shows the target phase margin. Apart from C12, this figure shows a decrease in phase margin with an increase in motion filter order. Figure 4.29 shows the disturbance phase margin and its predictions. The predictions show a higher phase margin for all conditions. This phase margin data does not allow to identify effects of motion filter order. Generally, changing the break frequency does show a larger interaction than predicted.

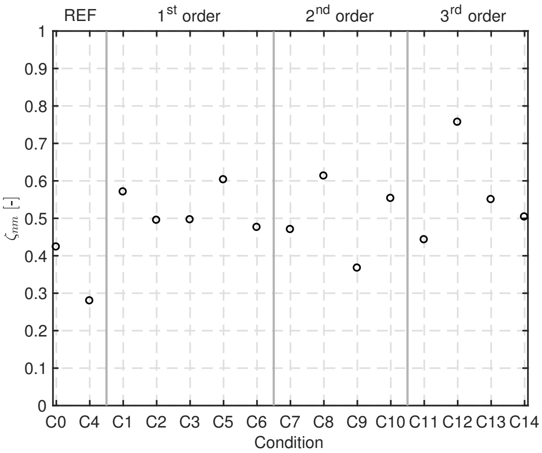

Figure 4.24: Pilot model neuromuscular damping constant ζ_{nm}

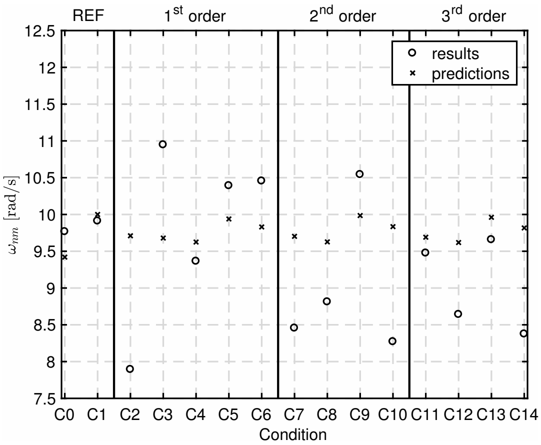

Figure 4.25: Pilot model neuromuscular frequency ω_{nm}

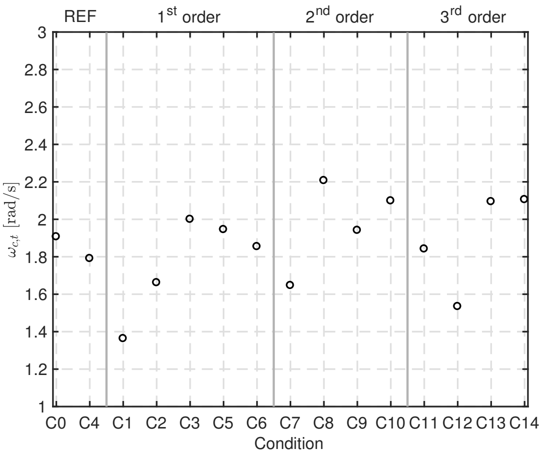

Figure 4.26: Open loop target crossover frequency $\omega_{c,t}$

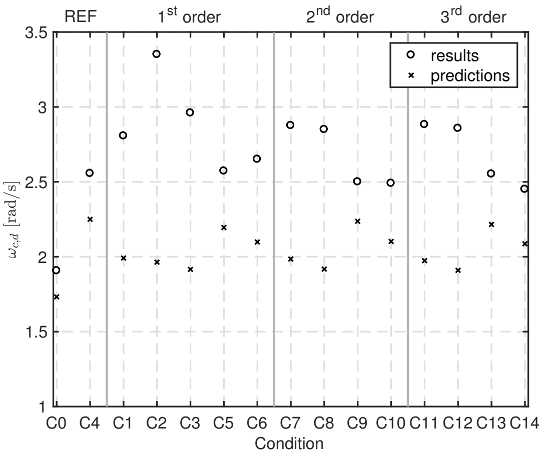

Figure 4.27: Open loop disturbance crossover frequency $\omega_{c,d}$

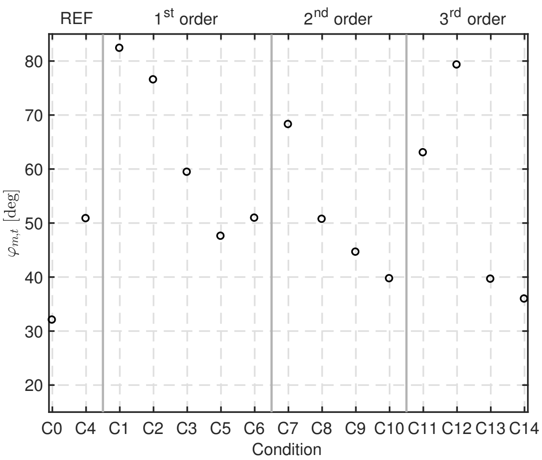

Figure 4.28: Open loop target phase margin $\varphi_{m,t}$

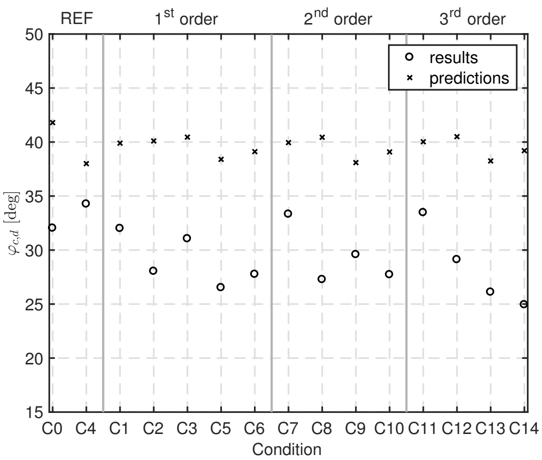

Figure 4.29: Open loop disturbance phase margin $\varphi_{m,d}$

4.7. Discussion

The results from the preliminary experiments gave some insights into the effects of the independent variables, which is discussed in this section. Then, using these results, several recommendations for future research into motion filter orders were made. An experiment is proposed in Chapter 5 that follows from these recommendations and could be performed on two simulators, which would allow for comparing the results in a benchmarking context.

In both preliminary experiments only one participant was present, making it difficult to draw conclusions on the effects of motion filter order, gain or break frequency. However, when abnormal results in some of the conditions were disregarded, it was possible to reflect on the hypotheses posed in Section 4.4. Furthermore, the goal of the preliminary experiments was to see if any interaction of the three independent variables could be identified and to test the experimental setup before simulator resources are allocated in an intensive manner.

The results of both preliminary experiments were verified by computing the Fourier Coefficients and overlaying the pilot model frequency responses. For most cases, the identified models followed the Fourier Coefficients. However, for some conditions the fit was less: an example can be seen in Figure 4.30. Here it can be seen that the motion magnitude deviates from the Fourier Coefficients at the higher frequencies: the pilot model motion response has a lower magnitude. This behavior was only present in some conditions, however. Identification using all six signals shown in Figure 4.13, showed similar results. The effects of the reference frame was determined by using the identified models to compute the VAF in the complementary frame. Figure 4.14 shows that the frame only resulted in a VAF decrease of several percent. Hence, the lower estimated pilot model, compared to the Fourier Coefficients, at higher frequencies, might be due to the control strategy of the single participant: it was decided to continue the analysis using the data, since it did not conflict with the purpose of the preliminary experiment.

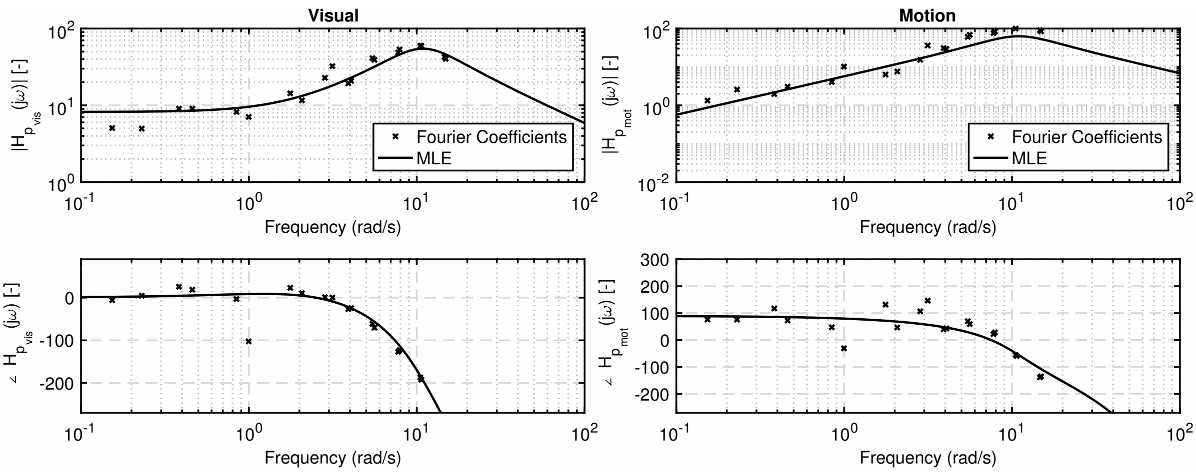

Figure 4.30: C2 pilot model frequency response and Fourier Coefficients

Using the parameter predictions and some of the results from the second experiment iteration, it was decided that Hypothesis 1 could be accepted: the motion filter break frequency showed more interaction on the results than the gain. The prediction equations presented in Section 4.3 depend on the motion filter only via the absolute of the motion filter at 1 rad/s, K_S, as explained in [2]. Hence, it is logical that the predicted results varied with motion filter gain and in a lesser manner with motion filter break frequency. However, in some conditions changing the motion filter frequency showed a larger interaction than changing the gain. Especially in the lead time constant T_L this was apparent. For this parameter the predictions of C7, C9, C11 and C13 matched the results. But when the break frequency was changed for these conditions, resulting in C8, C10, C12 and C14, larger variations than predicted were observed. Even when the predictions were disregarded, changing the break frequencies showed larger interactions than changing the gain in the final 8 conditions of the lead time constant. To some extent, the visual gain K_v showed similar effects. Hence, hypothesis 1 could be accepted. For a final experiment this means that the focus could lie on the motion filter break frequency ω_{mf} as a second independent variable, together with the motion filter order.

Looking at the effect of motion filter order separately, the RMS_e showed an increase with increasing filter order for most conditions. The lower fidelity motion that resulted from higher filter order apparently had a slightly degrading impact on performance. The control activity remained relatively constant with increasing filter order. This might be due to the participant having considerable experience with this kind of task. Also when looking at the simulated control activities of the motion and visual channels separated, the motion filter order effects could not be clearly identified. For the use of motion information versus visual information, Figure 4.18 shows a decreasing use of motion for increasing filter order. However, this was not true for all conditions. The fact that the participant was experienced with manual control tracking tasks might mean that a preferable control strategy had already formed, and hence less adaptation due to motion conditions was present.

Since increasing the motion filter order added phase distortion, a scenario where a participant might learn how to use this to enhance his or her performance is envisionable. This would translate into an increased performance in the higher motion filter order conditions, as compared to lower filter orders which induce less phase distortion. The results of the preliminary experiment did not indicate any such effects. However, the phase distortion is also dependent on the motion filter break frequency ω_{mf}, which is another reason to select this as a second independent variable.

The high phase distortions at lower frequencies might have a significant effect on the modelling quality of the pilot models. Furthermore, the VAF of this preliminary experiment indicates that relatively high percentages of the control signal can be explained by the chosen pilot model. No decrease of the VAF in the third order conditions was seen. However, since the phase distortions are large especially in the third order filters, in the final experiment this has to be verified as well, to ensure the pilot model structure is adequate.

Even though the use of a single participant limits the use of the data for the purpose of answering the hypotheses, the two goals of the preliminary experiment have been met. The task was tested and the results show effects of the independent variables. Furthermore, the focus was placed on motion filter order and motion filter break frequency using the results. The next section continues on this topic and proposes several recommendations for a final experiment into motion filter orders, which can be repeated on another simulator.

5

Recommendations for Future Experiment

An experiment into the effects of motion filter order is proposed which attempts to answer the question: *"How does changing the motion washout filter order influence human manual control behavior?"* Considering all the results from the preliminary experiment, the following two hypotheses relating to the effects of motion filter order are proposed for the experiment. Firstly, in both the analytic predictions as the preliminary experiment, the motion filter break frequency ω_{mf} showed more interaction on the results than the motion filter order. Furthermore, it is expected that with lower motion fidelity, the pilot will rely less on motion feedback. The behavior and performance are expected to be negatively impacted by lower fidelity motion.

1. Changing the motion filter order has a smaller interaction in influencing human control behavior than changing the motion filter break frequency.

2. With increasing motion filter order, a human operator will show:

   a. worse performance

   b. more control activity

   c. less contribution of motion feedback on his or her behavior

To link this experiment to simulator benchmarking, it is planned to perform it on two separate simulators. The following research question and hypotheses are appended to account for this element of the proposal: *"To what extent can a manual control tracking task be used as a benchmark for simulator fidelity comparisons?"* The hypotheses of this research question belong to a design approach and are therefore relatively difficult to measure objectively. If proven necessary after the experiment, they can be adapted to include other factors apart from these ones, which were the main factors of interest following from the literature review.

3. A manual control experiment executed on different simulators will show the same variations between conditions when care is taken to equalize the motion cues, the visual cues, the controlled dynamics, the control device, the participant type and the task itself.

4. A manual control tracking task can function as a human-centered baseline performance benchmark when care is taken to equalize the motion cues, the visual cues, the controlled dynamics, the control device, the participant type and the task itself.

For the final experiment it is proposed to make use of the same task as described in Section 4.1, with a condition matrix using two independent variables and eight conditions, such as Table 5.1. The conditions feature two extremes: a full-motion condition and a no-motion condition, which act as reference conditions for the simulator comparison. Between these two three filter orders with two frequencies each are proposed. The experiment is aimed to be performed by 16 general aviation pilots.

The two different motion filter break frequencies are $\omega_{mf_1} = 0.5$ rad/s and $\omega_{mf_2} = 2.0$ rad/s. To select them, the short period mode of the aircraft model was used as a reference, such that one of the conditions includes this motion and another filters it away. Figure 5.1 shows the frequency response of the aircraft model, with its short period mode and the selected frequency for the experiment. To find the second experimental motion filter break frequency, another was used: the mean OMCT results that are available in [23]. These

Table 5.1: Proposed experimental conditions

Condition	MF order	ω_{mf} [rad/s]
1	No motion: $H_{mf} = 0$	
2	1	0.5
3	1	2.0
4	2	0.5
5	2	2.0
6	3	0.5
7	3	2.0
8	Full motion: $H_{mf} = 1$	

OMCT results were also used in [6] for the selection of the motion fidelity criteria. They can be seen in Figure 5.2. The second motion filter break frequency was selected to be lie just above the break frequency of the mean OMCT filters, except for heave. The heave degree of freedom shows a notably higher break frequency in the mean OMCT results, which would have resulted in an unpractical experimental condition.

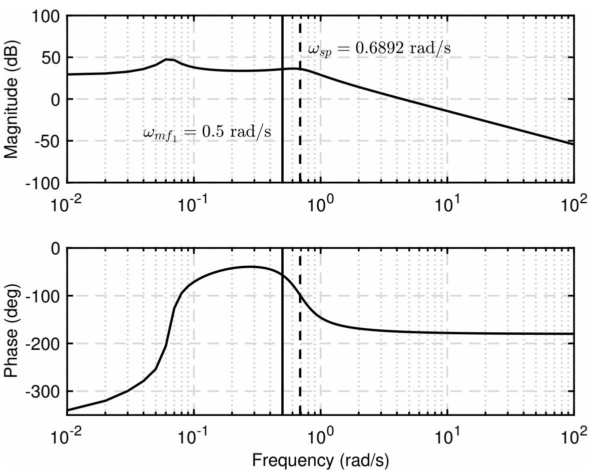

Figure 5.1: Controlled dynamics bode plot

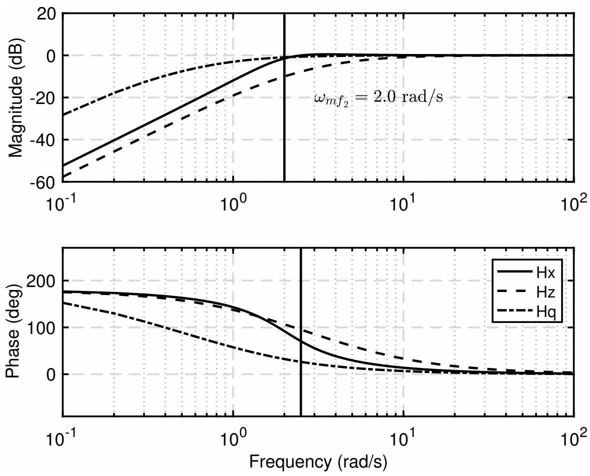

Figure 5.2: Mean OMCT results [6]

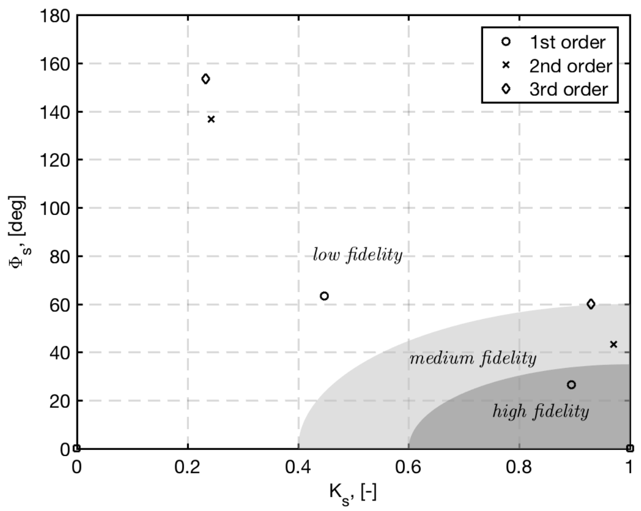

Figure 5.3: Eight proposed conditions on motion fidelity criteria plot

The data analysis will be similar to the one presented in this chapter. Using the same dependent variables allows to reflect on the hypotheses of the motion filter order experiment. Furthermore, even thought attention is paid to equalizing simulator cues between the two simulators, differences might still be present. The dependent variables following from the pilot models might help in identifying where these differences might originate from, such that in a following attempt into creating a benchmark this can be taking into account.

6 Preliminary Phase Conclusion

Human control flight simulation experiments have not been replicated frequently and no standard benchmark to compare results exists for this type of experiments. Furthermore, there has been little research directly looking at the effects of varying the motion filter order on pilot performance and behavior, while many filters of different orders exist in operational flight simulators. In literature, only one experiment with motion filters of different orders was found. However, no direct comparisons were made. Investigating a human-centered simulator benchmark by performing an experiment which looks into the order of motion filters combines these two research gaps.

Looking more closely at benchmarking, it was found to be complex problem where confounding factors can easily find their way into the experiment set-up. Some of the most important systems to compare between simulators are the motion system, the visual system and the control device. Furthermore, experimental factors such as the task, the participants and the procedures should be as similar as possible as well. In several experiment replications these factors have all (individually) been applied to experiment replications. It could thus be concluded that they provide a place to start to equalize simulator behavior. Five criteria for a benchmark task were derived from the domain of computer science. By taking into account the experiment replication factors found in literature in the proposed experiment plan, all five criteria are considered.

A cybernetic manual tracking task could function as a benchmark task, as it allows to compute pilot control behavior analytically, which is favorable to compare results. Hence, a manual control tracking task experiment is proposed which will be performed on two simulators to asses the suitability as a benchmark test. The task is a pitch target-disturbance manual tracking task. The independent variables of the experiment are motion filter order and motion filter break frequency, which followed from the results of two iterations of a preliminary experiment.

With this research, another step is taken in understanding commonly used motion washout filters, by focusing on the effects of their order. Furthermore, this thesis aims at developing a human-centered simulator benchmark, which can be used in future piloted flight simulation experiments to compare results to. Ultimately, a simulator benchmark aids in verifying experimental results, with the goal of understanding human-machine interaction challenges pilots face when operating aircraft.

Bibliography

[1] Royal Aeronautical Society, "Call for papers brochure: BENCHMARKING FOR IMPROVING FLIGHT SIMULATION," Online: http://www.raes-fsg.org.uk/uploads/170322020440_844_FSG%20June%2017_C4P.pdf, 2017.

[2] Pool, D. M., Damveld, H., van Paassen, M. M., and Mulder, M., "Tuning Models of Pilot Tracking Behavior for a Specific Simulator Motion Cueing Setting," *AIAA Modeling and Simulation Technologies Conference*, 2011.

[3] Pool, D. M., van Paassen, M. M., and Mulder, M., "Effects of Motion Filter Gain and Break Frequency Variations on Pilot Roll Tracking Behavior," *AIAA Modeling and Simulation Technologies Conference*, 2013.

[4] Sinacori, J. B., "The Determination of Some Requirements for a Helicopter Research Simulation Facility," Tech. rep., NASA-CR-152066, Systems Technology Inc., 1977.

[5] Schroeder, J. A., "Helicopter Flight Simulation Motion Platform Requirements," Tech. rep., NASA Ames Research Center, 1999.

[6] Zaal, P. M. T., Schroeder, J. A., and Chung, W. W., "Transfer of Training on the Vertical Motion Simulator," *Journal of Aircraft*, Vol. 52, No. 6, pp. 1971–1984, 2015.

[7] Stroosma, O., van Paassen, M. M., Mulder, M., Hosman, R. J. A. W., and Advani, S. K., "Applying the Objective Motion Cueing Test to a Classical Washout Algorithm," *AIAA Modeling and Simulation Technologies (MST) Conference*, 2013.

[8] Reid, L. D. and Nahon, M., "Flight Simulation Motion-Base Drive Algorithms: Part 1 - Developing and Testing the Equations," Tech. rep., UTIAS, 1985.

[9] Gouverneur, B., Mulder, J. A., van Paassen, M. M., Stroosma, O., and Field, E., "Optimisation of the SIMONA Research Simulator's Motion Filter Settings for Handling Qualities Experiments," *AIAA Modeling and Simulation Technologies Conference and Exhibit*, 2003.

[10] Jex, H. R., Magdaleno, R. E., and Junker, A. M., "Roll tracking effects of G-vector tilt and various types of motion washout," *The 14th Annual Conference on Manual Control*, pp. 463–502, 1978.

[11] Bray, R. S., "Visual and Motion Cueing in Helicopter Simulation," *TM-86818, NASA Ames Research Center*, 1985.

[12] Pool, D. M., Zaal, P. M. T., van Paassen, M. M., and Mulder, M., "Effects of Heave Washout Settings in Aircraft Pitch Disturbance Rejection," *Journal of Guidance, Control, and Dynamics*, Vol. 33, No. 1, pp. 29–41, 2010.

[13] Steurs, M., Mulder, M., and van Paassen, M. M., "A Cybernetic Approach to Assess Flight Simulator Fidelity," *AIAA Modelling and Simulation Technologies Conference and Exhibit*, 2004.

[14] Wieringen, A. T. V., Pool, D. M., van Paassen, M. M., and Mulder, M., "Effects of Heave Washout Filtering on Motion Fidelity and Pilot Control Behavior for a Large Commercial Airliner," *AIAA Modeling and Simulation Technologies Conference*, 2011.

[15] Zaal, P. M. T. and Zavala, M. A., "Effects of Different Heave Motion Components on Pilot Pitch Control Behavior," *AIAA Modeling and Simulation Technologies Conference*, 2016.

[16] Bergeron, H. P., "Investigation of Motion Requirements in Compensatory Control Tasks," *IEEE Transactionson Man-Machine Systems*, Vol. MMS-11, No. 2, pp. 123–125, 1970.

[17] van Gool, M. F. C., "Influence of Motion Washout Filters on Pilot Tracking Performance," *Piloted Aircraft Environment Simulation Techniques*, , No. AGARD-CP-249, pp. 19–1 – 19–5, 1978.

[18] Valente Pais, A. R., Pool, D. M., De Vroome, A. M., van Paassen, M. M., and Mulder, M., "Pitch Motion Perception Thresholds During Passive and Active Tasks," *Journal of Guidance, Control, and Dynamics*, Vol. 35, No. 3, pp. 904–918, 2012.

[19] Zaal, P. M. T., Pool, D. M., de Bruin, J., Mulder, M., and van Paassen, M. M., "Use of Pitch and Heave Motion Cues in a Pitch Control Task," *Journal of Guidance, Control, and Dynamics*, Vol. 32, No. 2, pp. 366–377, 2009.

[20] Huppler, K., *The Art of Building a Good Benchmark*, Springer Berlin Heidelberg, 2009, pp. 18–30.

[21] Oberkampf, W. L. and Smith, B. L., "Assessment Criteria for Computational Fluid Dynamics Validation Benchmark Experiments," *Proceedings of 52nd Aerospace Sciences Meeting*, 2014.

[22] Schroeder, J. A. and Grant, P. R., "Pilot Behavioral Observations in Motion Flight Simulation," *AIAA Modeling and Simulation Technologies Conference*, 2010.

[23] ICAO, "Document 9625, Volume 1, Attachement F: Frequency-Domain Motion Cueing System Performance Test," Tech. rep., ICAO, 2009. ISBN 978-92-9231-341-8, obtained online.

[24] Lean, D., Gerlach, O. H., Dusterberry, J. C., Erdmann, F., Falco, D., Koevermans, W. P., Staples, K. J., Vallee, J., and Kemmerling, P. T., "AGARD Advisory Report No. 144: Dynamics Characteristics of Flight Simulator Motion Systems," Tech. Rep. AGARD-AR-144, North Atlantic Treaty Organization, Advisory Group for Aerospace Research and Development, 1979.

[25] Sheridan, T., "Space teleoperation through time delay: review and prognosis," *IEEE Transactions on Robotics and Automation*, Vol. 9, No. 5, pp. 592–606, 1993.

[26] Miall, R. C. and Jackson, J. K., "Adaptation to visual feedback delays in manual tracking: evidence against the Smith Predictor model of human visually guided action," *Experimental Brain Research*, Vol. 172, No. 1, pp. 77–84, 2006.

[27] Allerton, D., *Principles of Flight Simulation*, 1st ed., John Wiley & Sons Inc, 2009.

[28] Pool, D. M., Mulder, M., van Paassen, M. M., and van der Vaart, J. C., "Effects of Peripheral Visual and Physical Motion Cues in Roll-Axis Tracking Tasks," *Journal of Guidance, Control, and Dynamics*, Vol. 31, No. 6, pp. 1608–1622, 2008.

[29] Stroosma, O., van Paassen, M. M., Mulder, M., and Postema, F., "Measuring Time Delays in Simulator Displays," *AIAA Modeling and Simulation Technologies Conference and Exhibit*, 2007.

[30] McRuer, D. and Jex, H., "A Review of Quasi-Linear Pilot Models," *IEEE Transactions on Human Factors in Electronics*, Vol. HFE-8, No. 3, pp. 231–249, 1967.

[31] Rogers, D. B., McCally, M., and Cappell, K. L., "The Dynamic Environment Simulator - A Multi-Environmental Man-Rated Centrifuge," Tech. rep., AIR FORCE AEROSPACE MEDICAL RESEARCH LAB WRIGHT-PATTERSON AFB OH, 1970.

[32] Haas, R., Hots, H., and Mills, G., "The Large Amplitude Multi-Mode Aerospace Research LAMAR Simulator," *Visual and Motion Simulation Conference*, 1973.

[33] Jex, H. R., Jewell, W. F., Magdaleno, R. E., and Junker, A. M., "Effects of Various Lateral-Beam Washouts on Pilot Tracking and Opionio in the Lamar Simulator," Tech. rep., AFFDLTR-79-3134, 1979.

[34] Jordan, H., "LAMAR Simulator Image," Online: http://www.wpafb.af.mil/News/Article-Display/Article/819130/afrl-helps-evaluate-safety-of-cold-weather-flight-ensemble/, 2014.

[35] Meiry, J. L., "The Vestibular System and Human Dynamic Space Orientation," Tech. Rep. CR-628, NASA, 1966.

[36] Schroeder, J. A., "Simulation motion effect on single axis compensatory tracking," *Proceedings of the AIAA Flight Simulation Technologies Conference*, 1993.

[37] Schroeder, J. A., “Evaluation of Simulation Motion Fidelity Criteria in the Vertical and Directional Axes,” *Journal of the American Helicopter Society*, Vol. 41, No. 2, pp. 44–57, 1996.

[38] Hosman, R. J. A. W., Grant, P. R., and Schroeder, J. A., “Pre and Post Pilot Model Analysis Compared to Experimental Simulator Results.” *AIAA Modeling and Simulation Technologies Conference and Exhibit*, 2005.

[39] Grant, P. R., Yam, B., Hosman, R. J. A. W., and Schroeder, J. A., “The Effect of Simulator Motion on Pilot’s Control Behavior for Helicoptor Yaw Tasks,” *AIAA Modeling and Simulation Technologies Conference and Exhibit*, 2005.

[40] Aponso, B. L., Beard, S. D., and Schroeder, J. A., “The NASA Ames Vertical Motion Simulator – A Facility Engineered for Realism,” *Royal Aeronautical Society Spring 2009 Flight Simulation Conference, London, UK*, 2009.

[41] Grant, P. R., “Motion characteristics of the UTIAS flight research simulator motion-base,” , 1986.

[42] Ellerbroek, J., Stroosma, O., Wentink, M., Groen, E., and Smaili, H., “Effect of Sway and Yaw Motion on Perception and Control: A Multi-Simulator, Follow-Up Study,” *AIAA Modeling and Simulation Technologies Conference and Exhibit*, 2006.

[43] Ellerbroek, J., Stroosma, O., Mulder, M., and van Paassen, M. M., “Role Identification of Yaw and Sway Motion in Helicopter Yaw Control Tasks,” *Journal of Aircraft*, Vol. 45, No. 4, pp. 1275–1289, 2008.

[44] Hodge, S., Perfect, P., Padfield, G., and White, M., “Optimising the yaw motion cues available from a short stroke hexapod motion platform,” *The Aeronautical Journal*, Vol. 119, No. 1211, pp. 1–21, 2015.

[45] Groen, E., Smaili, H., and Hosman, R. J. A. W., “Simulated Decrab Maneuver: Evaluation with a Pilot Perception Model,” *AIAA Modeling and Simulation Technologies Conference and Exhibit*, 2005.

[46] Groen, E. L., Smaili, M. H., and Hosman, R. J. A. W., “Perception Model Analysis of Flight Simulator Motionfor a Decrab Maneuver,” *JOURNAL OF AIRCRAFT*, Vol. 44, No. 2, pp. 427–435, 2007.

[47] Smaili, M. H., Jansen, H., Naseri, A., Groen, E., and Stroosma, O., “Pilot Motion Perception and Control During a Simulated Decrab Maneuver,” Tech. Rep. NLR-TP-2017-097, National Aerospace Laboratory (NLR), 2017.

[48] Nieuwenhuizen, F. M., Mulder, M., van Paassen, M. M., and Bülthoff, H. H., “Influences of Simulator Motion System Characteristics on Pilot Control Behavior,” *Journal of Guidance, Control, and Dynamics*, Vol. 36, No. 3, pp. 667–676, 2013.

[49] Pool, D. M., Zaal, P. M. T., Damveld, H., van Paassen, M. M., and Mulder, M., “Evaluating Simulator Motion Fidelity using In-Flight and Simulator Measurements of Roll Tracking Behavior,” *AIAA Modeling and Simulation Technologies Conference*, 2012.

[50] Mulder, J., van Staveren, W., van der Vaart, J., de Weerdt, E., de Visser, C., in t Veld, A., and Mooij, E., *Flight Dynamics: Lecture Notes*, Delft University of Technology, 2013.

[51] van Paassen, M. M. and Mulder, M., “Identification of Human Operator Control Behaviour in Multiple-Loop Tracking Tasks,” *IFAC Proceedings Volumes*, Vol. 31, No. 26, pp. 455–460, 1998.

[52] Sokal, R. R. and Rohlf, F. J., *Biometry: The Principles and Practices of Statistics in Biological Research*, W. H. Freeman, 1994.

[53] Scheirer, C. J., Ray, W. S., and Hare, N., “The Analysis of Ranked Data Derived from Completely Randomized Factorial Designs,” *Biometrics*, Vol. 32, No. 2, p. 429, 1976.

[54] Field, A., *Discovering Statistics Using SPSS (Introducing Statistical Methods series)*, Sage Publications Ltd, 2005.

[55] Toothaker, L. E. and Horng Shing Chang, “On "The Analysis of Ranked Data Derived from Completely Randomized Factorial Designs",” *Journal of Educational Statistics*, Vol. 5, No. 2, p. 169, 1980.

III

Appendices of Final Experiment

To be graded as part of AE5310 - Thesis Control and Operations

A

Detailed Analysis of Results

This appendix presents an overview of all the results of the final experiment. Firstly, in Section A.1, the procedure for verifying the pilot model parameters is presented. In the results of the paper, in Part I, two SRS pilots were omitted. Therefore, in Section A.2, the results of all experiment participants are presented. Four VMS pilots controlled with a notably larger control activity. To investigate their effects on the results, the results of the experiment with these four VMS pilots excluded are presented in Section A.3. In the final experiment a non-parametric statistical test was used, of which Section A.4 presents the procedure and a comparison with the results of an ANOVA. Finally, Section A.5 presents the estimated pilot model frequency responses of all participants.

A.1. Procedure for Verification of Pilot Model Estimates

Before the data analysis was commenced, a thorough investigation of all results was performed. By minimizing a quadratic cost function, pilot models were fitted through Fourier coefficients, which were calculated using the procedure described in [51]. Section A.5 presents all estimated pilot models and their respective fourier coefficients. All estimated pilot models were compared to their respective Fourier coefficients in order to identify the cases which required further attention. Several pilot model estimates were found which were incorrect or which required extra verification.

These cases were divided in three categories. The first category consisted of pilot model estimates with faulty parameters, such as incorrect estimates for the neuromuscular dynamics or time delays. The second category contained cases where the pilots used little motion, which was mainly visible in the estimates of K_m and τ_m. Finally, the third category contained a single cases where the VAF was 40%. Table A.1 presents the three categories and the cases within each category.

Pilot models were placed in the first category when one (or more) of the following criteria was true: $T_L > 2.0$ s, $\tau_v < 0.20$ s, $\zeta_{nm} > 1.0$, $\omega_{nm} > 14.8796$ rad/s (the highest frequency in the forcing functions), or when the pilot model frequency response was found to differ considerably from the Fourier coefficients. The pilot models were placed in the second category when the estimates for K_m was low or τ_m was disproportionately high, or when the frequency response showed a small contribution from the motion channel.

The three categories of Table A.1 required different approaches. For the cases in the first category, the faulty parameters were replaced with the estimates of the Fourier coefficient fit and the MLE algorithm was performed again with these "new" parameters fixed. Figure A.1 illustrates the differences between the initial result (MLE line), the Fourier coefficient fit (FC fit line) and the final pilot model (MLE via FC fit line) for SRS subject 1, condition 0. For all cases in this category acceptable final VAF results were found because of this procedure.

The cases in the second category were verified using the open-loop parameters, which could be calculated in two ways: by using the Fourier transformed signals and by using the pilot models (see Equations 4.5 and 4.6). Figure A.2 illustrates the similary in the found open-loop parameters for SRS subject 1, condition 1. Furthermore, once again, the pilot model frequency responses were compared to the Fourier coefficients, which resulted in the conclusion that for all cases in this category the pilot model estimates found by the MLE algorithm were correct and no further action was required to use them in the analysis. Table A.1 indicates that in the SRS these effects were present mainly in C4 and C6, which are both conditions with $\omega_{mf} = 2.0$ rad/s

Table A.1: Overview of faulty pilot model estimates

VMS		SRS	
Faulty pilot model parameters			
Subject and condition	Visible parameters	Subject and condition	Visible parameters
Subject 1, C0	ζ_{nm}, ω_{nm}	Subject 1, C0	$\zeta_{nm}, \omega_{nm}, T_L$
Subject 1, C6	ζ_{nm}, ω_{nm}	Subject 2, C0	ζ_{nm}, ω_{nm}
Subject 2, C6	ζ_{nm}, ω_{nm}	Subject 4, C0	ζ_{nm}, ω_{nm}
Subject 14, C0	T_L	Subject 9, C0	ζ_{nm}, ω_{nm}
		Subject 7, C6	ζ_{nm}, ω_{nm}
		Subject 9, C6	ζ_{nm}, ω_{nm}
		Subject 12, C6	ζ_{nm}, ω_{nm}
		Subject 14, C0	τ_v
Low motion usage			
Subject and condition	Visible parameters	Subject and condition	Visible parameters
Subject 4, C4, C6	τ_m	Subject 1, C1, C2, C4, C5, C6	K_m
Subject 6, all conditions	K_m	Subject 5, C4, C6	K_m
Subject 9, C6	K_m	Subject 7, C4, C6	K_m
Subject 10, all conditions	K_m	Subject 8, C4, C6	K_m
Subject 12, all conditions	K_m	Subject 14, C6	K_m
		Subject 17, C6	K_m
		Subject 18, C6	K_m
VAF (identifiability) problems			
Subject 4, C0	VAF of 40%	-	

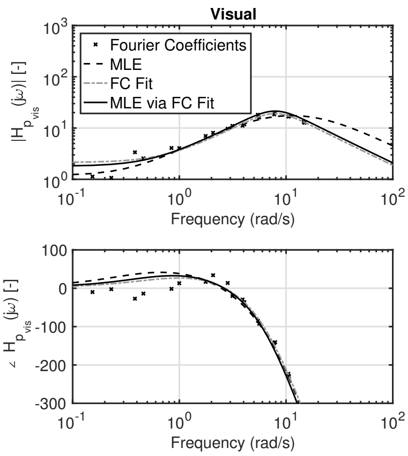

Figure A.1: Comparison of results with neuromuscular parameters fixed via Fourier coefficients

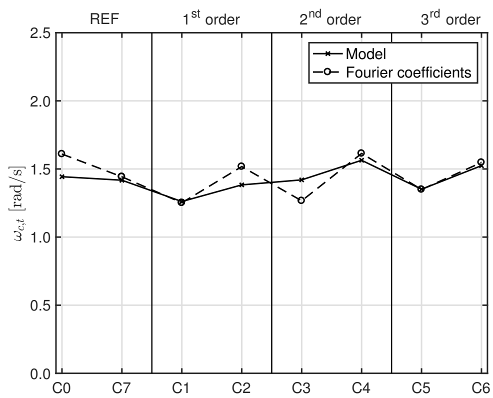

Figure A.2: Comparison of $\omega_{c,t}$ computed using Fourier coefficients and pilot model

and the lowest motion fidelity. In the VMS pilots displayed these effects also in the other conditions.

For the single case in the third category, in three of the five measurement runs the pilot made severe control errors, resulting in low performance. For this reason, the MLE algoritm was not able to estimate a pilot model with an adequate VAF. In the training runs preceding the measurement runs of the experiment this subject performed adequately, with a constant score. Hence, two of the three low-performance runs were replaced with runs from the training phase of the experiment. The resulting pilot model had a VAF of 82%.

A.2. Results of All Tested Participants

In the results of the scientific paper presented in Part I, two SRS pilots were omitted, due to the assumptions of the statistical test (see Section A.4). This section presents the results of all pilots of which pilot models could be estimated: 17 VMS pilots and 19 SRS pilots. The results are presented on both boxplots and 95% confidence interval (CI) plots. In both types of figures the mean and medians are indicated, with circles and horizonal dashes, respectively. Adding the two SRS pilots to the dataset did not alter the validity of the assumptions of the ANOVA, as compared to the results section of Part I.

A.2.1. Tracking Performance and Control Activity

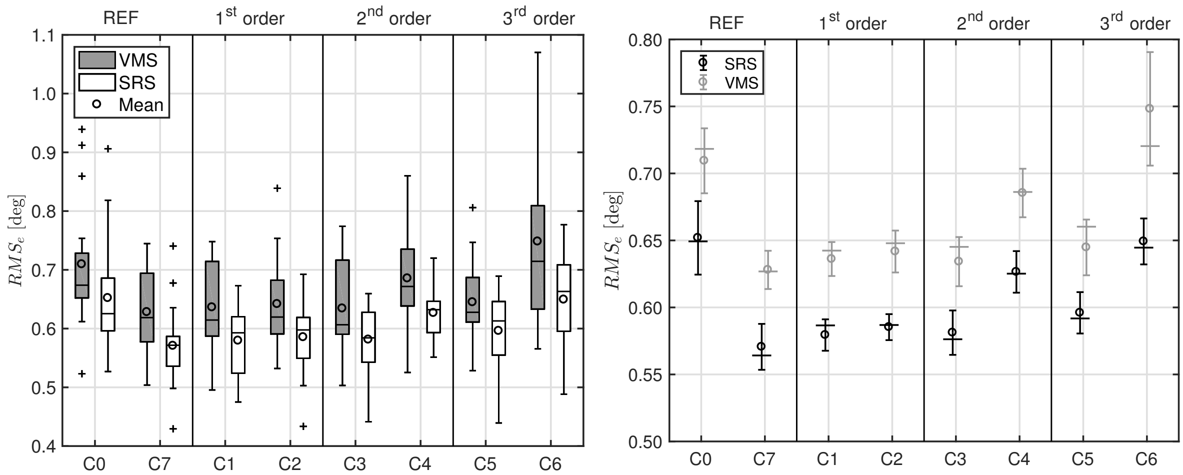

(a) boxplot (b) 95% CI plot

Figure A.3: RMS_e of all pilots

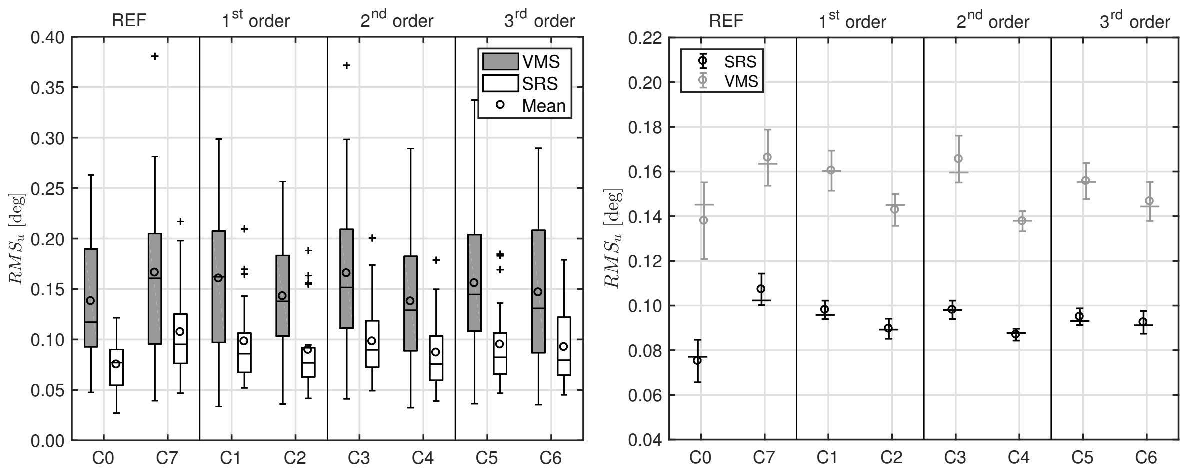

(a) boxplot (b) 95% CI plot

Figure A.4: RMS_u of all pilots

A.2.2. Pilot Model Parameters

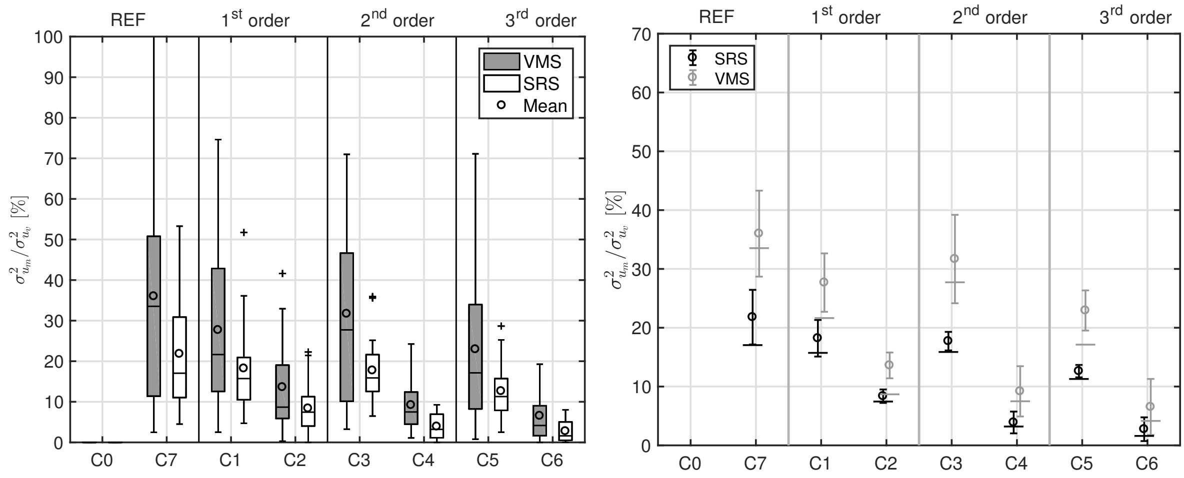

(a) boxplot (b) 95% CI plot

Figure A.5: $\sigma^2_{u_m}/\sigma^2_{u_v}$ of all pilots

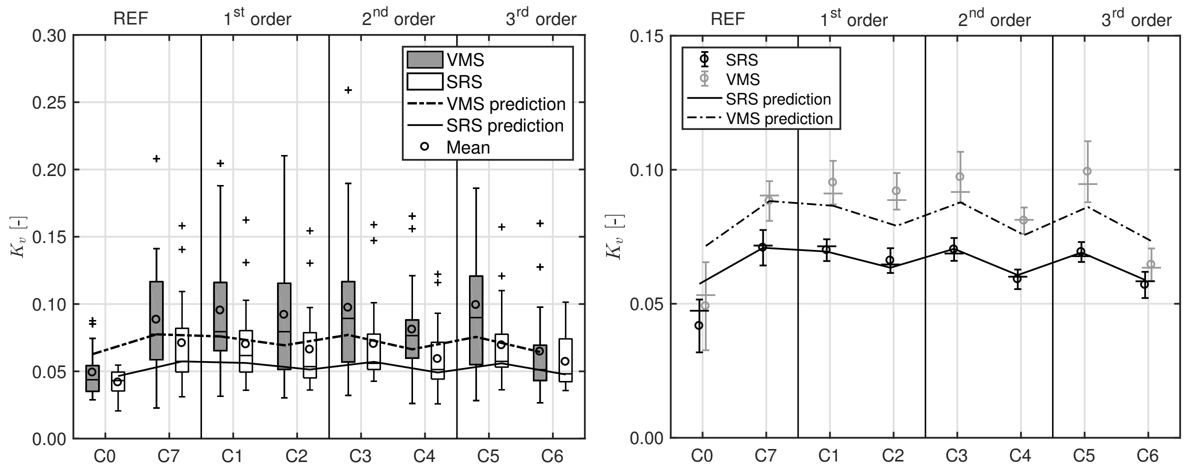

(a) boxplot (b) 95% CI plot

Figure A.6: K_v of all pilots

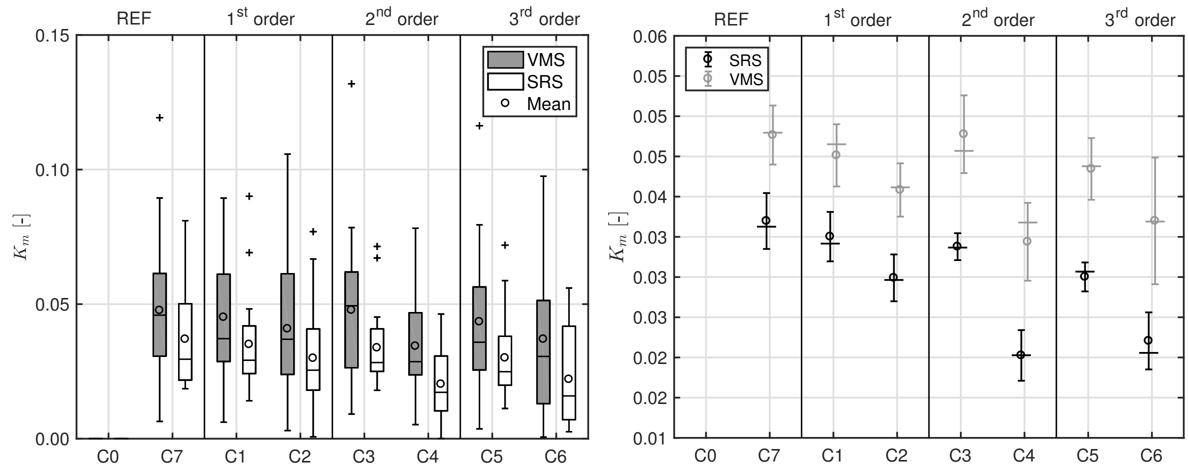

(a) boxplot

(b) 95% CI plot

Figure A.7: K_m of all pilots

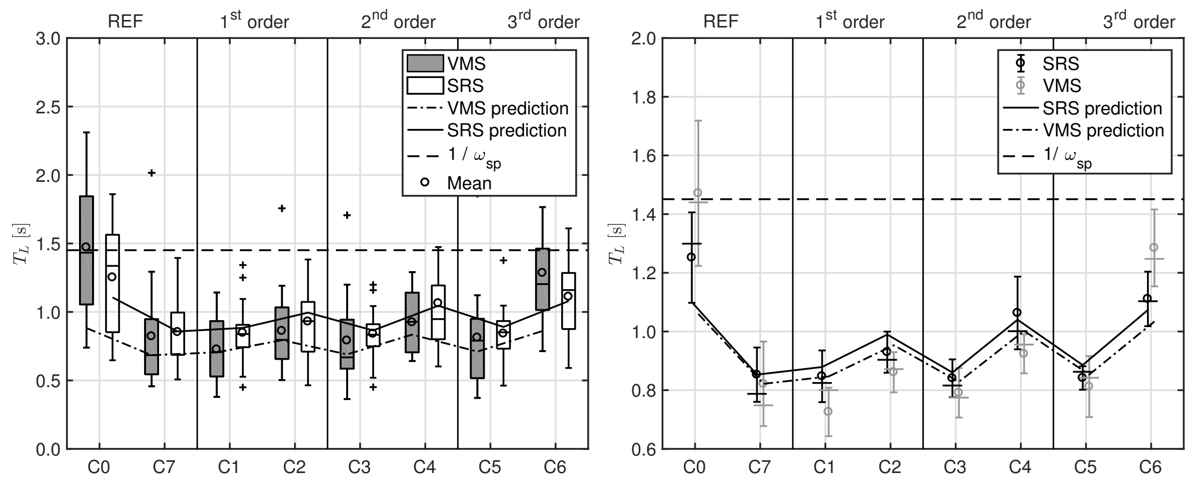

(a) boxplot

(b) 95% CI plot

Figure A.8: T_L of all pilots

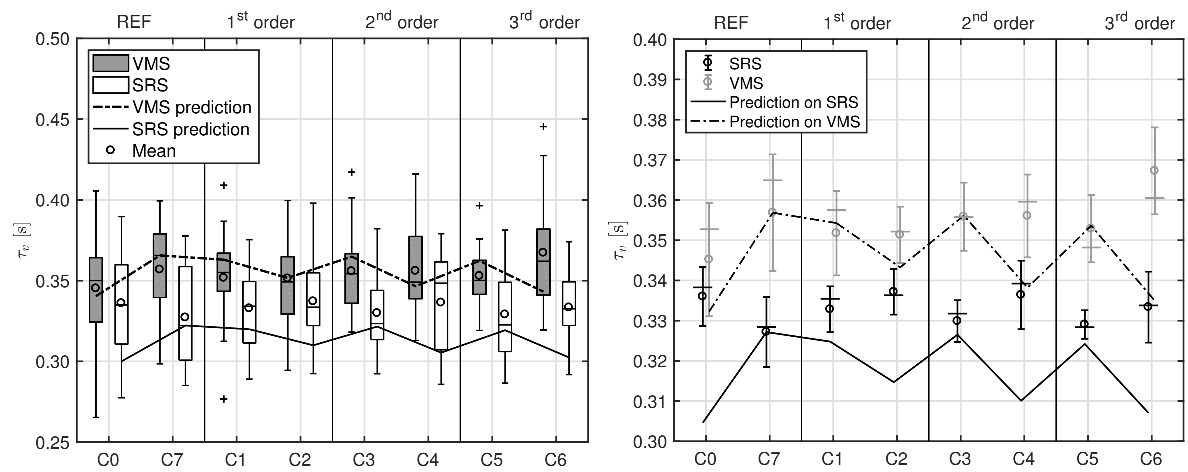

(a) boxplot

(b) 95% CI plot

Figure A.9: τ_v of all pilots

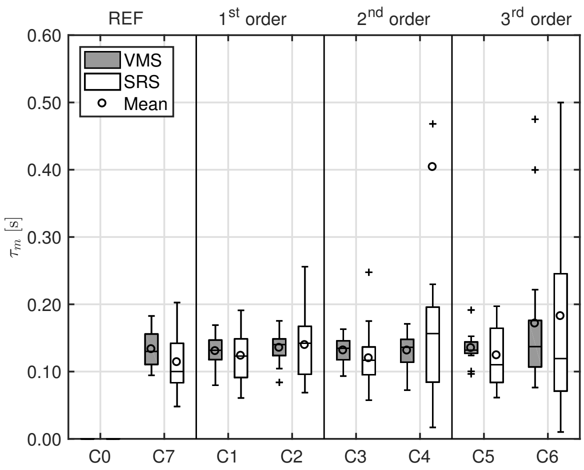

(a) boxplot

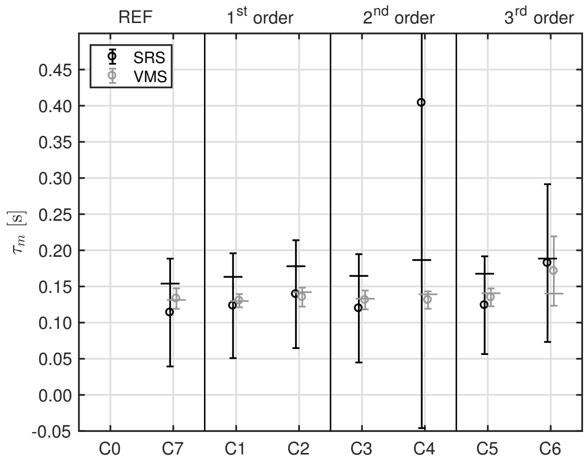

(b) 95% CI plot

Figure A.10: τ_m of all pilots

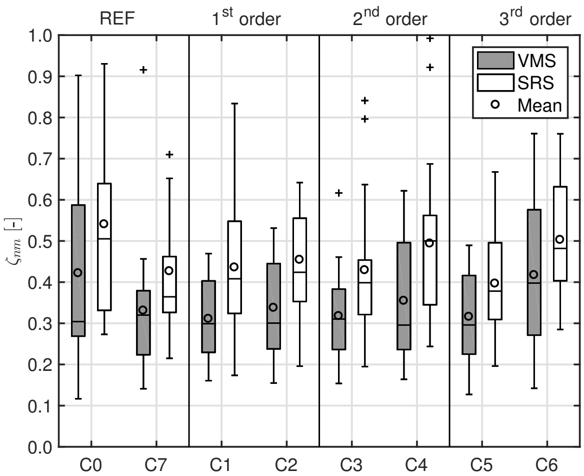

(a) boxplot

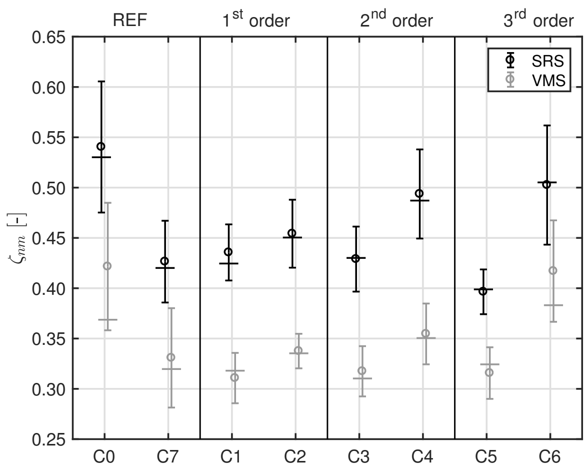

(b) 95% CI plot

Figure A.11: ζ_{nm} of all pilots

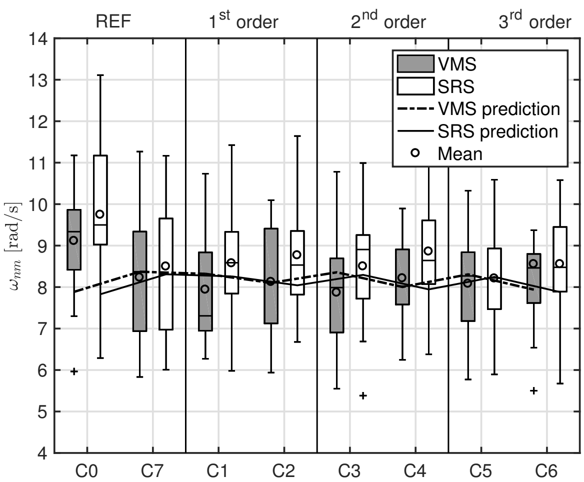

(a) boxplot

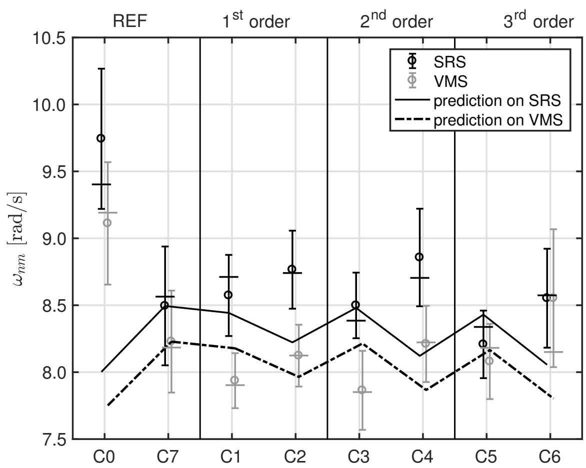

(b) 95% CI plot

Figure A.12: ω_{nm} of all pilots

A.2.3. Open-loop Parameters

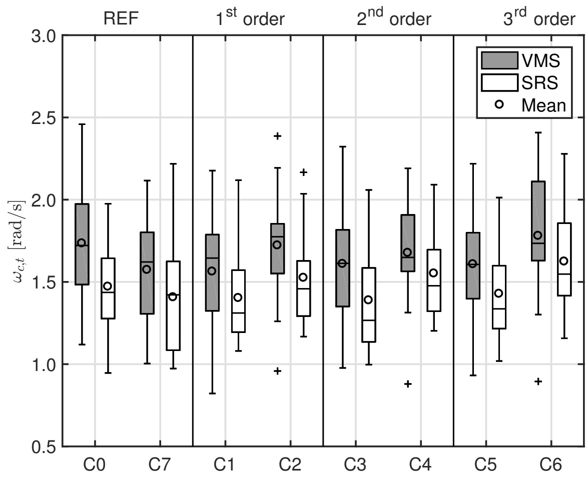

(a) boxplot

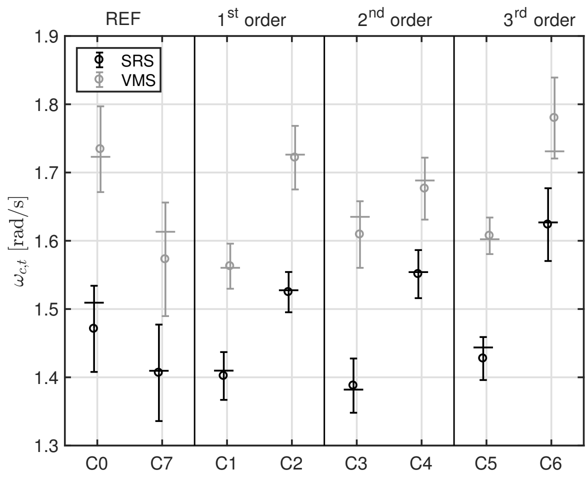

(b) 95% CI plot

Figure A.13: $\omega_{c,t}$ of all pilots

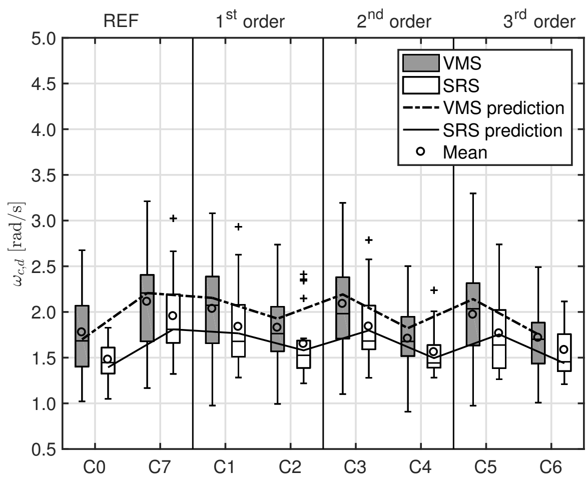

(a) boxplot

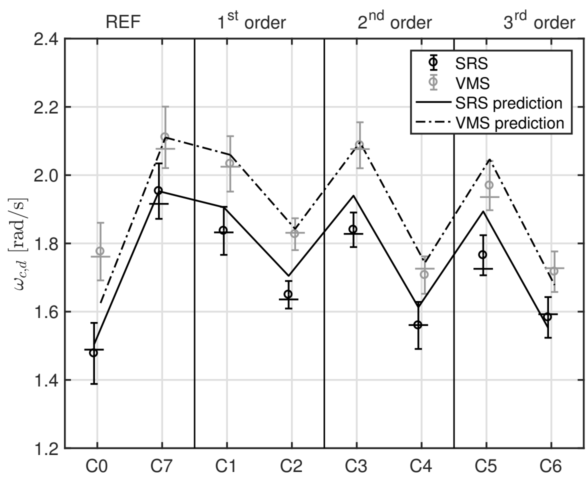

(b) 95% CI plot

Figure A.14: $\omega_{c,d}$ of all pilots

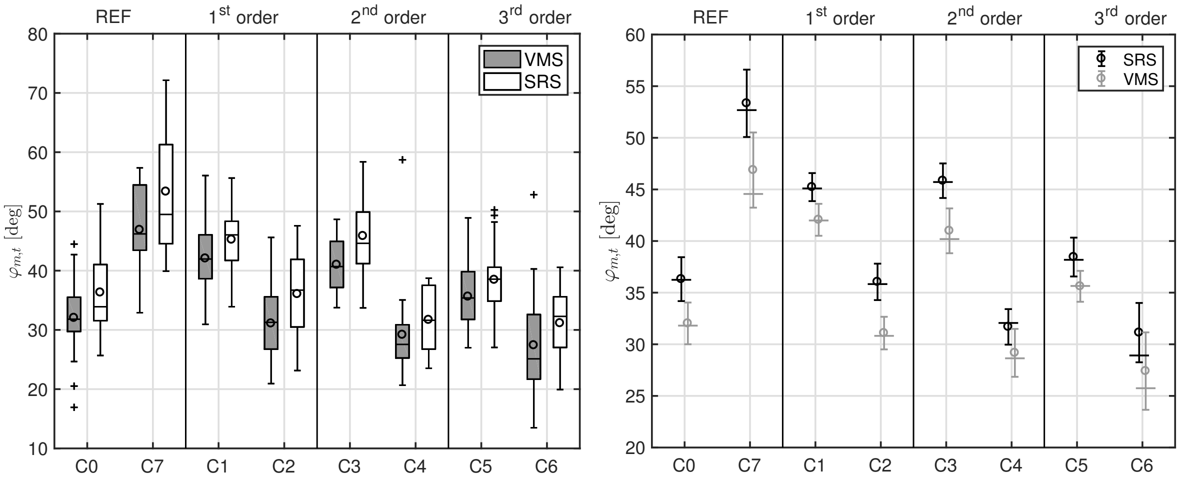

(a) boxplot (b) 95% CI plot

Figure A.15: $\varphi_{m,t}$ of all pilots

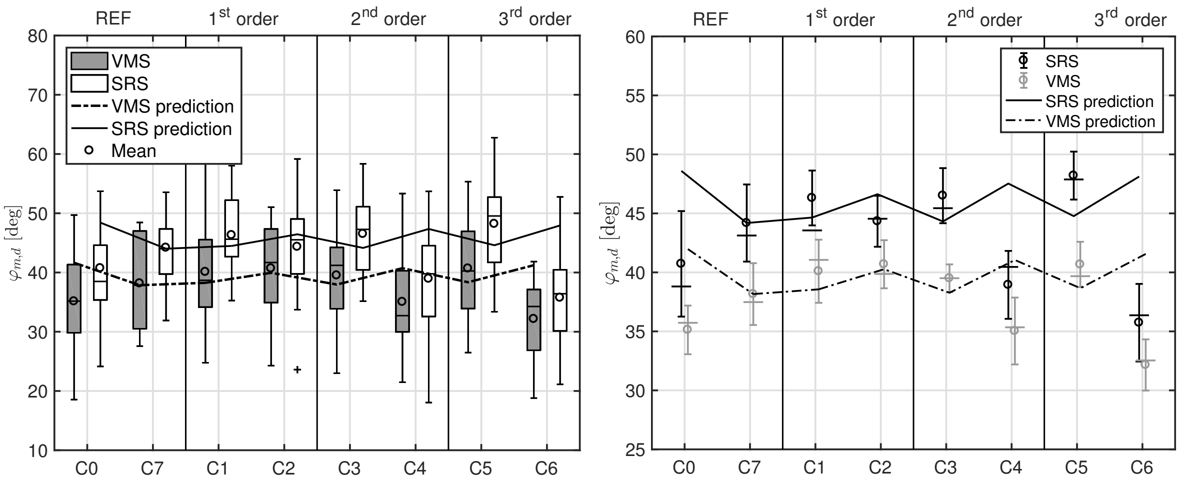

(a) boxplot (b) 95% CI plot

Figure A.16: $\varphi_{m,d}$ of all pilots

A.3. Four VMS Pilots Excluded

The pilot population of the VMS contained four pilots that controlled with notably larger control activity. Three of these four pilots had considerable experience with this kind of experiments. Their tracking performance RMS_e did not show any abnormalities. Figure A.17 shows the RMS_u of both simulators of all participants (5 runs averaged), with these four pilots indicated by cross symbols.

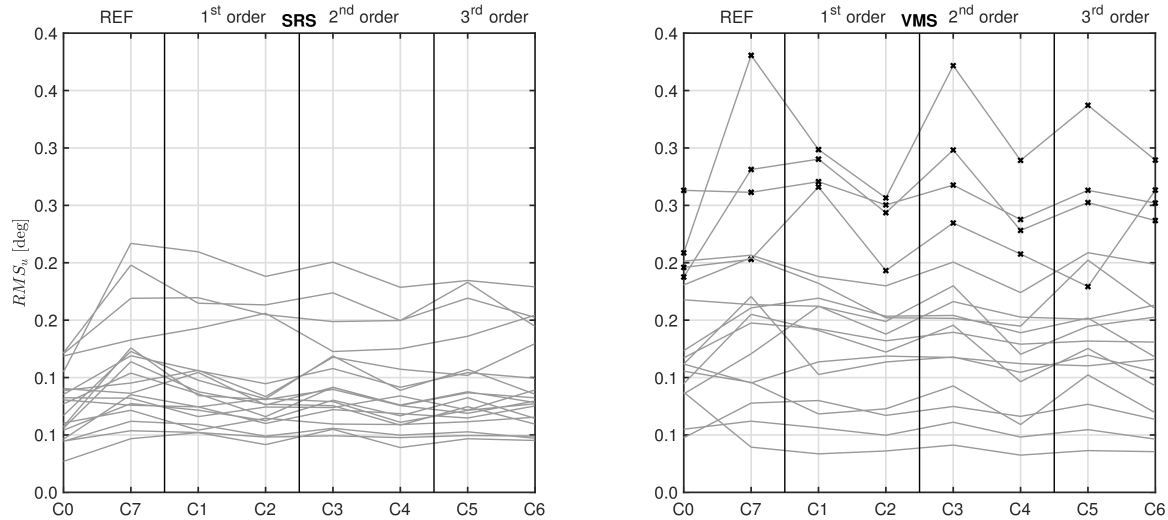

Figure A.17: RMS_u of all pilots (5 runs averaged) of both simulators, with black crosses indicating four abnormal VMS pilots

These four pilots had a direct effect on the results of RMS_u, K_v, K_m and the open-loop parameters. Furthermore, their effect is clearly visible in $\sigma^2_{u_m}/\sigma^2_{u_v}$. This section presents the results of all dependent measures, with these four pilots omitted. Comparing the figures in this section with their equavalent in Section A.2 illustrates the effect that these four pilots had on the results.

A.3.1. Tracking Performance and Control Activity

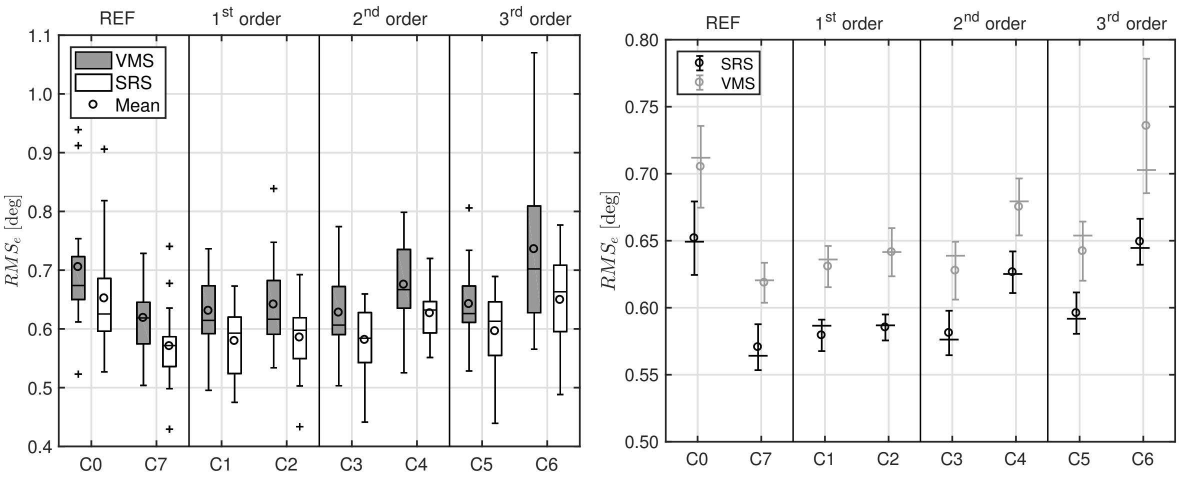

(a) boxplot (b) 95% CI plot

Figure A.18: RMS_e without 4 abnormal VMS participants

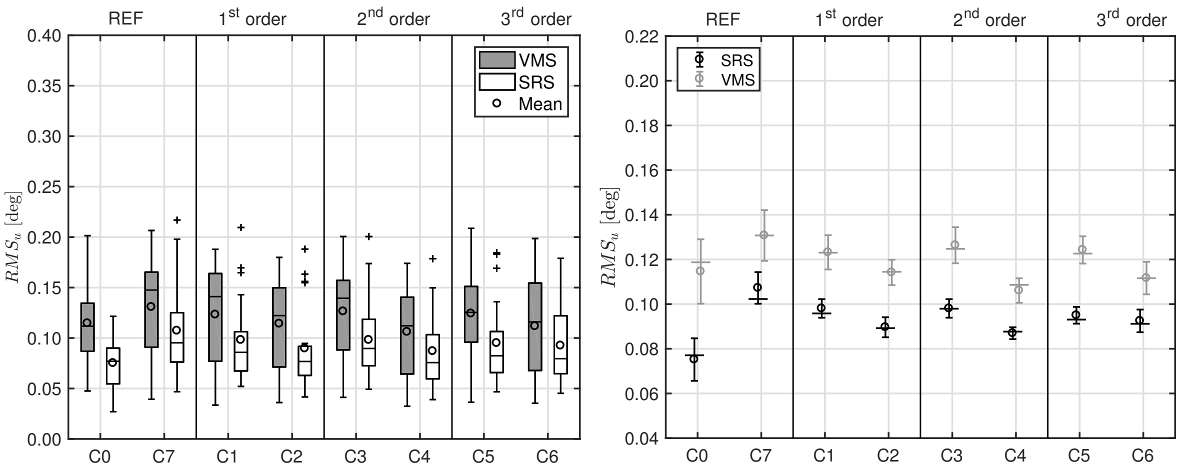

(a) boxplot (b) 95% CI plot

Figure A.19: RMS_u without 4 abnormal VMS participants

A.3.2. Pilot Model Parameters

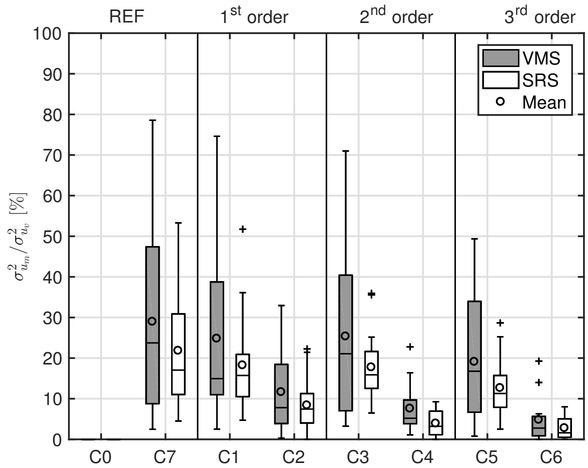

(a) boxplot

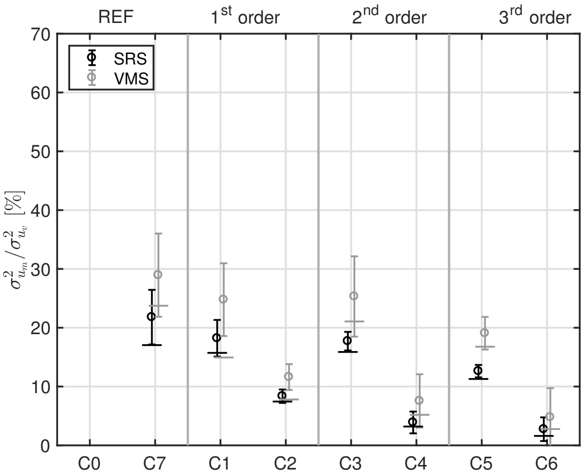

(b) 95% CI plot

Figure A.20: $\sigma^2_{u_m}/\sigma^2_{u_v}$ without 4 abnormal VMS participants

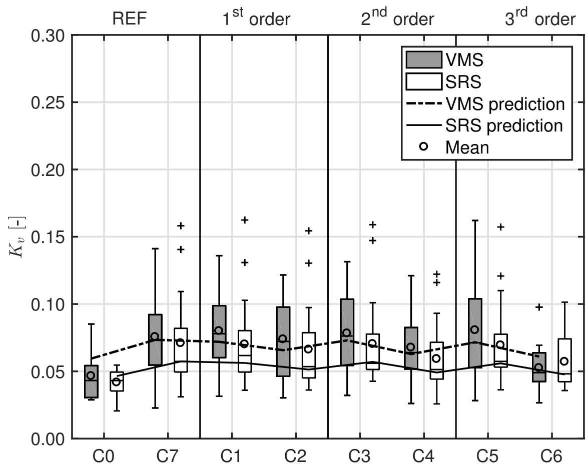

(a) boxplot

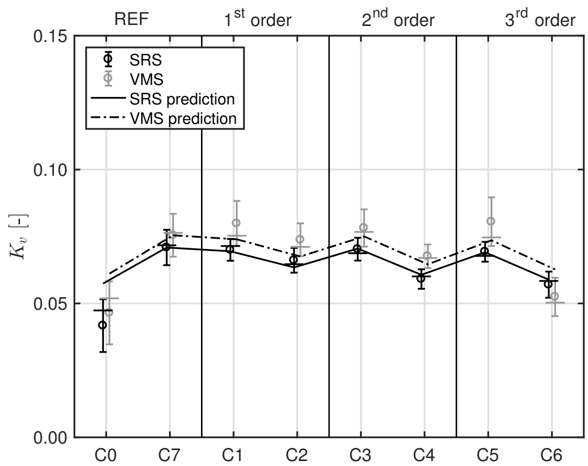

(b) 95% CI plot

Figure A.21: K_v without 4 abnormal VMS participants

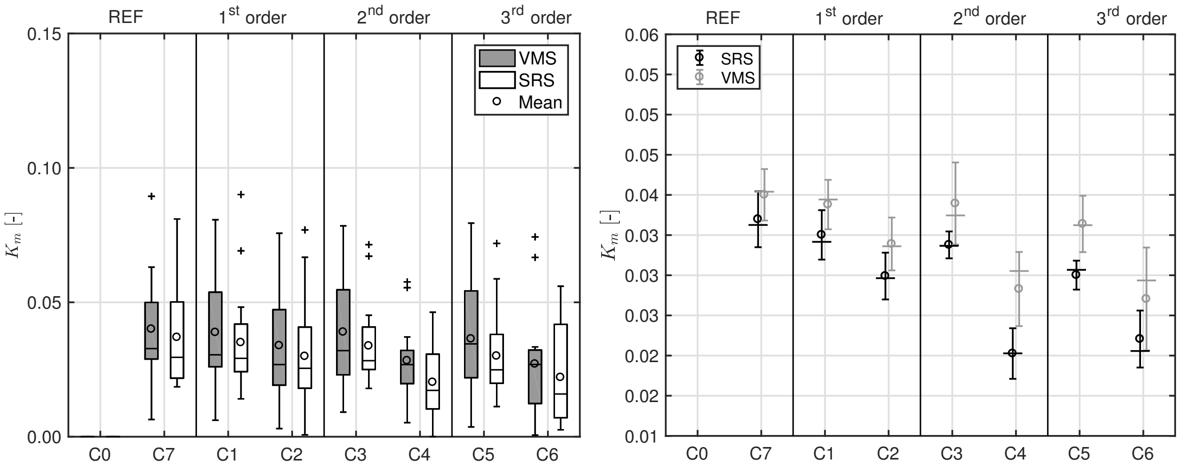

(a) boxplot (b) 95% CI plot

Figure A.22: K_m without 4 abnormal VMS participants

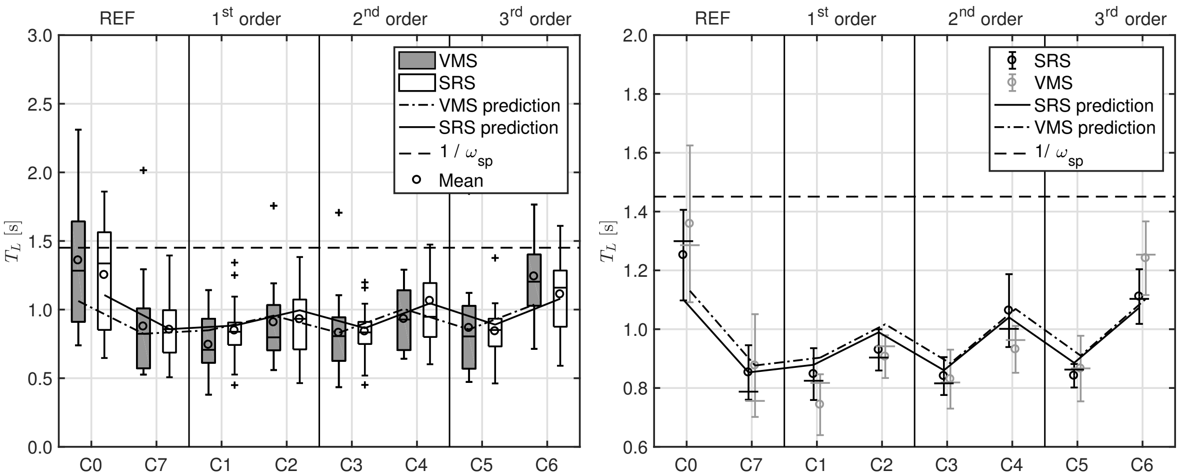

(a) boxplot (b) 95% CI plot

Figure A.23: T_L without 4 abnormal VMS participants

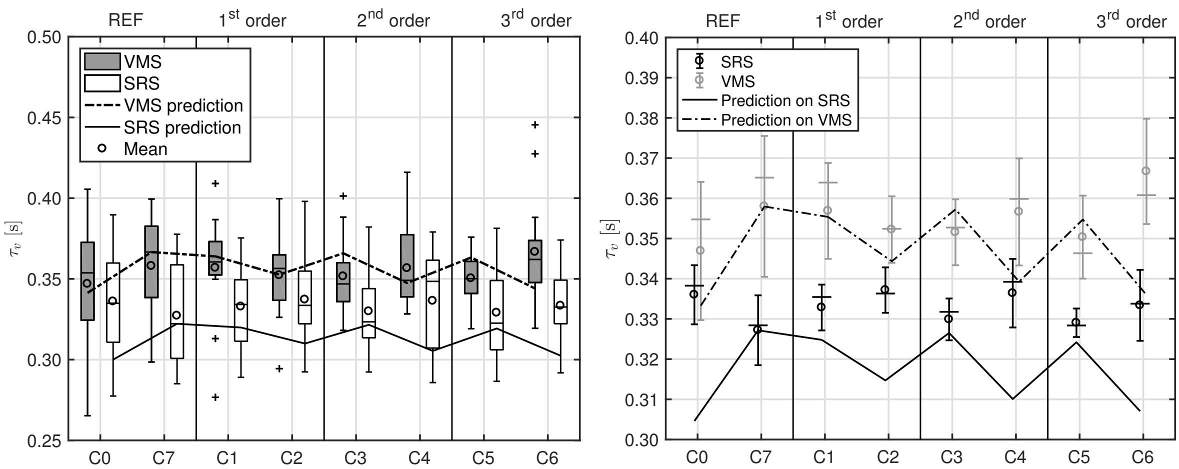

(a) boxplot (b) 95% CI plot

Figure A.24: τ_v without 4 abnormal VMS participants

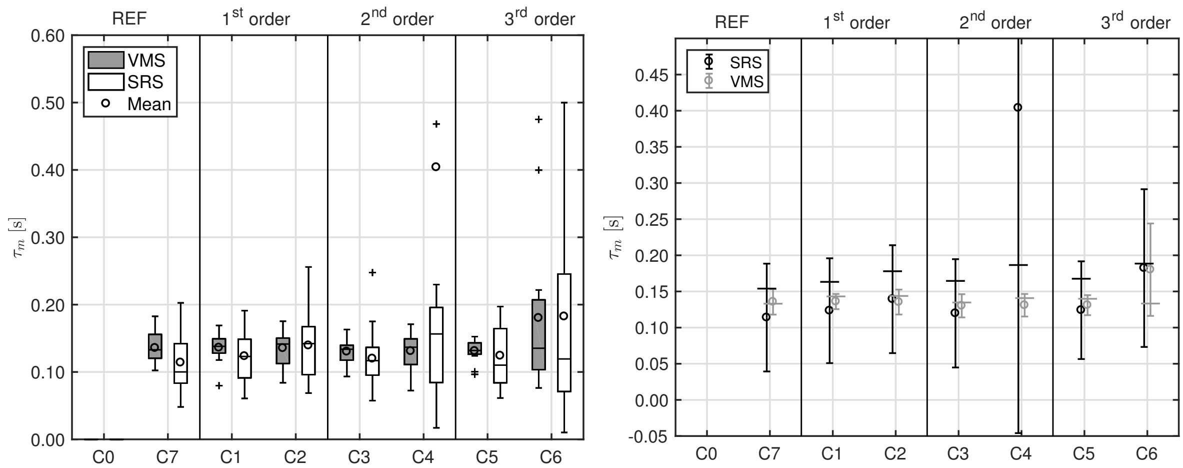

(a) boxplot (b) 95% CI plot

Figure A.25: τ_m without 4 abnormal VMS participants

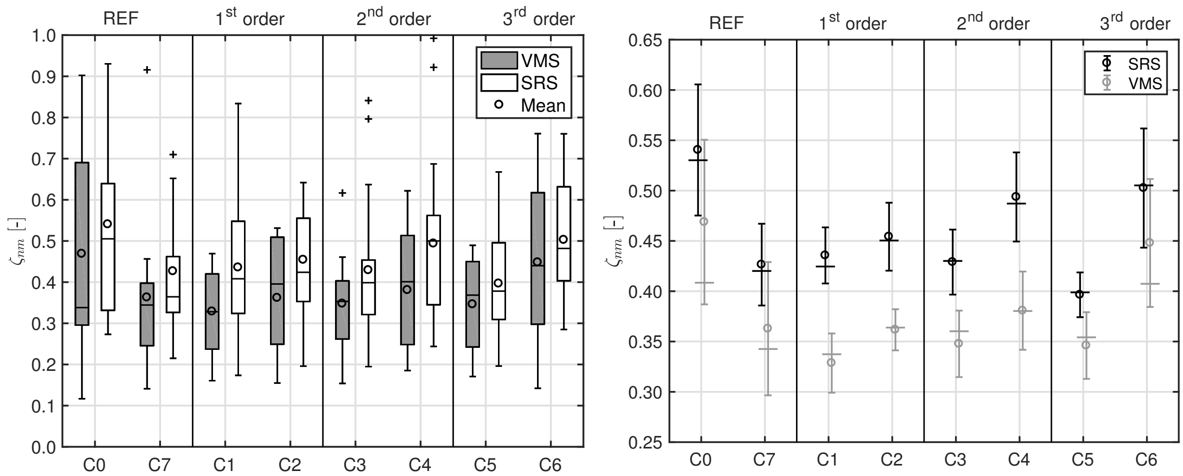

(a) boxplot (b) 95% CI plot

Figure A.26: ζ_{nm} without 4 abnormal VMS participants

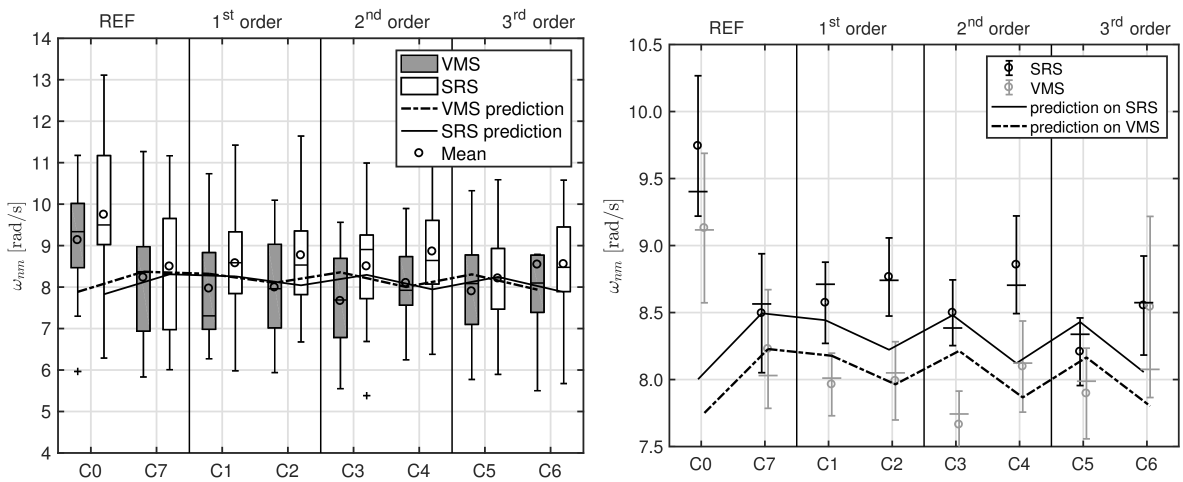

(a) boxplot (b) 95% CI plot

Figure A.27: ω_{nm} without 4 abnormal VMS participants

A.3.3. Open-loop Parameters

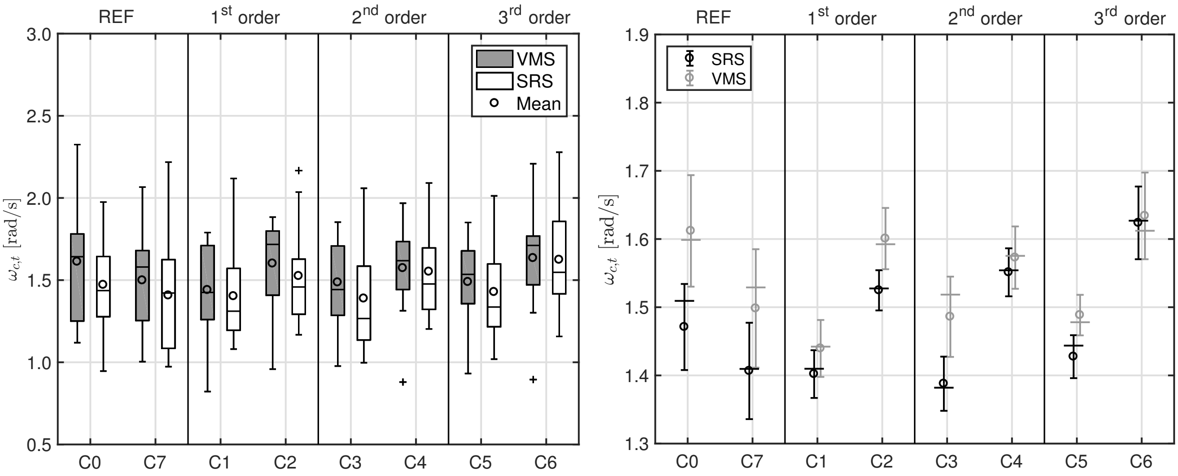

(a) boxplot (b) 95% CI plot

Figure A.28: $\omega_{c,t}$ without 4 abnormal VMS participants

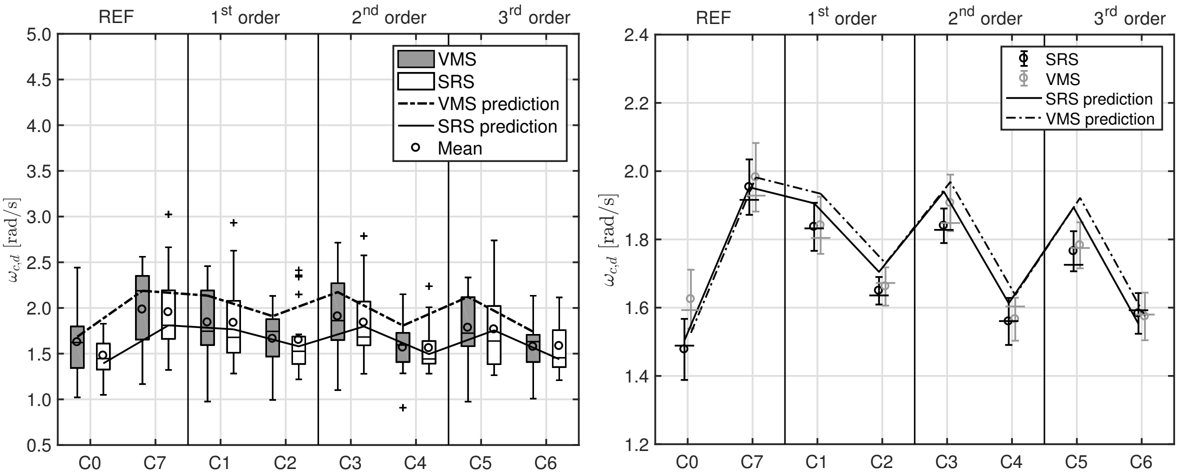

(a) boxplot (b) 95% CI plot

Figure A.29: $\omega_{c,d}$ without 4 abnormal VMS participants

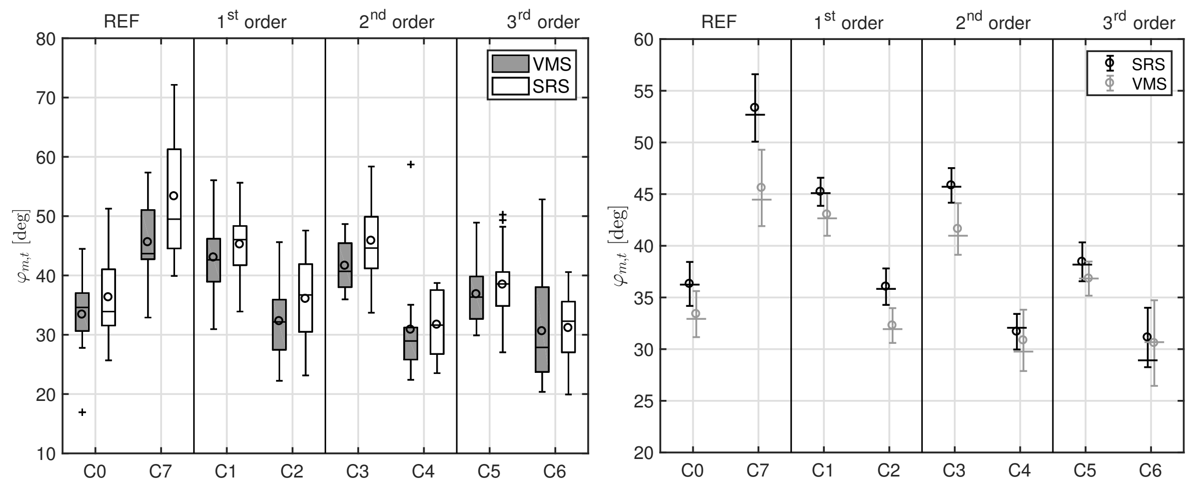

(a) boxplot (b) 95% CI plot

Figure A.30: $\varphi_{m,t}$ without 4 abnormal VMS participants

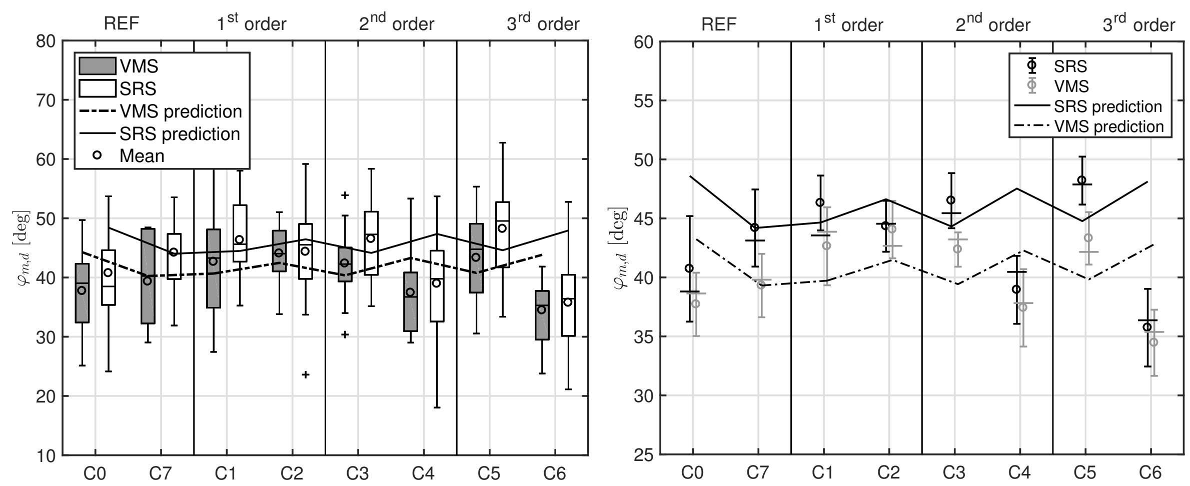

(a) boxplot (b) 95% CI plot

Figure A.31: $\varphi_{m,d}$ without 4 abnormal VMS participants

A.4. Non-parametric Statistical Analysis

In addition to an ANOVA, a non-parametric statistical test was used in the analysis of the results, because of violations of the ANOVA assumptions. Section IV of Part I of this report explains the criteria for selecting the non-parametric Schreirer-Ray-Hare extension of the Kruskall-Wallis (SRH-KW) test as an alternative for the ANOVA. This section explains the procedure of the SRH-KW test, based on a description in [52].

The Kruskall-Wallis test is a non-parametric alternative for a one-way ANOVA, based on ranked data. Scheirer et al. [53] proposed an extension to this test, which allows it to be used in the same way as a two-way ANOVA, for groups with equal sample sizes. The procedure of the SRH-KW test is as follows:

1. Group all observations into a single array and rank the observations in this array.

2. Replace the original observations by their ranks.

3. Compute the expected variance MS_{total} of the entire dataset with $MS_{total} = abn \cdot (abn+1)/12$, where a is the number of conditions ($a = 8$), b is the number of simulators ($b = 2$) and n is the number of participants ($n = 17$). As explained in [52], page 445: *"The expected variance of any array of n ranks is* $MS_{total} = n(n+1)/12$*"*.

4. Compute the sum-of-squares SS of the columns of the dataset (experimental motion conditions), the groups of the dataset (simulators) and the interaction term.

5. Compute the test statistic H for each of the above by dividing the corresponding SS by MS_{total}: $H = SS/MS_{total}$. This test statistic can be considered as a χ^2-variable, as explained in [52], page 445: *"The chi-square distribution is the ratio of a sum-of-squares devided by a parametric variance"*.

6. Test the significance of H as a χ^2-variable, with the degrees of freedom of the χ^2-distribution equal to the SS which is being tested.

To illustrate the differences between the two tests, Table A.2 presents the results of the first statistical analysis (simulator effects) of both the two-way mixed ANOVA and the SRH-KW test for the pilot model parameters. Generally, the two statistical tests showed the same results for these parameters. Differences were found in the significance of the main effect of motion condition of τ_m, the interaction term for ζ_{nm} and the main effect of simulator of ω_{nm}, see Table A.2.

Firstly, the main effect of motion condition of τ_m was found to be significant by the ANOVA, whereas the SRH-KW test did not find any significant interaction. For several pilots no accurate estimate of τ_m could be found, which is why the ANOVA assumptions were severely violated. The data of this variable violated the ANOVA assumption of normality in five out of sixteen cases. Furthermore, the assumption of equality of error variances was violated in four out of seven cases. Also, the assumption of equality of covariance was violated and 4 outliers were present in the data. According to the procedure followed in the analysis of the results, the non-parametric test was used. Because the ANOVA is a parametric test, it has a higher statistical power than the SRH-KW test, and hence a lower Type-II (false negative) error rate: it has a lower probability of falsely accepting the null-hypothesis. As Field states in [54], page 340: *"The Type I error rate and the statisficd power of a test are linked. Therefore, there is always a trade-off: if a test is conservative (the probability of a Type I error is small) then it is likely to lack statistical power (the probability of a Type II error will be high)"*. Therefore the ANOVA's probability of incorrectly rejecting the null-hypothesis (false positive, Type-I error rate) is higher, which could explain the positive main effect of motion condition for τ_m. As Figure A.10a and A.10b show, there was no variation of τ_m over the motion conditons. Another explanation lies in the fact that many of the identification issues regarding τ_m originated in C4 and C6, which were both conditions with $\omega_{mf} = 2.0$ rad/s. The quality of the motion cues was low and they were found to be more prone to identification issues than the other conditions. Because often τ_m was estimated disproportionally high, this could have promped the ANOVA to return a significant interaction as well.

In addition to a lowered statistical power, Toothaker and Chang [55] state that the SRH-KW test does not control α at the set level, based on a simulation study with a thousand simulation runs as dataset, for cases when effects other than the one being tested are present (ie. main effects and interaction effects). α relates to the Type-I error probability, which might explain the significant interaction between simulator and motion condition for ζ_{nm}, as the data did not show any differences in trends, see Figure A.11a and A.11b.

For ω_{nm}, the SRH-KW test found a significant difference between the two simulators. However, post-hoc Mann-Whitney U tests did not find any significant difference between the simulators for any motion condition. The data of the neuromuscular frequency ω_{nm} met the ANOVA assumptions. The results of the ANOVA are supported by post-hoc tests. This suggests that for this dataset, using the procedure to select the suitable statistical test, the ANOVA produces reliable results.

In conclusion, generally the results of both statistical tests are the same for the seven parameters in this analysis. In the case of ω_{nm}, the ANOVA assumptions were met and its results were supported by a second independent analysis. For τ_m however, the results of the ANOVA did not seem to correspond to the experimental data, which could be explained by the severe violations of its assumptions. This illustrates importance of selecting the suitable statistical test based on the assumptions it requires. Finally, the SRH-KW test suffers of some issues of statistical power and false positive error probability, as described in [55] as illustrated by the significant interaction in ζ_{nm}. This section serves to illustrate the importance of the role of statistics to support experimental results, as opposed to guiding the conclusions. The selection of the suitable statistical test, based on the required assumptions and the experiment data, is of paramount importance.

Table A.2: Comparison of statistical test results for pilot model parameter variables

	Two-way mixed ANOVA								
	Simulator			Motion Condition			Simulator × Motion Condition		
	df	F	p	df	F	p	df	F	p
K_v	1.0,32.0	4.435	**0.043**	2.6,81.6^{gg}	22.779	**<0.001**	2.6,81.6^{gg}	3.452	0.072
K_m	1.0,32.0	6.776	**0.014**	3.6,114.9^{gg}	14.08	**<0.001**	3.6,114.9^{gg}	0.217	0.913
T_L	1.0,32.0	0.006	0.938	2.7,91.4^{gg}	26.624	**<0.001**	2.7,91.4^{gg}	2.632	0.061
τ_v	1.0,32.0	6.760	**0.014**	4.5,143.6^{gg}	0.975	0.429	4.5,143.6^{gg}	1.491	0.202
τ_m	1.0,32.0	0.056	0.815	1.5,48.6^{gg}	5.147	**0.016**	1.5,48.6^{gg}	0.986	0.360
ζ_{nm}	1.0,32.0	6.336	**0.017**	3.5,118.8^{gg}	8.591	**<0.001**	3.5,118.8^{gg}	0.507	0.706
ω_{nm}	1.0,32.0	0.773	0.386	4.1,131.5^{gg}	9.591	**<0.001**	4.1,131.5^{gg}	1.017	0.347
	SRH-KW test								
	Simulator			Motion Condition			Simulator × Motion Condition		
	df	H	p	df	H	p	df	H	p
K_v	1.0,256.0	19.371	**<0.001**	7.0,256.0	41.357	**<0.001**	7.0,256.0	1.915	0.052
K_m	1.0,237.0	21.187	**<0.001**	6.0,237.0	18.051	**0.002**	6.0,237.0	1.278	0.054
T_L	1.0,256.0	1.741	0.127	7.0,256.0	63.546	**<0.001**	7.0,256.0	6.259	0.114
τ_v	1.0,256.0	27.392	**<0.001**	7.0,256.0	1.785	0.051	7.0,256.0	3.561	0.107
τ_m	1.0,237.0	1.537	0.149	6.0,237.0	6.600	0.100	6.0,237.0	3.998	0.135
ζ_{nm}	1.0,256.0	39.232	**<0.001**	7.0,256.0	13.724	**0.019**	7.0,256.0	0.419	**0.002**
ω_{nm}	1.0,256.0	8.6063	**0.002**	7.0,256.0	20.088	**0.002**	7.0,256.0	1.990	0.055

gg = Greenhouse-Geisser correction
(shaded) = significant ($p < 0.050$)
(unshaded) = not significant ($p \geq 0.050$)

A.5. Pilot Model Frequency Responses

This section presents the frequency responses of the estimated pilot models of all pilots for both simulators. First, the results of the 19 SIMONA Research Simulator pilots are presented, followed by the 18 Vertical Motion Simulator pilots. In all no-motion condition C0 plots, the results of a double-loop (DL) identification are also shown. The pilot model parameters corresponding to both the single-loop (SL) identification and the double-loop identification can be seen. Furthermore, in all cases where a second MLE iteration was performed, these final results results are presented together with the original pilot model estimation.

SRS Subject 1 of 19

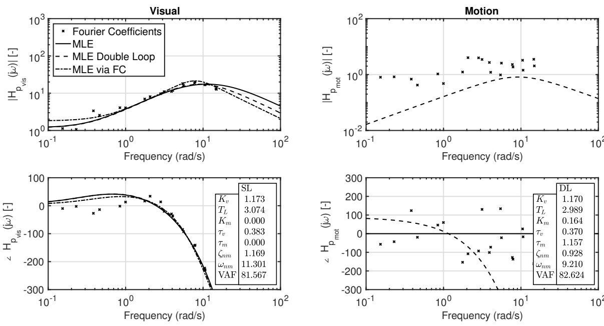

Figure A.32: Subject 1 C0

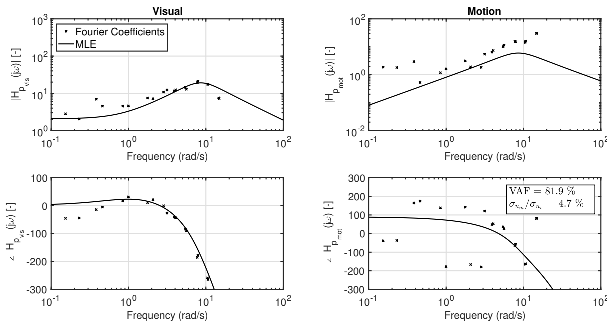

Figure A.33: Subject 1 C1

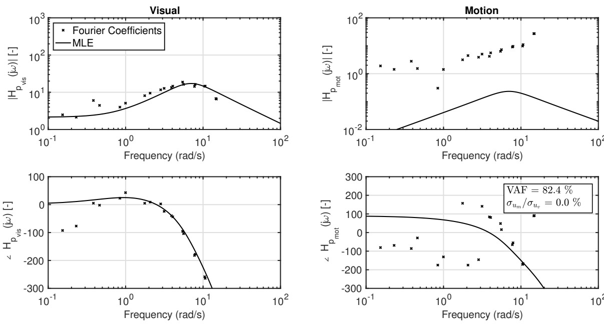

Figure A.34: Subject 1 C2

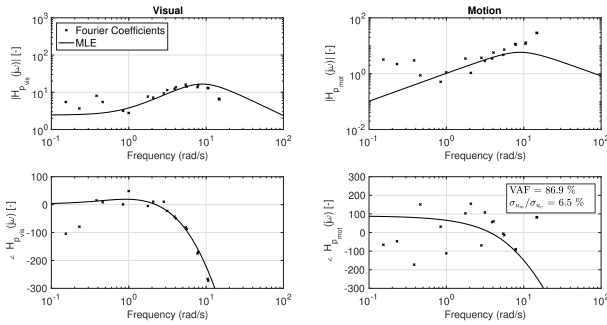

Figure A.35: Subject 1 C3

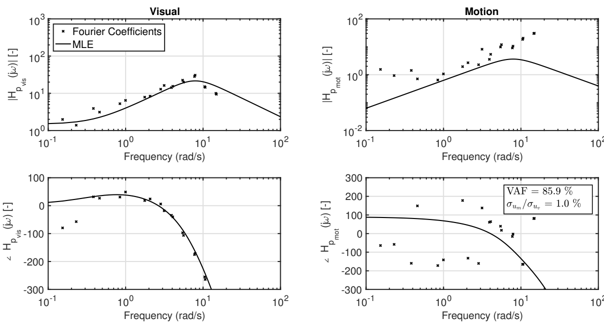

Figure A.36: Subject 1 C4

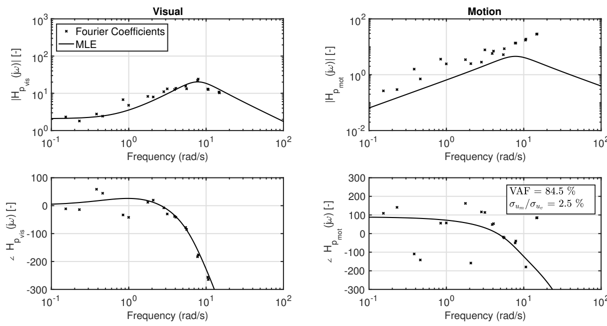

Figure A.37: Subject 1 C5

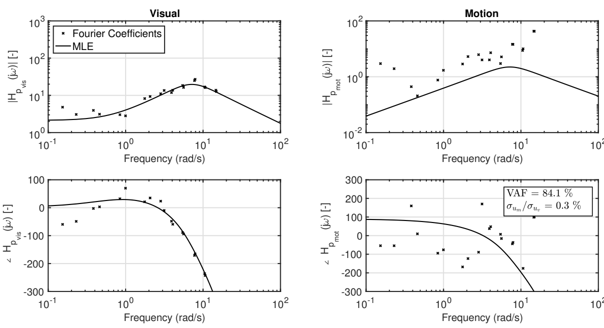

Figure A.38: Subject 1 C6

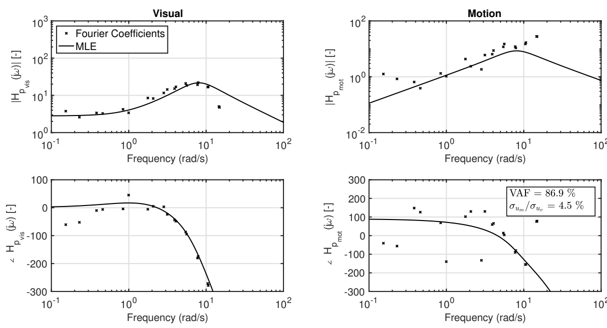

Figure A.39: Subject 1 C7

SRS Subject 2 of 19

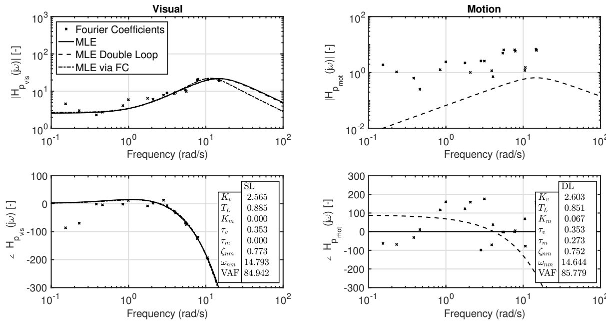

Figure A.40: Subject 2 C0

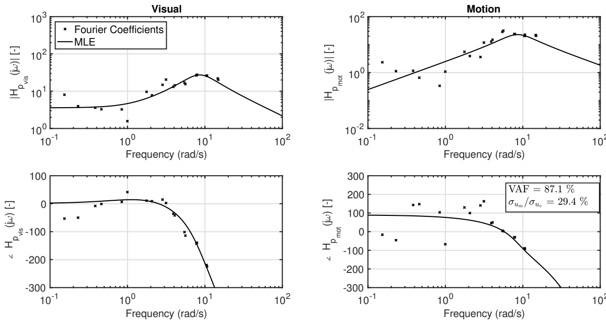

Figure A.41: Subject 2 C1

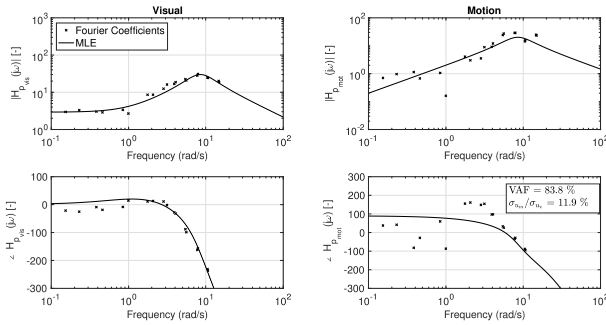

Figure A.42: Subject 2 C2

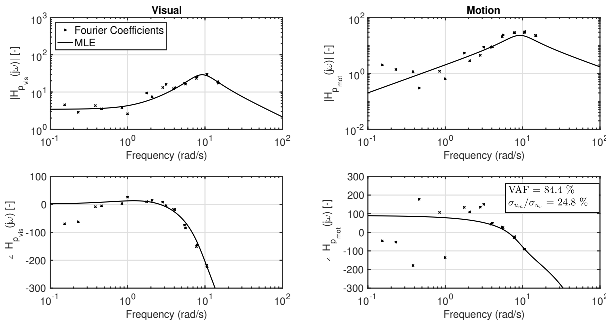

Figure A.43: Subject 2 C3

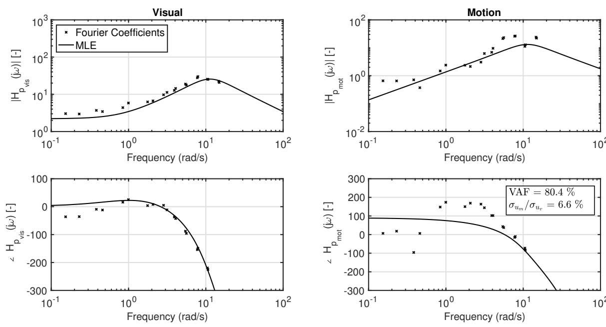

Figure A.44: Subject 2 C4

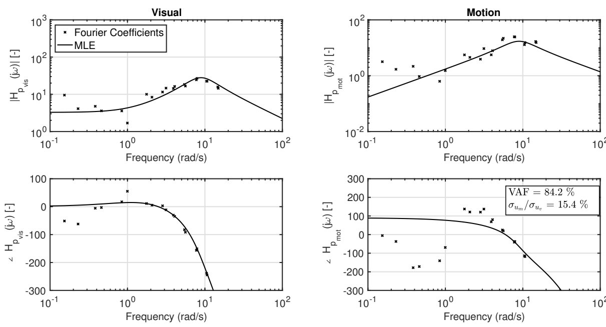

Figure A.45: Subject 2 C5

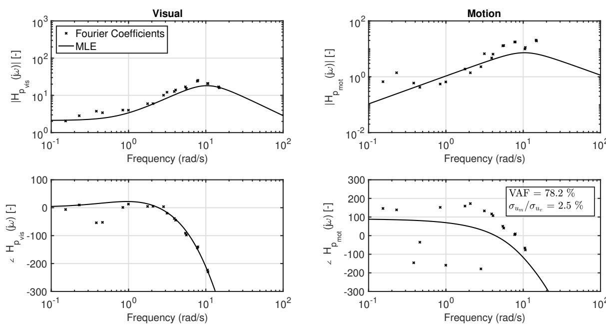

Figure A.46: Subject 2 C6

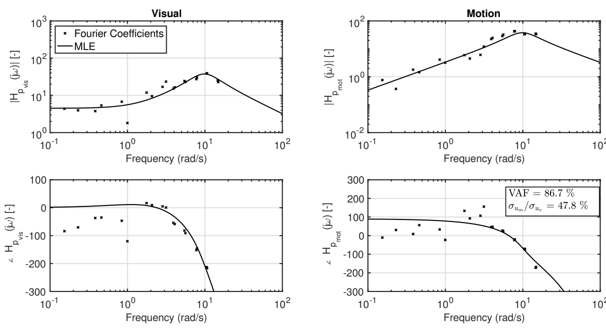

Figure A.47: Subject 2 C7

SRS Subject 3 of 19

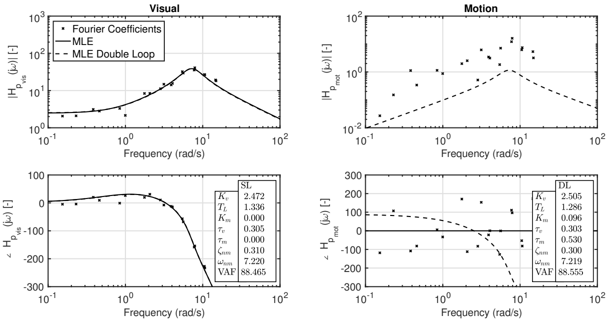

Figure A.48: Subject 3 C0

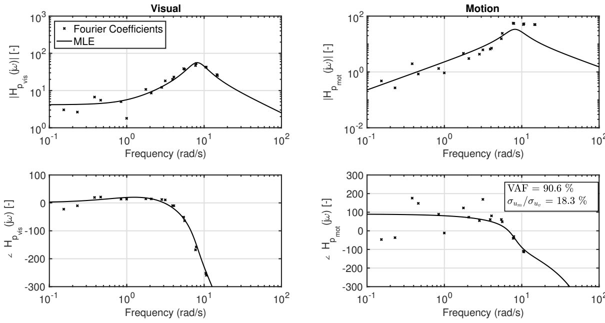

Figure A.49: Subject 3 C1

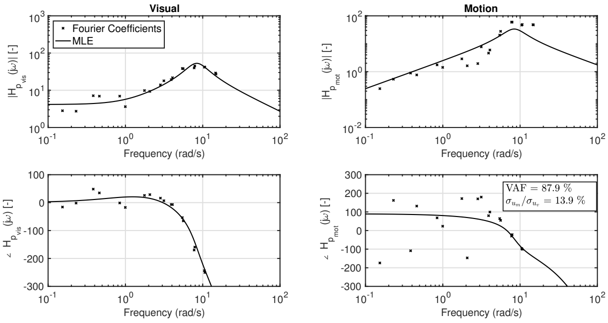

Figure A.50: Subject 3 C2

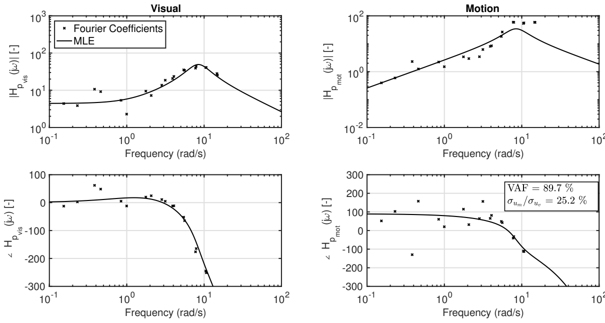

Figure A.51: Subject 3 C3

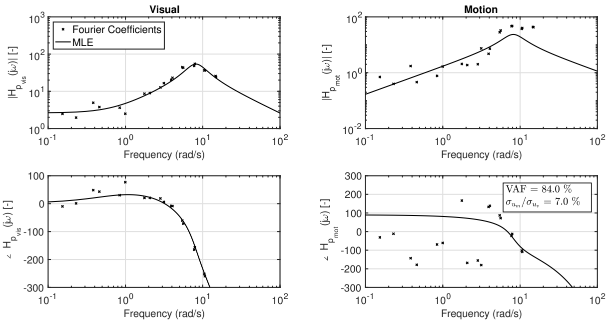

Figure A.52: Subject 3 C4

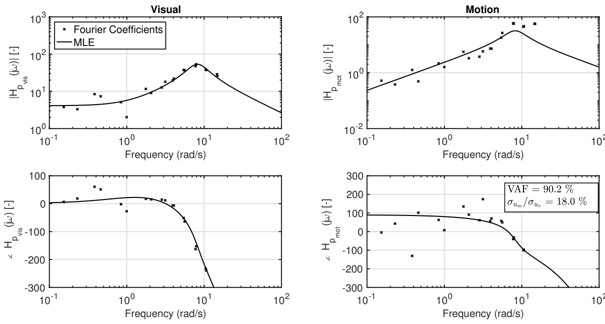

Figure A.53: Subject 3 C5

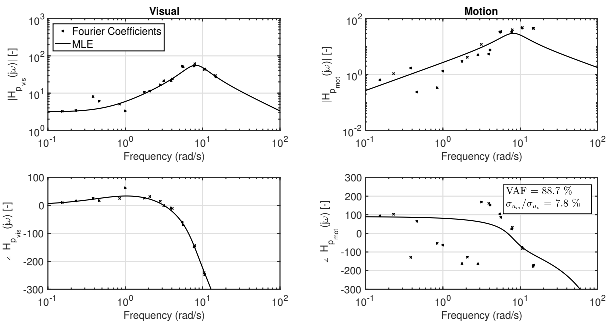

Figure A.54: Subject 3 C6

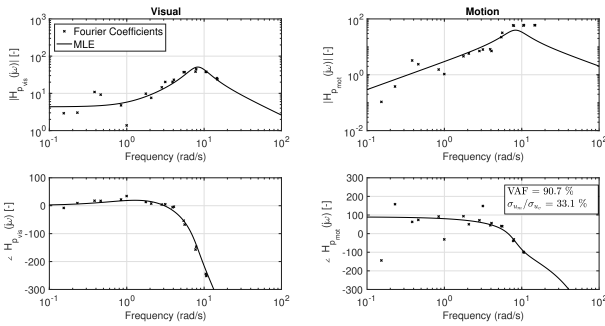

Figure A.55: Subject 3 C7

SRS Subject 4 of 19

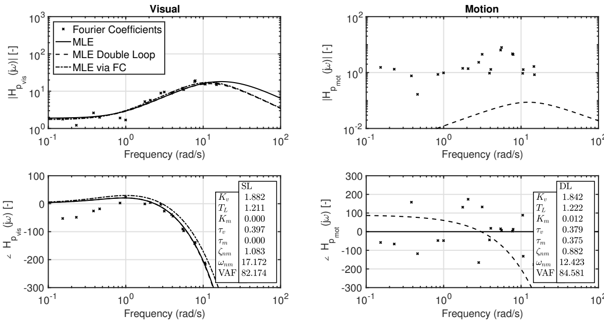

Figure A.56: Subject 4 C0

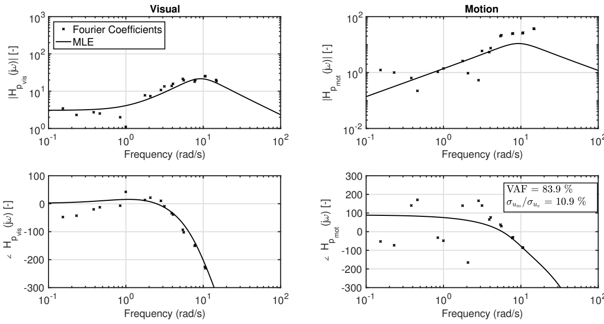

Figure A.57: Subject 4 C1

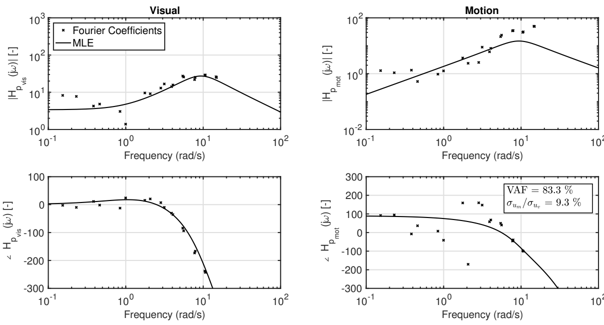

Figure A.58: Subject 4 C2

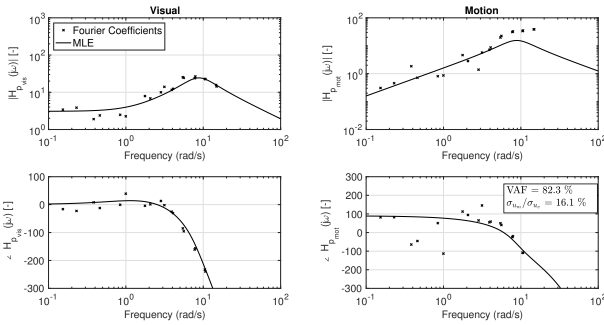

Figure A.59: Subject 4 C3

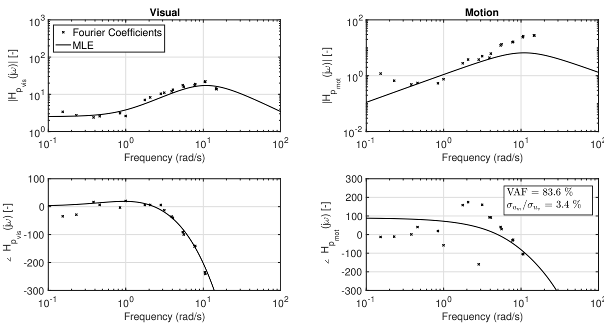

Figure A.60: Subject 4 C4

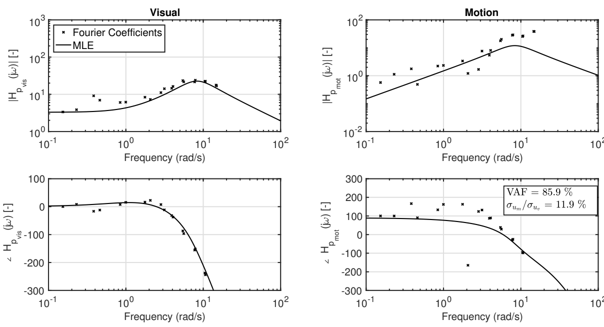

Figure A.61: Subject 4 C5

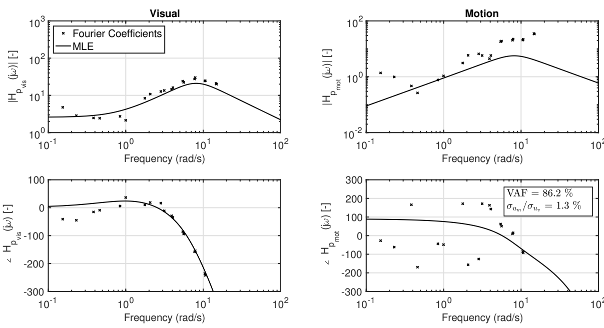

Figure A.62: Subject 4 C6

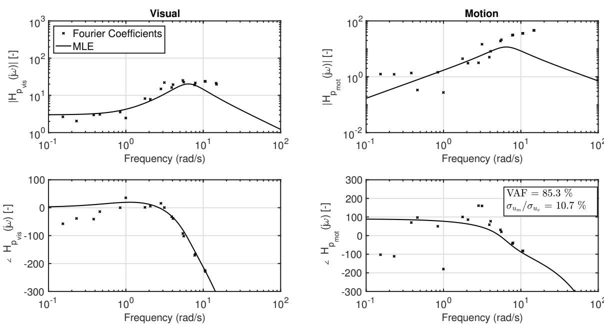

Figure A.63: Subject 4 C7

SRS Subject 5 of 19

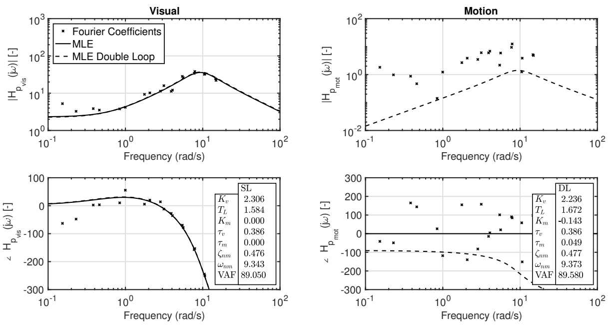

Figure A.64: Subject 5 C0

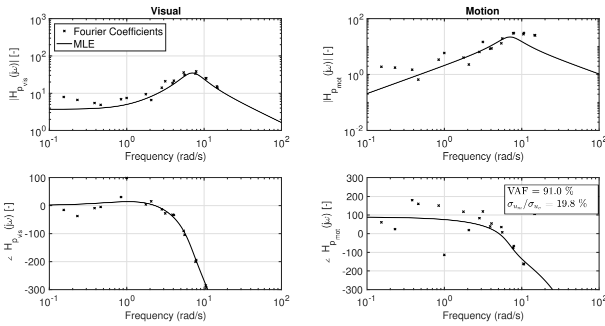

Figure A.65: Subject 5 C1

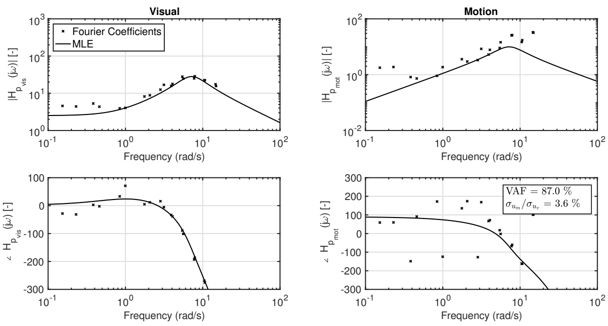

Figure A.66: Subject 5 C2

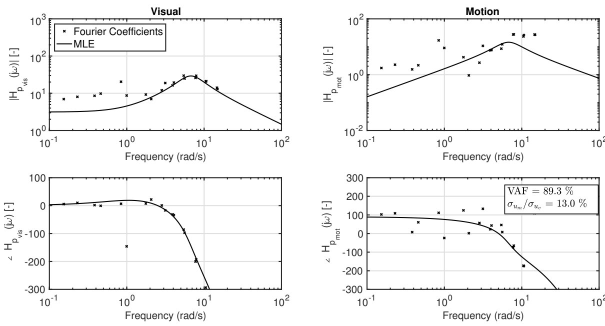

Figure A.67: Subject 5 C3

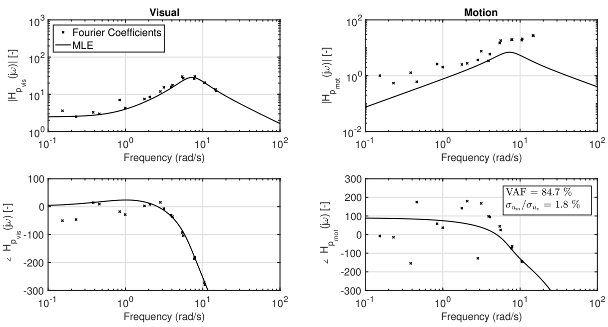

Figure A.68: Subject 5 C4

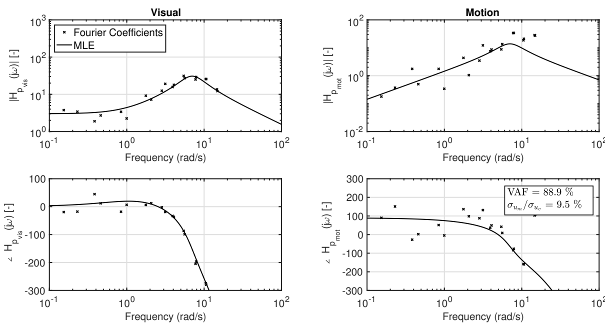

Figure A.69: Subject 5 C5

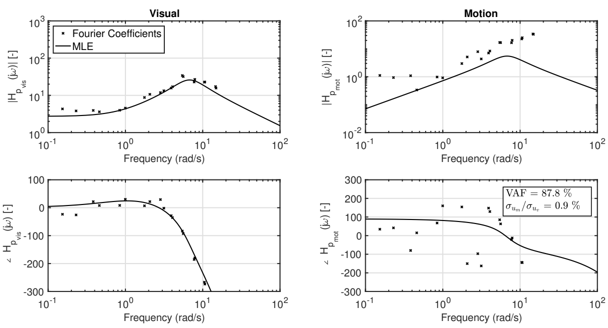

Figure A.70: Subject 5 C6

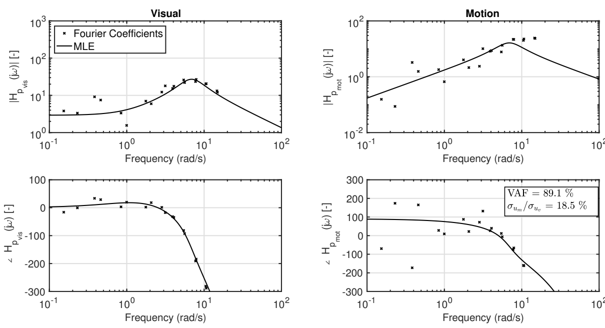

Figure A.71: Subject 5 C7

SRS Subject 6 of 19

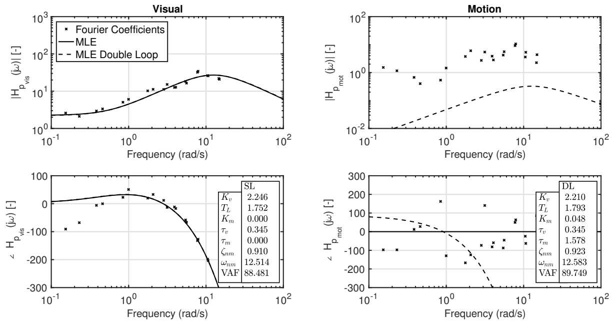

Figure A.72: Subject 6 C0

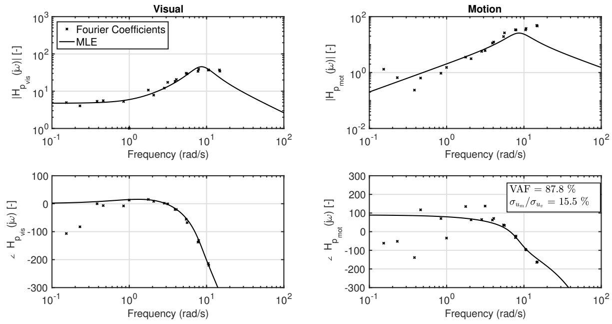

Figure A.73: Subject 6 C1

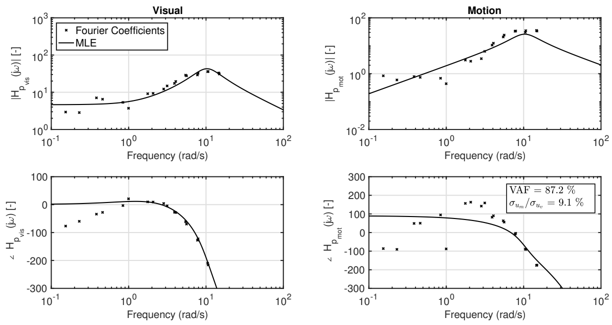

Figure A.74: Subject 6 C2

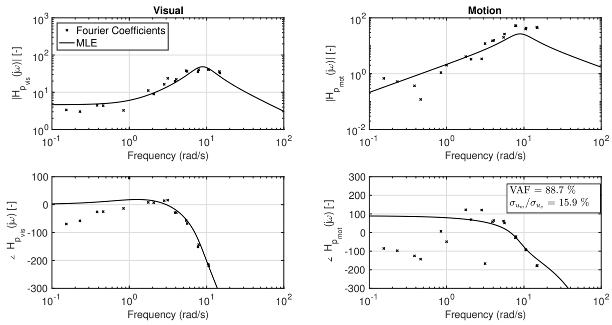

Figure A.75: Subject 6 C3

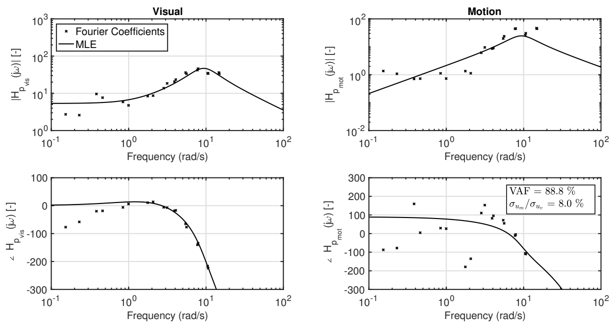

Figure A.76: Subject 6 C4

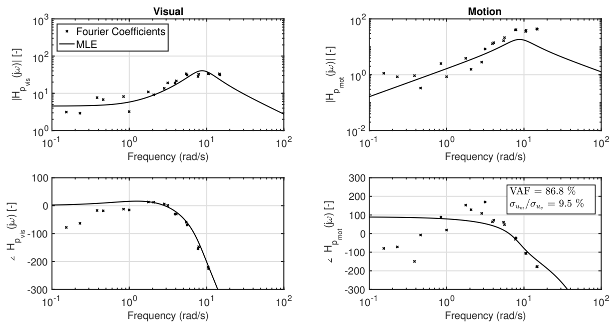

Figure A.77: Subject 6 C5

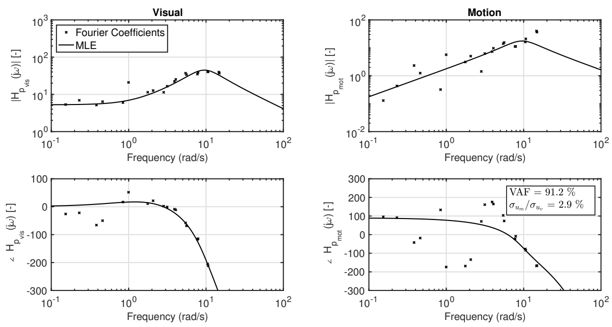

Figure A.78: Subject 6 C6

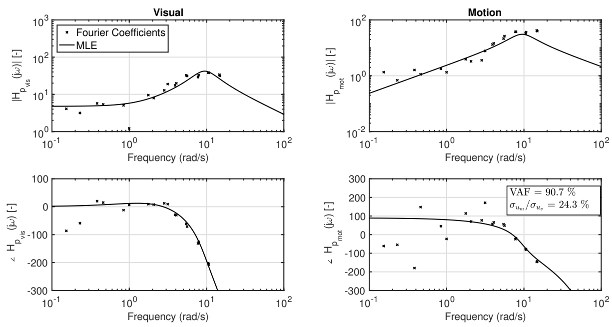

Figure A.79: Subject 6 C7

SRS Subject 7 of 19

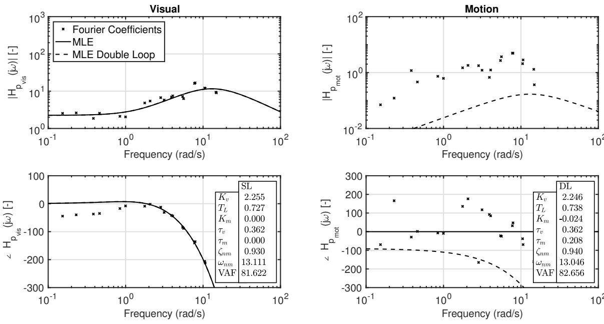

Figure A.80: Subject 7 C0

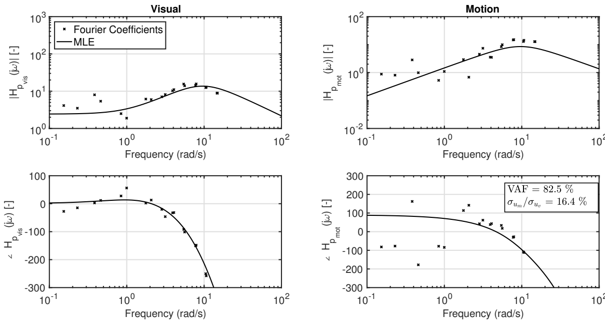

Figure A.81: Subject 7 C1

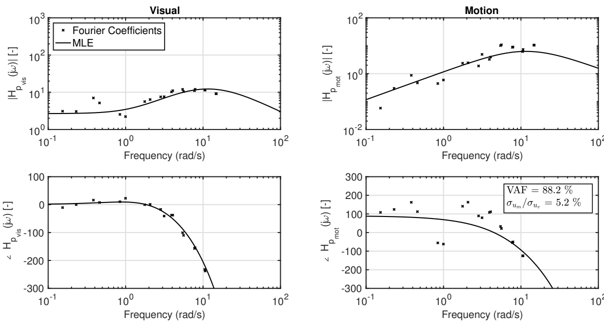

Figure A.82: Subject 7 C2

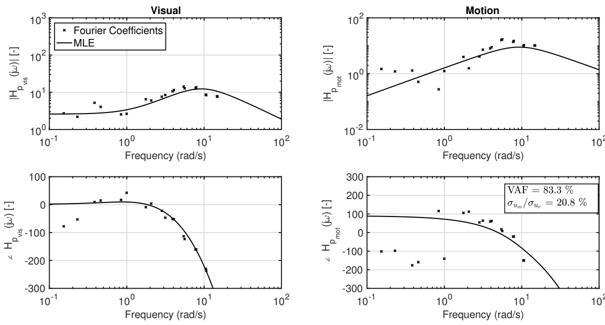

Figure A.83: Subject 7 C3

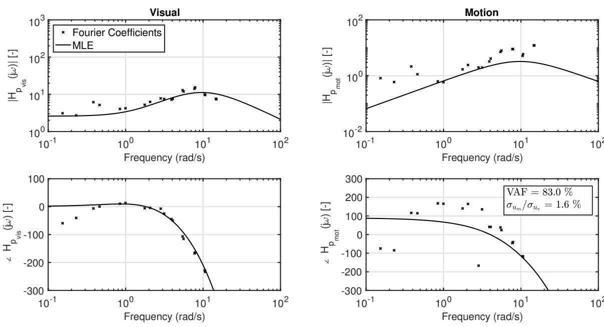

Figure A.84: Subject 7 C4

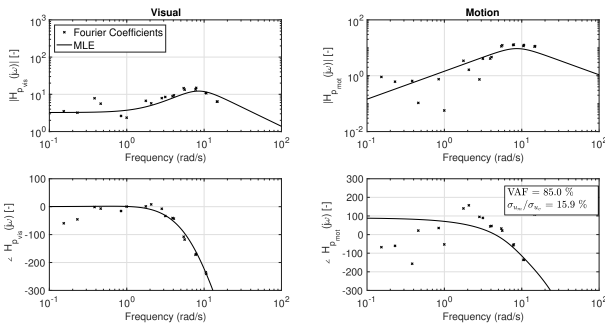

Figure A.85: Subject 7 C5

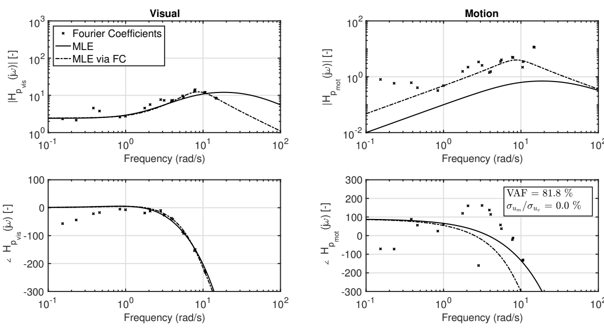

Figure A.86: Subject 7 C6

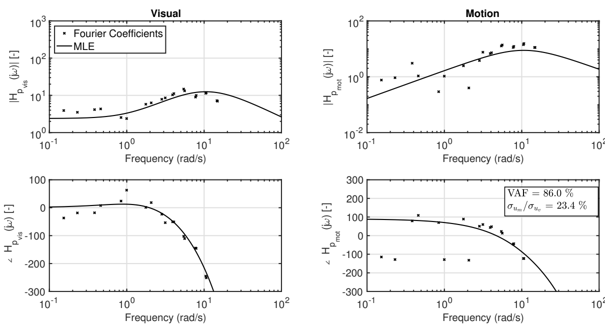

Figure A.87: Subject 7 C7

SRS Subject 8 of 19

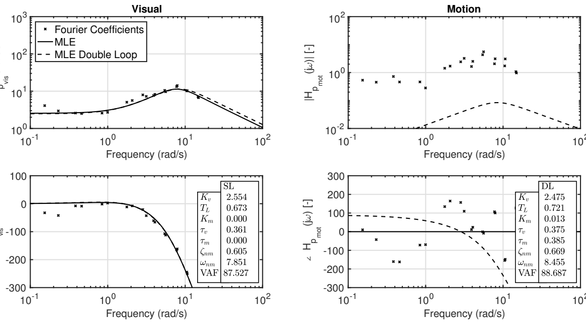

Figure A.88: Subject 8 C0

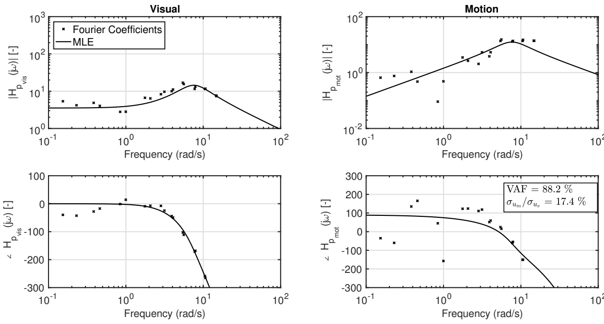

Figure A.89: Subject 8 C1

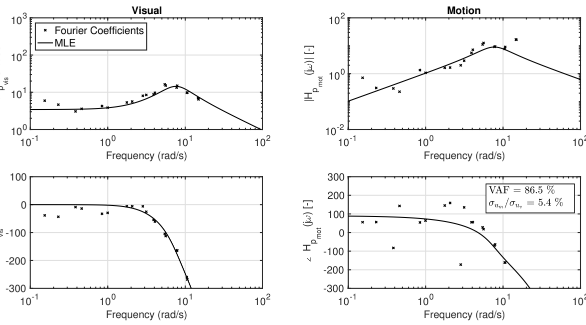

Figure A.90: Subject 8 C2

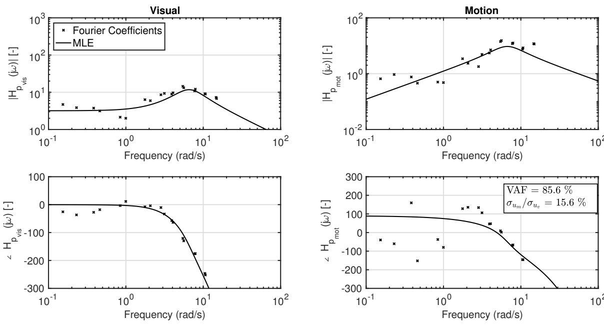

Figure A.91: Subject 8 C3

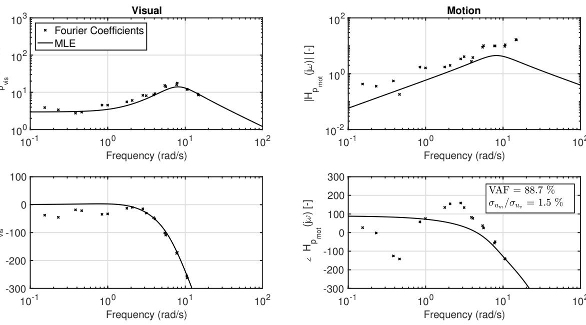

Figure A.92: Subject 8 C4

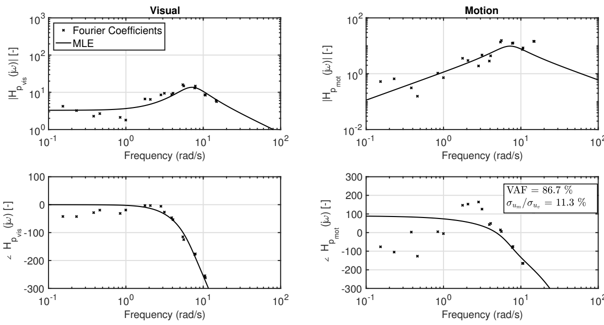

Figure A.93: Subject 8 C5

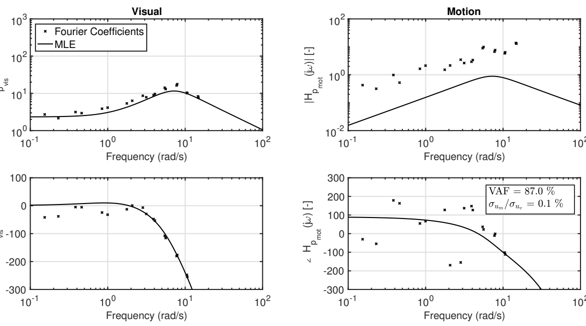

Figure A.94: Subject 8 C6

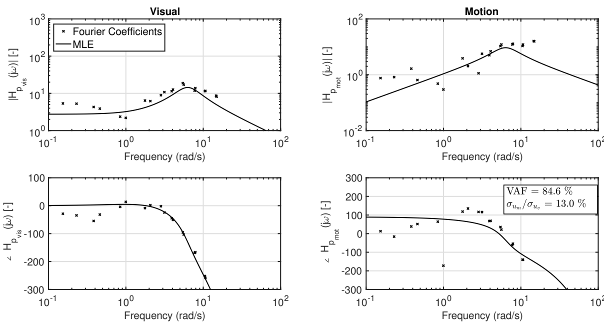

Figure A.95: Subject 8 C7

SRS Subject 9 of 19

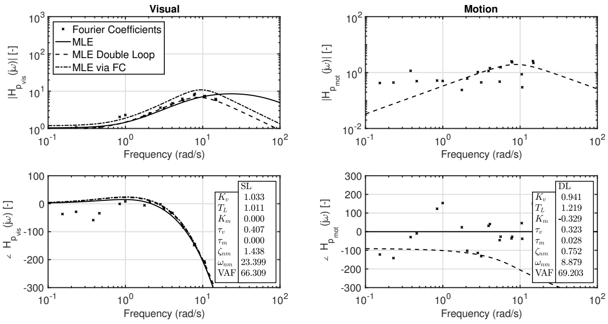

Figure A.96: Subject 9 C0

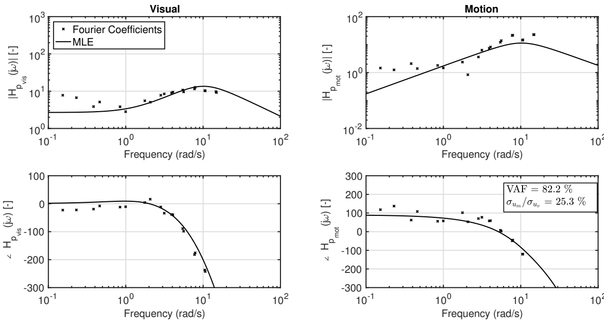

Figure A.97: Subject 9 C1

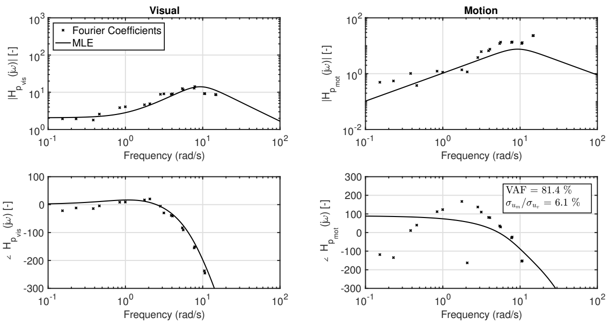

Figure A.98: Subject 9 C2

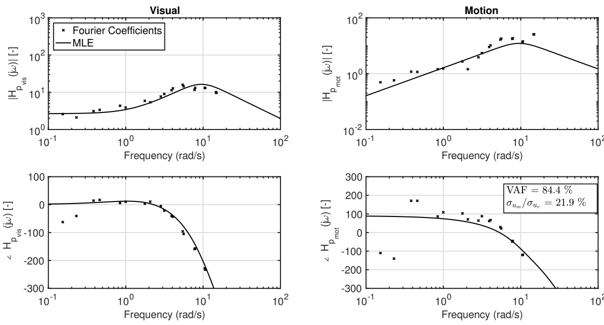

Figure A.99: Subject 9 C3

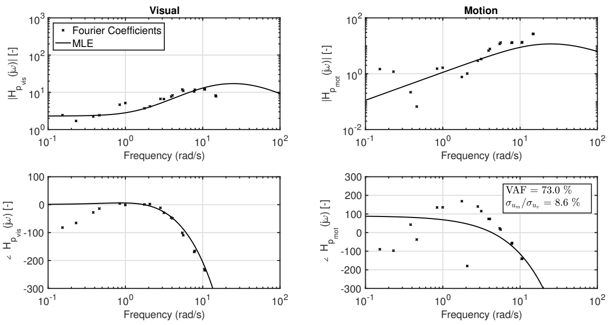

Figure A.100: Subject 9 C4

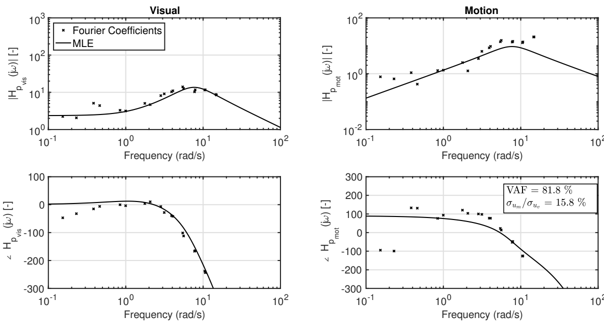

Figure A.101: Subject 9 C5

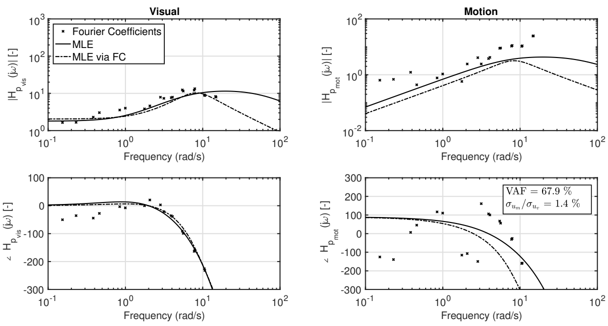

Figure A.102: Subject 9 C6

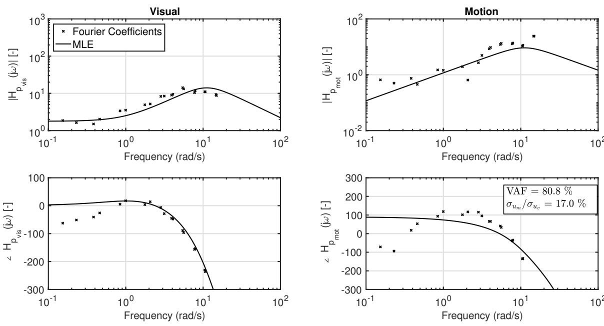

Figure A.103: Subject 9 C7

SRS Subject 10 of 19

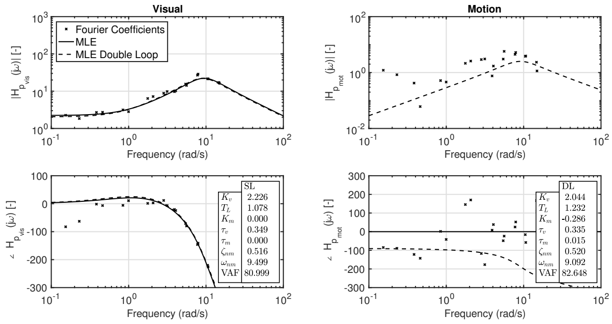

Figure A.104: Subject 10 C0

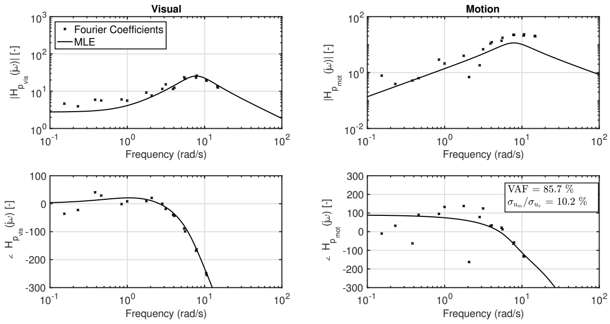

Figure A.105: Subject 10 C1

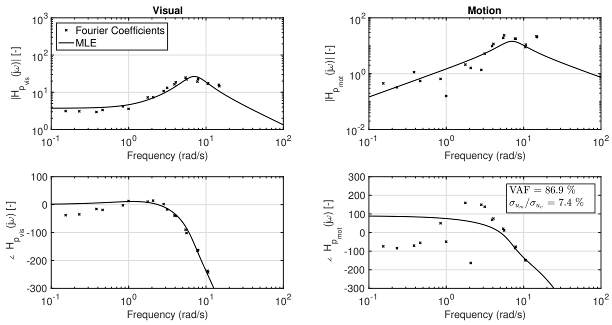

Figure A.106: Subject 10 C2

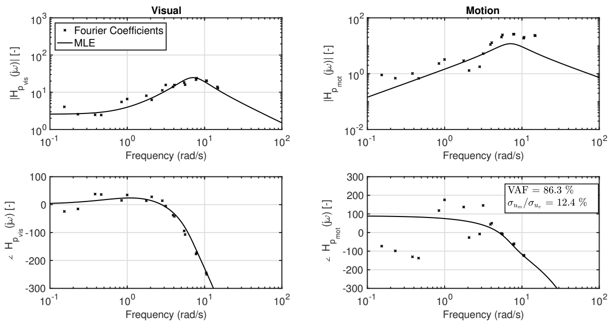

Figure A.107: Subject 10 C3

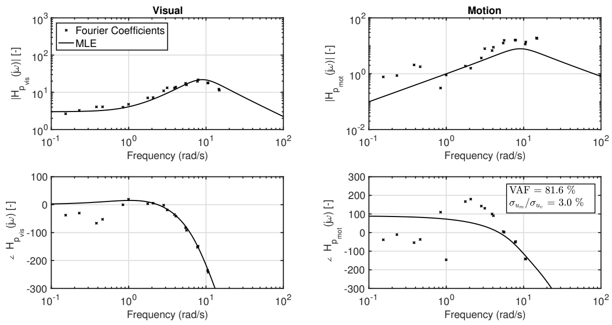

Figure A.108: Subject 10 C4

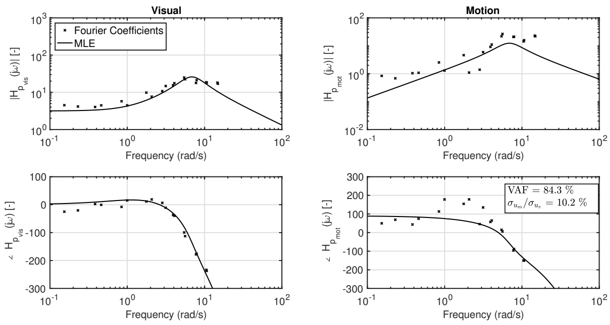

Figure A.109: Subject 10 C5

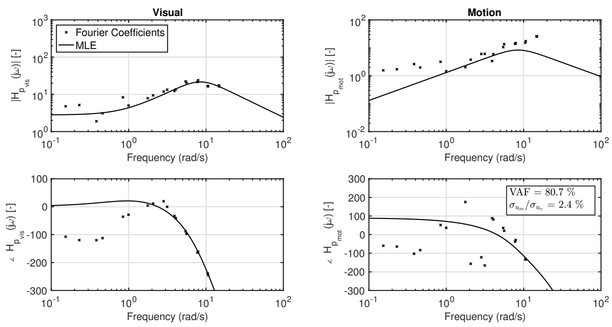

Figure A.110: Subject 10 C6

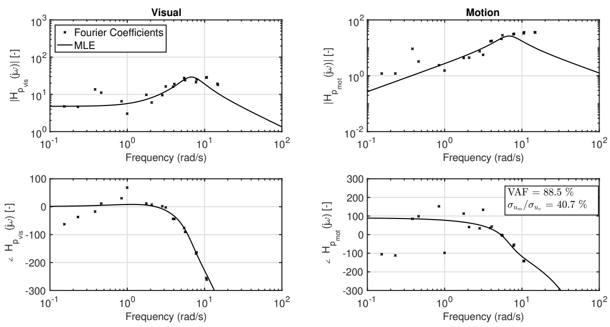

Figure A.111: Subject 10 C7

SRS Subject 11 of 19

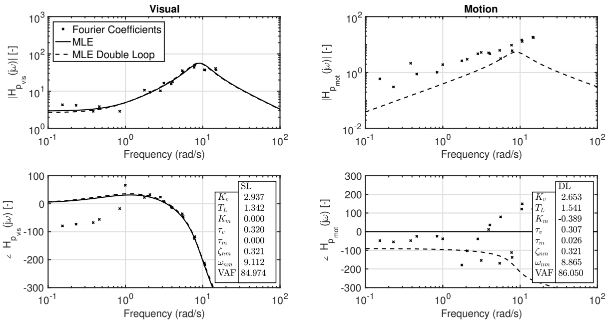

Figure A.112: Subject 11 C0

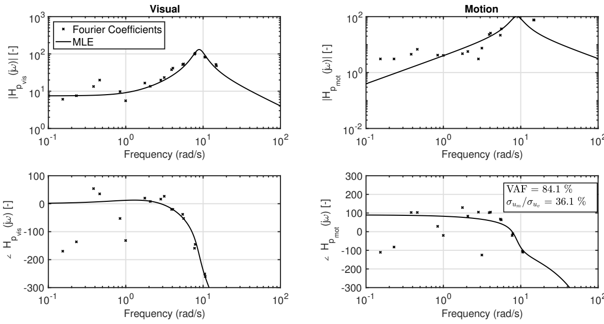

Figure A.113: Subject 11 C1

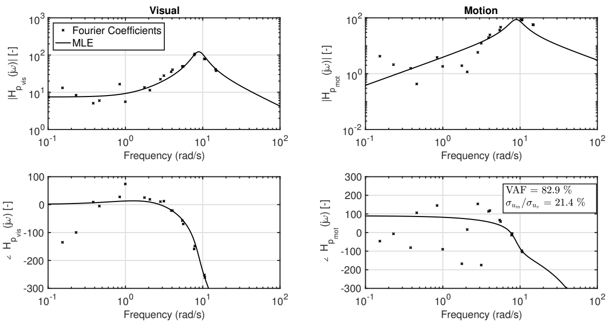

Figure A.114: Subject 11 C2

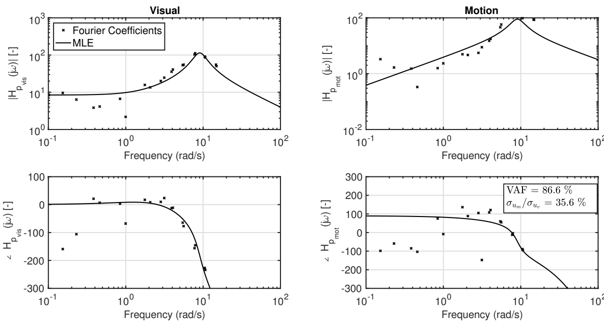

Figure A.115: Subject 11 C3

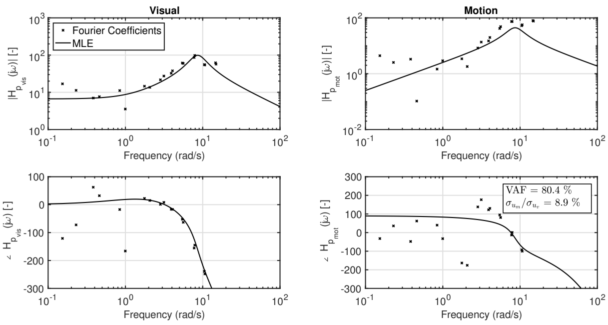

Figure A.116: Subject 11 C4

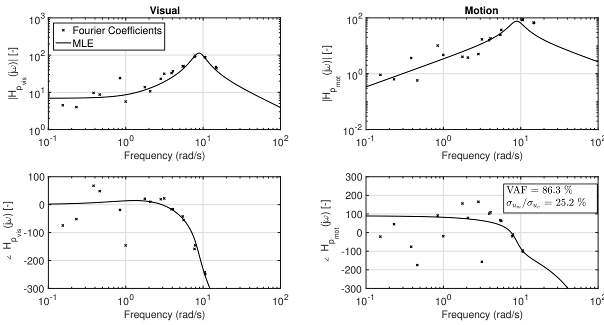

Figure A.117: Subject 11 C5

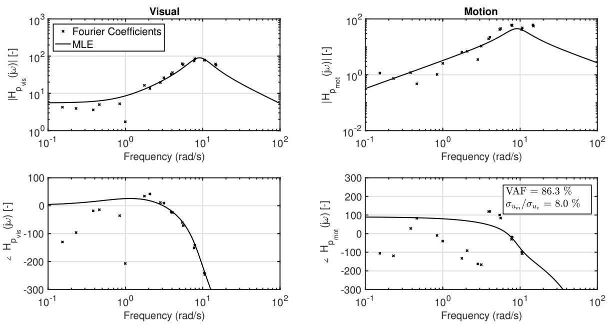

Figure A.118: Subject 11 C6

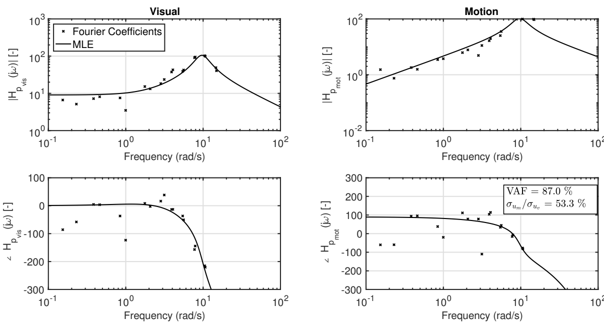

Figure A.119: Subject 11 C7

SRS Subject 12 of 19

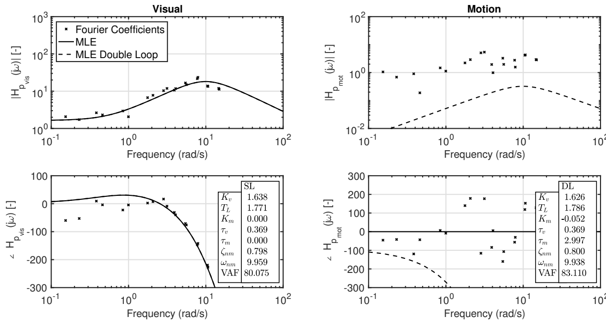

Figure A.120: Subject 12 C0

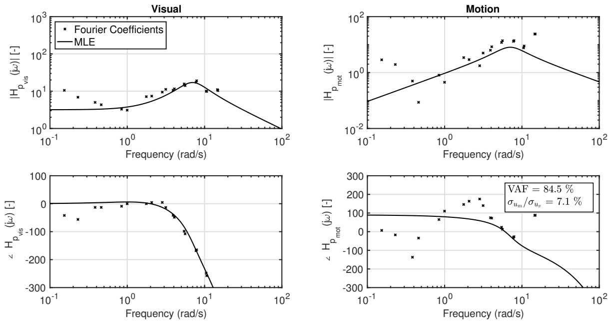

Figure A.121: Subject 12 C1

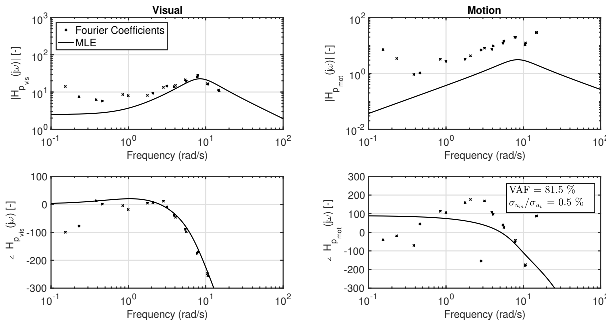

Figure A.122: Subject 12 C2

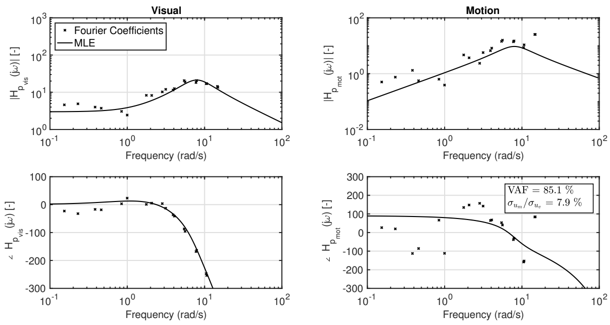

Figure A.123: Subject 12 C3

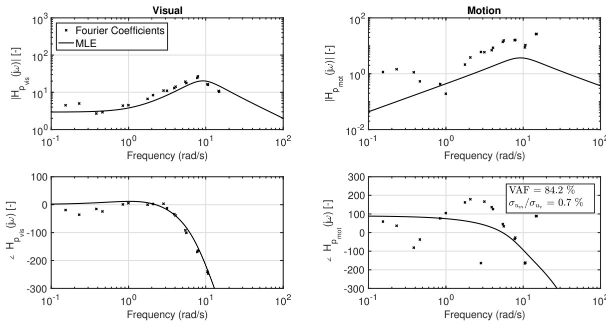

Figure A.124: Subject 12 C4

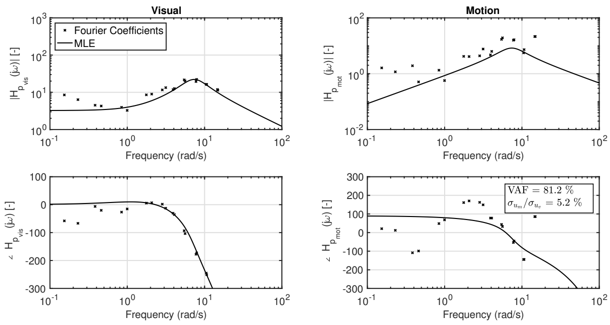

Figure A.125: Subject 12 C5

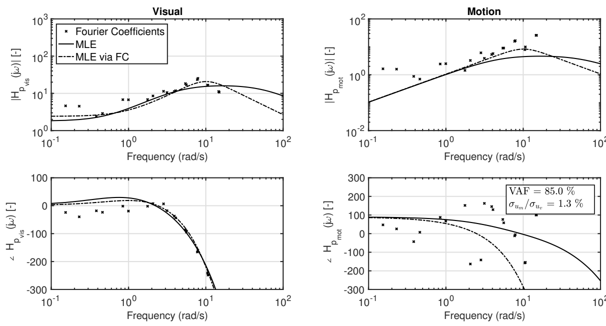

Figure A.126: Subject 12 C6

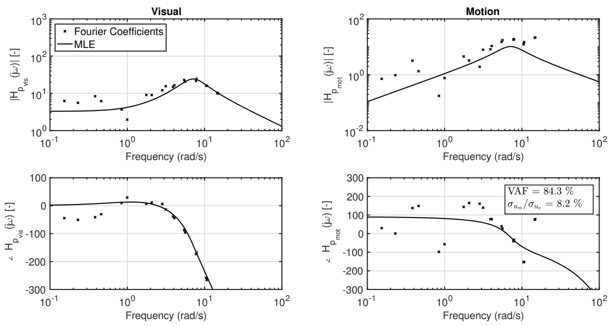

Figure A.127: Subject 12 C7

SRS Subject 13 of 19

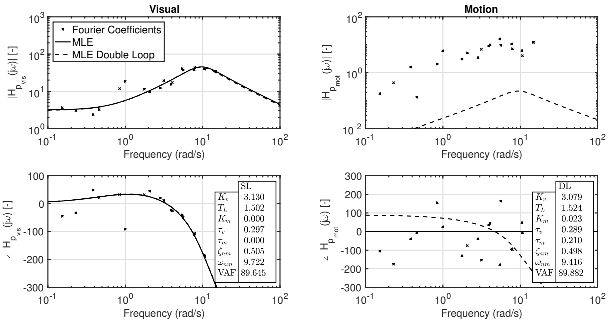

Figure A.128: Subject 13 C0

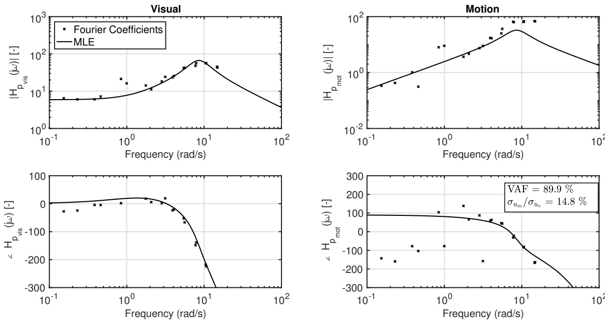

Figure A.129: Subject 13 C1

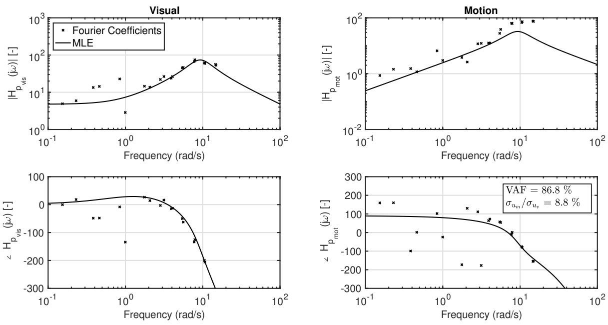

Figure A.130: Subject 13 C2

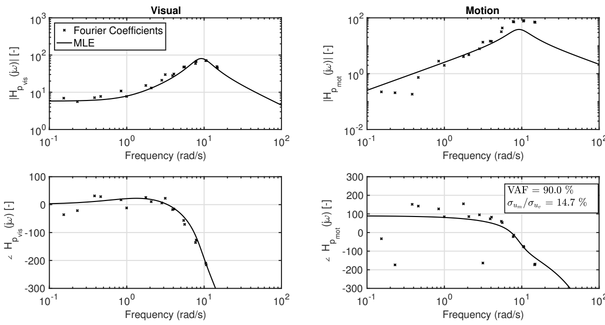

Figure A.131: Subject 13 C3

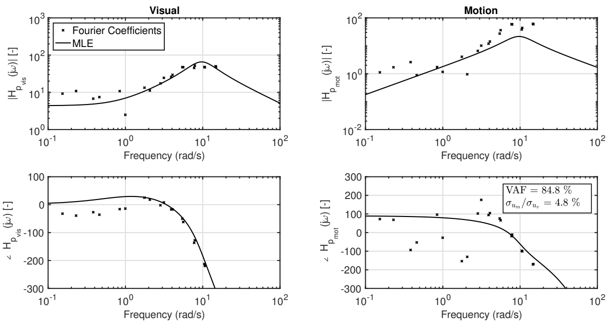

Figure A.132: Subject 13 C4

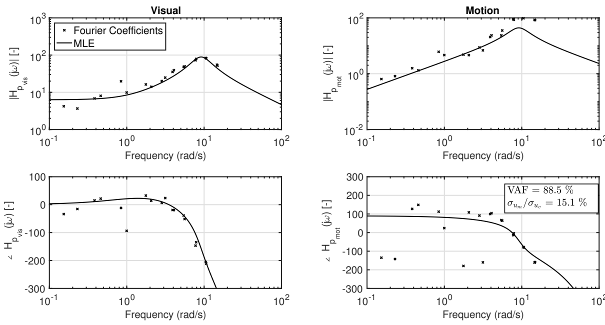

Figure A.133: Subject 13 C5

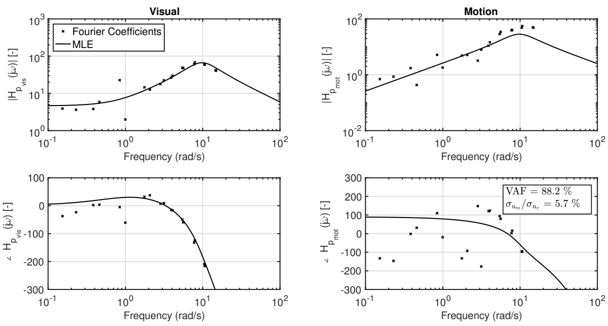

Figure A.134: Subject 13 C6

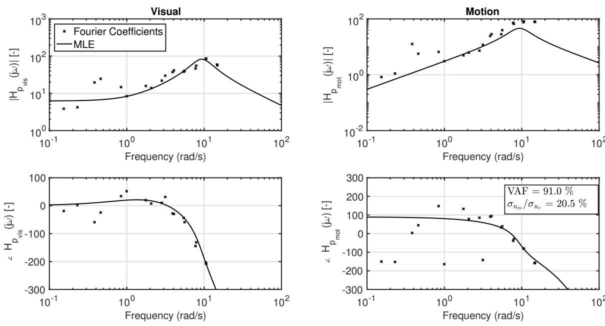

Figure A.135: Subject 13 C7

SRS Subject 14 of 19

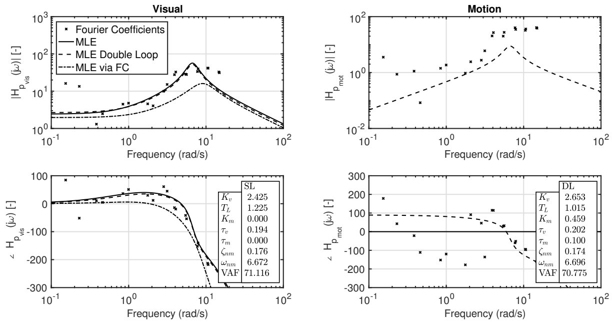

Figure A.136: Subject 14 C0

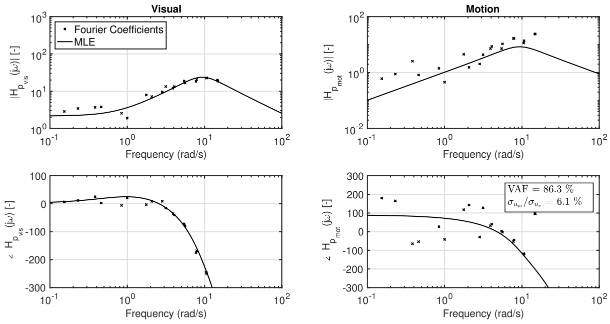

Figure A.137: Subject 14 C1

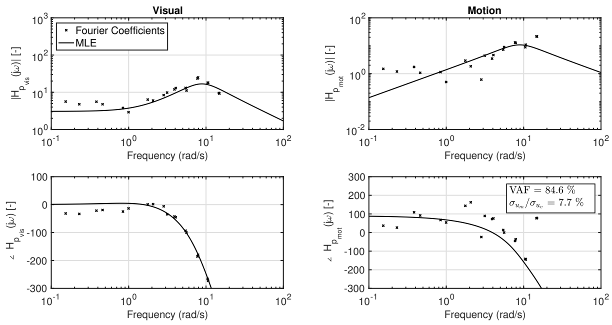

Figure A.138: Subject 14 C2

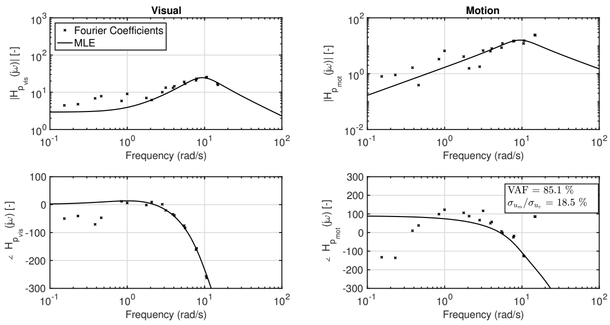

Figure A.139: Subject 14 C3

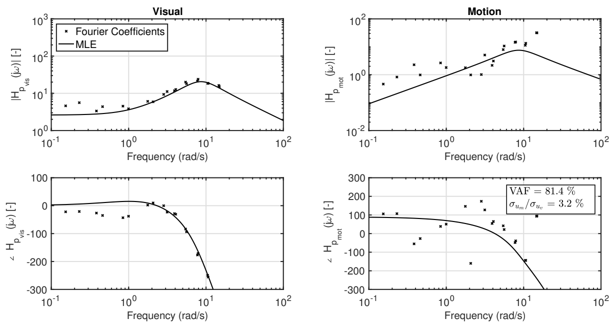

Figure A.140: Subject 14 C4

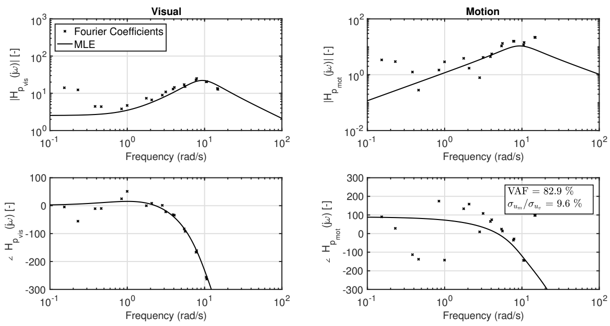

Figure A.141: Subject 14 C5

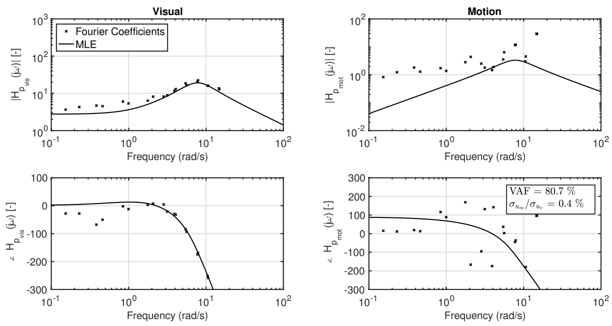

Figure A.142: Subject 14 C6

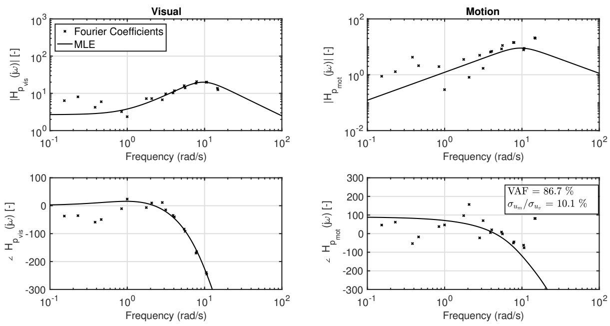

Figure A.143: Subject 14 C7

SRS Subject 15 of 19

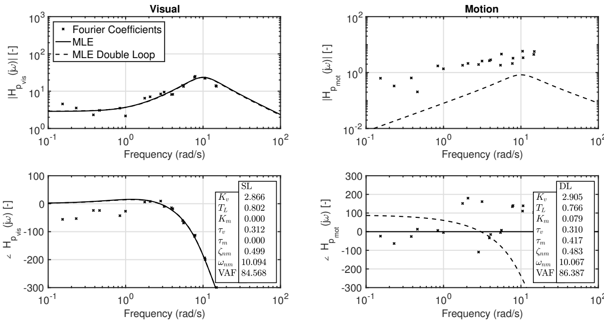

Figure A.144: Subject 15 C0

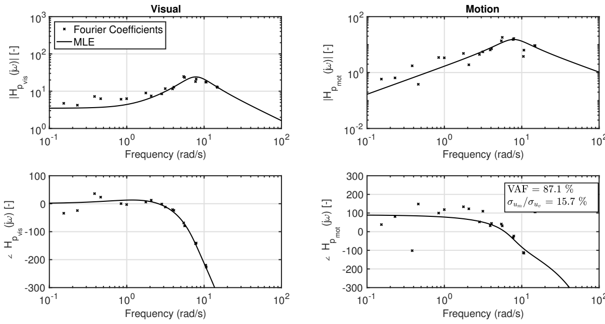

Figure A.145: Subject 15 C1

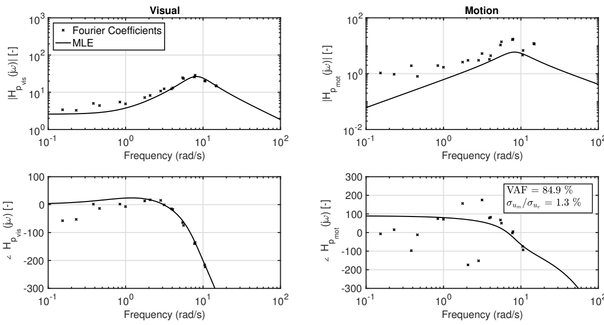

Figure A.146: Subject 15 C2

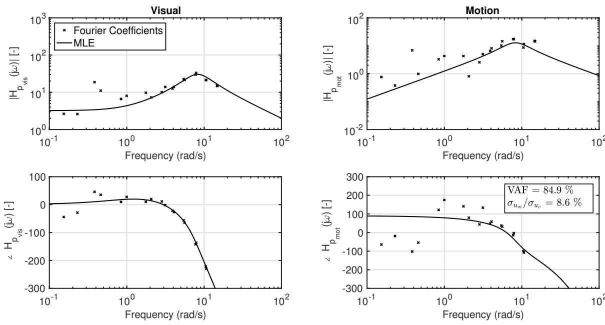

Figure A.147: Subject 15 C3

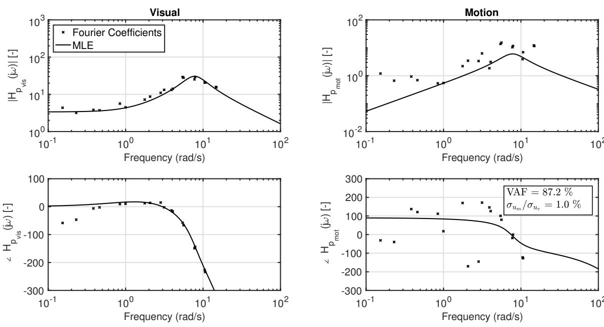

Figure A.148: Subject 15 C4

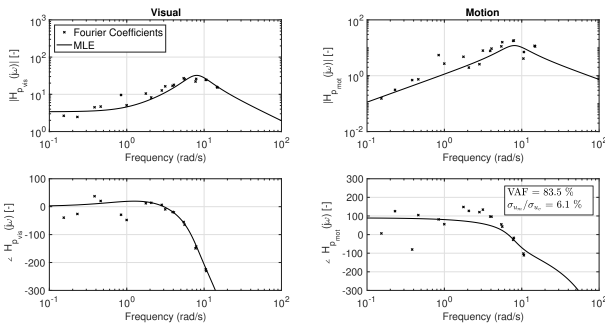

Figure A.149: Subject 15 C5

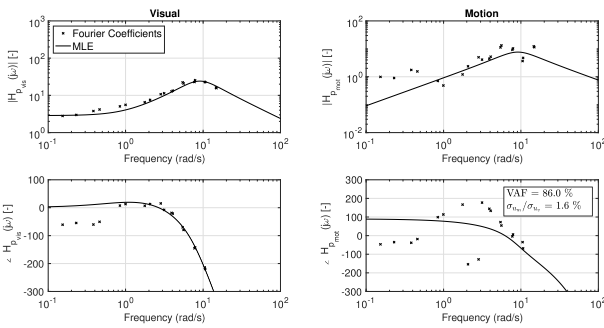

Figure A.150: Subject 15 C6

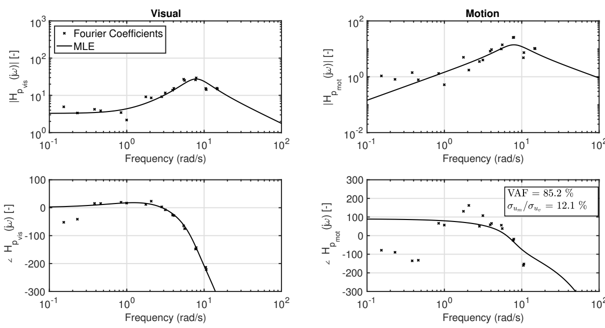

Figure A.151: Subject 15 C7

SRS Subject 16 of 19

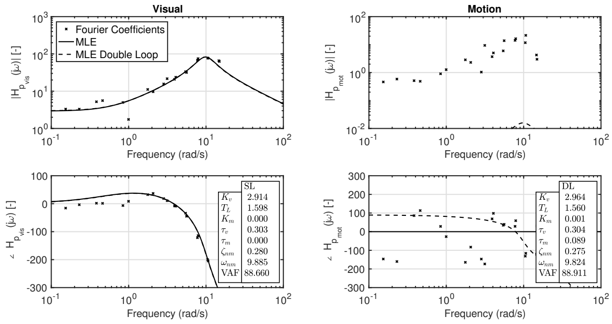

Figure A.152: Subject 16 C0

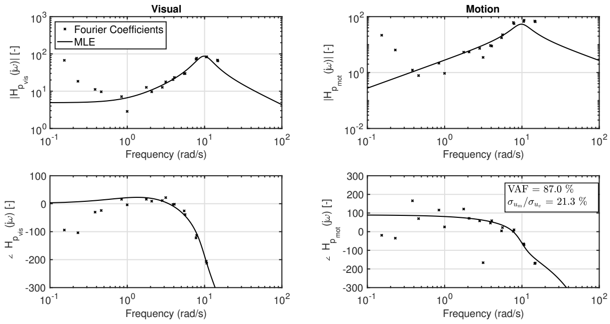

Figure A.153: Subject 16 C1

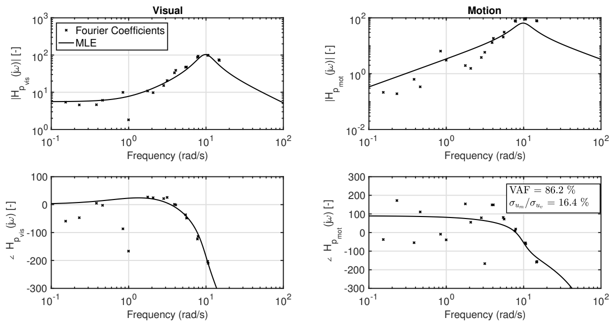

Figure A.154: Subject 16 C2

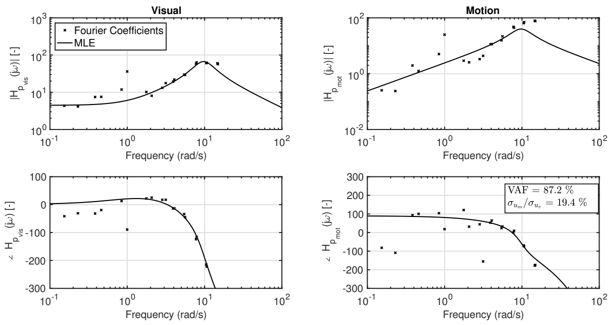

Figure A.155: Subject 16 C3

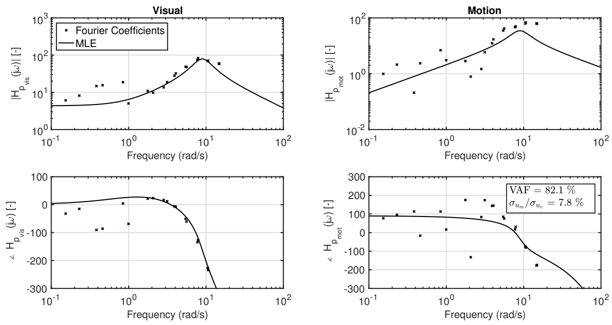

Figure A.156: Subject 16 C4

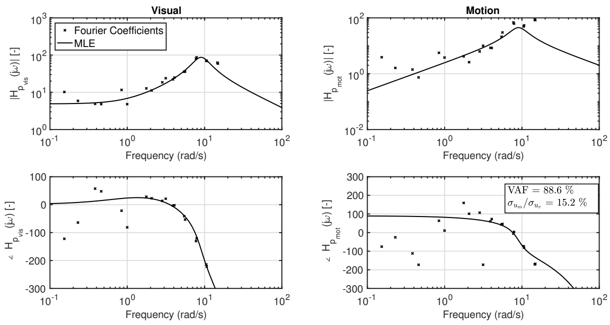

Figure A.157: Subject 16 C5

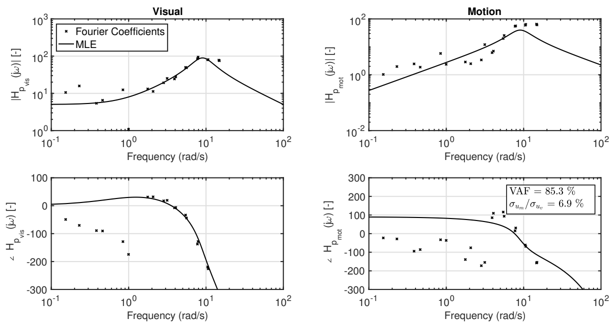

Figure A.158: Subject 16 C6

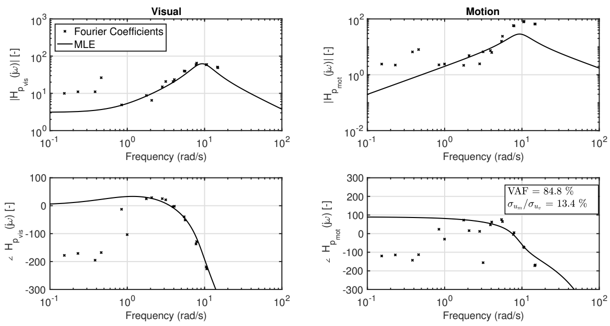

Figure A.159: Subject 16 C7

SRS Subject 17 of 19

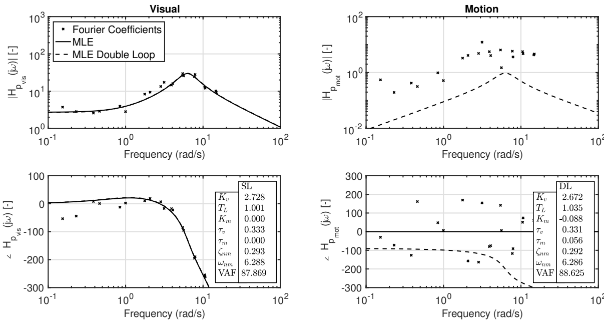

Figure A.160: Subject 17 C0

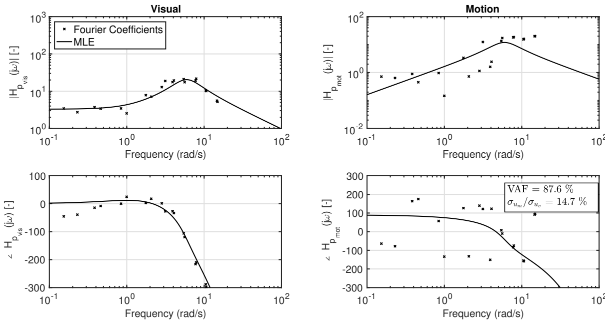

Figure A.161: Subject 17 C1

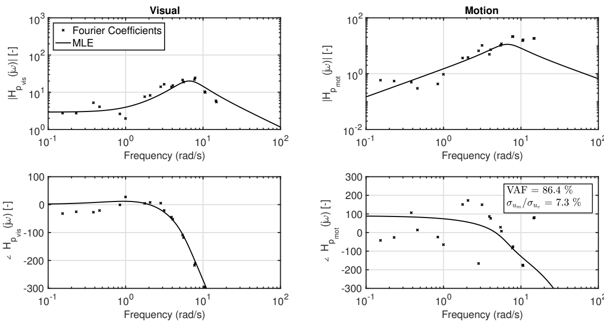

Figure A.162: Subject 17 C2

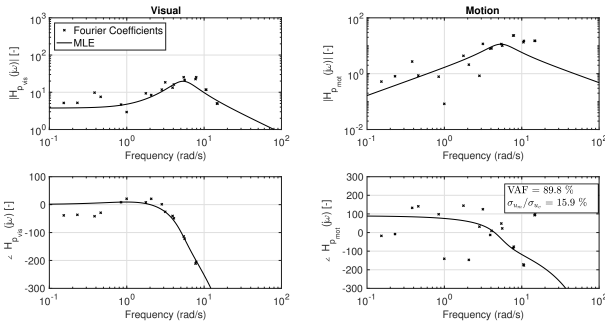

Figure A.163: Subject 17 C3

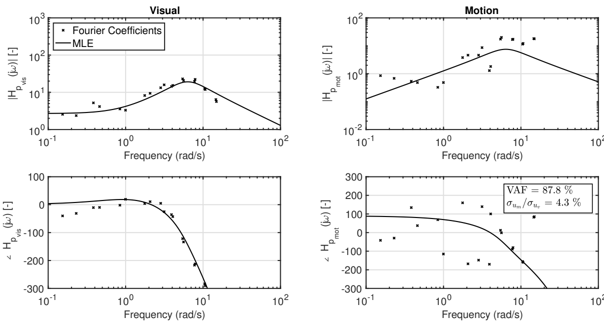

Figure A.164: Subject 17 C4

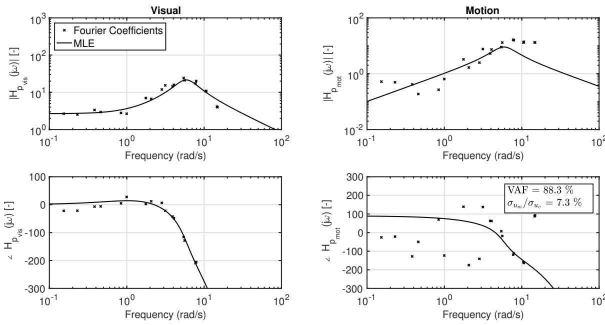

Figure A.165: Subject 17 C5

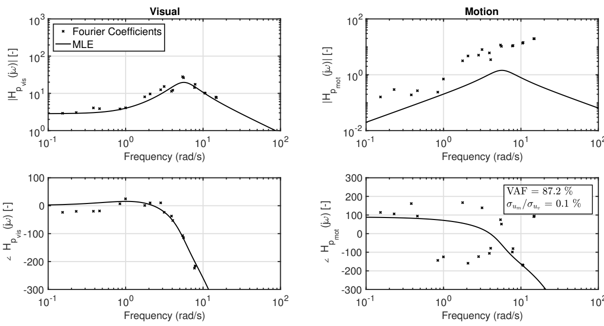

Figure A.166: Subject 17 C6

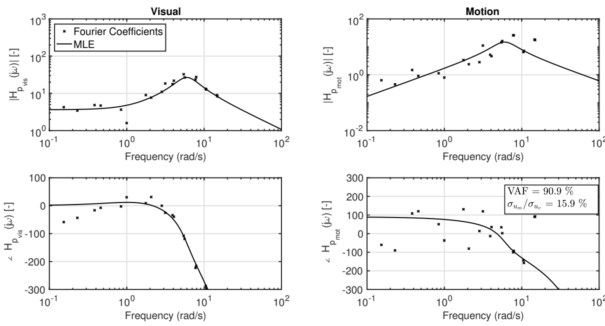

Figure A.167: Subject 17 C7

SRS Subject 18 of 19

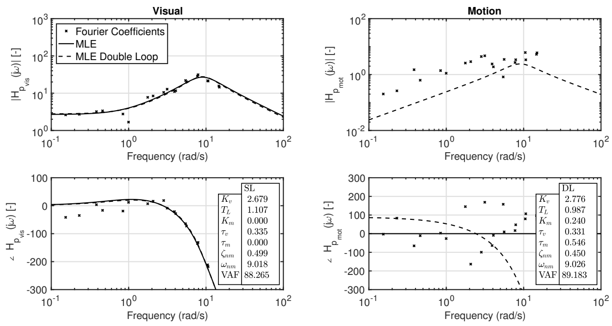

Figure A.168: Subject 18 C0

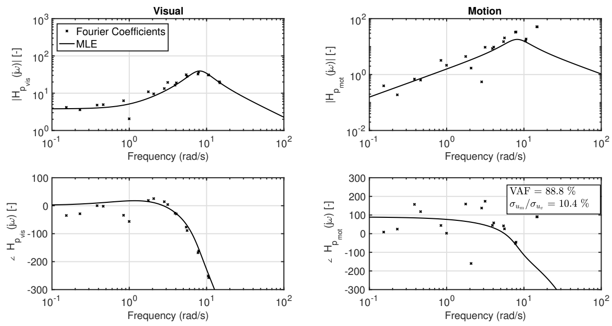

Figure A.169: Subject 18 C1

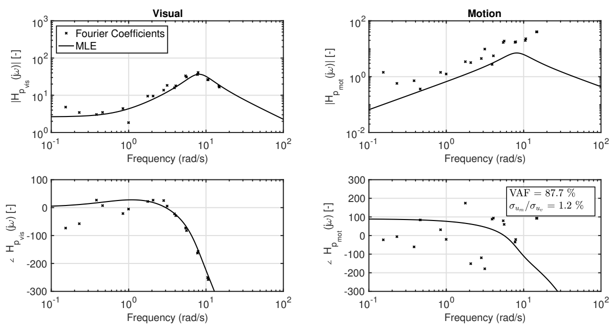

Figure A.170: Subject 18 C2

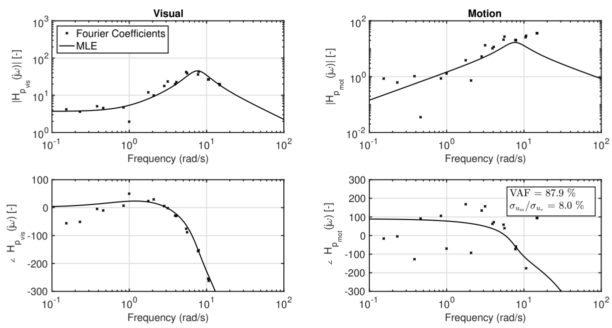

Figure A.171: Subject 18 C3

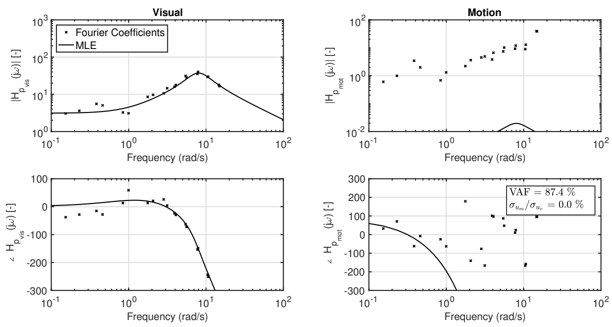

Figure A.172: Subject 18 C4

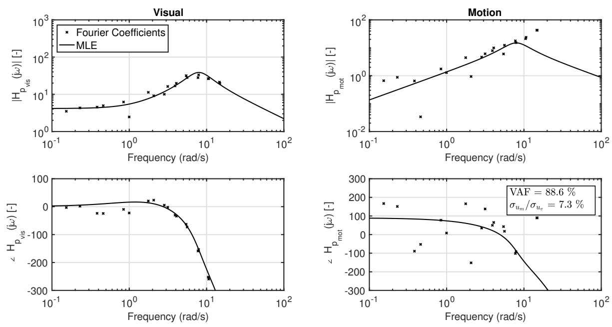

Figure A.173: Subject 18 C5

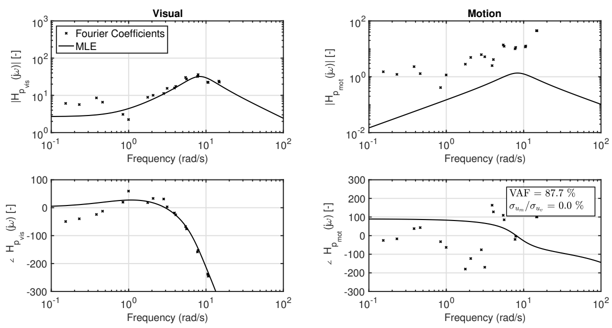

Figure A.174: Subject 18 C6

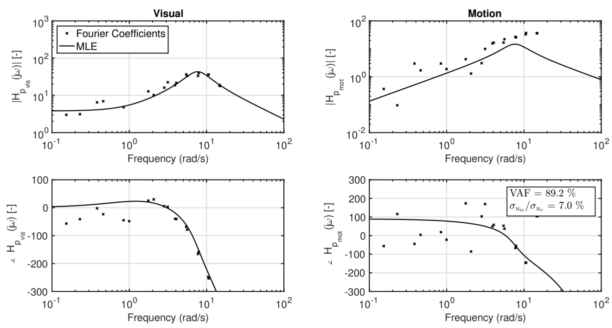

Figure A.175: Subject 18 C7

SRS Subject 19 of 19

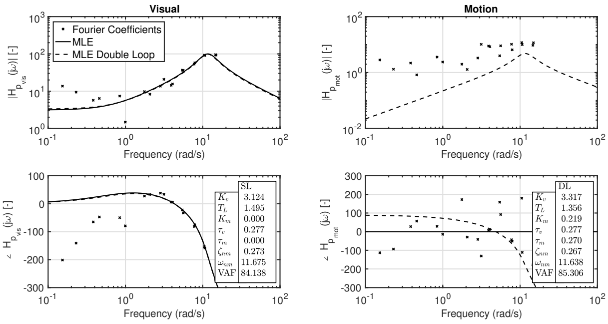

Figure A.176: Subject 19 C0

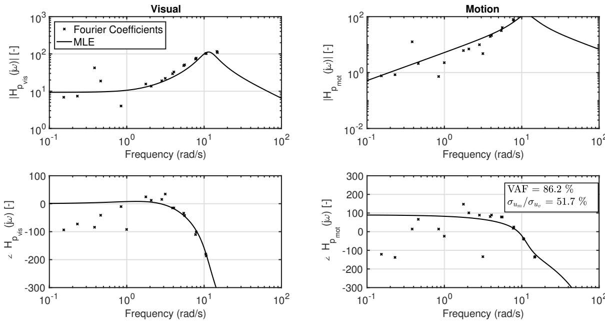

Figure A.177: Subject 19 C1

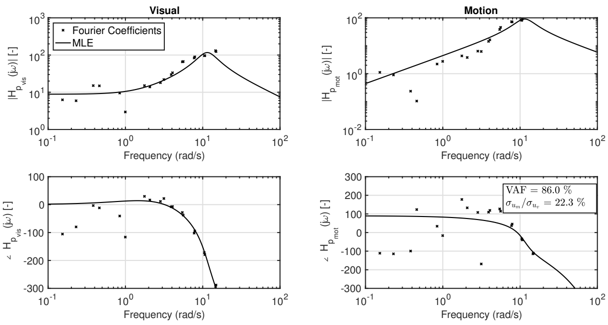

Figure A.178: Subject 19 C2

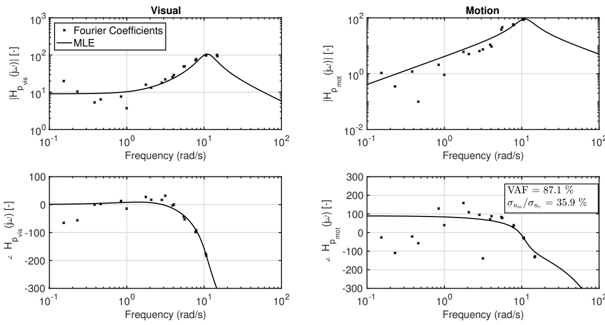

Figure A.179: Subject 19 C3

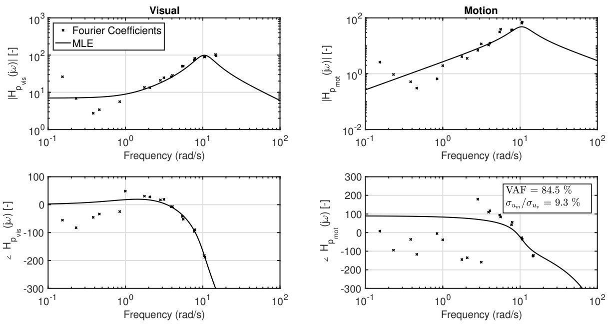

Figure A.180: Subject 19 C4

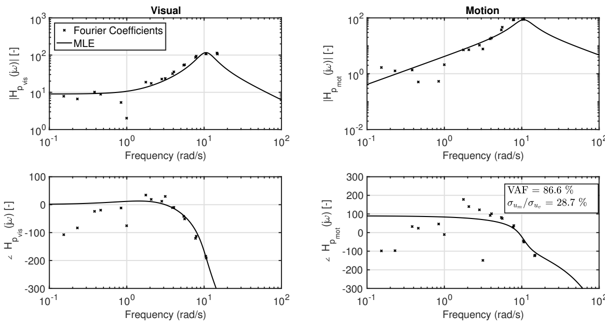

Figure A.181: Subject 19 C5

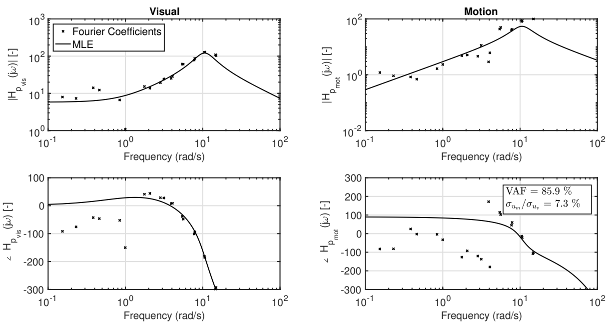

Figure A.182: Subject 19 C6

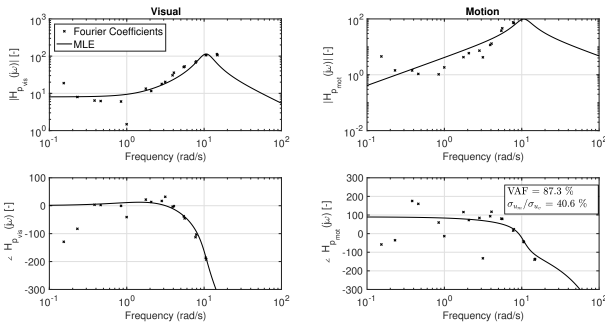

Figure A.183: Subject 19 C7

VMS Subject 1 of 18

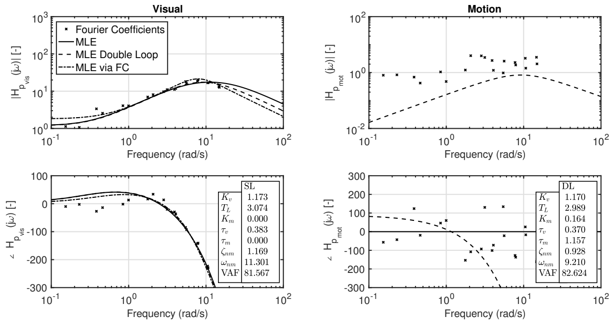

Figure A.184: Subject 1 C0

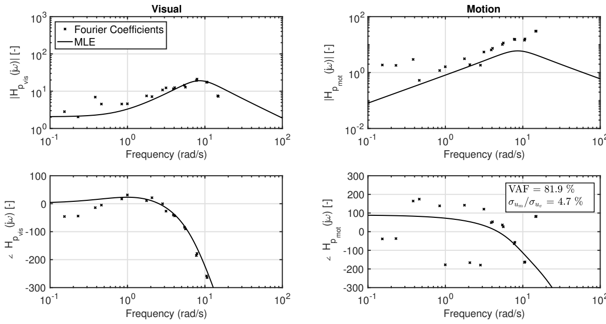

Figure A.185: Subject 1 C1

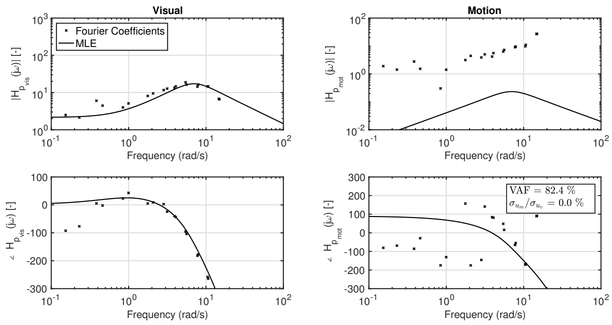

Figure A.186: Subject 1 C2

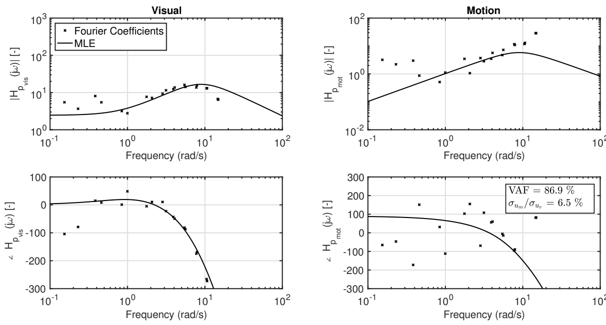

Figure A.187: Subject 1 C3

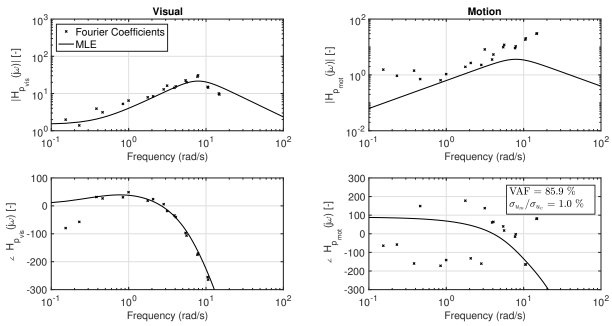

Figure A.188: Subject 1 C4

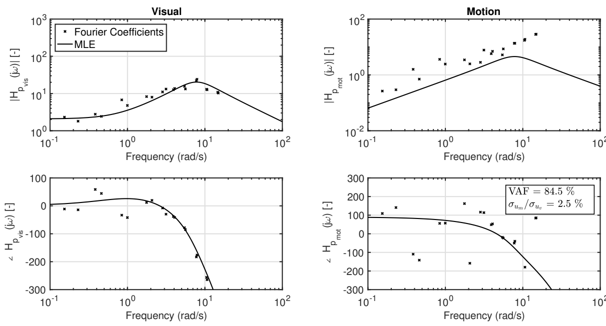

Figure A.189: Subject 1 C5

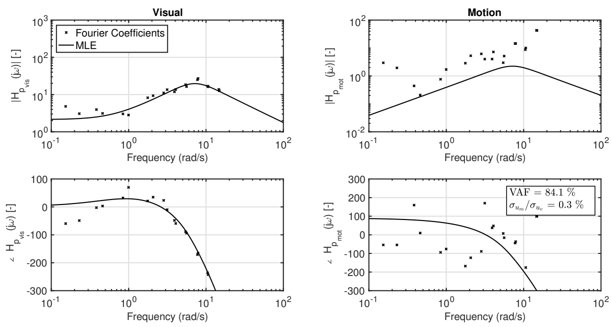

Figure A.190: Subject 1 C6

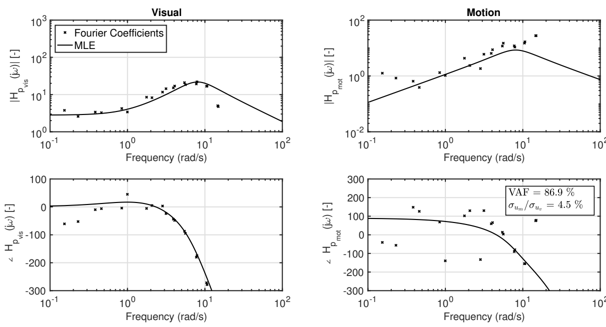

Figure A.191: Subject 1 C7

VMS Subject 2 of 18

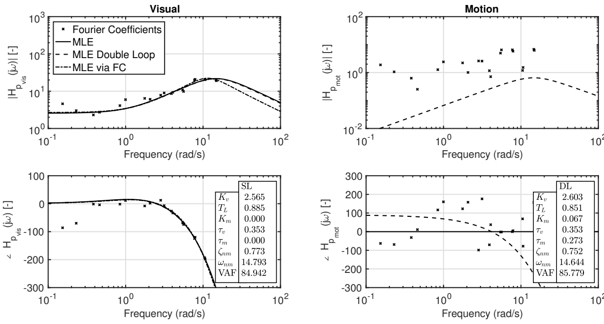

Figure A.192: Subject 2 C0

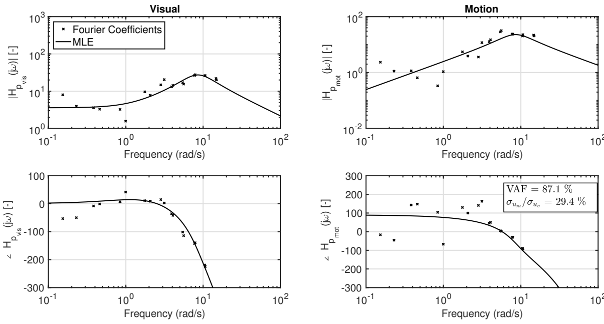

Figure A.193: Subject 2 C1

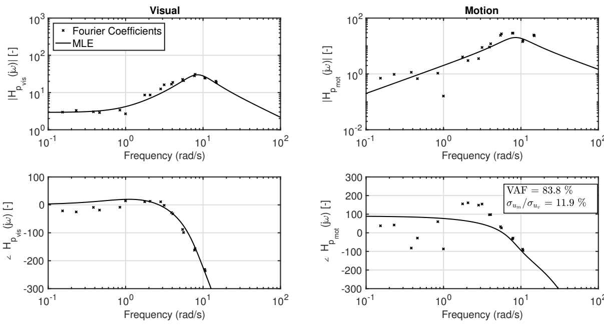

Figure A.194: Subject 2 C2

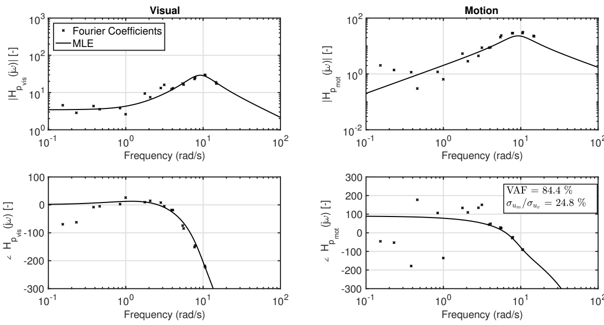

Figure A.195: Subject 2 C3

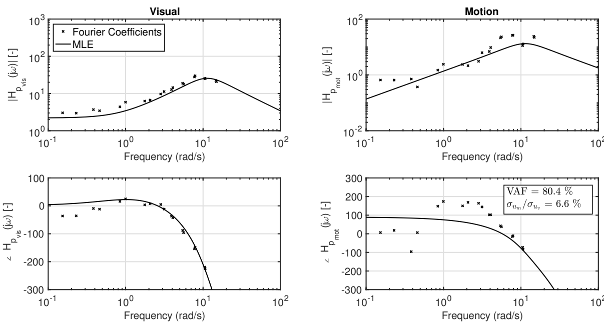

Figure A.196: Subject 2 C4

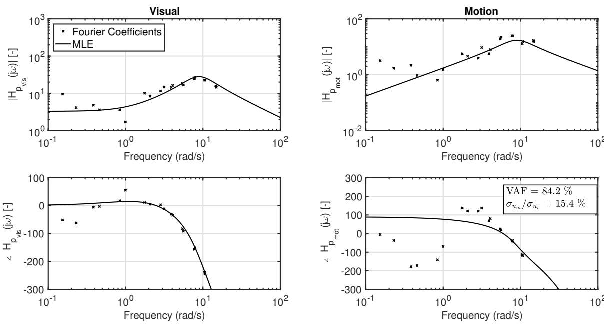

Figure A.197: Subject 2 C5

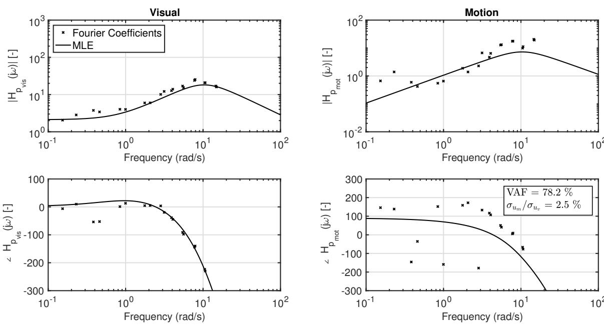

Figure A.198: Subject 2 C6

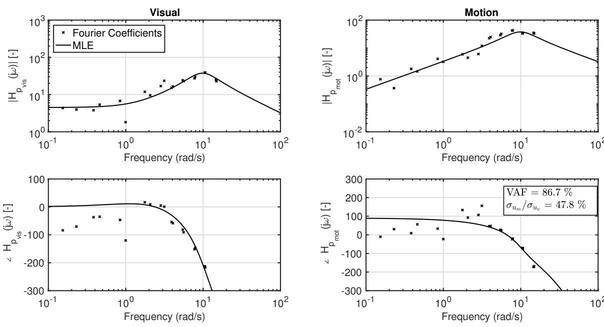

Figure A.199: Subject 2 C7

VMS Subject 3 of 18

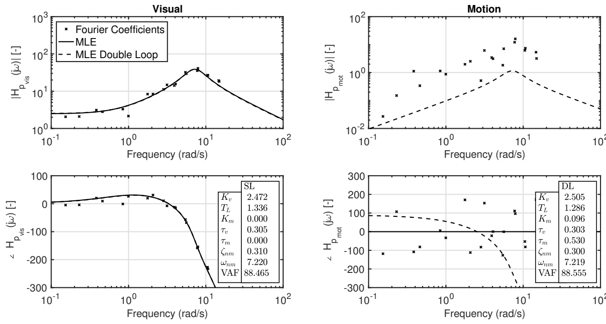

Figure A.200: Subject 3 C0

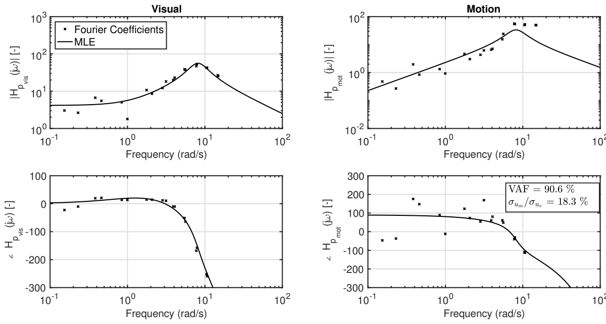

Figure A.201: Subject 3 C1

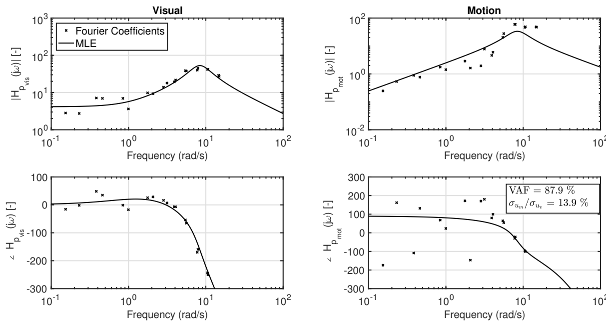

Figure A.202: Subject 3 C2

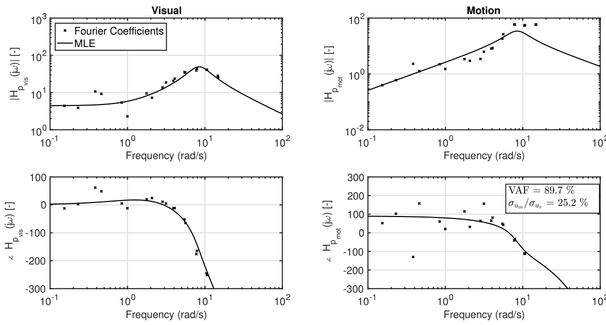

Figure A.203: Subject 3 C3

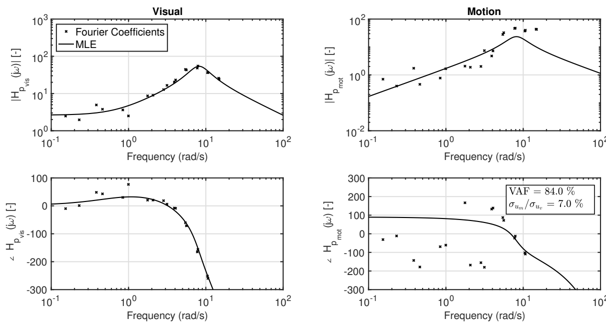

Figure A.204: Subject 3 C4

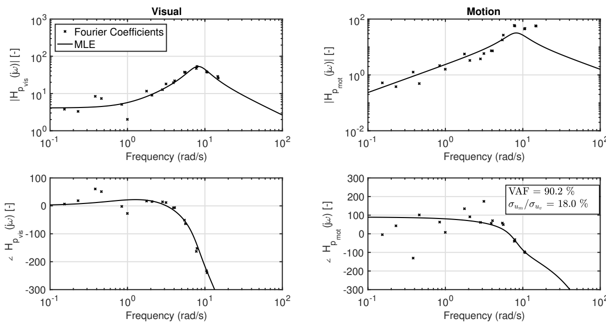

Figure A.205: Subject 3 C5

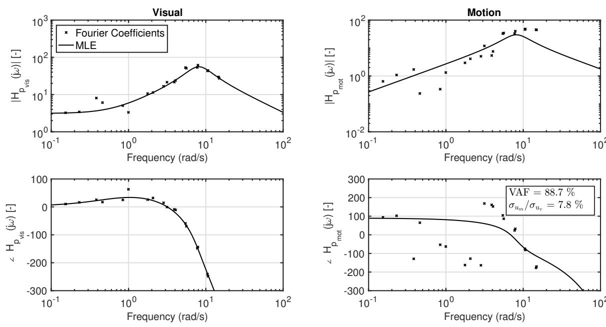

Figure A.206: Subject 3 C6

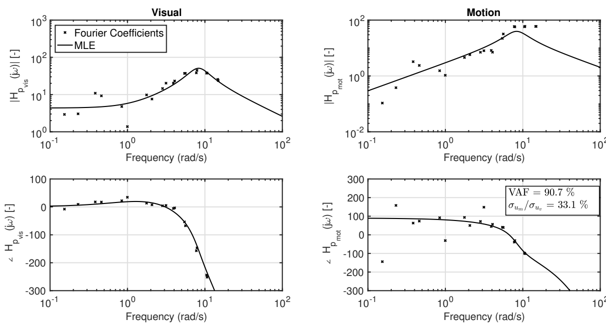

Figure A.207: Subject 3 C7

VMS Subject 4 of 18

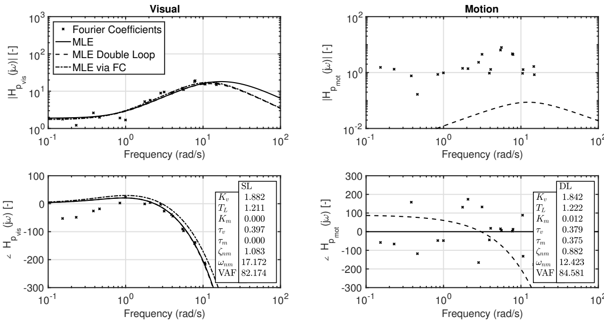

Figure A.208: Subject 4 C0

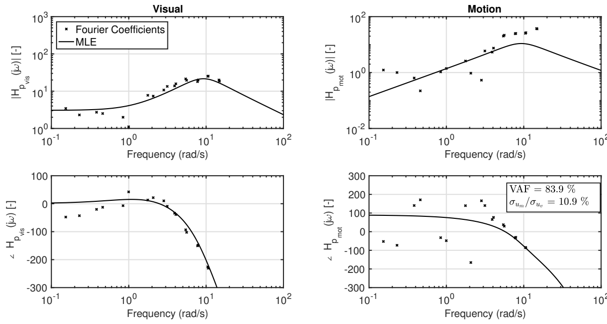

Figure A.209: Subject 4 C1

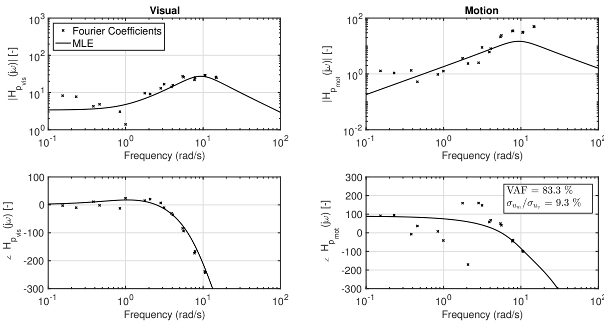

Figure A.210: Subject 4 C2

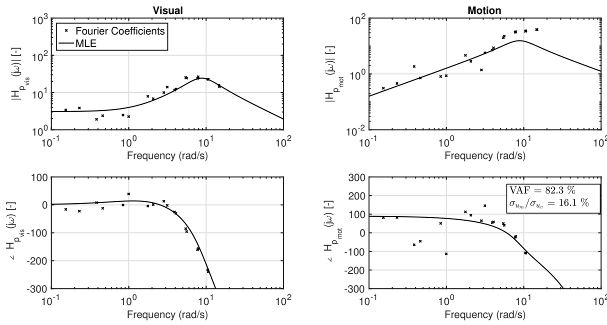

Figure A.211: Subject 4 C3

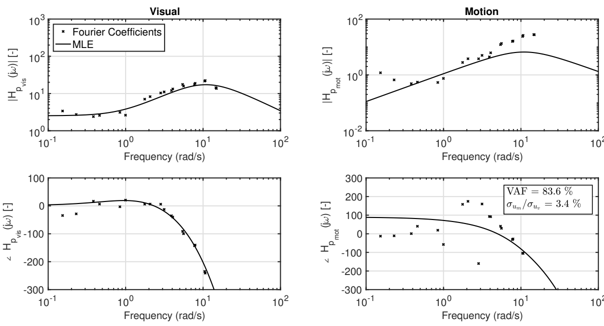

Figure A.212: Subject 4 C4

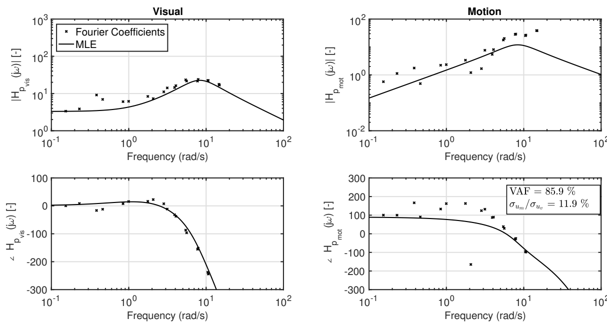

Figure A.213: Subject 4 C5

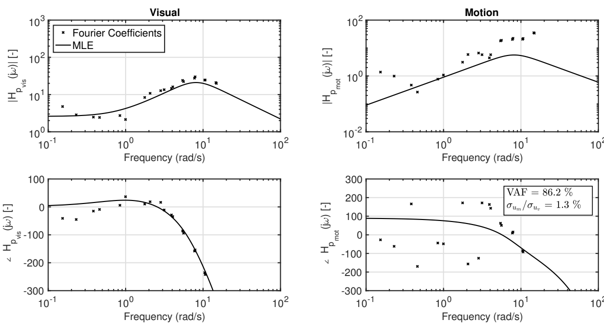

Figure A.214: Subject 4 C6

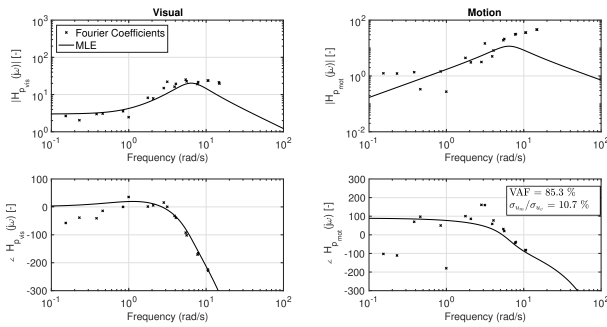

Figure A.215: Subject 4 C7

VMS Subject 5 of 18

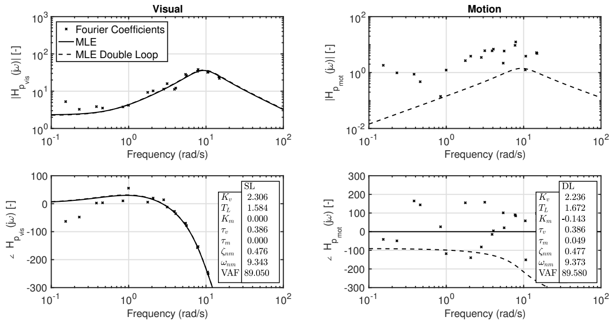

Figure A.216: Subject 5 C0

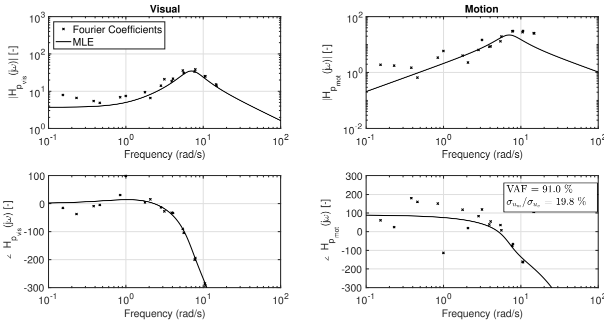

Figure A.217: Subject 5 C1

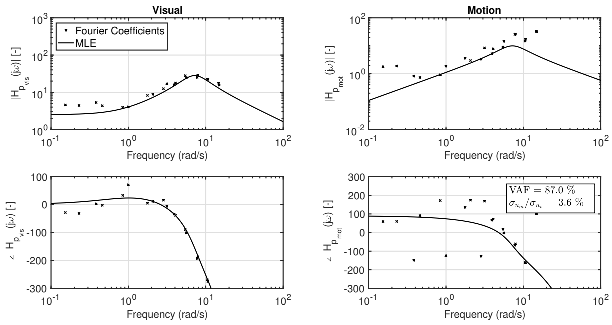

Figure A.218: Subject 5 C2

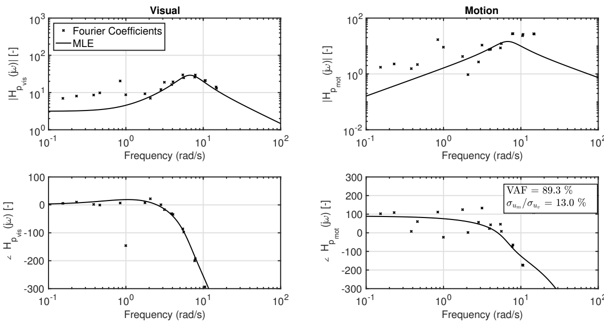

Figure A.219: Subject 5 C3

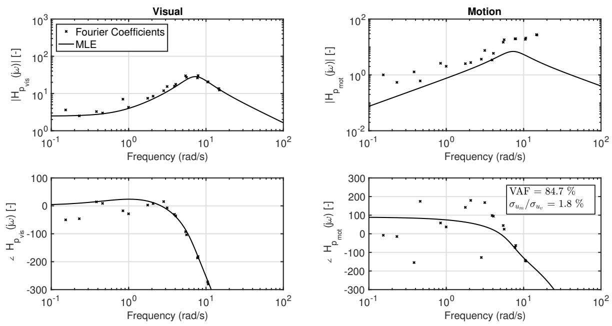

Figure A.220: Subject 5 C4

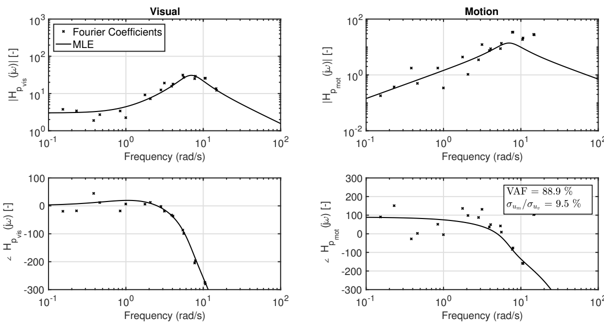

Figure A.221: Subject 5 C5

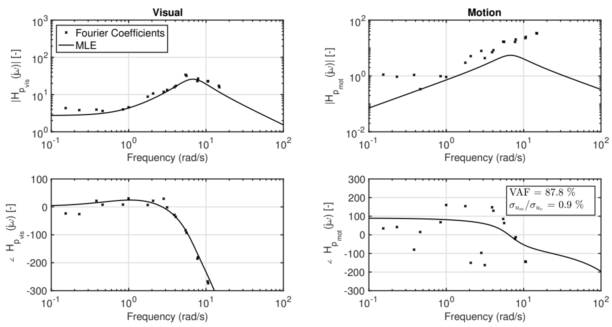

Figure A.222: Subject 5 C6

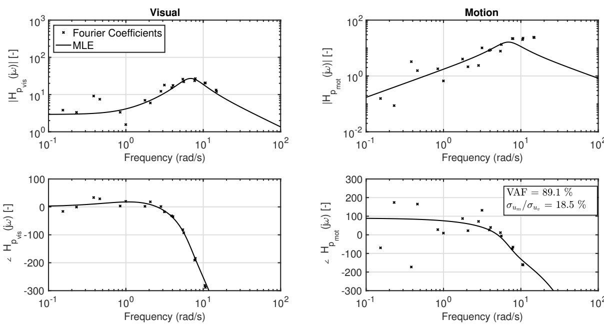

Figure A.223: Subject 5 C7

VMS Subject 6 of 18

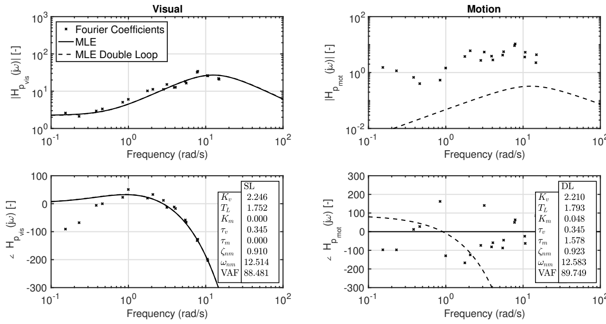

Figure A.224: Subject 6 C0

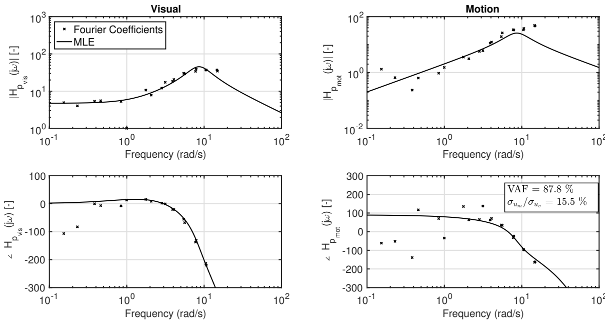

Figure A.225: Subject 6 C1

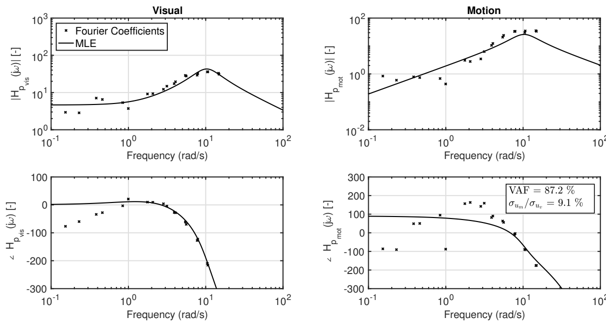

Figure A.226: Subject 6 C2

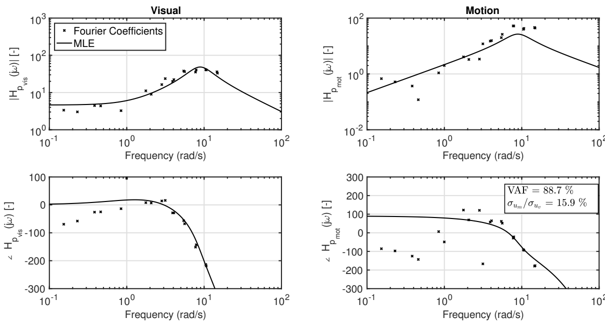

Figure A.227: Subject 6 C3

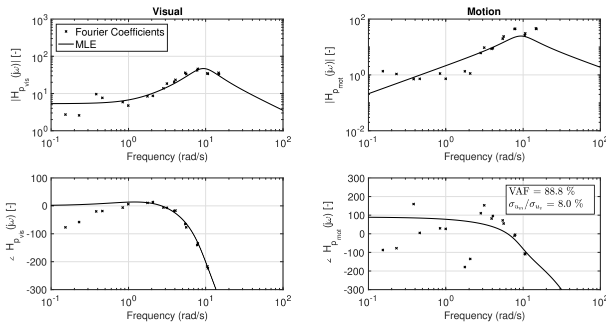

Figure A.228: Subject 6 C4

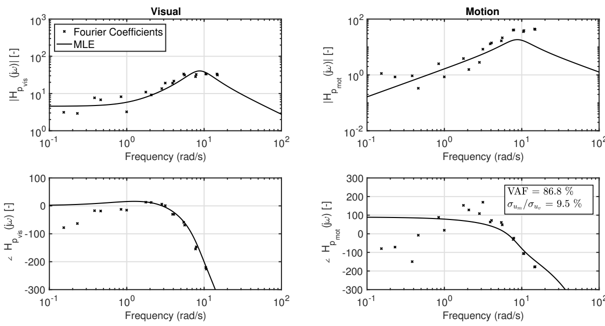

Figure A.229: Subject 6 C5

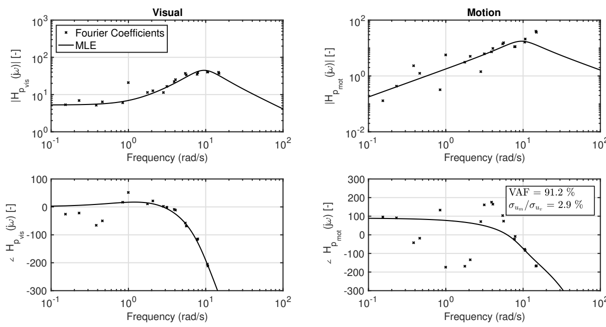

Figure A.230: Subject 6 C6

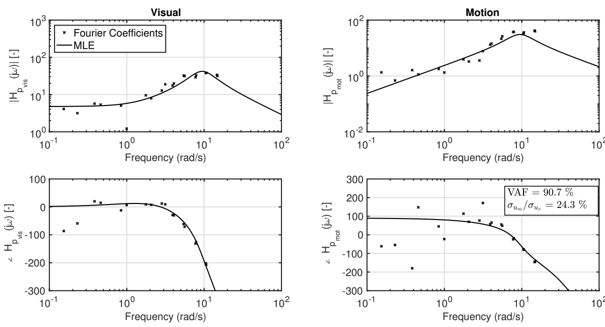

Figure A.231: Subject 6 C7

VMS Subject 7 of 18

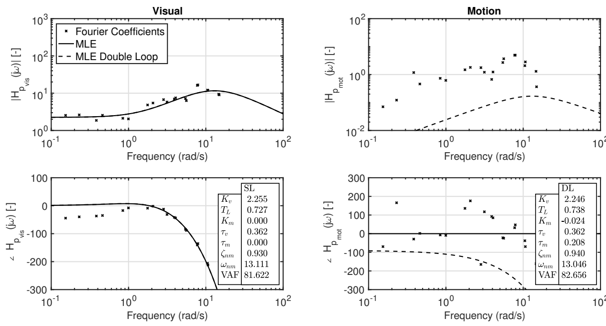

Figure A.232: Subject 7 C0

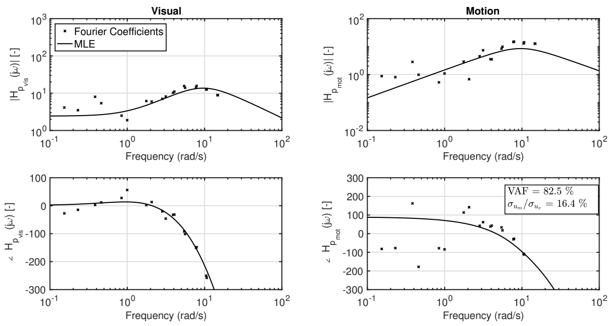

Figure A.233: Subject 7 C1

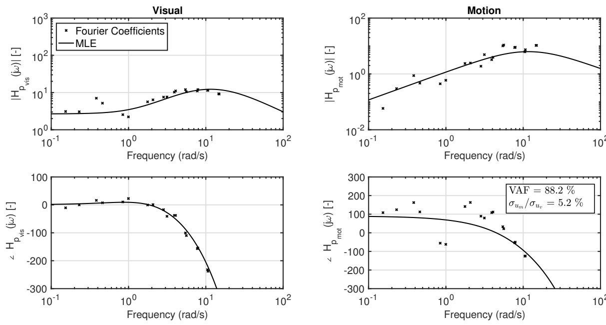

Figure A.234: Subject 7 C2

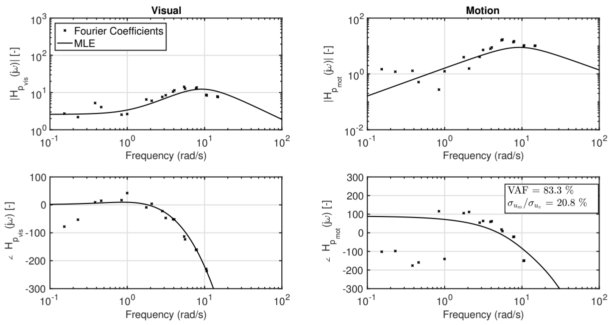

Figure A.235: Subject 7 C3

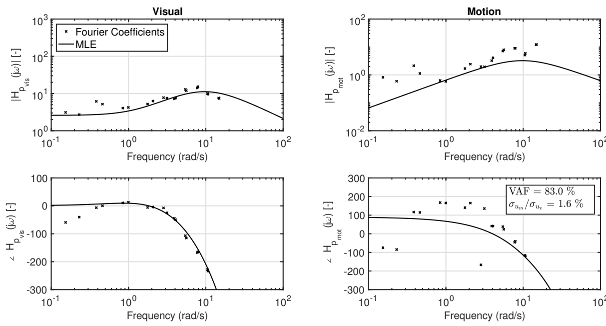

Figure A.236: Subject 7 C4

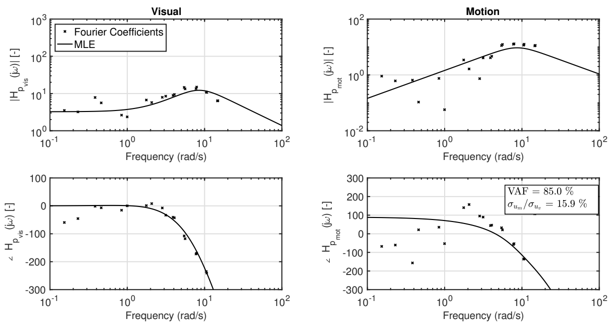

Figure A.237: Subject 7 C5

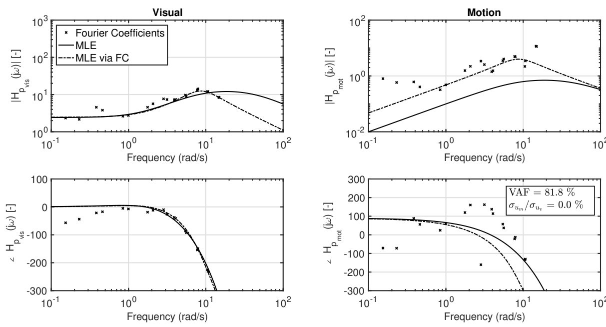

Figure A.238: Subject 7 C6

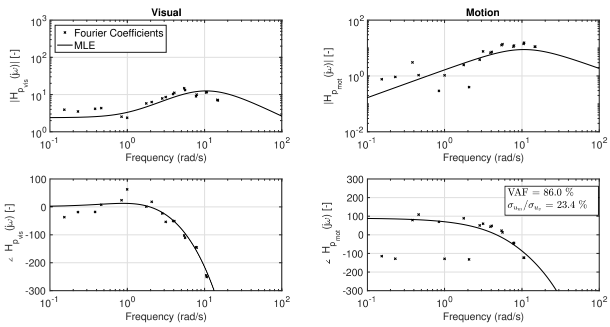

Figure A.239: Subject 7 C7

VMS Subject 8 of 18

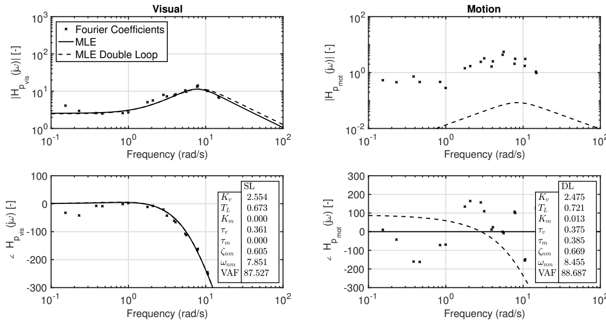

Figure A.240: Subject 8 C0

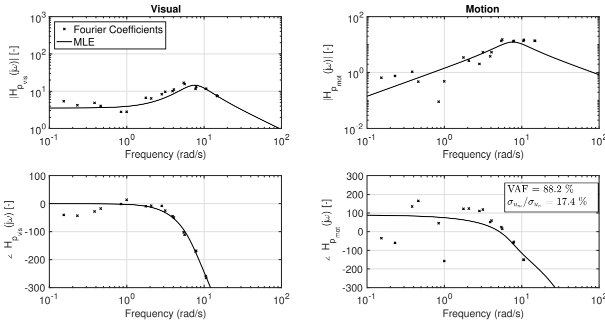

Figure A.241: Subject 8 C1

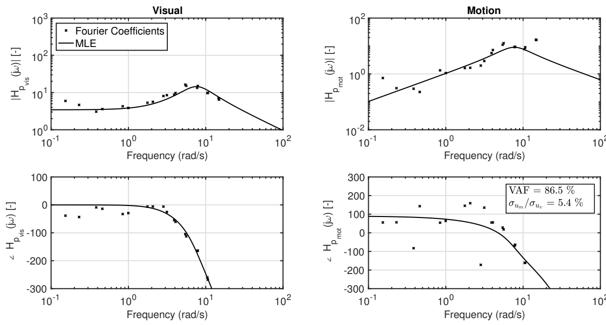

Figure A.242: Subject 8 C2

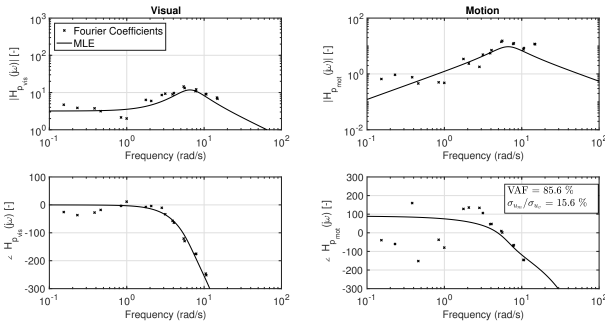

Figure A.243: Subject 8 C3

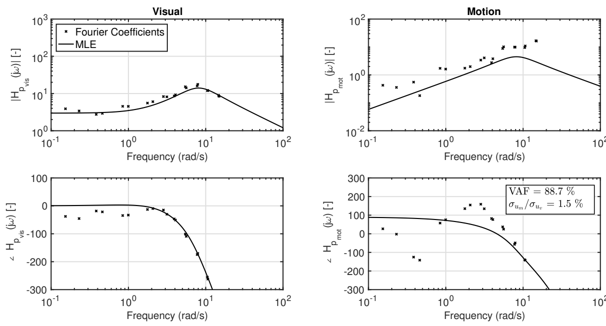

Figure A.244: Subject 8 C4

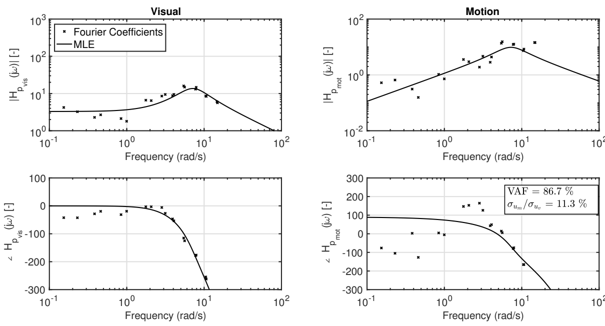

Figure A.245: Subject 8 C5

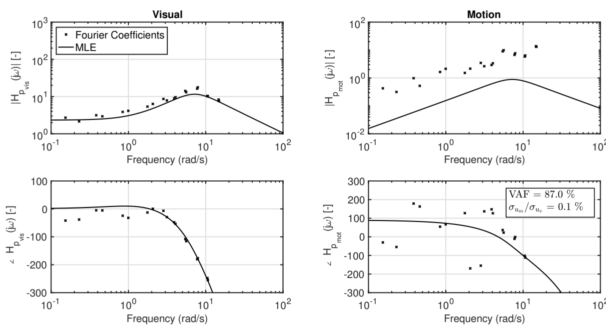

Figure A.246: Subject 8 C6

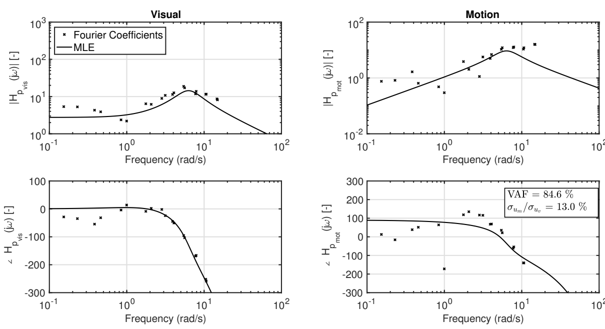

Figure A.247: Subject 8 C7

VMS Subject 9 of 18

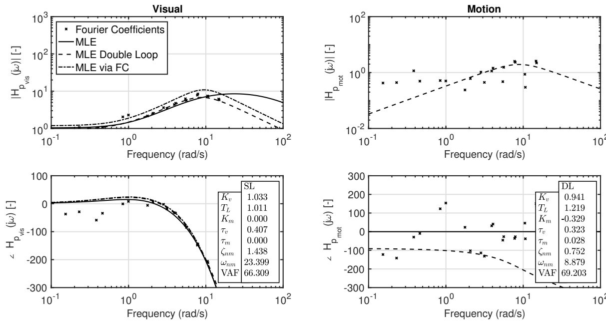

Figure A.248: Subject 9 C0

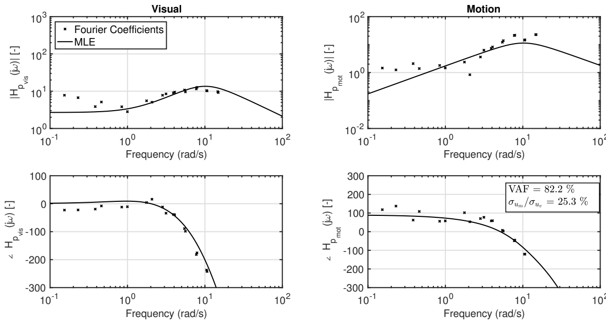

Figure A.249: Subject 9 C1

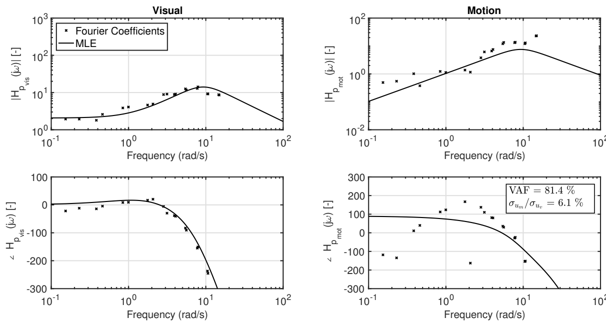

Figure A.250: Subject 9 C2

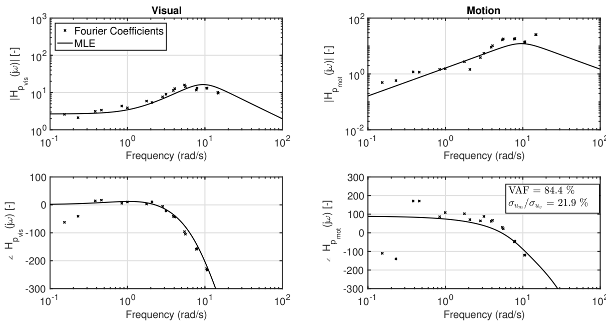

Figure A.251: Subject 9 C3

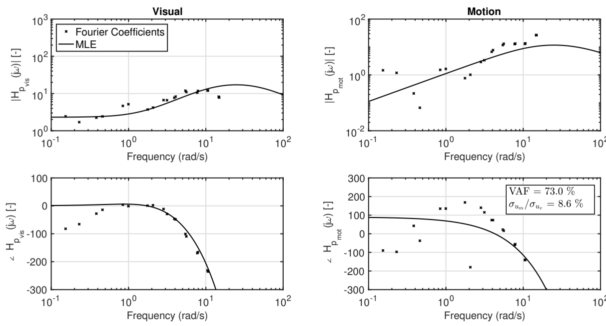

Figure A.252: Subject 9 C4

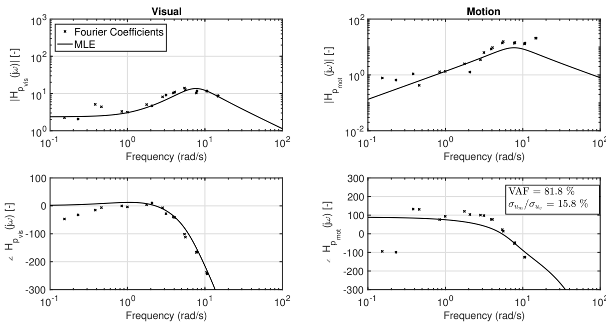

Figure A.253: Subject 9 C5

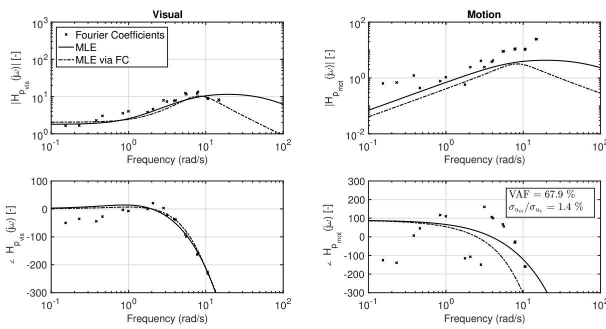

Figure A.254: Subject 9 C6

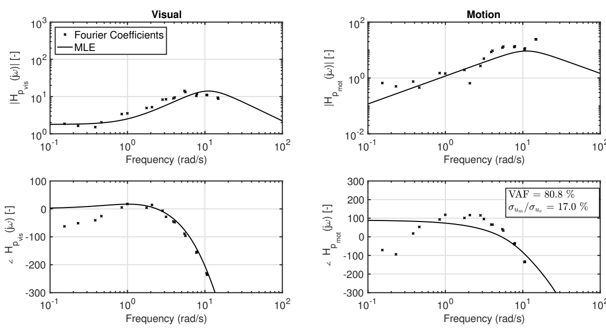

Figure A.255: Subject 9 C7

VMS Subject 10 of 18

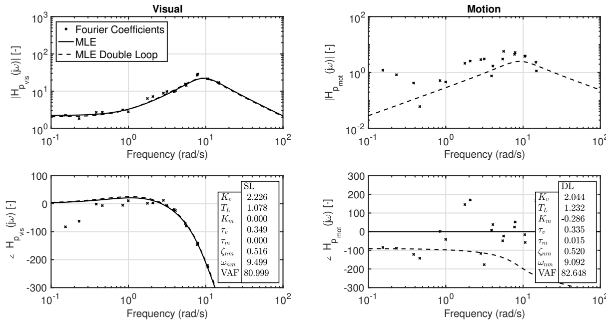

Figure A.256: Subject 10 C0

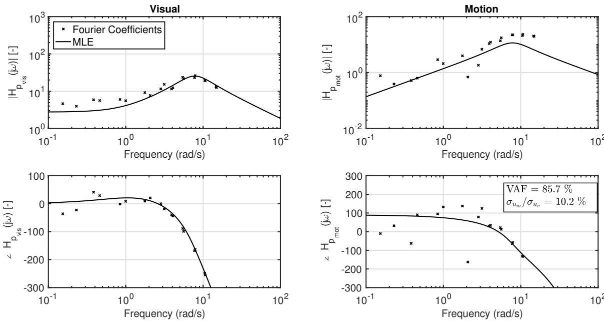

Figure A.257: Subject 10 C1

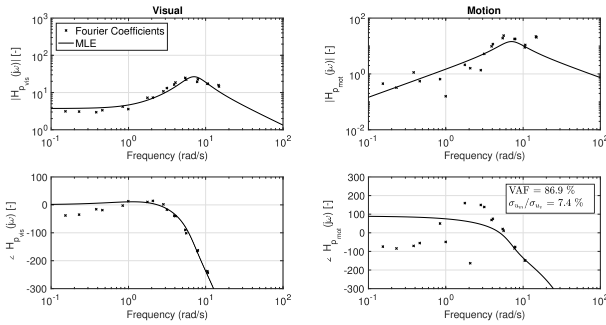

Figure A.258: Subject 10 C2

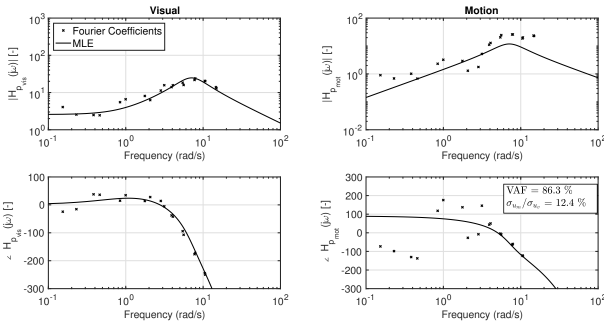

Figure A.259: Subject 10 C3

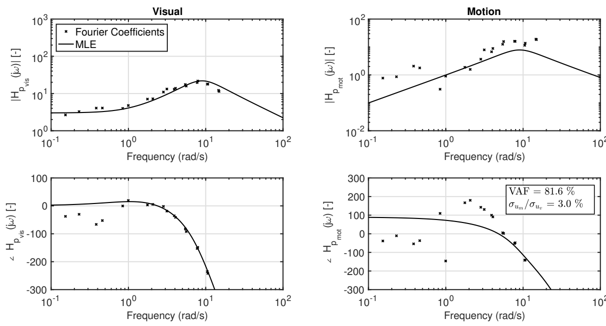

Figure A.260: Subject 10 C4

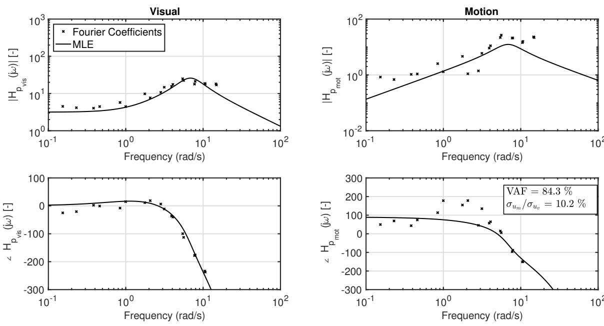

Figure A.261: Subject 10 C5

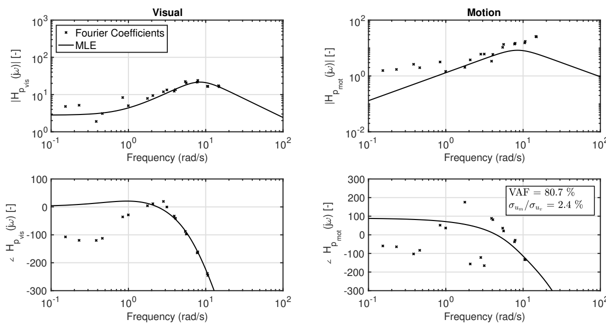

Figure A.262: Subject 10 C6

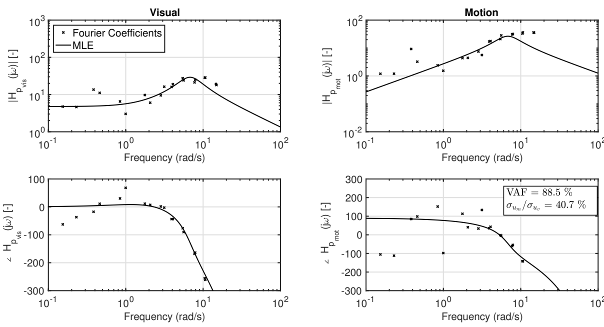

Figure A.263: Subject 10 C7

VMS Subject 11 of 18

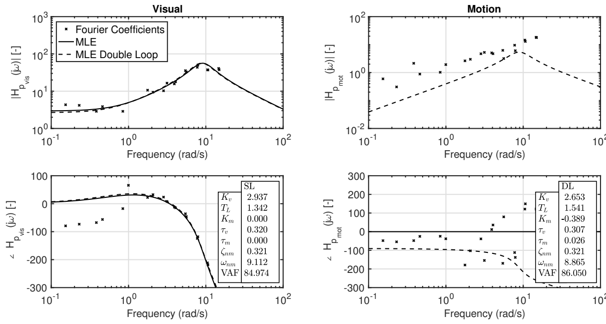

Figure A.264: Subject 11 C0

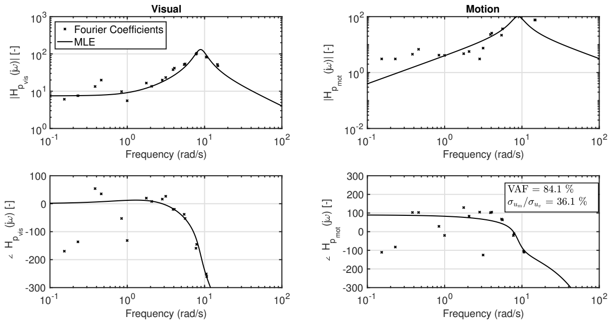

Figure A.265: Subject 11 C1

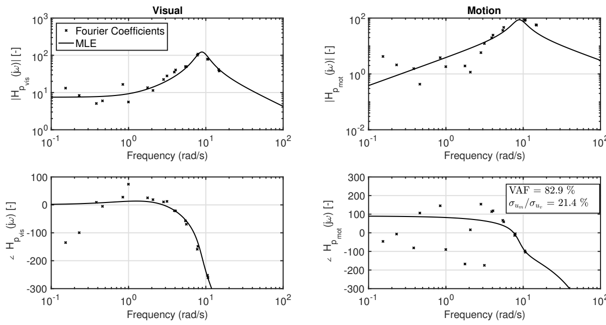

Figure A.266: Subject 11 C2

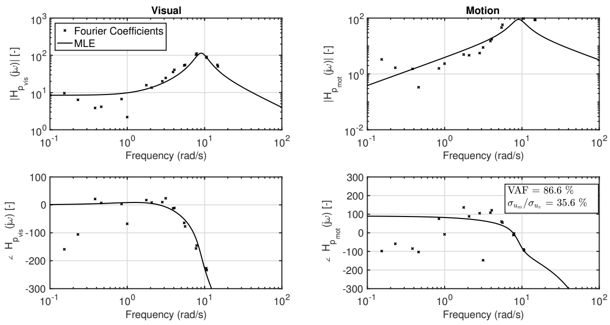

Figure A.267: Subject 11 C3

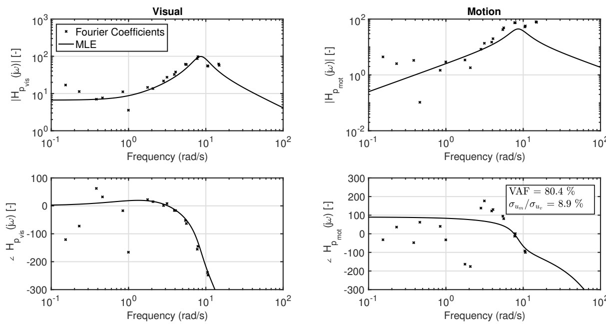

Figure A.268: Subject 11 C4

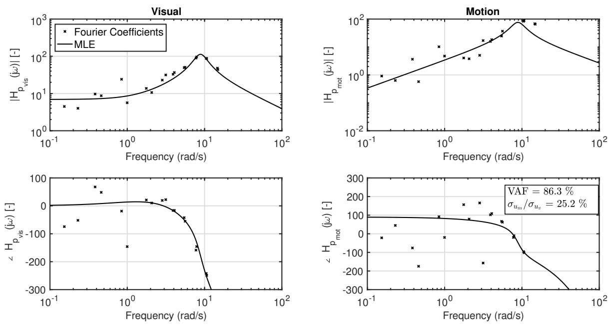

Figure A.269: Subject 11 C5

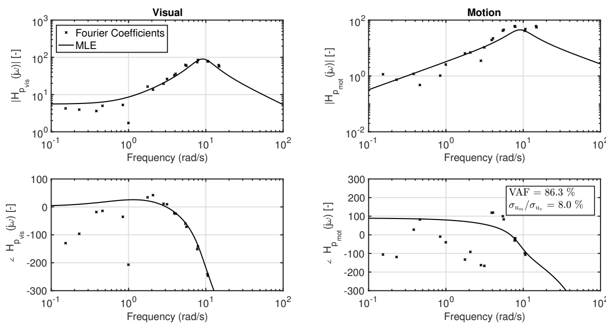

Figure A.270: Subject 11 C6

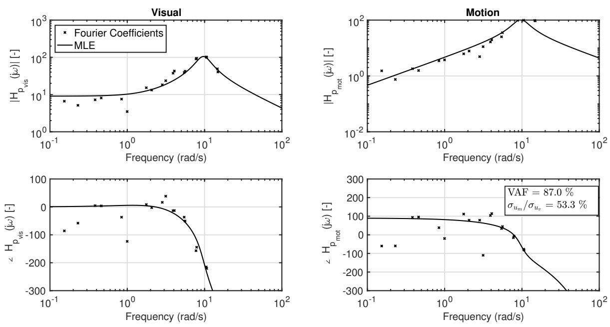

Figure A.271: Subject 11 C7

VMS Subject 12 of 18

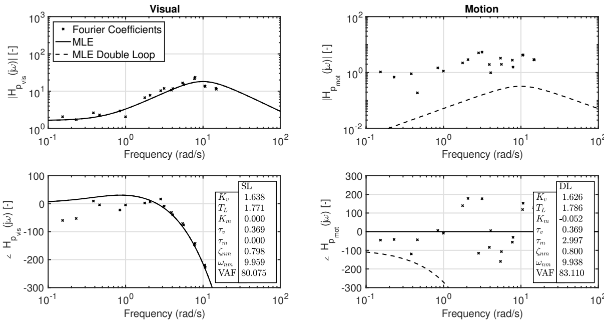

Figure A.272: Subject 12 C0

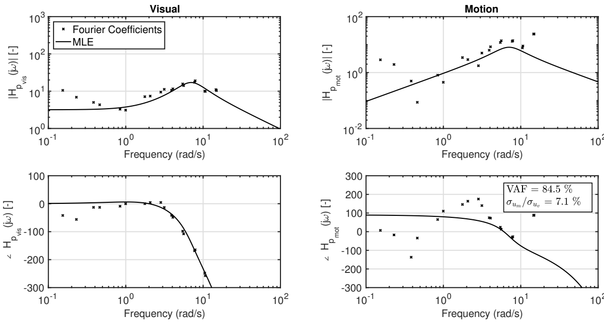

Figure A.273: Subject 12 C1

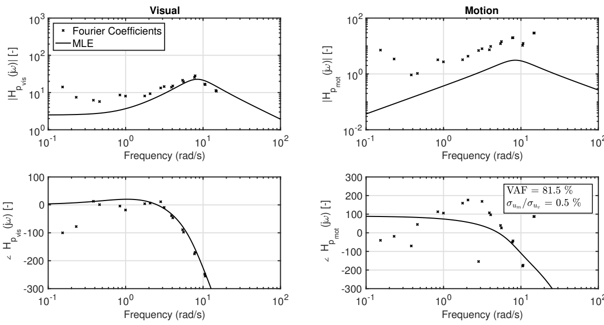

Figure A.274: Subject 12 C2

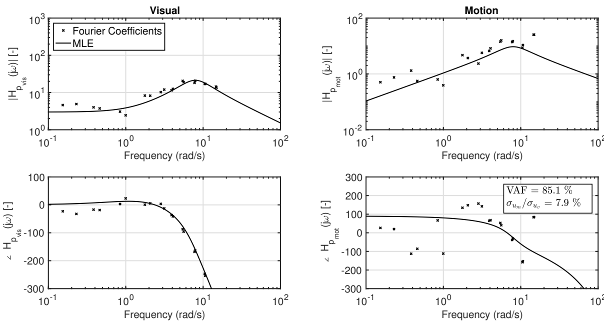

Figure A.275: Subject 12 C3

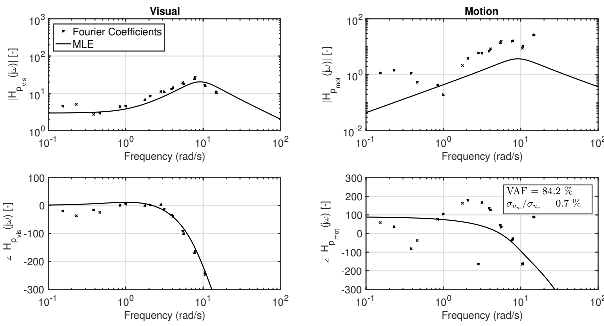

Figure A.276: Subject 12 C4

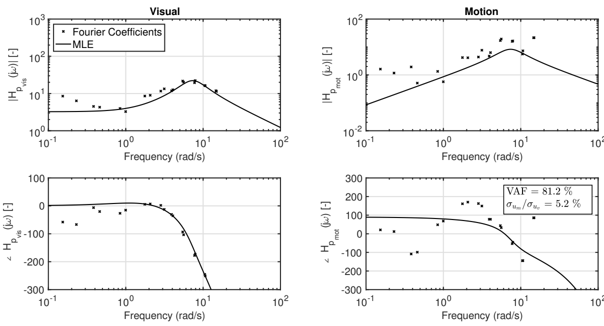

Figure A.277: Subject 12 C5

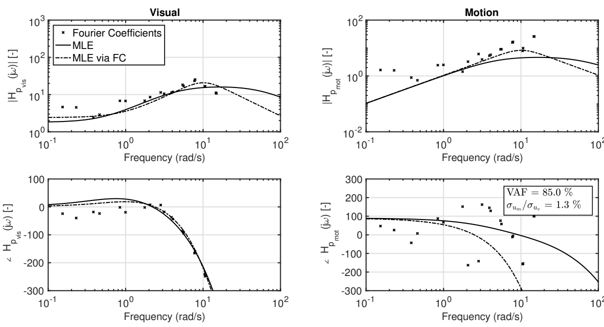

Figure A.278: Subject 12 C6

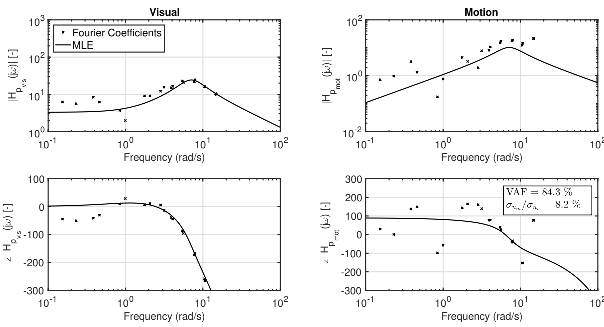

Figure A.279: Subject 12 C7

VMS Subject 13 of 18

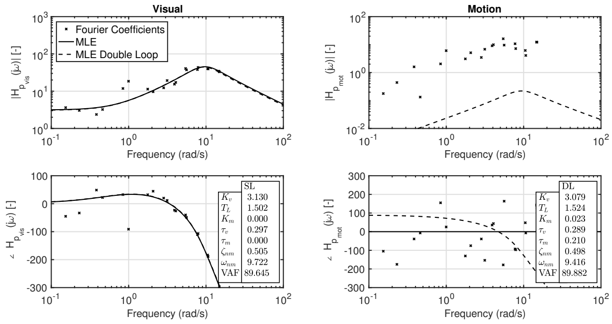

Figure A.280: Subject 13 C0

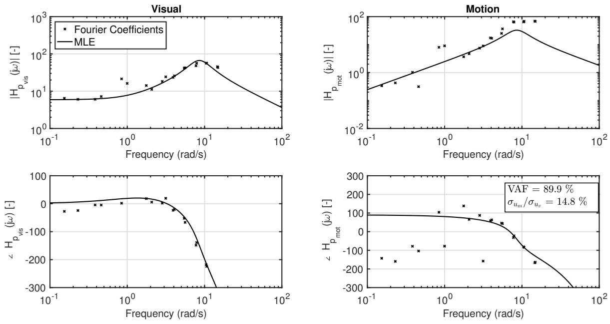

Figure A.281: Subject 13 C1

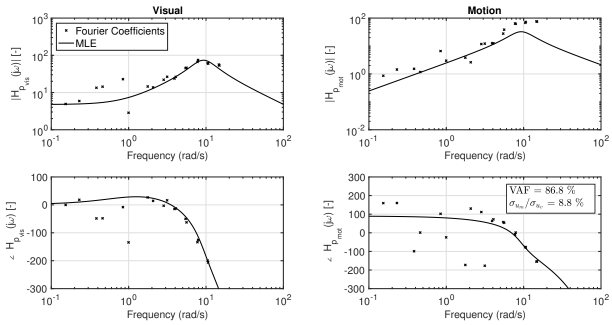

Figure A.282: Subject 13 C2

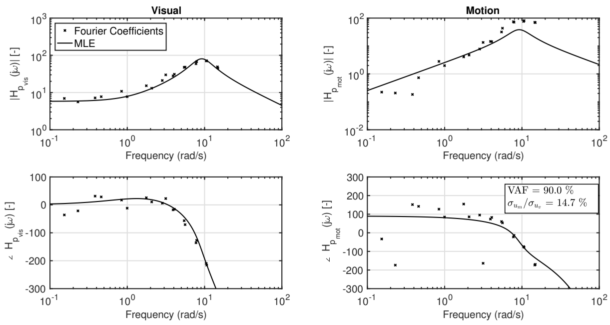

Figure A.283: Subject 13 C3

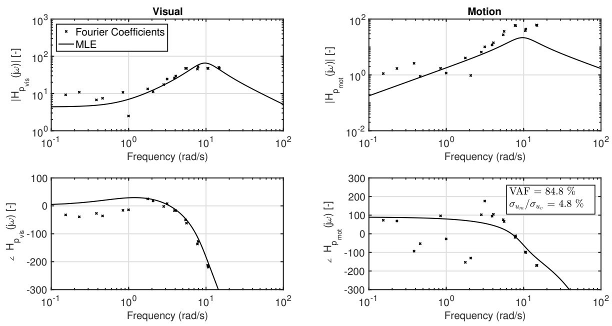

Figure A.284: Subject 13 C4

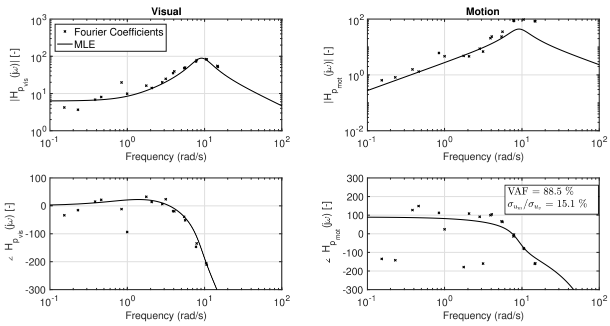

Figure A.285: Subject 13 C5

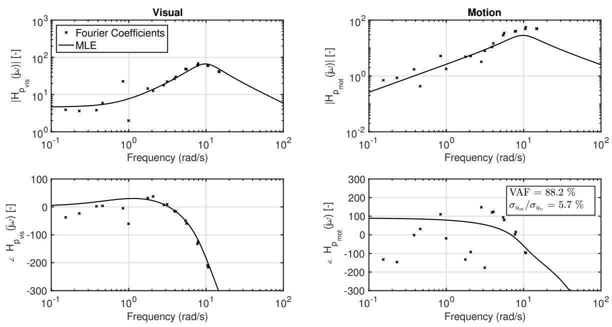

Figure A.286: Subject 13 C6

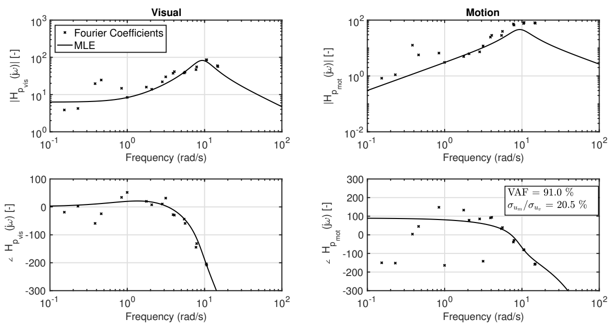

Figure A.287: Subject 13 C7

VMS Subject 14 of 18

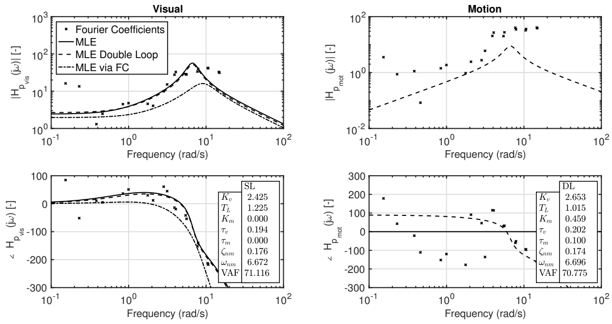

Figure A.288: Subject 14 C0

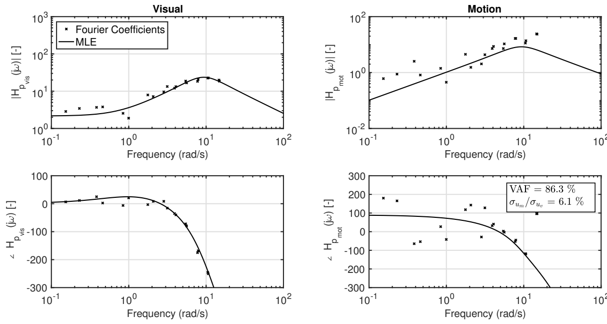

Figure A.289: Subject 14 C1

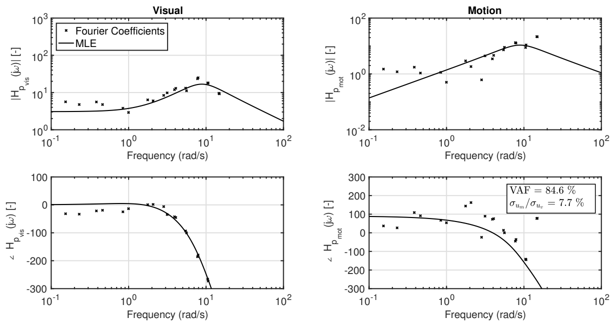

Figure A.290: Subject 14 C2

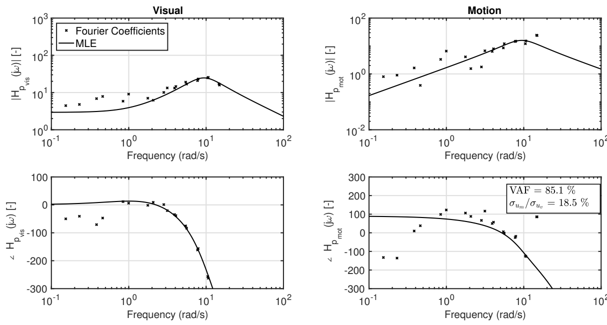

Figure A.291: Subject 14 C3

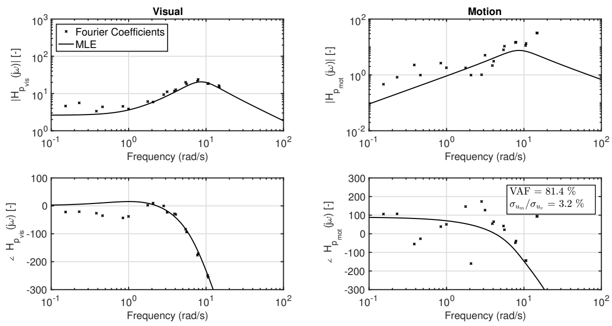

Figure A.292: Subject 14 C4

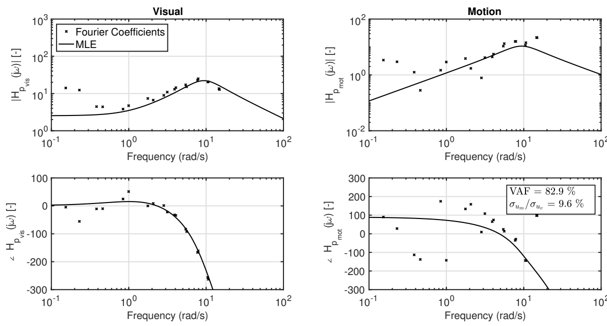

Figure A.293: Subject 14 C5

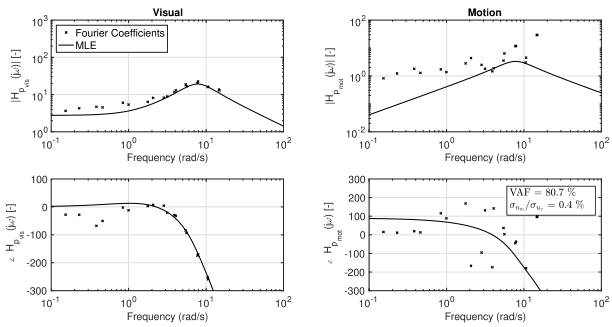

Figure A.294: Subject 14 C6

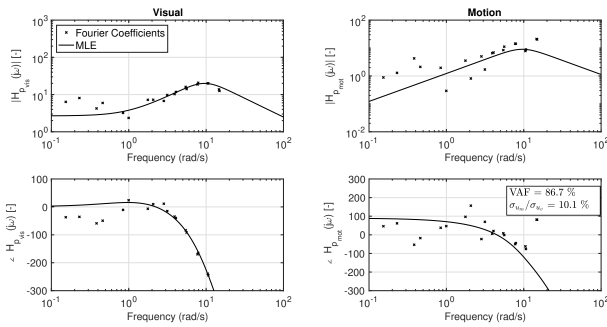

Figure A.295: Subject 14 C7

VMS Subject 15 of 18

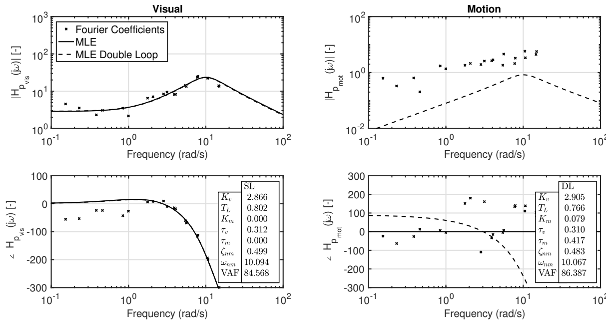

Figure A.296: Subject 15 C0

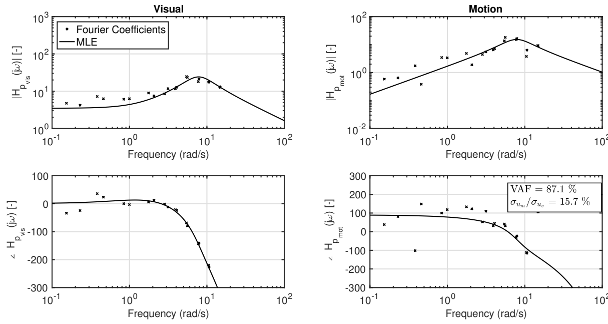

Figure A.297: Subject 15 C1

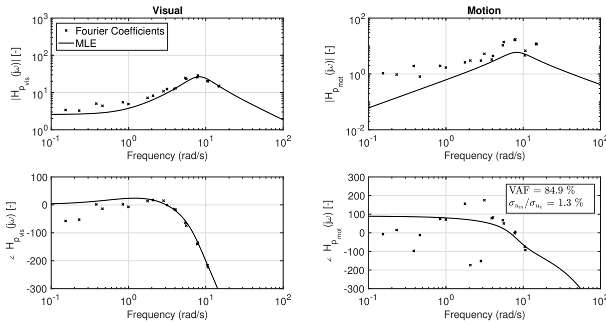

Figure A.298: Subject 15 C2

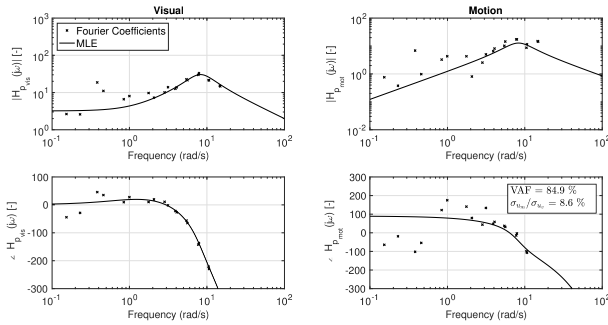

Figure A.299: Subject 15 C3

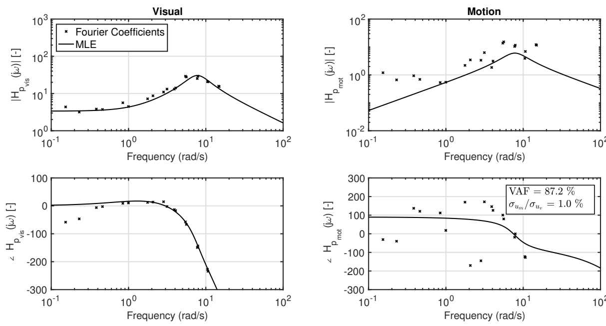

Figure A.300: Subject 15 C4

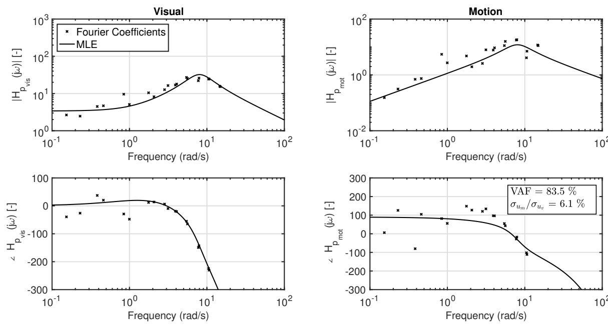

Figure A.301: Subject 15 C5

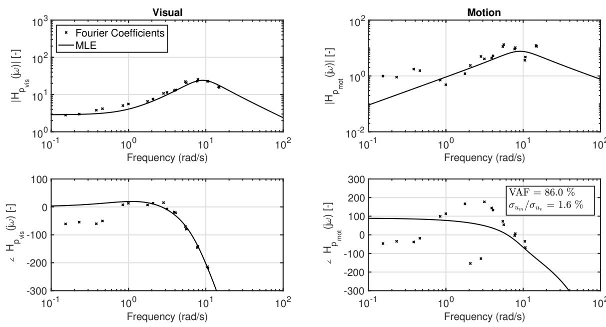

Figure A.302: Subject 15 C6

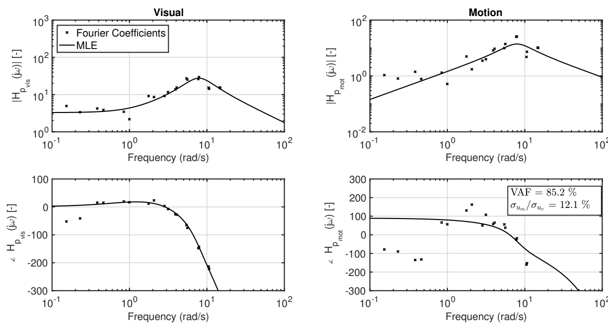

Figure A.303: Subject 15 C7

VMS Subject 16 of 18

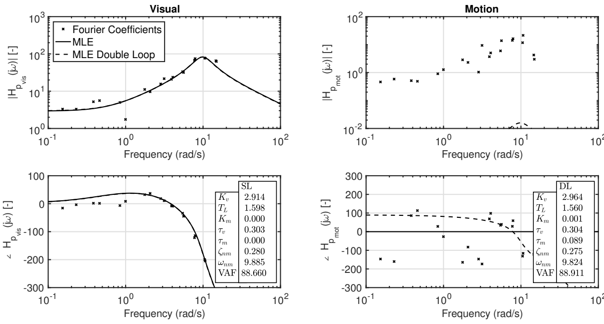

Figure A.304: Subject 16 C0

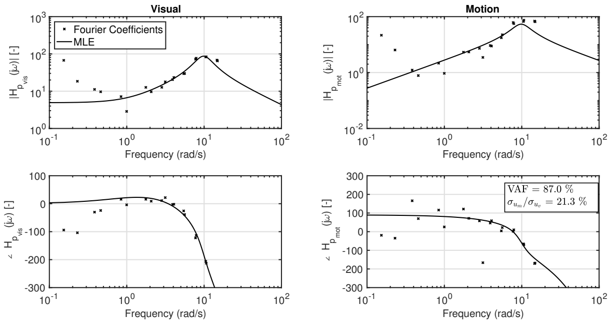

Figure A.305: Subject 16 C1

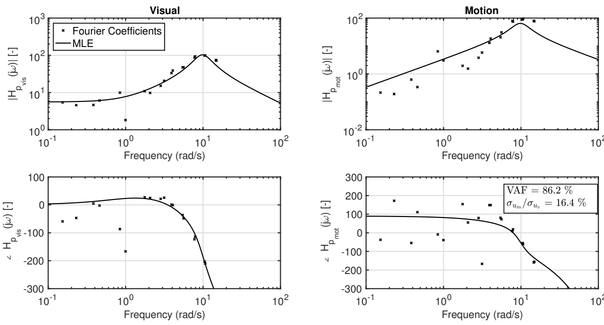

Figure A.306: Subject 16 C2

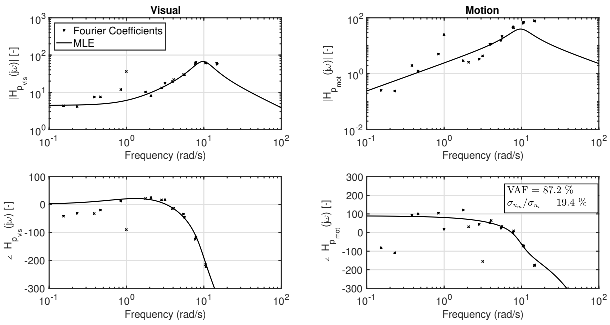

Figure A.307: Subject 16 C3

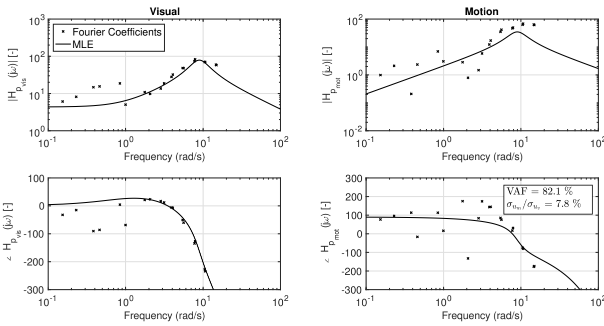

Figure A.308: Subject 16 C4

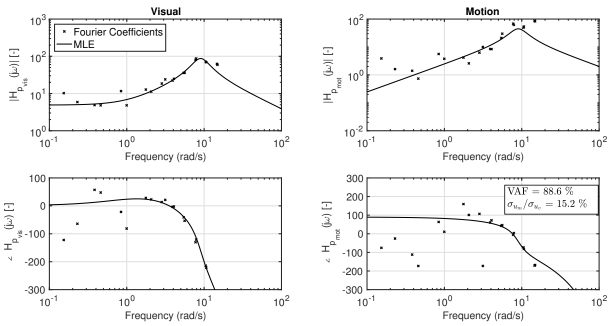

Figure A.309: Subject 16 C5

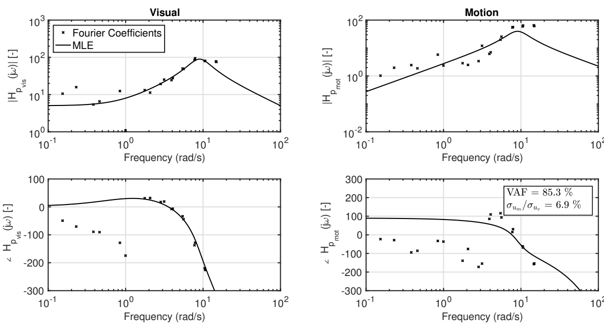

Figure A.310: Subject 16 C6

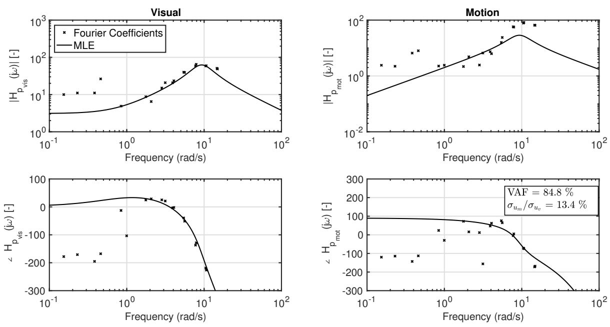

Figure A.311: Subject 16 C7

VMS Subject 17 of 18

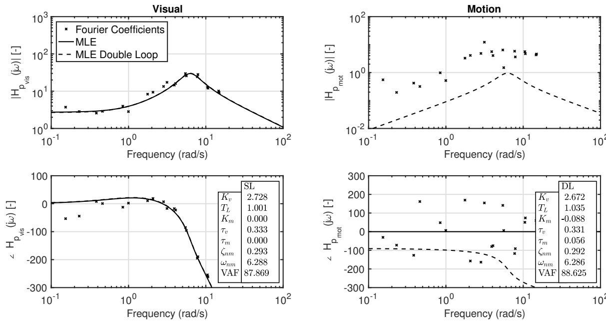

Figure A.312: Subject 17 C0

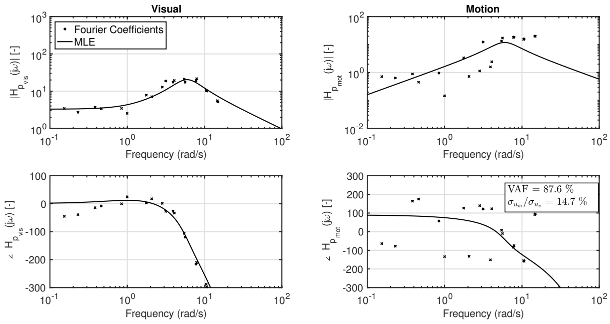

Figure A.313: Subject 17 C1

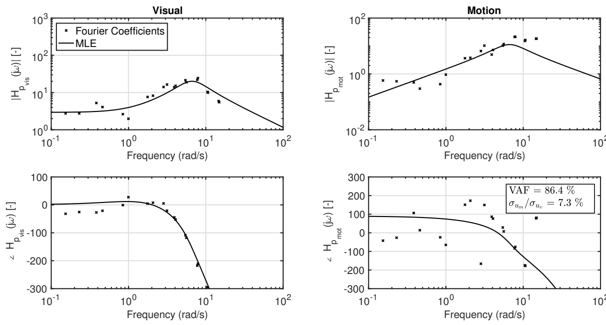

Figure A.314: Subject 17 C2

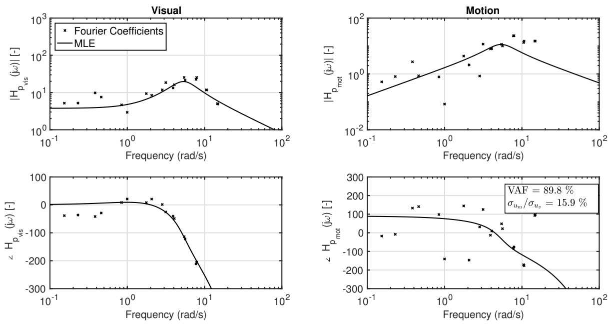

Figure A.315: Subject 17 C3

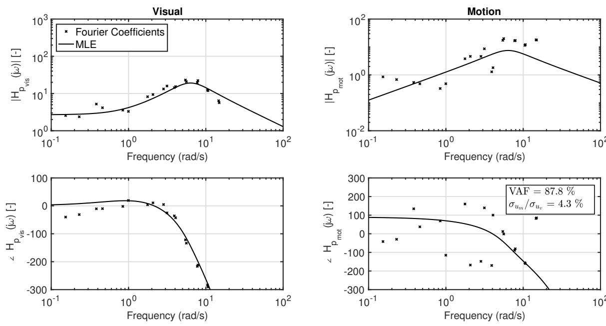

Figure A.316: Subject 17 C4

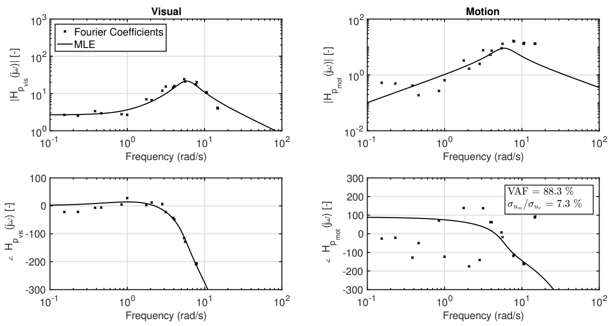

Figure A.317: Subject 17 C5

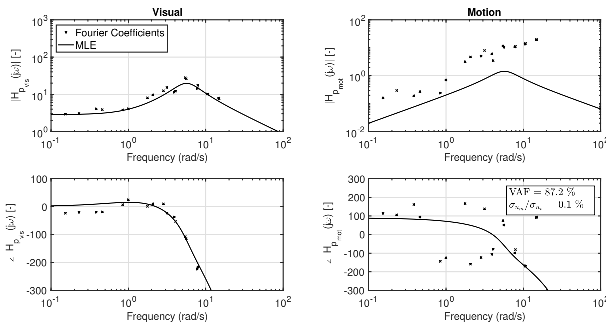

Figure A.318: Subject 17 C6

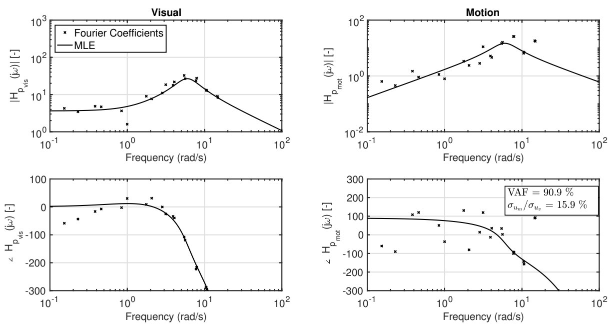

Figure A.319: Subject 17 C7

VMS Subject 18 of 18

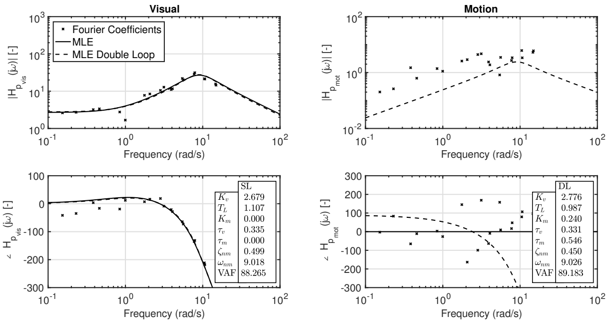

Figure A.320: Subject 18 C0

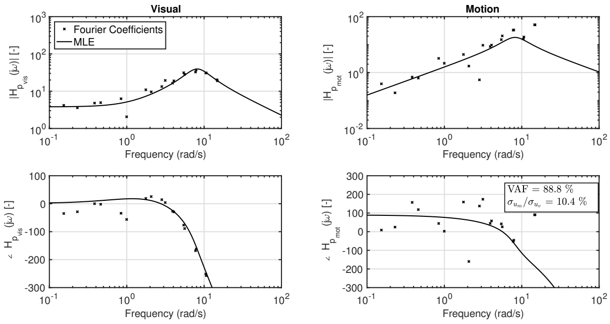

Figure A.321: Subject 18 C1

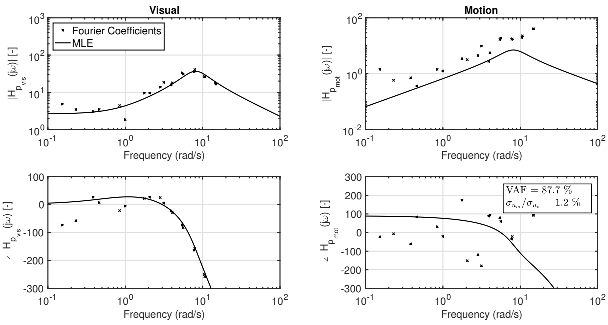

Figure A.322: Subject 18 C2

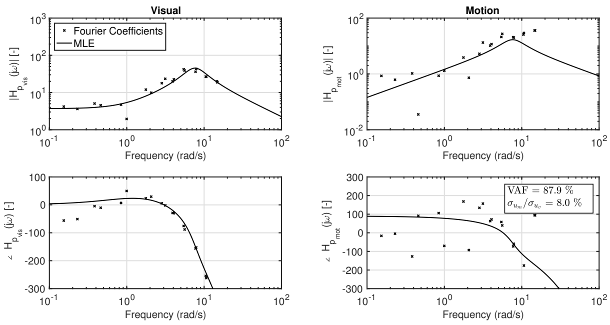

Figure A.323: Subject 18 C3

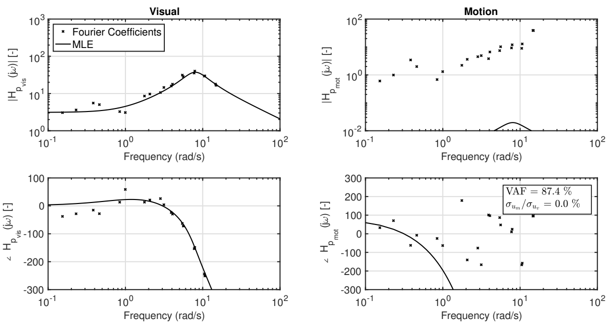

Figure A.324: Subject 18 C4

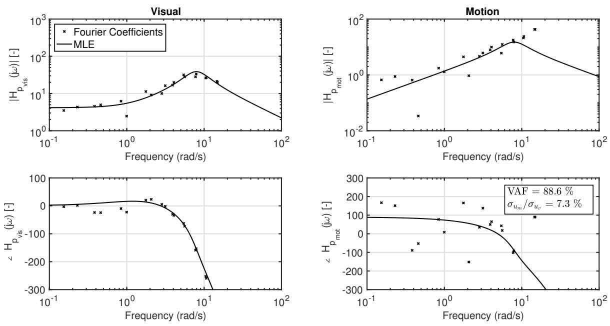

Figure A.325: Subject 18 C5

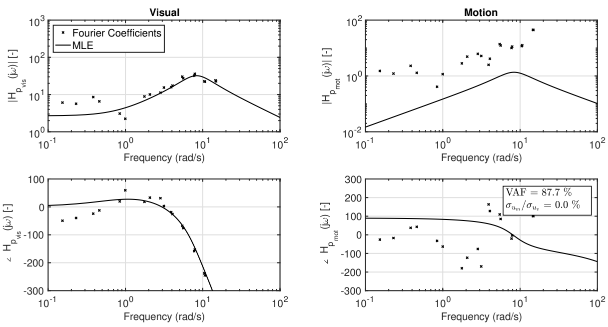

Figure A.326: Subject 18 C6

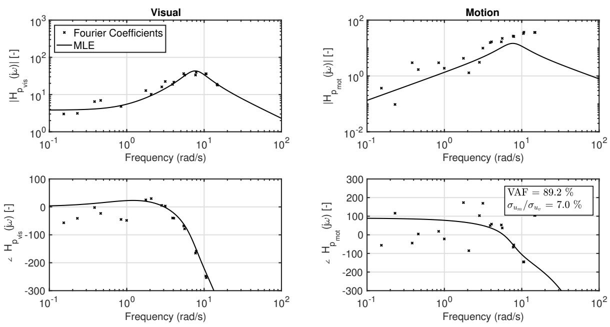

Figure A.327: Subject 18 C7

B

Motion System Matching

This appendix presents all OMCT results for both simulators. Furthermore, the shaping filters are explained.

The OMCT was used in the process of matching the simulator motion systems since it offered an objective standardized method of characterizing the simulator motion systems. As visible in Figure 3.2 (Part II, Chapter 3.1.1), the OMCT uses signals in the pilot station reference frame F^{ps}. This allows the OMCT test results to relate directly to what the pilot in an aircraft feels. The OMCT commanded signal is sent through the motion algoritm and subsequently to the motion base itself. The resulting movement of the motion base is measured. Figure B.1 shows an example of the signals of the OMCT test. In this case, the tenth frequency of the heavy test is shown. The measured singal shows a slight time delay compared to the commanded signal.

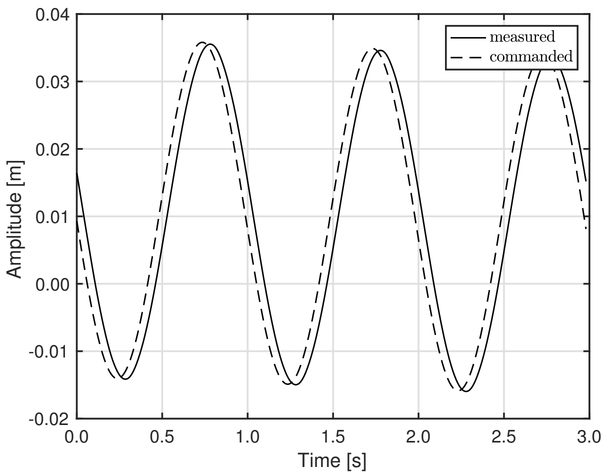

Figure B.1: OMCT commanded and measured signals for heave frequency number 10

Figure B.4 to B.6 show the OMCT results for the full-motion experimental condition that was used to generate the shaping filters. Figure B.7 to B.9 show the results of the verification condition C5. By making use of a cost function, transfer functions of the form presented in Equation B.1 were fitted through the twelve OMCT response measurement points [43], to determine the simulator motion dynamics.

$$H_{SRS,VMS}(s) = \frac{A \cdot s^2}{B \cdot s^2 + C \cdot s + D} \cdot e^{-E \cdot s} \tag{B.1}$$

Equations B.2 to B.7 show the resulting simulator motion dynamics for the pitch, surge and heave:

$$H_{VMS_q}(s) = 0.893 \cdot \frac{s^2}{0.916s^2 + 0.254s + 0.035} \cdot e^{-0.0445s} \tag{B.2}$$

$$H_{VMS_x}(s) = 0.926 \cdot \frac{s^2}{0.862s^2 + 0.282s + 0.032} \cdot e^{-0.0981s} \tag{B.3}$$

$$H_{VMS_z}(s) = 0.911 \cdot \frac{s^2}{0.883s^2 + 0.280s + 0.036} \cdot e^{-0.0975s} \tag{B.4}$$

$$H_{SRS_q}(s) = 0.908 \cdot \frac{s^2}{0.891s^2 + 0.259s + 0.035} \cdot e^{-0.0257s} \tag{B.5}$$

$$H_{SRS_x}(s) = 0.918 \cdot \frac{s^2}{0.883s^2 + 0.266s + 0.035} \cdot e^{-0.0526s} \tag{B.6}$$

$$H_{SRS_z}(s) = 0.908 \cdot \frac{s^2}{0.900s^2 + 0.256s + 0.036} \cdot e^{-0.0436} \tag{B.7}$$

The shaping filters had the form of Equation B.8.

$$H_{shaping}(s) = H^{-1}_{SRS}(s) \cdot H_{VMS}(s) \tag{B.8}$$

Equation B.9, B.10 and B.11 show the shaping filters as implemented in the SRS motion logic.

$$H_{shaping_{pitch}}(s) = \frac{0.796 \cdot s^4 + 0.231 \cdot s^3 + 0.032 \cdot s^2}{0.831 \cdot s^4 + 0.230 \cdot s^3 + 0.032 \cdot s^2} \cdot e^{-0.0188 \cdot s} \tag{B.9}$$

$$H_{shaping_{heave}}(s) = \frac{0.820 \cdot s^4 + 0.233 \cdot s^3 + 0.032 \cdot s^2}{0.801 \cdot s^4 + 0.254 \cdot s^3 + 0.033 \cdot s^2} \cdot e^{-0.0539 \cdot s} \tag{B.10}$$

$$H_{shaping_{surge}}(s) = \frac{0.817 \cdot s^4 + 0.246 \cdot s^3 + 0.033 \cdot s^2}{0.810 \cdot s^4 + 0.257 \cdot s^3 + 0.033 \cdot s^2} \cdot e^{-0.0455 \cdot s} \tag{B.11}$$

In both simulators, the motion systems used signals in the simulator intertial reference frame F^{si}, see Figure B.3. However, the shaping filters were implemented in the SRS motion logic in the body reference frame F^{sb}, right before the signal transformation from the aircraft body frame to the intertial reference frame, since the OMCT input signals that were used to generate the shaping filters were also in the body reference frame. Figure B.2 presents the different reference frames: X_b denotes the body x-axis and X_I denotes the intertial x-axis.

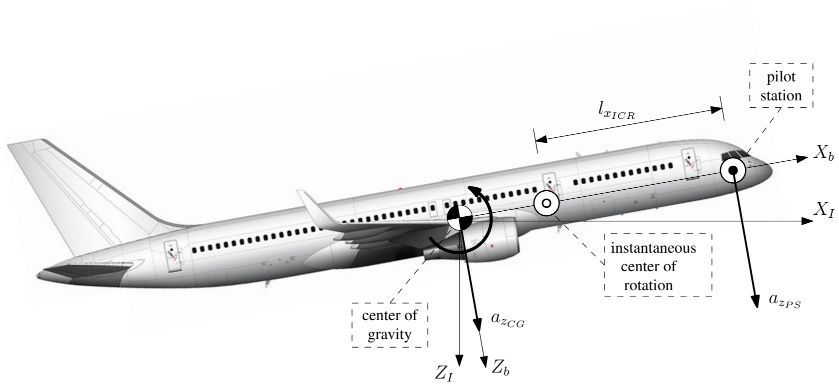

Figure B.2: Aircraft reference frames

Figure B.3 shows the location of the shaping filter in the SRS motion logic for the heave path, where $H_{motion}(s)$ represents the simulator motion hardware dynamics. Because only ICR pitch-heave is present in the simulation, the heave acceleration at the pilot station $a_{z_{PS}}$ is equal to the ICR pitch-heave: $a_{z_{PS}} = a_{z_{\theta,ICR}}$. The transformation matrix from aircraft body to interial reference frame is given in Equation B.12.

$$\mathbb{T}_{Ib} = \begin{bmatrix} \cos\theta & 0 & \sin\theta \\ 0 & 1 & 0 \\ -\sin\theta & 0 & \cos\theta \end{bmatrix} \tag{B.12}$$

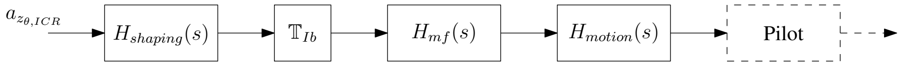

Figure B.3: Detailed view on heave motion path in pitch control task

For the surge degree-of-freedom the situation was analogous. However, because no CG surge was present in the experiment, and the pilot station was located on the X_b-axis, no surge motion was present in the aircraft body frame pilot station. The surge motion of the simulator resulted from the transfer of the rotation point from the aircraft to the simulator upper gimbal point. The corresponding acceleration is $a_{x_{I_{rpt}}}$, where the subscript "rpt" denotes "rotation point transfer". The corresponding heave component is indicated with $a_{z_{I_{rpt}}}$. Equation B.13 shows how $a_{x_{I_{rpt}}}$ and $a_{z_{I_{rpt}}}$ were computed from the shaped and filtered pitch rate signal. The simulator horizontal offset dx was 0, which left only the Eulerian acceleration term $-\dot{q}\cdot dz$, which is the angular acceleration due to the increased lever arm dz, and the centripital acceleration term $q^2 \cdot dz$ due to the rotation point offset dz.

$$\begin{bmatrix} a_{x_{I_{rpt}}} \\ a_{z_{I_{rpt}}} \end{bmatrix} = \mathbb{T}_{Ib} \cdot \begin{bmatrix} a_{x_{B_{rpt}}} \\ a_{z_{B_{rpt}}} \end{bmatrix} = \mathbb{T}_{Ib} \cdot \begin{bmatrix} q.^2 \cdot dx - \dot{q} \cdot dz \\ \dot{q} \cdot dx + q^2 \cdot dz \end{bmatrix} = \mathbb{T}_{Ib} \cdot \begin{bmatrix} -\dot{q} \cdot dz \\ q^2 \cdot dz \end{bmatrix} \tag{B.13}$$

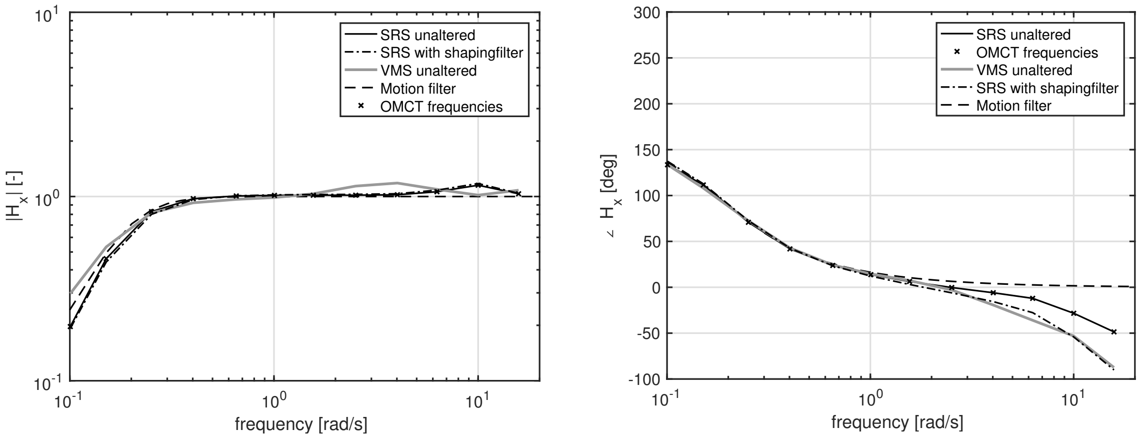

(a) Magnitude

(b) Phase

Figure B.4: Surge motion response of C7

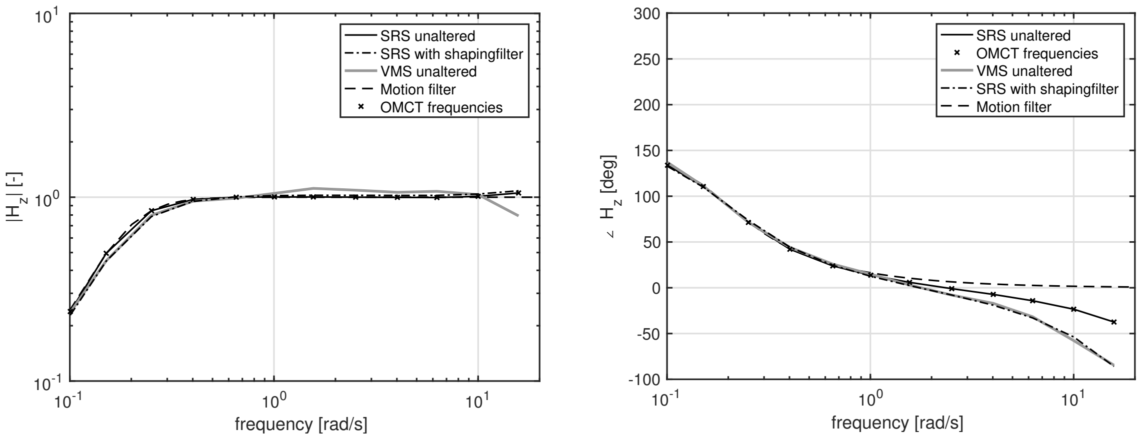

(a) Magnitude

(b) Phase

Figure B.5: Heave motion response of C7

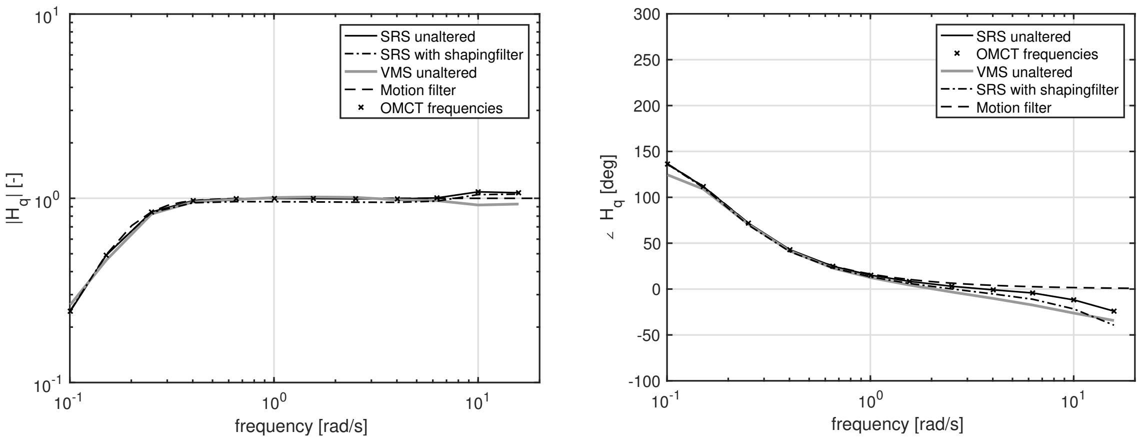

(a) Magnitude

(b) Phase

Figure B.6: Pitch motion response of C7

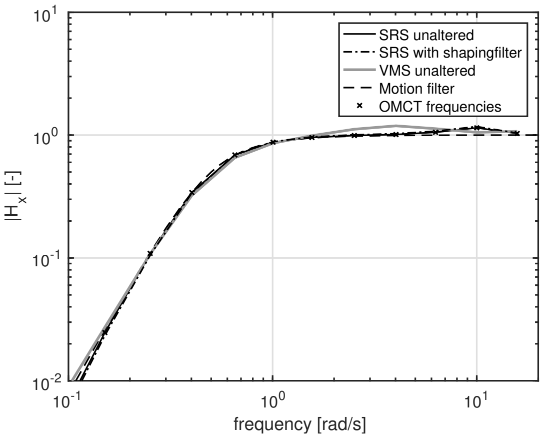

(a) Magnitude

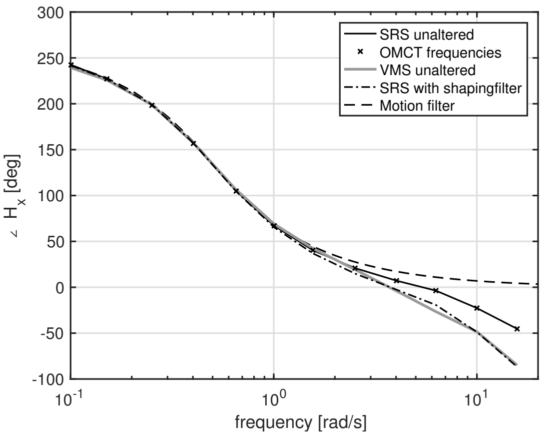

(b) Phase

Figure B.7: Surge motion response of C5

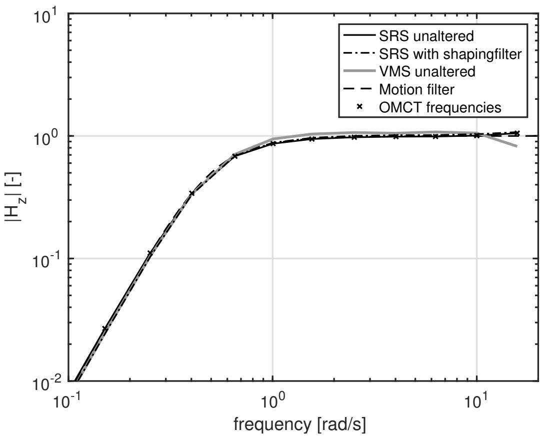

(a) Magnitude

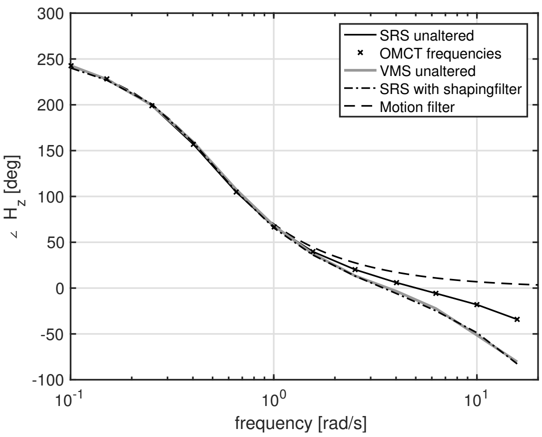

(b) Phase

Figure B.8: Heave motion resonse of C5

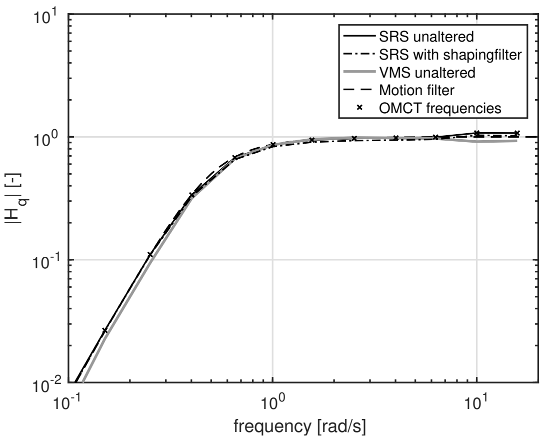

(a) Magnitude

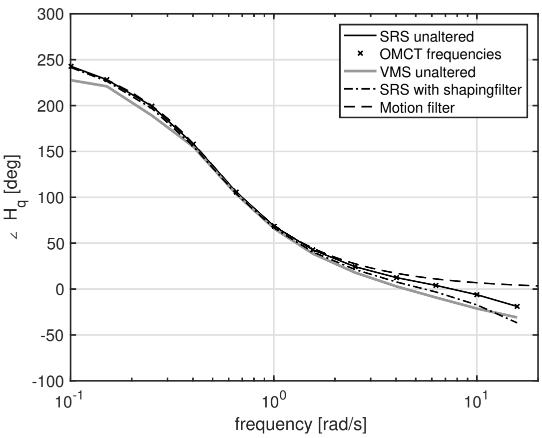

(b) Phase

Figure B.9: Pitch motion response of C5

C

Stick Gains

This appendix provides information on the stick gains that were present in order to match the control input signals of both the VMS McFadden sidestick and the SRS Moog sidestick. The input singal of the VMS stick was measured in inches of displacement, with the trigger point being the reference, as can be seen in Figure C.1a. The arm of the VMS stick was 9 inches long, which is equal to 0.229 m. This meant that in order to get the input singal u in the interval ± 1, a gain of 0.3596 was present. For the SRS, the angle of rotation in degrees of the sidestick was measured. In order to get the control signal u in the desired form, the input signal was first multiplied with $\pi/180$ and subsequently with 3.1827. Figure C.1 shows the block diagram of the sidestick input signal to the control signal u for both simulators, including a schematic drawing of the stick arm.

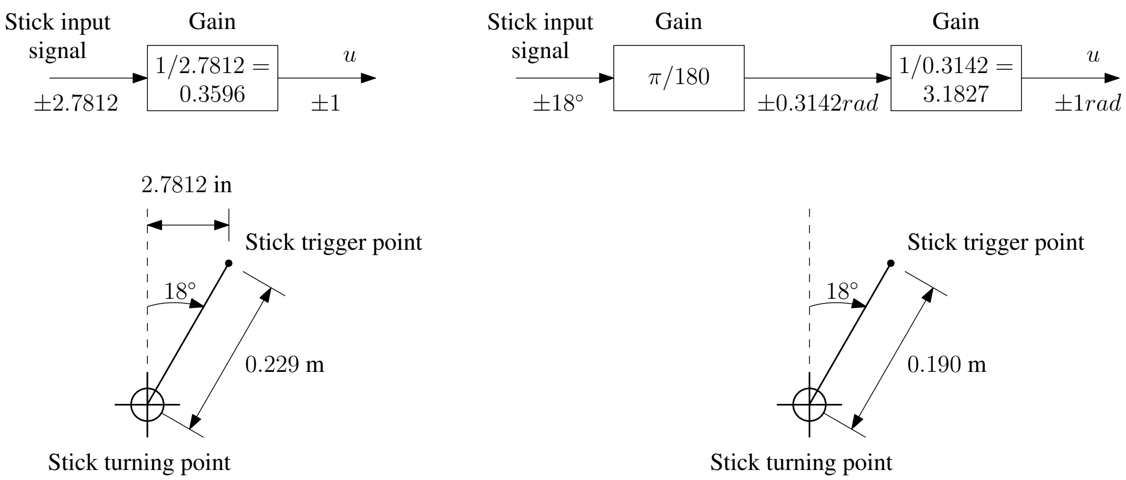

(a) VMS (b) SRS

Figure C.1: Side stick gains of both simulators

D

Experiment Documents

This appendix contains the documents that were prepared for, or required in, running the experiment. Section D.1 contains the experiment briefing. Section D.2 contains the runtables for all participants. Section D.3 contains the Institutional Review Board documents that were prepared for the NASA ethics committee. Finally, Section D.4 contains the consent form according to the guidelines of the Human Research Ethics Committee of Delft University of Technology.

D.1. Experiment Briefing

Motion Algorithm Development

Briefing

The experiment will be performed in the SIMONA Research Simulator [SRS] at the faculty of aerospace engineering, Delft University of Technology. The experiment is part of a comparison with the NASA Vertical Motion Simulator, the largest flight simulator in the world. A large commercial airliner will be simulated.

It is your task to keep the aircraft symbol on the horizon on a primary flight display [PFD] while the aircraft is perturbed by random disturbances similar to heavy atmospheric turbulence. The aircraft dynamics are controlled with a joystick, located on the right of the pilot seat in the simulator cab. The PFD is depicted in Figure 1.

It is important to adopt a consistent control strategy throughout the duration of the experiment. Provide smooth, continuous control inputs. Focus should be kept on the primary flight display in front of you.

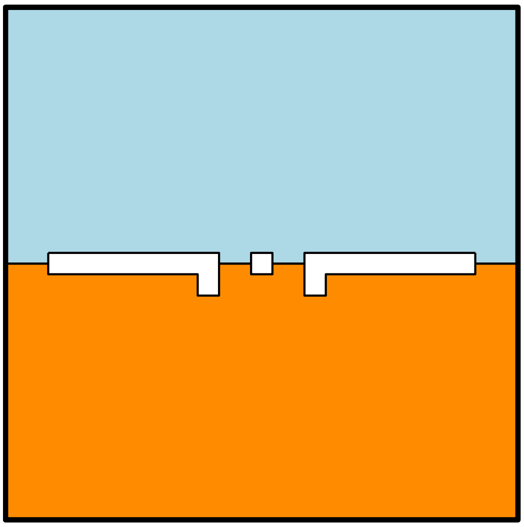

Fig 1: Primary Flight Display

Over the runs the motion settings of the simulator will change. Your performance will be evaluated with these different motion conditions.

Breaks will be taken regularly to alleviate any discomfort that might occur after sitting in a fixed position for a prolonged period of time. The total duration of the experiment is expected to be three hours, including breaks.

If you have any remaining questions, feel free to email me at m.a.pieters@student.tudelft.nl

Thank you for participating in this study!

D.2. Experiment Runtables

This appendix presents the experiment matrix that was used in both the Vertical Motion Simulator and SIMONA Research Simulator. Each participant performed 7 repetitions of all 8 conditions, in a randomized order. The first two repetitions were used as training runs.

Table D.1: Experiment matrix for 20 pilots

Pilot	p1	p2	p3	p4	p5	p6	p7	p8	p9	p10	p11	p12	p13	p14	p15	p16	p17	p18	p19	p20
Run 1	2	4	5	6	1	7	0	3	1	6	7	3	2	4	0	5	1	5	4	6
Run 2	0	2	3	4	7	5	6	1	0	5	6	2	1	3	7	4	2	6	5	7
Run 3	4	6	7	0	3	1	2	5	4	1	2	6	5	7	3	0	7	3	2	4
Run 4	6	0	1	2	5	3	4	7	7	4	5	1	0	2	6	3	3	7	6	0
Run 5	1	3	4	5	0	6	7	2	2	7	0	4	3	5	1	6	6	2	1	3
Run 6	3	5	6	7	2	0	1	4	6	3	4	0	7	1	5	2	0	4	3	5
Run 7	7	1	2	3	6	4	5	0	5	2	3	7	6	0	4	1	5	1	0	2
Run 8	5	7	0	1	4	2	3	6	3	0	1	5	4	6	2	7	4	0	7	1
Run 9	4	2	0	7	5	6	3	1	1	2	3	6	7	4	5	0	1	3	7	0
Run 10	0	6	4	3	1	2	7	5	2	3	4	7	0	5	6	1	0	2	6	7
Run 11	1	7	5	4	2	3	0	6	6	7	0	3	4	1	2	5	5	7	3	4
Run 12	6	4	2	1	7	0	5	3	4	5	6	1	2	7	0	3	3	5	1	2
Run 13	5	3	1	0	6	7	4	2	0	1	2	5	6	3	4	7	6	0	4	5
Run 14	2	0	6	5	3	4	1	7	7	0	1	4	5	2	3	6	7	1	5	6
Run 15	3	1	7	6	4	5	2	0	3	4	5	0	1	6	7	2	4	6	2	3
Run 16	7	5	3	2	0	1	6	4	5	6	7	2	3	0	1	4	2	4	0	1
Run 17	7	5	3	1	6	2	0	4	7	6	1	3	2	4	0	5	6	5	1	3
Run 18	5	3	1	7	4	0	6	2	1	0	3	5	4	6	2	7	7	6	2	4
Run 19	1	7	5	3	0	4	2	6	2	1	4	6	5	7	3	0	3	2	6	0
Run 20	3	1	7	5	2	6	4	0	6	5	0	2	1	3	7	4	1	0	4	6
Run 21	0	6	4	2	7	3	1	5	0	7	2	4	3	5	1	6	4	3	7	1
Run 22	6	4	2	0	5	1	7	3	4	3	6	0	7	1	5	2	5	4	0	2
Run 23	2	0	6	4	1	5	3	7	5	4	7	1	0	2	6	3	2	1	5	7
Run 24	4	2	0	6	3	7	5	1	3	2	5	7	6	0	4	1	0	7	3	5
Run 25	6	3	1	7	5	2	0	4	7	5	6	4	0	3	2	1	3	5	1	4
Run 26	3	0	6	4	2	7	5	1	0	6	7	5	1	4	3	2	4	6	2	5
Run 27	2	7	5	3	1	6	4	0	4	2	3	1	5	0	7	6	6	0	4	7
Run 28	1	6	4	2	0	5	3	7	3	1	2	0	4	7	6	5	7	1	5	0
Run 29	5	2	0	6	4	1	7	3	6	4	5	3	7	2	1	0	0	2	6	1
Run 30	4	1	7	5	3	0	6	2	1	7	0	6	2	5	4	3	1	3	7	2
Run 31	0	5	3	1	7	4	2	6	5	3	4	2	6	1	0	7	2	4	0	3
Run 32	7	4	2	0	6	3	1	5	2	0	1	7	3	6	5	4	5	7	3	6
Run 33	5	0	2	3	7	4	6	1	2	0	3	5	4	6	7	1	5	7	0	4
Run 34	1	4	6	7	3	0	2	5	5	3	6	0	7	1	2	4	2	4	5	1
Run 35	4	7	1	2	6	3	5	0	7	5	0	2	1	3	4	6	3	5	6	2
Run 36	0	3	5	6	2	7	1	4	4	2	5	7	6	0	1	3	1	3	4	0
Run 37	3	6	0	1	5	2	4	7	3	1	4	6	5	7	0	2	0	2	3	7
Run 38	2	5	7	0	4	1	3	6	0	6	1	3	2	4	5	7	6	0	1	5
Run 39	7	2	4	5	1	6	0	3	6	4	7	1	0	2	3	5	7	1	2	6
Run 40	6	1	3	4	0	5	7	2	1	7	2	4	3	5	6	0	4	6	7	3
Run 41	1	4	3	0	2	6	7	5	5	0	3	1	6	7	2	4	0	3	2	7
Run 42	2	5	4	1	3	7	0	6	6	1	4	2	7	0	3	5	2	5	7	1
Run 43	7	2	1	6	0	4	5	3	0	3	6	4	1	2	5	7	5	0	4	4
Run 44	6	1	0	5	7	3	4	2	2	5	0	6	3	4	7	1	1	4	3	0
Run 45	0	3	2	7	1	5	6	4	7	2	5	3	0	1	4	6	7	2	1	6
Run 46	4	7	6	3	5	1	2	0	3	6	1	7	4	5	0	2	3	6	5	2
Run 47	3	6	5	2	4	0	1	7	4	7	2	0	5	6	1	3	6	1	0	5
Run 48	5	0	7	4	6	2	3	1	1	4	7	5	2	3	6	0	4	7	6	3
Run 49	7	1	6	2	5	0	4	3	6	5	0	4	3	1	7	2	2	0	4	6
Run 50	0	2	7	3	6	1	5	4	4	3	6	2	1	7	5	0	5	3	7	1
Run 51	1	3	0	4	7	2	6	5	2	1	4	0	7	5	3	6	7	5	1	3
Run 52	2	4	1	5	0	3	7	6	3	2	5	1	0	6	4	7	4	2	6	0
Run 53	6	0	5	1	4	7	3	2	1	0	3	7	6	4	2	5	0	6	2	4
Run 54	3	5	2	6	1	4	0	7	5	4	7	3	2	0	6	1	3	1	5	7
Run 55	4	6	3	7	2	5	1	0	7	6	1	5	4	2	0	3	1	7	3	5
Run 56	5	7	4	0	3	6	2	1	0	7	2	6	5	3	1	4	6	4	0	2

- training runs
- measurement data

D.3. NASA Institutional Review Board Documents

To perform an experiment with human participants at NASA, it is required to have the experiment reviewed by the IRB. The IRB ensures that adequate measures are taken to protect the participants. This appendix contains two of the documents that were submitted to the IRB for review: a proposal of the experiment and a participant consent form. All participants at NASA reviewed and signed this consent form.

PROTOCOL

National Aeronautics and Space Administration

AMES RESEARCH CENTER

Moffett Field, California 94035-1000

HUMAN RESEARCH PROPOSAL

1. Title

The Effects of Motion Filter Order on Human Control Behavior

2. Organization and Location

The research will be performed by Peter Zaal (PI) and Marc Pieters (I) in the Vertical Motion Simulator (VMS) Lab in building N-243 at NASA Ames Research Center.

3. Investigators

Principal Investigator: Peter M. T. Zaal, Ph.D.
Investigator: Marc Pieters, B.Sc.

4. Purpose

The objective of this experiment is to investigate the effects of different motion washout filter orders on manual control behavior and performance.

5. Background

In the last decades, there has been a lot of research investigating the effects of different parameters commonly found in the algorithms used for motion cuing in flight simulators on human control behavior and performance. These filters appear in operational simulator with many different gains, break frequencies and in different orders. The effects of varying the filter parameters (the gain and the frequencies) has received a lot of attention. However, the effect of washout filter order on control behavior has not been investigated in detail, even though filters of different orders exist in different operational simulators, and even within simulators. This experiment investigates the effects of varying the washout filter order on pilot control behavior and performance.

6. Why Human Research is Required

The goal of this study is to determine how pilot control behavior and performance are affected by different simulator motion cuing settings. Human control behavior can only be investigated using human subjects in an experimental setting, as no accurate models of human control behavior exist.

7. Plan of Study

The experiment will be conducted in the Vertical Motion Simulator (VMS) with the commercial transport aircraft cab (T-cab), see Figure 1. This cab has two seats. The left seat will have a wheel and column to make control inputs. Participants will perform the experiment from the right seat, which will have a sidestick to make control inputs. In addition, rudder pedals will be available for both seats; however, these will not be operational during the experiment. Throttle levers are located in between the seats; however, also the throttles will not be operational. A simple primary flight display (PFD) will be located in front of both seats (Figure 2). The out-the-window visual system will provide a visual scene in the clouds, without visual features that can be used to determine the attitude of the aircraft. Participants will control an aircraft model used in an earlier VMS experiment [1], which represents a medium-large commercial airliner trimmed at its cruise altitude close to stall.

Participants will perform a disturbance-rejection task in the pitch degree of freedom (Figure 3). Roll and yaw are fixed in this experiment. It is the pilots' task to minimize the disturbances by keeping the aircraft pitch at the desired attitude. To allow for the identification of pilot control behavior, disturbance forcing functions will be used that are a summation of ten sine waves. These forcing functions induce disturbances similar to atmospheric turbulence. An artificial horizon line on the PFD will provide the desired pitch attitude.

Aircraft pitch attitude (θ) is subtracted from the desired pitch attitude to create a pitch error (e_θ) which is depicted on the PFD (Figures 2 and 3). The error is perceived visually by pilots and, from a control-theoretic perspective, it is the input to the pilot model. Pilots will use a sidestick to make control inputs (u). The differences between the pilot model response function outputs and the measured pilot control inputs is the remnant (n), which accounts for nonlinear behavior and noise. Using the measured error and control input signals, the linear response functions of the pilot model can be identified using the Maximum Likelihood Estimation technique discussed in [2].

The experiment has a within-subjects design with two independent variables. The independent variables are the motion washout filter order and the motion washout filter break frequency. Motion cues will be provided by the VMS motion system using the standard motion logic. There will be a no-motion condition (NM) present: the simulator will be operating with motion, however, with all motion parameters set to zero. A full VMS motion condition (FM) uses the entire VMS motion envelope to simulate motion with the highest possible fidelity. Between these two extremes 6 to 8 conditions will be present, in which the motion filter order and break frequency are varied. The conditions will be presented in random order according to a balanced Latin square design. The condition matrix can be seen in Table 1.

Table 1: Experiment Conditions.

Condition	Filter Order	Break Frequency [rad/s]	Motion Filter
1	No Motion		$H_{mf}(s) = 0.0$
2	1	0.5	$H_{mf}(s) = K\ \frac{s}{s+0.5}$
3	1	1	$H_{mf}(s) = K\ \frac{s}{s+1.0}$
4	2	0.5	$H_{mf}(s) = K\ \frac{s^2}{s^2+2\cdot\zeta_{mf}\cdot 0.5\cdot s+0.5^2}$
5	2	1.0	$H_{mf}(s) = K\ \frac{s^2}{s^2+2\cdot\zeta_{mf}\cdot 1.0\cdot s+1.0^2}$
6	3	0.5	$H_{mf}(s) = K\ \frac{s^2}{s^2+2\cdot\zeta_{mf}\cdot 0.5\cdot s+0.5^2}\cdot\frac{s}{s+\omega_b}$
7	3	1.0	$H_{mf}(s) = K\ \frac{s^2}{s^2+2\cdot\zeta_{mf}\cdot 1.0\cdot s+1.0^2}\cdot\frac{s}{s+\omega_b}$
8	Full VMS motion		$H_{mf}(s) = 1.0$

Varying the order and break frequency of the motion filter, as depicted in Figure 3, influences simulator motion fidelity. Figure 4 presents the frequency responses of 4 motion filters with different orders. Higher filter orders attenuate the lower frequencies more and induce a larger phase distortion. This leads to lower fidelity motion cuing, as can be seen in Figure 5.

Pilots will perform a minimum of eight runs per condition (including training) for a total minimum of 80 runs. Each run lasts 90 seconds. Anticipating a 20-second break between each run for preparing for the next run, the total run time of the experiment is at least 2.8 hours, excluding breaks. We expect that it will take three and a half hours for a participant to complete the experiment, including briefing and break time. Preferably two or three runs for each condition will be performed in between longer breaks. This anticipates two longer breaks over the course of the experiment. However, participants can get a break whenever they choose.

Before the start of the experiment, pilots will receive an extensive briefing explaining the main purpose of the experiment and the general procedures. No specifics will be given about the different experimental conditions.

Figure 1: Commercial transport aircraft cockpit.

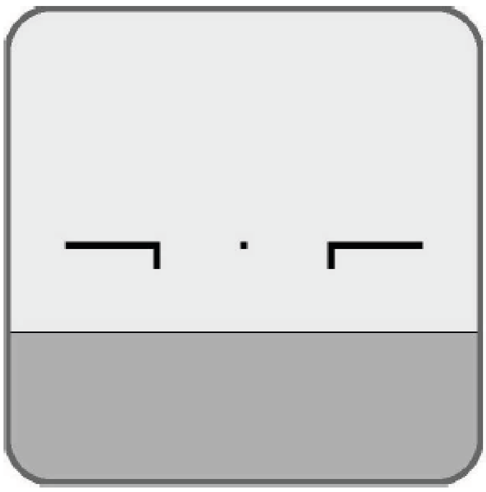

Figure 2: Primary flight display [1].

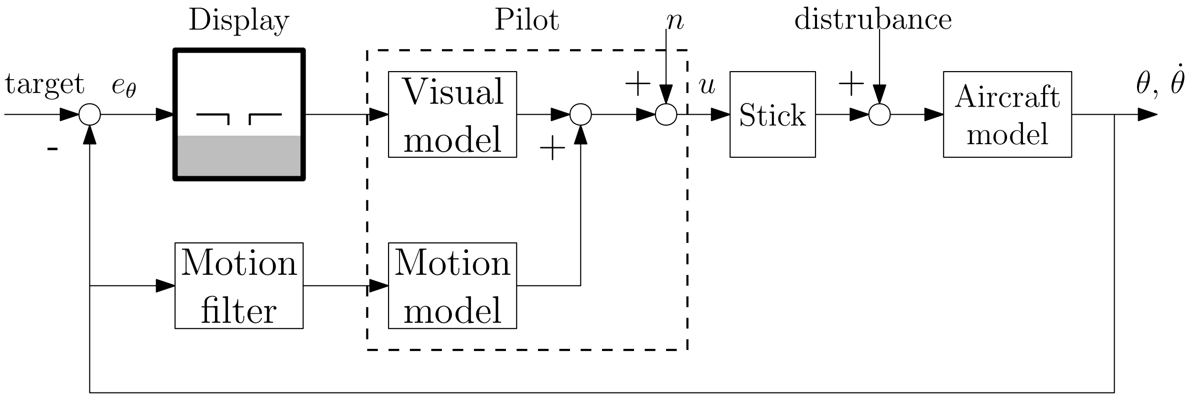

Figure 3: Control diagram.

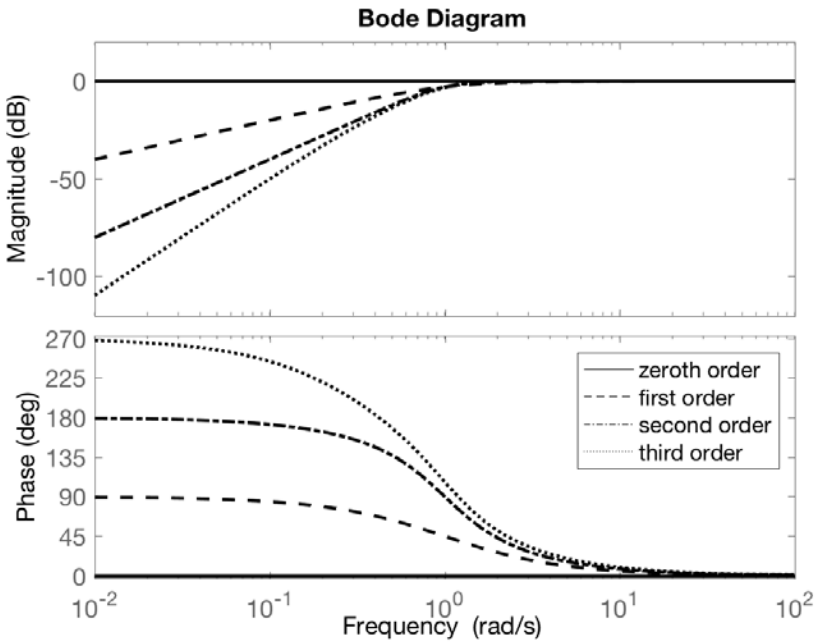

Figure 4: Frequency response of motion filters with different orders.

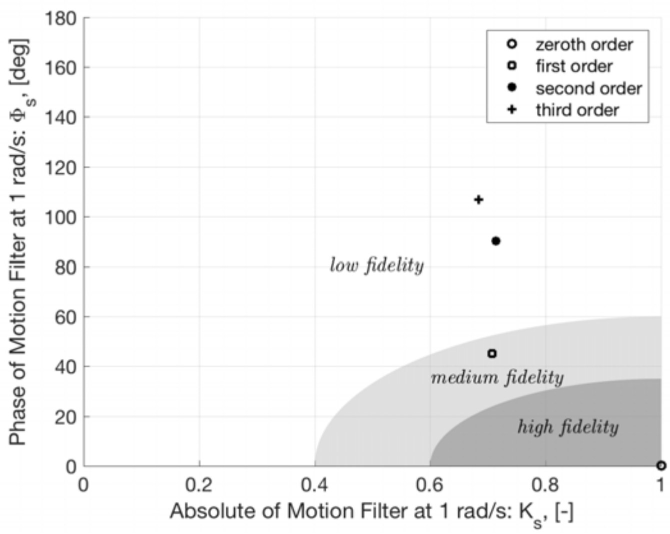

Figure 5: Motion fidelity criteria for motion filters with different orders.

8. Proposed Test Schedule

We aim to test participants from 21 May to 30 June, 2018. Two pilots may be tested per day. The first time slot runs from 8:00 am to 11:30 am and the second time slot runs from 12:30 pm to 4:00 pm. It is anticipated that every participant will be able to finish the experiment in three hours.

9. Safety Precautions

The VMS has been used in many pilot evaluation studies in the past. The standard operating procedures (SOP) for the VMS, including all safety procedures, are always followed for all motion simulations. In case of motion sickness or any other discomfort, the participant can stop the simulation at any time both verbally or by the push of a button. In addition, the PI, simulator engineer, or motion operator can stop the simulation if necessary.

For the current experiment, discrete data runs do not exceed 90 seconds. Participants will be told that they can take a break whenever they choose. After every experiment run, participants are asked if they are ready for the next run, allowing them substantial opportunity to ask for breaks. Short breaks between runs can be taken inside the simulator cab. After the training phase of the experiment, a longer break is scheduled outside of the simulator cab.

10. Number, Sources, and Pertinent Characteristics of the Participants.

Up to 12 general aviation pilots will be recruited by San Jose State University Research Foundation from an existing pool of subjects. This is similar to the number of pilots used in previous similar studies in the VMS. Both male and female participants may be included. Since the stick is a right-handed sidestick, participants need to either be right handed or be comfortable with making right-handed control inputs. Preferably, participants will be familiar with the type of control task used in the experiment, but this is not a requirement.

11. Possible Inconvenience, Discomfort, Pain, and Risks to the Subjects

Abrupt Acceleration/Decelerations Risks: The VMS system is capable of producing high fidelity motion effects including accelerations/decelerations. Although not planned, maneuvers could result in significant accelerations/decelerations. The simulator is equipped with control systems, seats and harness to protect participants and mitigate those risks as much as possible.

Motion Sickness: Possible discomfort from motion sickness due to the accelerations of the simulator.

Injury due to contact: Very remote risk of injury due to exposure to the motion of, or contact with, objects in the simulator cab.

Confidentiality: Although the following efforts will be taken to ensure confidentiality, there remains a remote risk of personal data becoming identifiable. A non-identifying code number will be assigned to the participant’s data records, which will be stored in accordance with federal regulatory procedures and accessible only to the investigator. No identifying individual medical information will be requested. Results from this study will typically be reported in an aggregate statistical format. Any use of individual data to illustrate specific performance features will be labeled in a manner to preserve the participants' anonymity. Any photographs or video of participants involved in the study will not be released without their prior written consent. While all stated precautions will be taken to protect participant anonymity, there is a small risk that some or all data could become identifiable.

12. What Measures Will Be Taken to Minimize the Discomfort or Risks

The seat in the simulator cabin will be adjusted for individual participants to provide them with the most comfortable position to perform the experiment. Sessions will be discontinued if participants experience any discomfort. Participants are able to stop the simulation at any time both verbally or by using a button in the simulator cab. Standard VMS safely procedures will be followed to mitigate any further risks.

13. Conditions on Withdrawal from the Experiment

Participants will be informed that they are free to withdraw from the experiment at any time. A subject may terminate participation at any time without explanation and without financial or other penalty. Compensation will be provided for time worked.

14. Remuneration for Participation

The wage to be paid each subject will be determined by the contractor by whom they will be employed (currently, San Jose State University Research Foundation).

15. Compensation in the Event of Injury

In the event of physical injury resulting from this study and calling for immediate action or attention, NASA will provide, or cause to be provided, the necessary treatment. If the subject is eligible for California Workers Compensation benefits while participating in this study, their employer cannot be sued as the law makes Workers Compensation the only remedy against their employer. The subject may have other remedies against other persons or organizations depending on the circumstances of the injury. NASA will pay for any claims of injury, loss of life or property damage to the extent required by the Federal Employees Compensation Act or the Federal Tort Claims Act.

16. Consent Form

See attachment to this proposal.

17. Responsible Ames Employee

Brent R. Beutter, Ph.D.

18. Provide details on how confidentiality and/or anonymity of research participants will be maintained.

Participants' confidentiality will be maintained by keeping consent forms and other identifying information in a secure place and ensuring that no personally identifying information is included in any publications reporting this experiment. For example, demographic information will be stated using statistical information, and pilots will simply be numerically identified in all publications (that is, pilot 1, pilot 2, etc.). All stated precautions will be taken to protect anonymity, and there is little risk that some or all of the participants' data could become identifiable.

19. References

[1] P. M. T. Zaal and M. A. Zavala. "Effects of Different Heave Motion Components on Pilot Pitch Control Behavior", AIAA Modeling and Simulation Technologies Conference, AIAA AVIATION Forum, (AIAA 2016-3371)

[2] P.M. T. Zaal, D. M. Pool, Q. P. Chu, M. Mulder, M. M. Van Paassen, and J. A. Mulder. "Modeling Human Multimodal Perception and Control Using Genetic Maximum Likelihood Estimation", Journal of Guidance, Control, and Dynamics, Vol. 32, No. 4 (2009), pp. 1089-1099.

National Aeronautics and Space Administration
AMES RESEARCH CENTER
Moffett Field, California 94035

HUMAN RESEARCH CONSENT FORM

Part 1

TITLE: The Effects of Motion Filter Order on Human Control Behavior

A. PURPOSE:
The objective of this experiment is to investigate the effects of different motion washout filter orders on manual control behavior and performance.

B. INVESTIGATORS:
Principal Investigator: Peter M. T. Zaal, Ph.D. (San José State University)
Investigator: Marc Pieters, B.Sc. (San José State University)

C. NATURE OF THE EXPERIMENT:
Background: By performing a variation of the order of the (high-pass) motion filters of the simulator, insight into the effects of the motion filter orders – an underexplored but critical motion tuning parameter – on pilot manual control behavior is gained.

Overview: The experiment will be conducted in the Vertical Motion Simulator (VMS) with the commercial transport aircraft cab (T-cab). This cab has two seats. The left seat will have a wheel and column to make control inputs. You will perform the experiment from the right seat, which will have a sidestick to make control inputs. In addition, rudder pedals will be available for both seats; however, these will not be operational during the experiment. Throttle levers are located between the seats; also the throttles will not be operational. A primary flight display (PFD) will be located in front of both seats. The out-the-window visual system will be turned off.

You will perform a disturbance-rejection task in pitch. It is your task to minimize the disturbances by keeping the aircraft pitch at the desired attitude while the aircraft is perturbed by atmospheric turbulence. The desired attitude will be provided by the PFD.

The experiment has several different motion conditions. Some conditions represent motion that is typical for a hexapod training simulator (smaller motion excursions) and some will use the full VMS motion capability (large motion excursions). The motion conditions will be presented in random order.

Typical session: After having read this document and providing your informed consent, you will be briefed about the purpose, procedures, and conditions of the experiment. Next, you will be given a safety briefing at the VMS explaining the safety features of the simulator and showing you the escape routes. After this, we will familiarize you with the simulator cab layout and flight controls, and adjust the seat to provide you with the most comfortable position to perform the experiment.

You will perform a minimum of eight runs per condition (including training) for a total minimum of 80 runs. Each run lasts 90 seconds. Anticipating a 20-second break between each run for preparing for the next run, the total run time of the experiment is at least 3 hours, excluding breaks. We expect that it will take three hours for a participant to complete the experiment, including briefing and break time. Preferably two or three runs for each condition will be performed in between longer breaks. This anticipates two longer breaks over the course of the experiment. However, you may take a break whenever you choose if you experience any discomfort.

D. MANNER IN WHICH TEST OR EXPERIMENT WILL BE CONDUCTED:
You will be one of up to 12 volunteer participants who will be recruited to come to the Vertical Motion Simulator Lab at NASA Ames Research Center for this study.

E. DURATION AND LOCATION:
Your participation is requested over a three-hour period in May/June 2018. The location of the tests will be the Vertical Motion Simulator Lab (Building N-243) at NASA Ames Research Center. Excluding travel, your total time commitment in this experiment will not exceed three hours.

F. FORESEEABLE INCONVENIENCE, DISCOMFORT, AND/OR RISKS:
Abrupt Acceleration/Decelerations Risks: The VMS system is capable of producing high fidelity motion effects including accelerations/decelerations. Although not planned, maneuvers could result in significant accelerations/decelerations. The simulator is equipped with control systems, seats and harness to protect participants and mitigate those risks as much as possible.

Motion Sickness: Possible discomfort from motion sickness due to the accelerations of the simulator.

Injury due to contact: Very remote risk of injury due to exposure to the motion of, or contact with, objects in the simulator cab.

Confidentiality: Although the following efforts will be taken to ensure confidentiality, there remains a remote risk of personal data becoming identifiable. A non-identifying code number will be assigned to the participant's data records, which will be stored in accordance with federal regulatory procedures and accessible only to the investigator. No identifying individual medical information will be requested. Results from this study will typically be reported in an aggregate statistical format. Any use of individual data to illustrate specific performance features will be labeled in a manner to preserve the participants' anonymity. Any photographs or video of participants involved in the study will not be released without their prior written consent. While all stated precautions will be taken to protect participant anonymity, there is a small risk that some or all data could become identifiable.

G. RENUMERATION:
The wage to be paid will be determined by the San José State University Research Foundation.

H. RIGHT TO WITHDRAW FROM THE STUDY; HAZARDS ASSOCIATED WITH WITHDRAWAL:
You have the right to withdraw from this study at any time for any reason, although we hope you will not consent to the study unless you intend to complete it.

I. ANSWERS TO QUESTIONS:
You may receive answers to any questions related to this study by making contact with the Principal Investigator, Peter M. T. Zaal at (650) 604-5805. Should any problems related to the study occur during its course, please contact the Principal Investigator at that number. You may also call Dr. Ralph Pelligra, MD, Ames's Chief Medical Officer and Chair of Ames's Human Research Institutional Review Board at (650) 604-5163. Dr. Pelligra is your advocate and you can speak with him confidentially about any concerns and questions relating to this study.

J. REMEDY IN THE EVENT OF INJURY:
In the unlikely event of injury or death, civil servant employees will be compensated according to federal insurance regulations. If you are a contractor or other non-federal employee, you will be covered by Worker's Compensation insurance during the course of your participation in this study. If you sustain an injury caused by this study, the benefits you will receive are those currently provided under the Worker's Compensation law in California. You cannot sue your employer because the law makes Workers' Compensation your only remedy against him/her. You may have other remedies against other persons or organizations, depending on the circumstances or your injury.

I certify that the series of tests for which ________________________________ is to serve as a subject has been explained to him/her in detail.

____ __________

Signature of Test Subject Date

____ __________

Signature of Principal Investigator Date

TO THE SUBJECT: Please read Part 1 CAREFULLY. Make sure all of your questions have been answered to your satisfaction. Do not sign this form until Part 1 has been read by you and signed by the Principal Investigator (P.I.). You will receive a signed copy of the Consent Form.

A. I, ____
agree to participate as a subject in this study and experiment described in Part 1 of this form.

B. I am aware of possible foreseeable consequences that may result from participation, and that such participation may otherwise cause me inconvenience or discomfort as described in Part 1.

C. My consent has been freely given. I may withdraw my consent, and thereby withdraw from the study, at any time. I understand (1) that the Principal Investigator may request my withdrawal from the study if I am not conforming to the requirements of the study as outlined in Part 1 and (2) that the NASA Facility Safety Manager may terminate the study in the event that unsafe conditions develop that cannot be immediately corrected. I understand that if I withdraw from the study, or am dismissed, I will be paid for the time served up to the point of my departure, but not thereafter.

D. I am not releasing NASA or any other person or organization from liability for any injury arising as a result of this study. I understand that I will receive emergency care if I am injured during the study, but payment for any follow-on care will depend on whether I have some form of applicable insurance, or whether I have made some other arrangements for such follow-on care. I may have other remedies against other persons or organizations, depending upon the circumstances of my injury.

E. I hereby agree that all records collected by NASA in the course of this experiment are available to the NASA Medical Officer, Principal Investigator and Co-Investigators and duly authorized research review committee. I grant NASA permission to reproduce and publish all records, notes or data collected from my participation provided that there will be no association by name with the collected data and that confidentiality is maintained unless specifically waived by me. All stated precautions will be taken to protect your anonymity, but there is a small risk that some or all of your data could become identifiable.

F. I understand that I have the right to request the Chair of the Ames Human Research Institutional Review Board (HRIRB) to convene a Board if, at any time, I feel that my rights as a human research subject have been abused or violated.

G. I have had an opportunity to ask questions and I have received satisfactory answers to each question I have asked. I understand that the P.I. for the study is the person responsible for this activity and that any pertinent questions will be addressed to her during the course of this study. I have read the above agreement, the attached protocol and/or instructions prior to my signature and understand the contents.

Signature of Test Subject	Date	Signature of Principal Investigator	Date
Printed Name of Test Subject		Printed Name of Principal Investigator	
Address		Telephone Number of Principal Investigator	
City, State, Zip Code		Subject Signature: Authorization for Videotaping	
Telephone number of Test Subject		Subject Signature: Authorization for Release of Information to Non-NASA Source(s)	

D.4. Delft University of Technology Consent Form

Similar to the NASA IRB documents, Delft University of Technology also required a consent form to be signed by all participants stipulating the risks and protection measures taken. The consent form follows the format of the Human Research Ethics Comission (HREC).

Consent Form for SIMONA Research Simulator – Motion Algorithm Development Experiment

Please tick the appropriate boxes	**Yes**	**No**
Taking part in the study		
I have read and understood the study information dated, or it has been read to me. I have been able to ask questions about the study and my questions have been answered to my satisfaction.	▯	▯
I consent voluntarily to be a participant in this study and understand that I can refuse to answer questions and I can withdraw from the study at any time, without having to give a reason.	▯	▯
I understand that taking part in the study involves performing a manual control task in a full-motion simulator setup, under different motion conditions.	▯	▯
Risks associated with participating in the study		
I understand that taking part in the study involves the following risks: discomfort due to sitting down, dry eyes and motion sickness.	▯	▯
Use of the information in the study		
I understand that information I provide will be used for a report and publications.	▯	▯
I understand that personal information collected about me that can identify me, such as my name, will not be shared beyond the study team.	▯	▯
Future use and reuse of the information by others		
I give permission for the experiment data that I provide to be archived in an anonymous manner so it can be used for future research and learning.	▯	▯

Signatures

______________________	______________________	________
Name of participant [printed]	Signature	Date

I have accurately read out the information sheet to the potential participant and, to the best of my ability, ensured that the participant understands to what they are freely consenting.

_________________________	___________________	________
Researcher name [printed]	Signature	Date

Study contact details for further information:

Contact information researcher	Contact information supervisor
Marc Pieters	dr. ir. Daan Pool